SYNTHESIS AND CHARACTERIZATION OF NANOSTRUCTURED TITANIA FOR GAS SENSOR APPLICATIONS

THESIS SUBMITTED FOR THE AWARD OF THE DEGREE OF

Doctor of Philosophy

in

Applied Physics

by

Saroj Radheyshyam Sabhajeet
M.Sc., M. Phil.

Enrollment No. 582/12

Under the supervision

of

Dr. Bal Chandra Yadav

DEPARTMENT OF APPLIED PHYSICS
SCHOOL FOR PHYSICAL SCIENCES
BABASAHEB BHIMRAO AMBEDKAR UNIVERSITY,
LUCKNOW– 226025, U.P., INDIA

July, 2017

DECLARATION

I hereby declare that the thesis entitled **"Synthesis and Characterization of Nanostructured Titania for Gas Sensor Applications"** has been prepared by me under the supervision of Dr. Bal Chandra Yadav, Associate Professor, Department of Applied Physics, School for Physical Sciences, Babasaheb Bhimrao Ambedkar University, Lucknow. No part of this thesis has formed the basis for the award of any degree, diploma or fellowship previously. Further, I declare that the material embodied in the present work is based on original research work and the indebtedness to others has been duly acknowledged at relevant places.

(Saroj Radheyshyam Sabhajeet)

Department of Applied Physics, School for Physical Sciences,

Babasaheb Bhimrao Ambedkar University, Vidya Vihar,

Raebareli Road, Lucknow-226025, U.P., India.

Date: 28th July, 2017
Place: Lucknow

Dedicated to
My Teachers
and
Parents

CERTIFICATE

This is to certify that the thesis entitled **"Synthesis and Characterization of Nanostructured Titania for Gas Sensor Applications"** submitted by **Saroj Radheyshyam Sabhajeet** is an original research work and has not been previously submitted in part or full for the award of any other degree or diploma to this or any other university or institutions.

The thesis submitted to the Babasaheb Bhimrao Ambedkar University, Lucknow satisfies all the requirements as stipulated in the *Doctor of Philosophy (Ph.D.) regulations-1999 as amended in 2010* and it is fit for submission and evaluation for the award of Doctor of Philosophy of the University.

Dr. B. C. Yadav
(Supervisor)

Dr. Bal Chandra Yadav
Associate Professor & Ex-Head
Department of Applied Physics
School for Physical Sciences
B.B. Ambedkar University, Lucknow-226025

Dr. Devesh Kumar
(Head of the Department)

Head
विभागाध्यक्ष
Deptt. of Applied Physics
अनुप्रयुक्त भौतिकी विभाग
Babasaheb Bhimrao Ambedkar University
बाबासाहेब भीमराव अम्बेडकर विश्वविद्यालय
Lucknow-226025, U.P. INDIA
लखनऊ-226025, उ०प्र०, भारत

Date: 28th July, 2017
Place: Lucknow

ACKNOWLEDGEMENT

It is my firm belief that any major research work to result in a positive outcome including a worthy thesis requires the culmination of several factors such as a meaningful subject which can motivate a determined researcher to take up the challenge, a learned and sincere guide in the form of friend who selflessly encourage and help the researcher throughout the research. I had the honour and privilege to have **Dr. Bal Chandra Yadav** as an excellent guide and former head of the department who meticulously guided and supervised throughout my research. I take this opportunity to place on record my heart-felt and sincere gratitude and deep indebtedness to him without whose guidance this work could not have been meaningfully concluded.

I am extremely thankful to my teachers **Dr. Devesh Kumar, Dr. Ramesh Chandra, Dr. Anil Kumar Yadav, Dr. Khem Bhadur Thapa, Mr. Devendra Singh,** and Lab Staff, Department of Applied Physics, Babasaheb Bhimrao Ambedkar University, for providing friendly and motivating environment during the course of this work.

I am deeply thankful to **Prof. Raja Ram Yadav**, Vice-chancellor, Veer Bahadur Singh Purvanchal University, Jaunpur, U.P. and my supervisor of M.Phil. for providing me the basic training of research. I am also thankful to **Dr. Rakesh Kumar Sonker, NPDF, Delhi University** for his help and support in my progress of academic learning and exploration. I am grateful to him for providing useful suggestions at the hour of need. Also I am thankful to **Ms. Samiksha Sikarwar** for her suggestions and contributions.

I oblige to **Dr. Vivek Malviya,** Geological Survey of India, Lucknow, **Dr. Mukesh Kumar,** USIC, Babasaheb Bhimrao Ambedkar University, Lucknow, **Dr. Thakur Prasad Yadav,** Department of Physics, Banaras Hindu University, Varanasi, **Dr. Subodh Kumar**,

Birbal Sahni Institute of Paleobotany, Lucknow and **Mr. Rahul,** Indian Institute of Technology, Kanpur, Uttar Pradesh for technical help in XRD, SEM, FE-SEM, FTIR, TEM facilities.

I would like to acknowledge the contribution of my friends and colleagues, **Dr. Richa Srivastava, Dr. Sarita Yadav, Dr. Ravindra Kumar, Dr. Ravikant Tripathi, Ms. Monika, Mr. Utkarsh, Mr. Kuldeep** and **Ms. Priyanka,** who helped me throughout this journey. I am very thankful to my senior **Dr. Satyendra Singh** for their continuous moral support and encouragement.

I owe this thesis to my loving mother and father for their love, support and sacrifice from the very first day of my journey of life. I also express my sincere thanks to my brother **Mr. Ghanshyam Saroj** and sister **Ms. Sarita Devi** for providing me every kind of support. I would like to acknowledge the sweet smile of my daughter **Ms. Anjali** and moral support of my wife **Ms. Surekha Devi** who inspired and imparted happiness in my life and gave strength to overcome the failures and to start over again.

My final words of thanks will be for almighty God, for showering His blessings upon me and companionship through all turmoil of my life.

Saroj Radheyshyam Sabhajeet

(Ph.D. Scholar)

LIST OF PUBLICATIONS

Papers communicated/ published in the refereed journals:

1. **S. R. Sabhajeet**, Rakesh Kumar Sonker, B.C. Yadav, "Sol-gel processed Grape-like nanostructured Titania based Liquefied Petroleum Gas Sensor", communicated to *International Journal of Nanotechnology and Application*.
2. **S. R. Sabhajeet**, Rakesh Kumar Sonker, B.C. Yadav, "Zn-doped TiO_2 nanoparticles employed as room temperature Liquefied Petroleum Gas Sensor", communicated to *Journal of Electronic Materials*.
3. **S. R. Sabhajeet**, Rakesh Kumar Sonker, Samiksha Sikarwar, B.C. Yadav, "Synthesis and characterization of Ag-doped TiO_2 nanocomposites via sol-gel method for LPG sensor", communicated to *Sensor and Actuator B: Chemical.*
4. Rakesh Kumar Sonker, **S. R. Sabhajeet**, B.C. Yadav, "TiO_2–PANI nanocomposite thin film prepared by spin coating technique working as room temperature CO_2 gas sensing", *J Mater Sci: Mater Electron*, 27 (2016) 11726-11732.
5. Rakesh Kumar Sonker, B.C. Yadav, **S. R. Sabhajeet** "Preparation of PANI doped TiO_2 nanocomposite thin film and its relevance as room temperature liquefied petroleum gas sensor" *J Mater Sci: Mater Electron*, DOI 10.1007/s10854-017-7309-4.
6. B. C. Yadav, Nidhi Verma, Tripti Shukla, Satyendra Singh, **S. R. Sabhajeet**, "Fabrication and characterization of nanostructured (Sn–Ti)O_2 pellets and films for liquefied petroleum gas sensing", *J Mater Sci: Mater Electron*, 27 (2016) 7852-7863.
7. Rakesh Kumar Sonker, **S. R. Sabhajeet**, Satyendra Singh, B.C. Yadav, "Synthesis of ZnO nanopetals and its application as NO_2 gas sensor", *Materials Letters*, 152 (2015) 189-191.

International Conferences/workshop

1. **S. R. Sabhajeet,** Rakesh Kumar Sonker, B.C. Yadav, "Synthesis and characterization of Fe-doped TiO_2 for LPG sensor using precursor $TiCl_4$ at room temperature", **2nd International Conference Kathmandu Symposia on Advanced Material**, **2014,** held on Tribhuvan University, Kathmandu, **Nepal** from 7-10 September 2014.
2. **S. R. Sabhajeet,** Rakesh Kumar Sonker, B.C. Yadav, "Synthesis and ultrasonic characterization of Ag nanoparticles polymer suspension", **International Conference on Nanoscience and Nanotechnology-2013,** Babasaheb Bhimrao Ambedkar University, Lucknow, **India**, 18-20 November 2013.
3. Rakesh Kumar Sonker, **S. R. Sabhajeet**, Ravindra Kumar, B.C. Yadav, "Study of NO_2 Sensing metal oxide (SnO_2) thin film", **International Symposium on Advances in Materials Characterization**, Babasaheb Bhimrao Ambedkar University, Lucknow, **India**, 14 July 2014.
4. Rakesh Kumar Sonker, **S. R. Sabhajeet**, Ravindra Kumar, B.C. Yadav, "LPG detection for SnO_2, PANI-SnO_2 and Ag-SnO_2 composite film fabricated by Chemical route method", **2nd International Conference, Kathmandu Symposia on Advanced Material**, **2014,** Tribhuvan University, Kathmandu, **Nepal,** 7-10 September 2014.
5. Rakesh Kumar Sonker, **S. R. Sabhajeet**, B.C. Yadav, "PANI doped TiO_2 composite nanoparticles employed as room temperature Liquefied Petroleum Gas sensor" **International Conference on Energy Environment and Engineering "ICEEE-2016"**, Coimbatore Institute of Technology, Tamilnadu, **India,** Feb. 29-March 2, 2016.

National Conferences/workshop

1. **S. R. Sabhajeet,** Monika Singh, Rakesh Kumar Sonker, Manmeet Kaur, B. C. Yadav,

"Zn-doped TiO_2 nanoparticles employed as room temperature Liquefied Petroleum Gas sensor", **National conference on Emerging Trends In Nanoscience and Nanotechnology**, MVP Samaj's Arts, Science and Commerce College, Ozar, Nashik, **India,** 23-24 December 2014.

2. **S. R. Sabhajeet "18th National Symposium on Solid State Nuclear Track Detectors and their Applications"**, Faculty of Science, Agarwal College Ballabgarh, Faridabad (Haryana), **India,** 18-20 October 2013.
3. **S. R. Sabhajeet**, **UGC Networking Programme** a workshop on **"Nano Materials with Particular Reference to Energy Security"** Department of Physics, Banaras Hindu University, Varanasi-5, **India,** 11-17 March 2014.
4. **S. R. Sabhajeet, UGC Networking Programme** a winter school on **"Practical crystallography and structure solution",** Department of Physics, Banaras Hindu University, Varanasi-5, **India,** 5-11 March 2014.
5. Rakesh Kumar Sonker, **S. R. Sabhajeet**, Rahul, B.C. Yadav, "Effect of Polyaniline/ Titanium dioxide composite film for LPG sensing", **"National Conference on Nanotechnology and Renewable Energy"**, Delhi, **India**, 28-29 April 2014 (ISBN-978-93-81212-65-3).

SUMMARY

A gas sensor is a chemical sensor which provides an electrical output in response to the chemical collaborations with gas species only. It is commonly used for industrial applications where many gas storage containers are in use. In the industrial application gas sensors are used to determine gas leaks in order to prevent any harm to human health as well as to defend from any explosions that caused by leakage.

From the literature, it is observed that currently available sensors have two major inadequacies i.e. low sensitivity and high operating temperature [1]. We have to compromise with either sensitivity or operating temperature. A high sensitive gas sensor mostly works at a very high operating temperature which increases the power consumption. LPG is most harmful gas for its inflammable and explosive nature which gives many hazards to human and environment. The LPG sensor has become a very interesting topic in view of the fundamental research as well as industrial applications [2-3].

The growth of portable LPG sensors that are robust, tiny sized, long lifetime, quick response and have sufficient sensitivity to the ambient environment is necessary and demanded in order to prevent the explosion accidents in homes and industries for safety requirements. Solid-state LPG sensors of metal oxide are the most auspicious for the detection of LPG because of their solid structure, high selectivity, low price, and the ability of continuous monitoring [4]. The need for reliable, cheap and user-friendly gas sensors for the detection of LPG is industrially important and has led to a considerable expansion in the field of sensor research and development. The performances will be enhanced intensely by approving preparation conditions and by controlling deposition process. Numerous types of LPG sensors such as chemical sensors, the resistive and conductive type sensors using semiconductors and sensors based on metal polymer complexes have been investigated by different research groups in the world. So, a great attention has been recently remunerated to

the development of new material at the nano-scale.

Nanomaterials can enhance the performance of LPG sensor due to their much higher surface-to-volume ratio as compared to micro-size materials. To enhance the sensitivity verified by the nanostructured material based sensors, it gives a quick response. Grain size and porous structure have large effect on the gas-sensing properties of crystalline materials and their full characterization is the beginning of the study of materials [5].

Use of nanoscience and nanotechnology in manufacturing materials for sensor applications may improve the detection limit of gas sensors at lower temperatures. It is due to alterations of the space charge layers for each grain and improving other electronic properties of the material. The large surface to volume ratio of nanomaterials can be used for improvement in gas sensor development. The surface reaction is improved by the increase in the number of defect sites for the reaction. It will increase the sensitivity of the gas sensor.

The one-dimensional nanostructure with high aspect ratios makes it attractive in gas sensor production [6]. The space charge layer control of nanostructures make motivating since conduction can modify drastically with expansion and contraction of the layer in the presence of different gases. In sensing process, high non-equilibrium amount of oxygen vacancies in the oxide sensor material is important in achieving the goal, which would help to contribute in more effective movement of charge across the sensor material. At low operating temperature, the non-equilibrium exists and number of vacancies cannot be predicted. In next step, increasing the number of surface sites for gas interaction will help for detection of gas at room temperature. Further, the sensor material in modification of the space charge layer can be done by:

(i) Reducing the crystallite size,

(ii) Changing the defect chemistry within the space charge layer and surface of the material,

(iii) Changing the particle shape

Another motivating aspect of nanomaterials that makes it an interesting candidate for room temperature gas sensor which is because of the changes in the band gap reported at small sizes [7]. The band gap may be improved by changing the potential barrier energy required for charged species to conduct. Another enhanced feature of nanocrystallites is the conduction of electrons from the surface reaction. This conduction of electrons has to overcome a potential barrier induced by the space charge layer.

Even after half a century of research investigations on the fundamental properties of TiO_2 crystal phases remain a significant characteristic due to its important function to be successfully utilized as gas sensor and solar cell. The gap between valence and conduction bands and the optical absorption property are dynamic to all these applications. TiO_2 is an important metal oxide for broad range of gas sensing applications, because of its surface chemistry, charge transport and electrical properties. It is a versatile material widely used in industry, research and ecological cleaning. The bulk structure of titanium dioxide materials can exist in one of the three forms: rutile, anatase and brookite, rutile and anatase structure is shown in Figure 1. Each phase has its own structure along with a particular application [8-10]. TiO_2 is a versatile functional material due to its many unusual properties such as high refractive index, hydrophilicity [11], biocompatibility [12], semiconductivity, corrosion resistance, low cost, wide availability, nontoxicity and physicochemically stable nature [13] and also known for its gas sensing behavior [14-15]. Titanium dioxide has received considerable attention because of its excellent optical, electrical, mechanical, and catalytic properties, which makes it technologically useful. Its superior properties are due to chemical and biological inertness, non-toxicity, strong oxidizing/reducing power, cost-effectiveness and long-term stability against photo corrosion and chemical corrosion. The band gap of

titania is about 3.2 eV. The band gap further increases with decreasing the particle size and hence the utilization typically confined within the UV-radiation of electromagnetic spectrum.

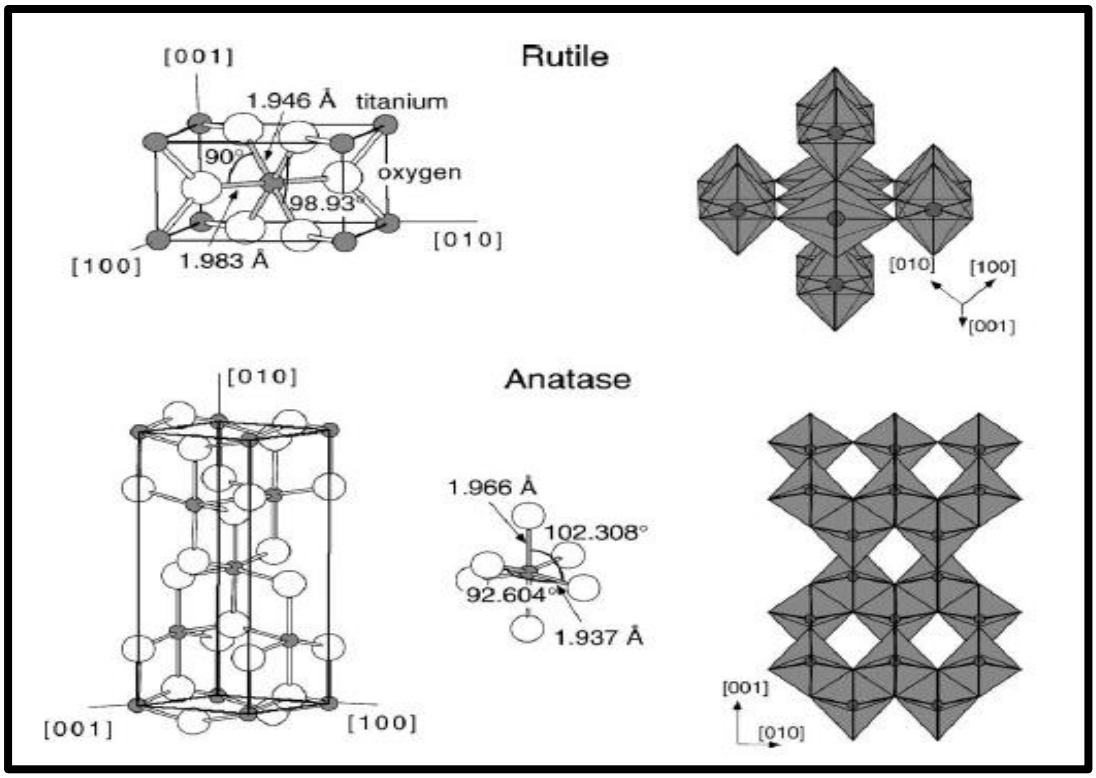

Figure 1: Bulk structure of rutile and anatase titanium dioxide showing the bond lengths and angles between atoms.

Basic requirement for the sensor is the change in electrical conductivity with exposure of LPG to surface of semiconducting oxides which depends on their band gaps, surface morphology, size, diffusion rate of gas and specific surface area. The semi-conducting properties of metal oxides represent the basis for their use as gas sensors, since the number of free charge carriers within the metal oxide and thus its electrical conductivity reversibly depends on the interactions with the ambient gas atmosphere.

Since the LPG sensing mechanism is based on the chemisorption reaction that takes place at the surface of the metal oxide. Thus increasing specific surface area of the sensing film leads to more sites for adsorption of surrounding gases. The oxygen adsorbed on the surface of the film influences the resistance of the titania based sensor. Initially oxygen from

the atmosphere adsorbs on the surface of the film and extracts electrons from its conduction bands to form O_2^- species on the surface, consequently resistance decreases. After that an equilibrium state is achieved between oxygen of TiO_2 and atmospheric oxygen.

Use of nanotechnology in engineering materials for sensor applications may improve the working detection limit of gas sensors to lower temperatures. This will be achieved predominantly by alterations of the space charge layers for each grain and enhancing other electronic properties of the material. The large surface to volume ratio of nanomaterials can be used as an advantage to contribute in gas sensor development. The surface reaction on the gas sensor is improved when the number of defect sites for reaction is increased. The large surface area to volume ratio of nanocrystalline structures increases the opportunity for this surface reaction to occur. This in turn will increase the sensitivity of the gas sensor. The surface of nanomaterials can comprise much of the actual material making them ideal for gas sensors.

The additives in metal oxide are chosen for improving the interactions among the gas species and the sensing surface. A study of synthesis, characterization and LPG sensing properties of titanium oxide, PANI-TiO_2, Zn-TiO_2, and Ag-TiO_2 is summarized here:

Chapter 2 includes the gas sensing of titania based nanostructured materials. Liquefied petroleum gas is an inflammable mixture of hydrocarbon gases used as a fuel in heating utilizations and vehicles. The structural, morphological and optical properties of the prepared sensor structure have been studied by X-ray diffraction (XRD), Scanning Electron Microscopy (SEM) and UV-Visible spectroscopy respectively. XRD revealed the crystallite size as 7 nm. SEM showed the regular and porous grape-like surface morphology before exposure to the LPG. The band gap of the material was found as 3.65 eV. The maximum sensing response was found as 1.34 for the exposure of 4% vol. of LPG and results were found reproducible. Figure 2 shows the lab model of experimental set-up for LPG sensing.

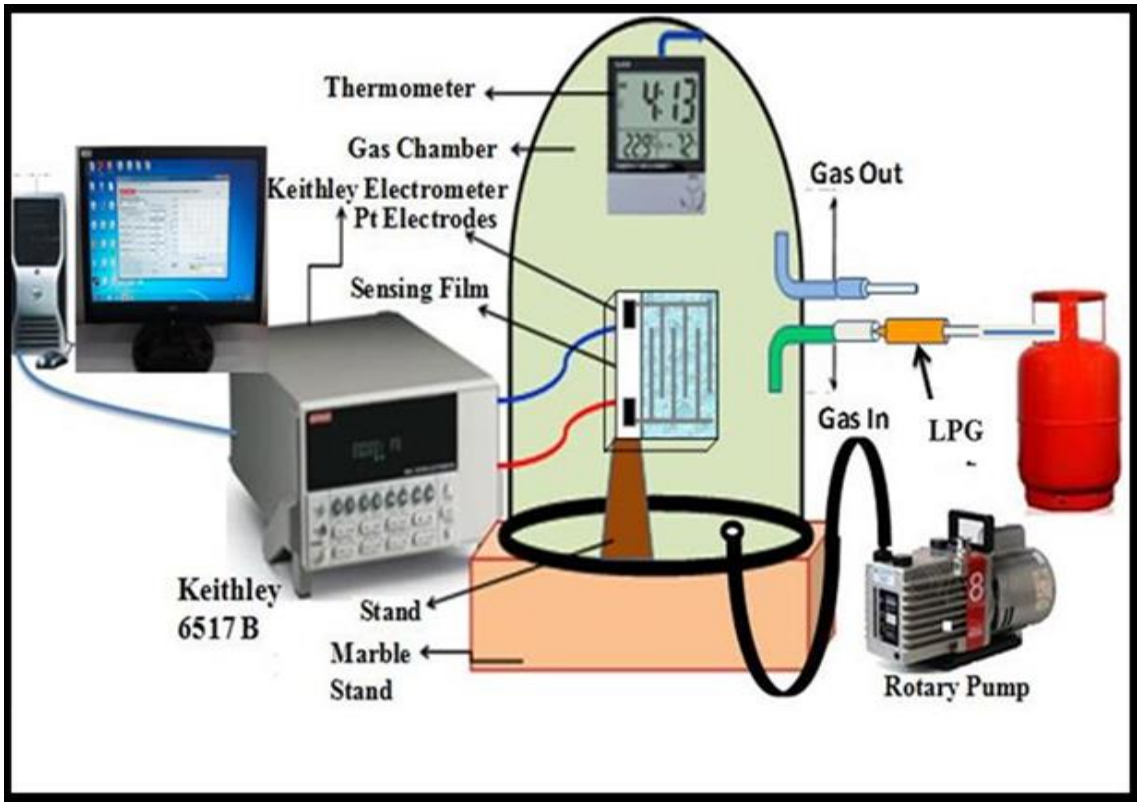

Figure 2. Gas sensing Set-up: Lab Model

Chapter 3 reports the utility of PANI doped titanium dioxide thin film on corning substrate with Inter Digital Electrodes (IDEs) prepared by spin coating technique as for LPG and CO_2 sensing. The increasing needs of carbon dioxide detection in various fields like air quality control, greenhouse monitoring and bio-related processes have been demanding high-quality CO_2 sensors in day to day. Optical properties were investigated using UV–Vis absorption spectroscopy. The surface morphology and structure of synthesised material were characterised by TEM and XRD analysis, respectively. The structural analysis confirmed the formation of PANI-TiO_2 having an average crystallite size 7 nm. The schematic of sensing mechanism and characteristics is shown in Figure 3. Variations in resistance with exposure of LPG to the sensing element were observed. Sensor response (S) as a function of time was calculated and its maximum value was found as 2.77 towards 2000 ppm of LPG, response time of the sensor was 156 s and recovery time was 140 s. Similarly, the sensor response (S) as a function of time was calculated and its maximum value was found as 53 for 1000 ppm of

CO_2. Response and recovery times of the sensor were observed as 9.2 min and 5.7 min respectively. The sensor was quite sensitive and results were found reproducible.

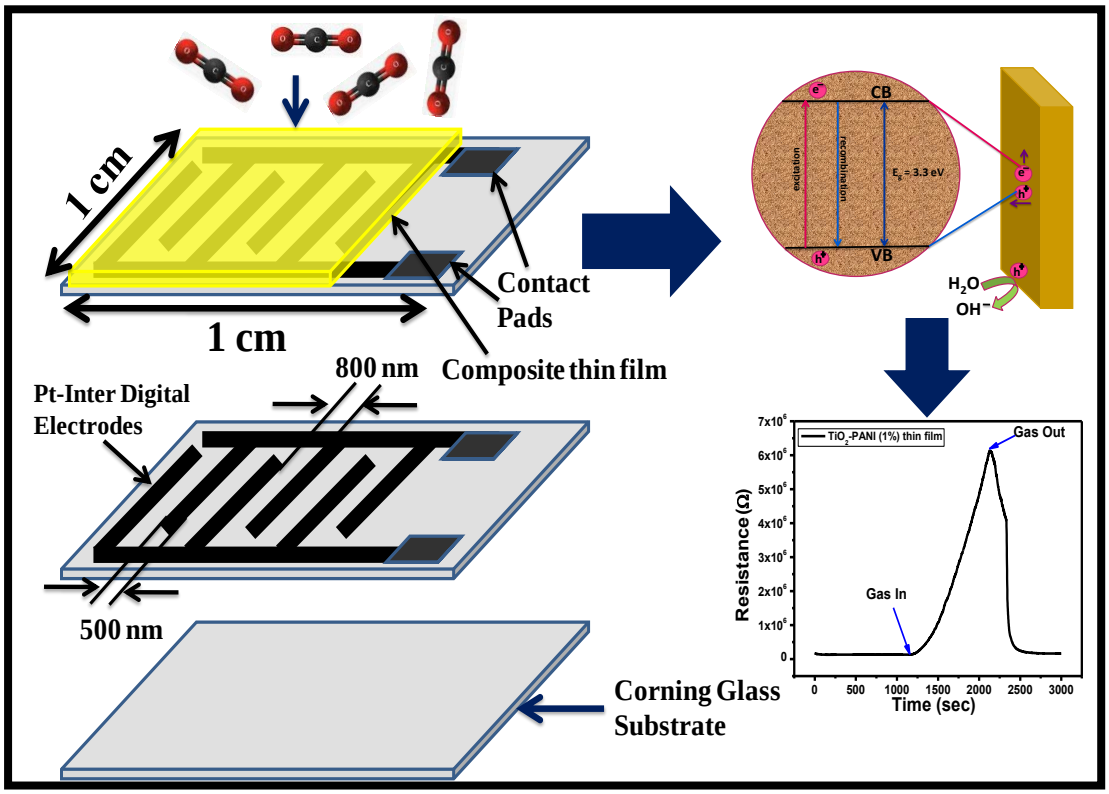

Figure 3 : Schematic of CO_2 sensing through PANI doped titanium dioxide composite thin film on corning substrate with IDEs

Chapter 4 describes the performance of a room temperature liquefied petroleum gas (LPG) sensor based on the Zn-doped titanium dioxide heterojunctions thin film prepared by spin coating technique. The surface morphology and structure of synthesised material were characterised by SEM and XRD analysis respectively. The structural analysis confirmed the formation of Zn-doped TiO_2 having an average crystallite size 76 nm with tetragonal rutile structure. Optical properties were investigated using UV–Vis absorption spectroscopy. Energy band gap of material was estimated as 3.26 eV. Variations in resistance with the exposure of LPG to the sensing element were observed. Sensor response (S) as a function of time was calculated and its maximum value was 2.92 towards 1.5 vol. % LPG, response time of the sensor was 120 s. The sensitivity of the

LPG sensor at 1.5 vol. % was found as 0.4625. Variations of average sensitivity of Zn-doped TiO_2 thin film with different volume concentrations of LPG is shown in Figure 4. The sensor was found moderately sensitive to LPG and results were found reproducible.

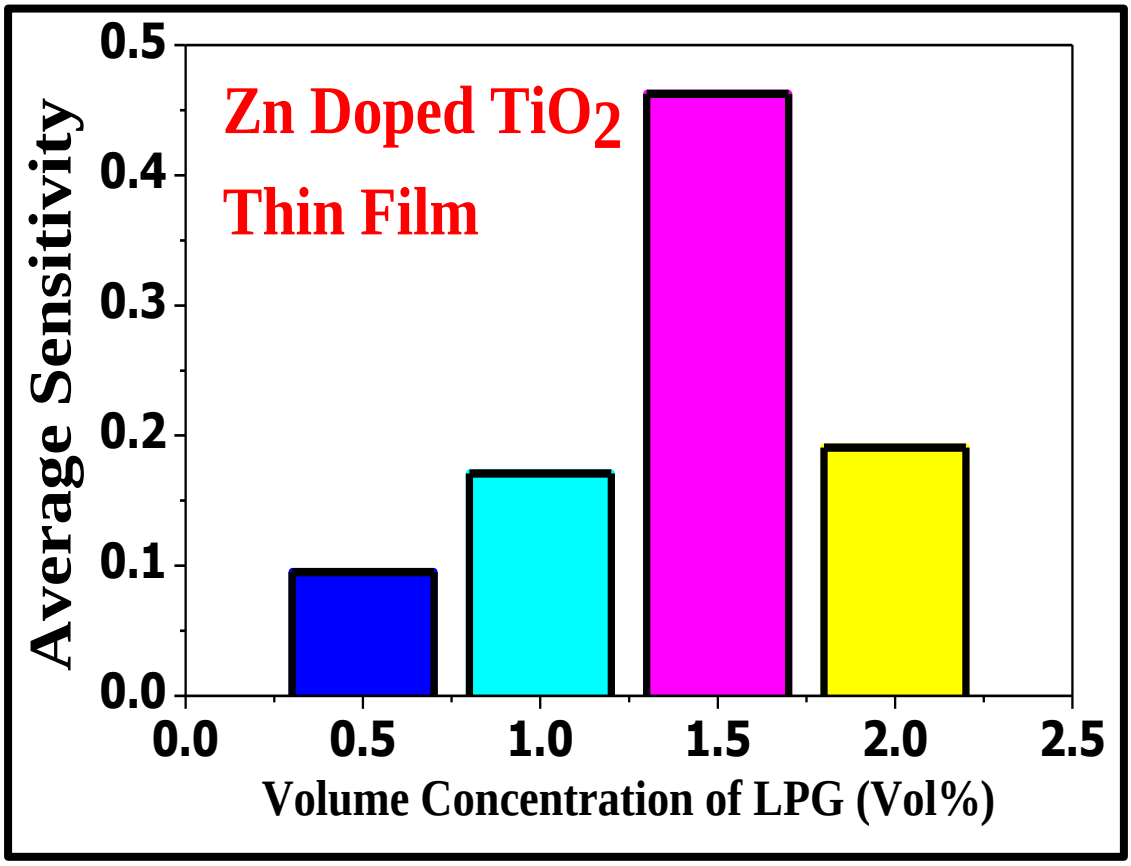

Figure 4: Variations of average sensitivity of Zn-doped TiO_2 thin film with different volume concentrations of LPG.

Chapter 5 includes the synthesis of Ag-doped TiO_2 nanocomposite via sol-gel method, its characterization and performance as liquefied petroleum gas (LPG) sensor. The synthesised material was characterised using XRD and confirmed the formation of (Ag-TiO_2) nanocomposite. The minimum crystallite size was found as 81 nm. XRD pattern revealed the tetragonal crystalline nature of the material. The material was also investigated through SEM and UV-Vis spectrophotometer. The energy band gap TiO_2 and Ag doped TiO_2 is found 3.29 eV and 2.6 eV by Tauc plot. The thin film was fabricated

for the sensing analysis. Further at room temperature, the film was exposed to LPG in a gas chamber under controlled conditions at room temperature and variations in resistance with the concentrations of LPG were observed. Figure 5 shows the schematic diagram of working mechanism of LPG sensor for 0.1M Ag doped TiO_2 thin film. The maximum value of sensor response for Ag-TiO_2 thin film based sensor was found 3.82 for 2 vol.% of LPG. The response and recovery times were obtained as 13.2 s and 6.6 s respectively.

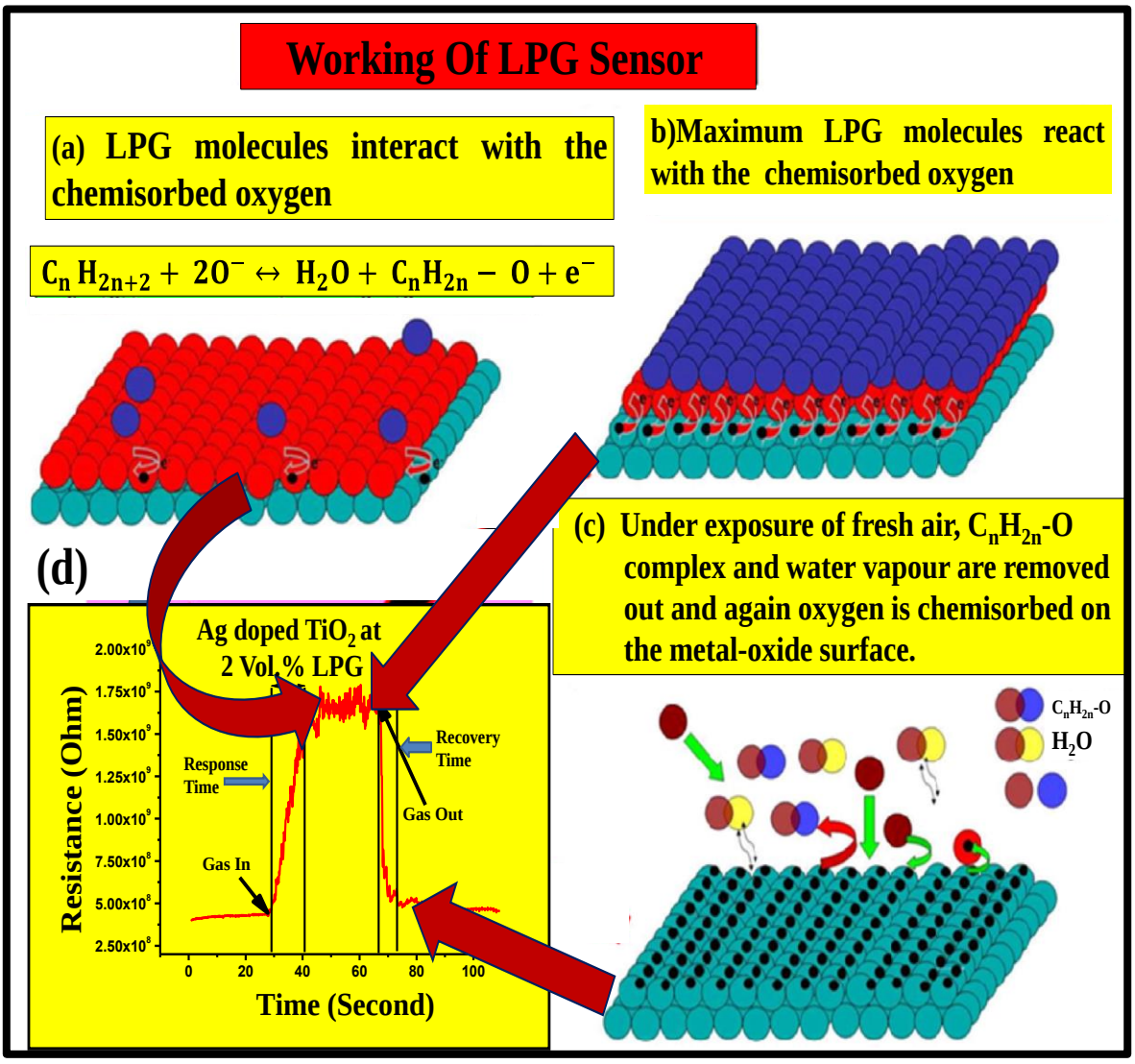

Figure 5: Schematic diagram showing the working of LPG sensor for 0.1M Ag doped TiO_2 thin film.

A chapter wise sketch of the thesis including the materials, percentage sensor response, crystallite size and concerned journals is depicted in Table 1. The main goal of our

research work carried out was to design and fabricate a LPG sensor which would be robust, cost effective and more sensitive than previously reported sensors.

Table 1: A chapter wise sketch of the Thesis.

Chapters	**Sensing Materials**	**Target Gas**	**Concentration Of gas**	**Sensor Response**	**Response time(s)**	**Recovery time(s)**
Chapter 1	Introduction					
Chapter 2	TiO_2	LPG	4.0 vol. %	1.34	117	148
Chapter 3	PANI-TiO_2	LPG	2000 ppm	2.77	156	140
Chapter 4	Zn doped TiO_2	LPG	1.5 vol. %	2.92	120	102
Chapter 5	Ag-TiO_2	LPG	2.0 vol. %	3.82	13.2	6.6
Chapter 6	Concluding Remarks					

From Table 1, we deduce that the nanocrystalline Ag doped titanium oxide is an excellent material for LPG sensing application at room temperature and using this material a commercialized model of LPG sensor applicable for both indoor and outdoor detection of LPG may be designed. Thus various configurations/systems described in the thesis and the detailed specifications given for each of them are expected to prove useful in fabricating a sturdy, robust and cost-effective LPG sensor suitable for operation over the entire range; from lower explosive limit (LEL) to upper explosive limit (UEL).

Scope of Further Research

(i) In future, the effect of swift heavy ion irradiation and gamma irradiation on metal oxide semiconductor and related effect on their sensitivities and sensor responses as gas sensor with exposure of harmful gases in environment may be investigated.

(ii) Detailed analysis of the evolution of the surface reactions with respect to temperature in order to get precise understanding of the reaction products may be carried out.

(iii) An effort may also be made to integrate the reduced graphene oxide (rGO) doped nanostructured ZnO and SnO_2 by CVD or chemical route for LPG sensing application.

(iv) Theoretical modeling on sensing mechanism of LPG and other oxidizing gases with the metal oxides may be undertaken for further investigations.

(v) The presence of crystallographic defects affects the sensing mechanism of gas sensor. A quantitative study that associates the presence of these defects with the density of states in the energy gap followed by the variations in the sensitivity of the sensor is to be done.

References:

[1] X.S. Niu, W.P. Du and W.M. Du, Preparation and gas sensing properties of ZnM_2O_4 (M = Fe, Co, Cr), Sens. Actuators B 99 (2004) 405-415.

[2] K.V. Gurav, U.M. Patil, S.W. Shin, S.M. Pawar, J.H. Kim, C.D. Lokhande, Morphology evolution of ZnO thin films from aqueous solutions and their application to liquefied petroleum gas (LPG) sensor, J. Alloys Compounds 525 (2012) 1-7.

[3] O.K. Tan, W. Cao, Y. Hu and W. Zhu, Nanostructured oxides by high-energy ball milling technique: application as gas sensing materials, Solid State Ionics 172 (2004) 309-331.

[4] Y.L. Liu, Z.M. Liu, Y. Yang, H.F. Yang, G.L. Shen and R.Q. Yu, Simple synthesis of $MgFe_2O_4$ nanoparticles as gas sensing materials, Sens. Actuators B 107 (2005) 600-604.

[5] R. Srivastava, B.C. Yadav, Ferrite Materials: Introduction, Synthesis Techniques, and Applications as Sensors, International Journal of Green Nanotechnology: Physics & Chemistry, Special Issue: New Advances in Phytochemicals-Mediated Green Nontechnology: Part I, 4 (2) (2012) 1-14.

[6] B.C. Yadav, Nanotechnology: An introduction and its application, Lucknow Journal of Science 4 (2) (2007) 1-10.

[7] K.K. Dey, D. Bhatnagar, A.K. Srivastava, M. Wan, S. Singh, R.R. Yadav, B.C. Yadav and M. Deepa, VO_2 nanorods for efficient performance in thermal fluids and sensors, Nanoscale, Royal Society of America, 7 (2015) 6159-6172.

[8] C. Xiabo, S.S. Mao, Titanium Dioxide Nanomaterials: Synthesis, Properties, Modifications, and Applications, Chem. Rev. 107 (2007) 2891-2906.

[9] A. Fujishima, K. Honda, Electrochemical photolysis of water at a semiconductor electrode, Nature, 238 (1972) 37-38.

[10] U. Diebold, The surface science of titanium dioxide, Surf. Sci. Rep., 28 (2003) 53-229.

[11] O. Carp, C.L. Huisman, A. Eller, Photoinduced reactivity of titanium dioxide., Solid State Chem., 32 (2004) 33-177.

[12] A.K. Jha, K. Prasad, Ferroelectric $BaTiO_3$ nanoparticles: biosynthesis and characterization, Colloids Surf., 5 (2010) 330-334.

[13] C.H. Kwon, H. Shin, J.H. Kim, W.S. Choi, K.H. Yoon, Degradation of methylene blue via photocatalysis of titanium dioxide, Mat. Chem. Phys. 86 (2004) 78-82.

[14] L.R. Skubal, N.M. Meshkov, M.C. Vogt, Detection and identification of gaseous organics using a TiO_2 sensor, J. Photochem. Photobiol., 148 (2002) 103-108.

[15] K.R. Meier, M. Gratzel, Redox Targeting of Oligonucleotides Anchored to Nanocrystalline TiO_2 Films for DNA Detection, Chem. Phys. Chem., 3 (2002) 371-374.

PREFACE

Over the past two decades, a lot of research efforts have been made towards the development of gas sensing devices for practical applications ranging from toxic/inflammable gas detection to continuous environmental monitoring. Gas sensors play a pivotal role in domestic and industrial fields and also help to keep a cleaner environment by giving an early warning of leakage of toxic gases. Metal oxide semiconductors TiO_2 and PANI, Zn, Ag, doped TiO_2 are extensively utilised for the detection of various gases due to their high chemical stability. Thus in the present work, an effort has been made to develop an efficient sensor based on the TiO_2 thin film for detecting trace level of LPG and CO_2 gas with enhanced response. The TiO_2 and doped TiO_2 thin films are prepared by sol-gel or chemical route. Structural and optical properties of pure TiO_2 and Zn, PANI, Ag doped TiO_2 thin films were found to be highly dependent on the film thickness. LPG and CO_2 sensing properties of TiO_2 and PANI, Zn, Ag-doped TiO_2 nanocomposite thin films were studied.

The present thesis is divided into six chapters. Chapter 1 introduces the materials, methods, characterization tools and describes the object of the present investigation. Detailed investigation on nanostructured Titania thin film synthesis, characterization and application as LPG sensor is depicted in Chapter 2. Chapter 3 describes the fabrication of PANI doped Titanium oxide nanocomposites thin film, its application as CO_2 and LPG sensor at room temperature. In Chapter 4, the synthesis, characterization and LPG sensing properties of Zn doped Titanium oxide is reported. Chapter 5 describes the synthesis of Ag doped TiO_2 thin film using the chemical route and its application as LPG sensor at room temperature. A study of synthesis, characterization and LPG and CO_2 sensing properties of TiO_2 and PANI, Zn, Ag, doped TiO_2 is summarised in Chapter 6. This chapter also gives the guidelines for further research work in the field of nanostructured materials and their composites as a gas sensor.

LIST OF ABBREVIATIONS

S. No.	Name	Full Name
1.	TiO_2	Titanium Oxide
2.	ZnO	Zinc Oxide
3.	FTIR	Fourier Transform Infrared spectroscopy
4.	PANI	Polyaniline
5.	CO_2	Carbon Dioxide
6.	LPG	Liquefied Petroleum Gas
7.	CVD	Chemical Vapor Deposition
8.	XRD	X-ray diffraction
9.	SEM	Scanning Electron Microscopy
10.	UV-vis	Ultra Violet-Visible spectroscopy
11.	TEM	Transmission Electron Microscopy
12.	IDE	Inter Digital Electrode
13.	NPs	Nanoparticles
14.	IPA	Isopropyl alcohol
15.	COP	Conducting Organic Polymer
16.	MOS	Metal Oxide Semiconductor
17.	1-D, 1D	One Dimensional
18.	CSA	Camphor Sulphonic Acid
19	LEL	Lower explosive limit
20	RT	Room temperature
21	VLS	Vapor liquid solid
22	COP	Conducting Polymer

LIST OF TABLES

LIST OF FIGURES

LIST OF APPENDICES

TABLE OF CONTENTS

Chapter 1

Introduction and aim of present work

This chapter introduces the motivation of the thesis and pronounces the objective of the present investigations. It explains the types of gas sensors and requirement of LPG sensor along with experimental techniques. Synthesis techniques of nanostructured materials and their characterization methods have also been depicted. At the end, future research directions in this field have been mentioned.

1.1 Motivation

1.1.1 Sensors

A sensor is a tool which responses by a physical stimulus such as heat, light, sound, pressure, magnetism, or motion and chemical stimulus such as adsorption of gases or surface reactions. It accumulates and measures the data about something of an incidence, object or material. Chemical sensors are classified in a number of different ways. One of the classifications uses the operating principle of the receptor [1]. Sensors are normally designed to operate under well-defined conditions for specified analyte in certain sample types. Therefore, it is not always necessary that a sensor responds specifically to certain analyte. Under carefully controlled operating conditions, the analyte signal may be independent of other sample components, thus allowing the determination of the analyte without any major preliminary treatment of the sample. Otherwise unspecific but satisfactory reproducible sensors can be used in series for multicomponent analysis using multivariate calibration software and signal processing. Such systems for multicomponent analysis are called sensor arrays [2].

The development of instrumentation, microelectronics and computers makes it possible to design sensors utilizing most of the known chemical, physical and biological principles that have been used in chemistry [3]. Sensors may be classified according to the operating principle of the transducer [4].

Using this principle, one can distinguish between the following sensors:

(i) Physical sensors

(ii) Chemical sensors

(iii) Biochemical sensors

(iv) Chemical gas sensor

1.1.1.1 Physical sensors

A physical sensor is a device that provides information about a physical property of the system. In physical sensors, no chemical reaction takes place at the receptor, and the signal is a result of a physical process, such as mass, absorbance, refractive index, turbidity, depth/pressure, temperature conductivity change and groundwater flow.

1.1.1.2 Chemical sensors

A chemical sensor is a device that converts chemical information, alternating from the concentration of a precise sample module to total composition analysis, into an analytically useful signal. Chemical sensors are based on chemical reactions between analyte molecules and the receptor. A chemical sensor is an essential component of an analyser. In addition to the sensor, the analyser may contain devices that perform the following functions: sampling, sample transport, signal processing, data processing. An analyser may be an essential part of an automated system. The analyser working according to a sampling plan as a function of time acts as a monitor. Chemical sensors contain two basic functional units: a receptor part and a transducer part. Some sensors may include a separator which is, for example, a membrane. In the receptor part of a sensor the chemical information is transformed into a form of energy which may be measured by the transducer. The transducer part is a device capable of altering the energy carrying the chemical information from the sample into a useful analytical signal. The receptor part of chemical sensors may be based upon various principles: physical, where no chemical reaction takes place. Some cases are those based upon measurement of absorbance, refractive index, conductivity, temperature or mass variation. Chemical, in which a chemical reaction with participation of the analyte gives rise to the analytical signal [5].

1.1.1.3 Biochemical sensors

In biochemical sensor, a biochemical procedure is the source of the analytical signal. Examples are microbial potentiometric sensors or immuno-sensors. It may be regarded as a subgroup of the chemical ones. Such sensors are called biosensors. The biosensors are not presented as a special class because the process on which they are based is, in general, common to chemical sensors. They may be also differentiated according to the biological elements used in the receptor. Those may be organisms, tissues, cells, organelles, membranes, enzymes, antibodies, etc. The biosensors may have several enzymatic systems coupled which serve for amplification of the signal [6-8].

1.1.1.4 Chemical gas sensors

A gas sensor is a device that yields an electrical signal on chemically interacting with the vapours or gas. Gas sensor has originated broad applications in both the home and industries. Even with its value, many challenges exist in manufacturing a reliable sensor earlier it can be working with assurance. Also, the sensor should only produce an electrical response when exposed to the gas of interest. Sensors should also have stable, reproducible electrical signals to reduce the amount of time needed for calibration. Other applied concerns exist, such as reducing size, weight, and power consumption, as well as the ability to place the sensor close to where the measurements essential to be made.

According to the definition of a gas sensor, given by the International Union of Pure and Applied Chemistry (IUPAC), “A chemical sensor is a device that transforms chemical information, ranging from the concentration of a specific sample component to total composition analysis, into an analytically useful signal”. The diagram of LPG sensor is shown in Figure 1.1. The chemical information mentioned above may originate from a chemical reaction of the analyte or from a physical property of the system investigated [9]. Normally, chemical sensors have two main parts, a receptor, and a transducer. The

sensors are an essential part of any measurement and automation applications. The sensor is responsible for converting some type of physical phenomenon into a quantity measurable by a data acquisition (DAQ) system. The receptor transforms chemical information into a form of energy, which can be measured by the transducer. The transducer converts this energy into a useful, typically electrical and analytical signal.

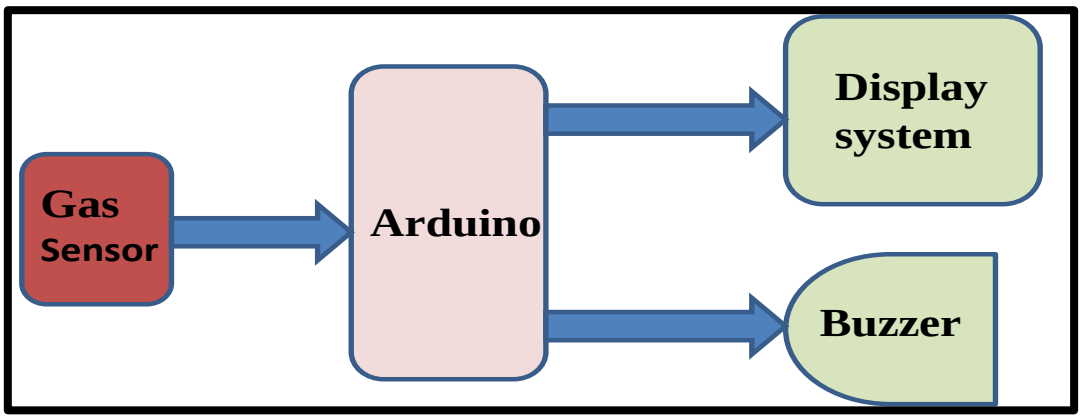

Figure 1.1: Schematic diagram of gas sensor

Sensors have also been classified according to the application to detect or determine a given analyte. Examples are sensors for pH, for metal ions or for determining oxygen or other gases. Another basis for the classification of chemical sensors may be according to the mode of application, for example, sensors intended for use in vivo, or sensors for process monitoring and so on. It is, of course, possible to use various classifications as long as they are based on clearly defined and logically arranged principles. Chemical sensors may be classified according to the operating principle of the transducer [10-12]:

(1) Optical devices transform variations of optical phenomena, which are the result of an interaction of the analyte with the receptor part. This group may be further sub-divided according to the type of optical properties which have been applied in chemical sensors:

(i) Absorbance, measured in a transparent medium, caused by the absorptivity of the analyte itself or by a reaction with some suitable indicator.

(ii) Reflectance is measured in non-transparent media, usually using an immobilized indicator.

(iii) Luminescence, based on the measurement of the intensity of light emitted by a chemical reaction in the receptor system.

(iv) Fluorescence, measured as the positive emission effect caused by irradiation. Also, selective quenching of fluorescence may be the basis of such devices.

(v) Refractive index, measured as the result of a change in solution composition. This may include also a surface plasmon resonance (SPR) effect.

(vi) Opto-thermal effect based on the measurement of the thermal effect caused by light absorption.

(vii) Light scattering, based on effects caused by particles of definite size present in the sample. It should be emphasized that fibre optics now commonly used are only technical devices applicable in a large group of optical sensors which can be based on various principles.

(2) Electrochemical devices transform the effect of the electrochemical interaction of analyte electrode into a useful signal. Such effects may be stimulated electrically or may result in a spontaneous interaction at the zero-current condition. The following sub-groups may be distinguished:

(i) Volta-metric sensors, including amperometric devices, in which current is measured in the D.C. or A.C. mode. This sub-group may include sensors based on chemically inert electrodes, chemically active electrodes and modified electrodes. This group includes sensors with and without (galvanic sensors) external current source.

(ii) Potentiometric sensors, in which the potential of the indicator electrode (ion-selective electrode, redox electrode, meta1 oxide electrode) is measured against a reference electrode.

(iii) Chemically sensitized field effect transistor in which the effect of the interaction between the analyte and the active coating is transformed into a change of the source-drain current. The interactions between the analyte and the coating are, from the chemical point of view, similar to those found in potentiometric ion-selective sensors.

(iv) Potentiometric solid electrolyte gas sensors work in high temperature solid electrolytes and are usually applied for gas sensing measurements.

(3) Electrical devices are based on measurements, where no electrochemical processes take place, but the signal arises from the change of electrical properties caused by the interaction of the analyte [13-15].

(i) Metal oxide semiconductor sensors are based on reversible redox processes of analyte gas components.

(ii) Organic semiconductor sensors, based on the formation of charge transfer complexes, modify the charge carrier density.

(iii) Electrolytic conductivity sensors.

(iv) Electric permittivity sensors.

(4) Mass sensitive devices transform the mass change at a specially modified surface into a change of a property of the support material. The mass change is caused by accumulation of the analyte.

(i) Piezoelectric devices used mainly in gaseous phase, but also in solutions, are based on the measurement of the frequency change of the quartz oscillator plate caused by adsorption of a mass of the analyte at the oscillator.

(ii) Surface acoustic wave devices depend on the modification of the propagation velocity of a generated acoustical wave affected by the deposition of a definite mass of the analyte.

(5) Magnetic devices are based on the change of paramagnetic properties of a gas being analysed. These are represented by certain types of oxygen monitors.

(6) Thermometric devices are based on the measurement of the heat effects of a specific chemical reaction on adsorption of the analyte. In this group the heat effects may be measured in various ways, for example in the so called catalytic sensors, the heat of a combustion reaction or an enzymatic reaction is measured by use of a thermistor. The devices based on measuring opto-thermal effects can alternatively be included in this group.

(8) Other physical properties as for example, α, β and γ radiation may form the basis for a chemical sensor, in case they are used for determination of chemical composition. This classification represents one of the possible alternatives. Sensors have, for example, been classified not according to the primary effect but to the method used for measuring the effect. As an example can be given to the so-called catalytic devices in which the heat effect evolved in the primary process is measured by the change in the conductivity of a thermistor. Also, the electrical devices are often put into one category together with the electrochemical devices.

1.2 Harmful Gases

Air pollution is one of the major consequences which continuously cause increasing threats to living being and vegetation. Air pollution may be defined as any atmospheric condition in which certain substances are present in such concentrations that may produce undesirable effects on human being and ecosystem. These substances include gases (sulphur dioxide, carbon dioxide, nitrogen oxides, carbon monoxide, LPG, etc.), particulate matters (smoke, dust, fumes, aerosols, etc.), radioactive materials and many others. It contributes to the formation of photochemical smog, which can have significant impacts on human health [16]. Gas sensors play a pivotal role in domestic and

industrial fields and also help to keep a cleaner environment by giving an early warning of leakage of toxic gases.

1.2.1 Liquefied Petroleum Gas

Liquefied petroleum gas (LPG) is commonly used in homes for central heating, hot-water, gas-fires, cooking, and in mobile heaters for leisure activities such as boats. This energy source is primarily composed of propane and butane which are highly flammable chemical compounds. Chemical formula of LPG is $C_nH_{2n+2}O$ where, n=1, 2, 3 etc.

1.2.1.1 Properties of LPG

The LPG consists of isobutane, propane, methane, etc. Butane includes temperately less than 70 % of the gas. Propane includes approximately 29 % of the gas, leaving just above 1% for the trace component [17]. Its biggest advantage is a lower boiling temperature, at -42.1 °C vs -0.5 °C for butane [18]. So, propane will continue to vaporize turn to gas even in colder climates. Conversely, butane vapor pressure is about one fourth that of propane, which is advantageous for some propellant applications. Propane energy content is slightly higher by weight but lower by volume. Butane (n-butane) is a flammable hydrocarbon gas liquefied through pressurization. Butane comes from natural gas process and oil refinery. It is used for heating, cooking and fuel. Isobutane is normally used in refrigerant/propellant. Propane is an inflammable hydrocarbon gas liquefied through pressurization.

In 1910 LPG [17], was first manufactured by Dr. Walter Snelling the U.S Bureau of mines investigated gasoline to see why it is evaporated so fast and discovered that the evaporating gases were propane, butane and other light hydrocarbons. Both LPG and natural gases are environmentally friendly and easily detected. These are normally stored in pressurised steel cylinders in liquid form and vaporise at normal temperatures. The

LPG is heavier in comparison of air. So, it flows along the floor and also settles in low points which make it difficult to disperse. The LPG is finding wide usage in homes, industries and in automobiles as fuel because of its desirable properties which include high calorific value produces less soot, produces so less smoke. Similarly, natural gas is another widely used fuel in homes. The gases are heavier than air not disperse easily and may lead to suffocation when gulped. There is a necessity of a system to detect and also prevent leakage of LPG. Gas leakages causing into fatal has become a serious problem for the household and other areas where household gas is handled and used. The property of LPG is depicted in Table 1.1. The explosion happens when the following three conditions are fulfilled [17].

(i) The concentration of gas is between LEL and UEL.

(ii) A sufficient amount of Oxygen exists.

(iii) There is a source of ignition

Table 1.1 Properties of LPG [17]

Gas Formula	**Vol.% LEL**	**Vol.% UEL**	**Ignition Temp. (°C)**	**Flash point (°C)**	**Liquid boiling point (b.p.)**	**Vapour /Gas (b.p.)**
C_3H_8	2.2	9.5	470	97	<-42°C	≥-42°C
C_4H_{10}	1.8	8.4	365	152	<-0.4°C	≥-0.4°C

1.2.2 Nitrogen based Oxide (NO_x)

Nitrogen oxides (NO_x), a mixture of nitric oxide (NO) and nitrogen dioxide (NO_2), are produced from natural sources, motor vehicles and other fuel combustion processes. Nitrogen dioxide (NO_2) is an intermediate product in the industrial synthesis of nitric acid, millions of tons which are produced every year [19]. Nitrogen dioxide is harmful to vegetation, can fade and discolor fabrics, reduce the visibility, and react with

the surfaces and furnishings. Vegetation exposure to high levels of nitrogen dioxide can be identified by damage to greenery, decreased growth or reduced crop yield. This reddish-brown toxic gas has a characteristic sharp and pungent odour. NO_2 is the main air pollutant in the combustion exhaust gases of automobiles, industrial, combustion of fossil fuels or domestic heater/burners. As a matter of fact, NO_2 associated with other pollutants like volatile organic compounds (VOCs) are responsible for the formation of ozone in lower atmosphere (troposphere) when interacts directly with sun rays and smog in urban areas. Ground level ozone is severe irritant, responsible for the choking, coughing and burning eyes. Chemical reaction of NO_2 gas with water vapour in atmosphere causes acid rain. Also it acts as a precursor to nitrates, which contribute to increase the irrespirable particle levels in the environment. Constantly increasing level of NO_2 gas is harmful to living beings as it is irritating to the upper respiratory tract and lungs even at low concentrations. Immediately dangerous to life or health Concentrations (IDLHs) of NO_2 gas has been declared to be 20 ppm by Occupational Safety and Health Administration, USA [20]. Thus it is very important to measure and control the increasing level of NO_2 gas using efficient sensors.

1.2.3 Carbon based Oxide (CO_x)

Carbon based oxides (CO_x) are carbon monoxide (CO) and carbon dioxide (CO_2). They are produced from ignition of some sources e.g. wood, coal, plastics and some waste substances, motor vehicles and other fuel combustion processes. CO_2 is the main greenhouse gas which causes global climatic changes on the larger scale. Recently, detection of greenhouse gases has become essential to control the damage causing to the environment and quality of life. Global warming is a major concern of researchers because of the massive emissions of CO_2. Hence, the detection and control of CO_2 concentrations in the environment are necessary. CO_2 is a chemically stable gas, therefore

its detection with the resistive methods is more difficult than that of other reducing gases [21]. The demand for a convenient and low-cost sensor for continuously monitoring gaseous emissions from various processes is steeply growing. CO_2 is the oxidising gas. Carbon monoxide (CO) gas has no color, odor and taste, which is less dense than air. It is toxic to animals and human beings when come in concentrations above about 35 ppm, it is also produced in normal animal metabolism in low quantities. [22]. In the presence of oxygen, including atmospheric concentrations, carbon monoxide burns with a blue flame, producing carbon dioxide [23].

1.2.4 Sulphur dioxide (SO_2)

Sulphur dioxide (SO_2) is complex of sulphur and oxygen molecules. It is colourless gas with an undurable bitter odour and simply soluble in water to form sulphuric acid. It is comparatively dense around 2.5 times heavier than air. Sulphur dioxide (SO_2) can trouble eyes and the breathing system (lungs) [24]. The emission sources of SO_2 is natural gas plants, oil sands, cement plants, petroleum refineries, pulp, ships and off-road diesel vehicles [25].

1.2.5 Other Gases

Other harmful gases are alcohol, ammonia, methane, chlorofluorocarbons (CFCs), and hydrofluorocarbons (HFCs). Chlorofluorocarbons (CFCs) are injurious to the ozone layer. These gases are released from air conditioners, refrigerators and aerosol sprays. On release in air, CFCs increase in the stratosphere come in contact to other gases and destroy the ozone layer. This allows dangerous ultraviolet rays to spread on the earth's surface. This causes skin cancer, eye disease and also damage to plants. Ammonia (NH_3) gas, with a characteristic bitter odour, is released from various agricultural processes and byproducts of different explosives. Ammonia contributes significantly to the nutritional needs of terrestrial organisms by serving as a precursor to foodstuffs and fertilizers. In

wide use, ammonia is corrosive and harmful. In the atmosphere, ammonia reacts with oxides of nitrogen and sulphur to form another compounds [26].

1.3 Requirement of gas sensor

Gas sensors have much importance in the field of industry and other areas. Although many difficulties are present in addressing these issues, gas sensors still have several specific roles in the world. For example, hydrogen sensors are needed in the rocket propulsion industry because hydrogen propellant leaks pose significant safety risks. In addition, the automotive industry routinely monitors the air to fuel ratio in vehicles with oxygen sensors that utilise an electrochemical cell containing ZrO_2 which conducts oxygen ions at high temperature. The automotive industry also has an interest in NO_x sensors because nitrogen oxide forms it when fuel burns at high temperatures. Nitrogen oxide is a unique danger because it can travel great distances from its emission source and result in ozone, smog, and particulate matter far from the actual source of pollution. For designing a robust gas sensor, the sensor material should possess following qualities given as under:

(i) The material should be sensitive in the lower explosive limit (LEL) for explosive gases.

(ii) The material should have high sensitivity over a wide range of gas and temperature.

(iii) It should quickly respond to any fast changes in the ambient.

(iv) The sensor material should have a rapid response to the variation of gas concentration and good reproducibility of the electrical signal.

(v) The sensitivity should be independent of the ambient temperature.

(vi) The material should not react with any chemical contaminants present in the application ambient.

(vii) It should show stable characteristics for a long time.

(viii) The construction of the sensor should preferably be simple using IC technology and of low cost.

(ix) The device should be portable and operated by a battery.

1.4 Liquefied Petroleum Gas Sensor

Coal gas and liquefied petroleum gas (LPG) are the combustible gases. They are potentially hazardous because explosion accidents might be caused when they leak accidently or by mistake. So its detection in domestic appliances is very important for safety [27]. The system has two main devices, the gas detector and the centralised alarm unit (Buzzer).

There can be more than one detector in the systems, which can be separately identified in the system. The centralised alarm unit detects the alerts sent by the detectors and releases the alarm. It has an indication of which detector has released the alert. The components of the device have been chosen considering the power consumption and the time intervals have been calculated concerning the current consumption of each component. Liquefied petroleum gas is a flammable mixture of hydrocarbon gases used as a fuel in heating appliances and vehicles. Varieties of LPG bought and sold include mixtures that are primarily propane (C_3H_8), primarily butane (C_4H_{10}) and includes both propane and butane depending on the application [27].

Unlike natural gas, the LPG is heavier than air and thus will flow along floors & tend to settle in lower spots, such as basements. There are two following main dangers from this [27].

(i) Explosion may occur if a certain mixture of LPG and air works as an ignition source.

(ii) Suffocation due to LPG displacing air and causing a decrease in oxygen concentration.

1.4.1 LPG Sensor: Working Principle

The gas sensing mechanism of TiO_2 thin film based sensor belongs to a surface controlled type, i.e. resistance change is controlled by surface area and the amount of chemisorbed oxygen. LPG consists of CH_4, C_3H_8, and some other hydrocarbons. In each composition, the reducing hydrogen species are bound to carbon atom therefore, LPG dissociates into the reactive reducing components hardly on the surface of the sensing element. As LPG is exposed to sensing element, the conductivity increases due to adsorption of oxide and capture more electrons that contribute to reducing the current. It was observed that as the concentration of LPG increases, the average sensitivity increases linearly in the beginning and later, it becomes saturated. The linear relationship between sensitivity and gas concentration may be attributed to the availability of a sufficient number of sensing sites on the film to act upon the LPG. The low concentration implies a lower surface coverage of gas molecules, resulting in a lower surface reaction between the surface adsorbed oxygen species and the gas molecules. The increase in LPG concentration increases the surface reaction due to a large surface coverage. Further, increase in the LPG concentration does not increase the surface reaction and eventually, saturation takes place. Thus, the maximum sensitivity was obtained at higher concentration of LPG for safety requirement.

The equilibrium of the chemisorption process results in stabilization of surface resistance (R_a). When the sensor is exposed to the atmosphere containing inflammable gases such as LPG at elevated temperature, the O^- adsorbate reacts with the inflammable gas and releases the electrons to the conduction band. The oxygen adsorbed on the surface of the film influences the resistance of the TiO_2 based sensor. Initially, oxygen from the atmosphere adsorbs on the surface of the film and extracts electrons from its conduction bands to form O_2^- species on the surface, consequently resistance increases.

After that an equilibrium state is achieved between the oxygen of TiO_2 and atmospheric oxygen.

$O_2\,(gas) \leftrightarrow O_2\,(ads)$ (Thin Film Surface) (1)

$O_2\,(gas) + e^- \leftrightarrow O_2^-$ (Thin Film Surface) (2)

When the thin film is exposing to LPG, it reacts with the chemisorbed oxygen. On interaction with hydrocarbons of LPG, the adsorbed oxygen is removed, forming gaseous species and water vapour. Consequently, the resistance changes, which is due to the change in the width of depletion layer after exposure to LPG. The overall reaction of LPG with the chemisorbed oxygen may take place as shown below:

$C_4H_{10} + 13O^- \rightarrow 4CO_2 + 5H_2O + 13e^-$ (3)

$C_4H_{10} + \frac{13}{2}O_2^- \rightarrow 4CO_2 + 5H_2O + \frac{13}{2}e^-$ (4)

$C_4H_{10} + 13O^{2-} \rightarrow 4CO_2 + 5H_2O + 26e^-$ (5)

$C_3H_8 + 10O^- \rightarrow 3CO_2 + 4H_2O + 10e^-$ (6)

$C_3H_8 + 5O_2^- \rightarrow 3CO_2 + 4H_2O + 10e^-$ (7)

$C_3H_8 + 10O^{2-} \rightarrow 3CO_2 + 4H_2O + 20e^-$ (8)

1.5 Metal Oxide Semiconductor (MOS) Based Gas Sensor

Metal oxide semiconductor (MOS) is one of the most important materials that could be applied for gas sensing measurements. Solid-state sensors, typically based on a titanium dioxide semiconductor, respond to gases by changing resistance. The quality of sensors reportedly varies widely from manufacturer to manufacturer with substantial variations in performance often found from a single manufacturer.

MOS sensors are constructed by applying a semiconducting material to a non-conducting substrate between two electrodes. The substrate is heated to a temperature

such that the target gas being monitored can cause a reversible change in the conductivity of the semiconducting material. When the target gas is not present, oxygen atoms or other electron acceptors adsorb on the surface of the semiconductor material and trap free electrons from the conduction band of the semiconductor. This process inhibits electrical flow (i.e. increased resistance). As the target gas is introduced, they react with the adsorbed oxygen atom, which releases the trapped electrons to the material thereby decreasing resistance. This change in resistance is measured electrically and is proportional to the concentration of the gas being measured. To achieve some specificity, the sensors can be impregnated with dopants or the working temperature can be changed so that the sensor's resistance changes when specific gases react with the adsorbed oxygen.

MOS sensors have a relatively long operating life (3-5 years). They have a high sensitivity to most combustible gases (i.e. saturated hydrocarbons), LPG and CO_2. MOS sensors have a fast response time, good reliability, good resistance to corrosive gases and humidity, high mechanical strength and low production cost.

However, MOS sensors have low selectivity and background gases can create inaccurate readings. This problem may be improved somewhat by dopants and temperature adjustment during the measurement. They also show the poor distinction between different polar compounds. Due to the high temperature operation, they consume more power than other similar sensors and the sensor's nonlinear output signal makes calibration more complicated.

1.6 Conducting Organic Polymers (COP) Based Sensors

Sensors based on changes in resistivity of polymer films to gas exposure have been studied extensively [28-29]. The most studied polymers are polypyrrole and

polyaniline. In general, all suitable polymers have a conjugated π–electron system along the polymer backbone. The choice of the polymer is limited to conducting polymers or those which can be made to conduct [30]. Polymers are made conductive by doping them with counter ions from an electrolyte solution by reducing or oxidising the polymer [31]. Figure 1.2 shows the polymerization of conducting polymer. The polymers are formally described as semiconductors because they have a band gap in their electronic structure at room temperature. Conducting polymers are fabricated by depositing a thin polymer film on a sensor structure consisting of a narrow gap. They are sensitive to polar compounds and the bulk absorption is normally reversible.

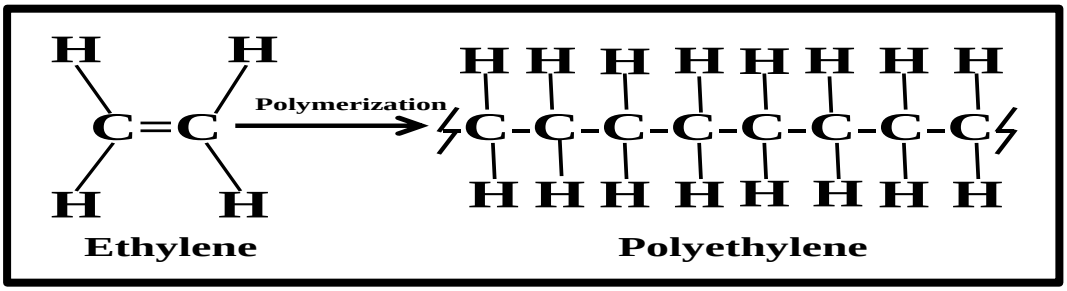

Figure 1.2: Conducting Polymer

The conductivity of the polymer is measured at a constant current or voltage over a resistor. As the target gases are absorbed into the polymer matrix, their interaction with the matrix causes a change in the conductivity of the polymer. Unfortunately, the response of the sensor is not necessarily a linear function of the target gas concentration. Therefore, quantification is difficult.

The sensitivity and selectivity of a conducting polymer array can be altered extensively by manipulating the chemistry of the polymer backbone, changing the selection of doping ions, varying the polymer chain length, and changing the method of polymerization. COP sensors can be used at ambient temperature unlike many of the gas monitoring sensors. However, they are also sensitive to temperature changes. Their primary advantages are high sensitivity and small size. Their primary disadvantage is

poor reproducibility of fabrication, which is dependent on polymer coating of the substrate. Water vapour is a strong interfering agent and the baseline may drift over time as a result of confirmation changes within the polymer after exposure to inappropriate compounds.

1.7 Sensor Parameters/Attributes

For optimising and standardising the performance of any device, it is necessary to define a set of operating parameters. Hence this section will be devoted to defining and understanding the basic operating parameters of a sensing device, namely: sensor response, sensitivity, selectivity, stability, response and recovery times, reproducibility and long-term stability.

1.7.1 Sensitivity

Sensitivity very roughly can be defined as the magnitude of response of a sensor to a particular target analyte. Mathematically, several definitions exist, and the usage primarily depends on the application.

1.7.2 Response and Recovery Times

Response time is defined as the time taken by the sensor to reach 90% of the final response value and recovery time is defined the time taken by the sensor to come to 10% value of the original baseline.

1.7.3 Reproducibility and Long Term Stability

Sensor stability refers to the long-term operation of a sensor without any change in the above operating parameters. Gradual changes in the properties of the sensing matrix that commonly accompany the prolonged usage of a sensor in changing gas environments at elevated temperatures is referred to as ‘drift’ and it is desirable to minimise the drift as much as possible.

1.7.4 Selectivity

Selectivity may be defined as the sensor response to a particular gas in a mixture of interfering gases. This parameter defines the specific response of the sensor.

1.8 Nanostructured Material

Nanomaterials can be metals, ceramics, polymeric materials, or composite materials. Their significant characteristic is due to their very small feature size in the range of 1-100 nanometres. The unit of nanometer creates its prefix nano from a Greek word meaning ‘dwarf’ or ‘extremely small’. Nanomaterials are not simply another step in miniaturisation, but a different arena entirely, the nanoworld lays midway between the scale of atomic and quantum phenomena and the scale of bulk materials. At the nano level, some material properties are affected by the laws of Atomic Physics, rather than behaving as traditional bulk materials do. Applications of nanoscience in manufacturing materials for sensor may improve the working detection limit of gas sensors from lower temperatures. It will be reached mainly by modifications of the space charge layers for each grain and improving other electronic properties of the material. Particles that are smaller than the characteristic lengths related with the specific phenomena often display new chemistry and new physics that lead to new properties that depend on size. When size of the material decreases, surface to volume ratio increases significantly and the surface phenomena dominate over the chemistry and physics in the bulk material. For better sensing the reduction in the size gives better results to reduce the size of devices. The nanoscience of materials for new sensor devices offers more advantage for sensing phenomena. The response of sensor can increase by the better conduction properties; the limits of detection can be lowered and very small quantities of samples to be analysed [32-33].

Inorganic nanomaterials with controllable sizes and shapes show a wide range of exceptional chemical, electrical, surface, and optical properties. A wonderful interaction can be attained by participating nanosensors based on plasmonics, electronics, photonics and conventional sensors on the same chip. The nanosensor field needs the identification of various self-organized nanostructures with special structural characteristics and physical properties for devices with suitable circuit incorporation [34].

1.9 Titania Nanomaterials

Nanomaterials [35-37] play an imperative role in the recent development of science due to its small size and large surface area. In this chapter, several synthesis methods to prepare ceramic nanoparticles, characterization techniques and different properties of gas sensors are described.

Nanoparticle research presents wide scope for the development of novel solutions in the field of healthcare, cosmetics, optics and electronics altering their molecular and atomic states results with unexpected outcomes, which may not be possible by using the materials in their original states. This article deals with the properties and applications of titanium oxide nanoparticles. Titanium oxide (TiO_2) is available in the form of nanocrystals or nanodots having a high surface area. Titania is an inventive material used broadly in industry, research and environmental cleaning. Titania occurs in a number of crystalline forms; the most significant of which are anatase and rutile. Pure titanium dioxide does not occur in nature but is derived from ilmenite or leucoxene ores. It is also willingly mined in one of the purest forms, rutile beach sand. These ores are the major raw materials used in the production of titanium dioxide pigment. The first step is to purify the ore [38-42]. It is generally a refinement step. Either the sulphate process, which uses sulphuric acid as an elimination agent or the chloride process, which uses chlorine,

may achieve this. After purification, the powders may be treated (coated) to enhance their performance as pigments.

Titania has created strong grounds in today's industrial and engineering world. Titanium dioxide pigment is a fine white powder. When used in paints, plastics or paper, it provides for maximum whiteness and opacity. It gives paint of high power, meaning thereby ability to cover substrate. It does this more effectively than any other white pigment. The exceptional properties of TiO_2 are derived from the refractive index 2.3 at λ = 550 nm of titanium dioxide [43]. The refractive index expresses the capability to bend and scatter the light [44]. Titanium dioxide requires the highest refractive index of any material known to man, greater even than diamond [45]. To take advantage of this property, titanium dioxide must be excavated, refined and ground to a fine, uniform particle size. Titanium dioxide is one of the most preferential compounds from this class of semiconductors because it is non-toxic, cheap, highly photoactive and simply synthesised and handled.

Some metal oxides such as TiO_2 [46-49], SnO_2 [50-53] and ZnO [54-57] etc. are the semiconducting materials. The electrical properties of these oxides are sensitive to the oxygen partial pressure since it changes the concentration of electrons or holes in the oxides. Owing to the fact that the porosity within the oxides may alter their inside oxygen partial pressure, the porosity in a semiconducting oxide should affect its electrical properties. Therefore, there should be a relationship between the electrical properties and the microstructural features in a semiconducting oxide. TiO_2 has been widely investigated in linked to surface properties.

1.9.1 Lattice Structure of TiO_2

The bulk structure of titanium dioxide materials can exist in one of the three forms: rutile, anatase and brookite as shown in Figure 1.3. The basic structural

characteristics of both anatase and rutile materials have been reviewed as they are often used for experimental investigations. Both the rutile and anatase crystal structures are in the distorted octahedron. In rutile, the distortion is slightly orthorhombic where the unit cell is stretched beyond a cubic shape. In anatase, the distortion of the cubic lattice is more significant, and thus the resulting symmetry is less than orthorhombic. Figure 1.4 shows a structural lattice arrangement of the bulk rutile and anatase materials. The bond lengths and angles between atoms are depicted.

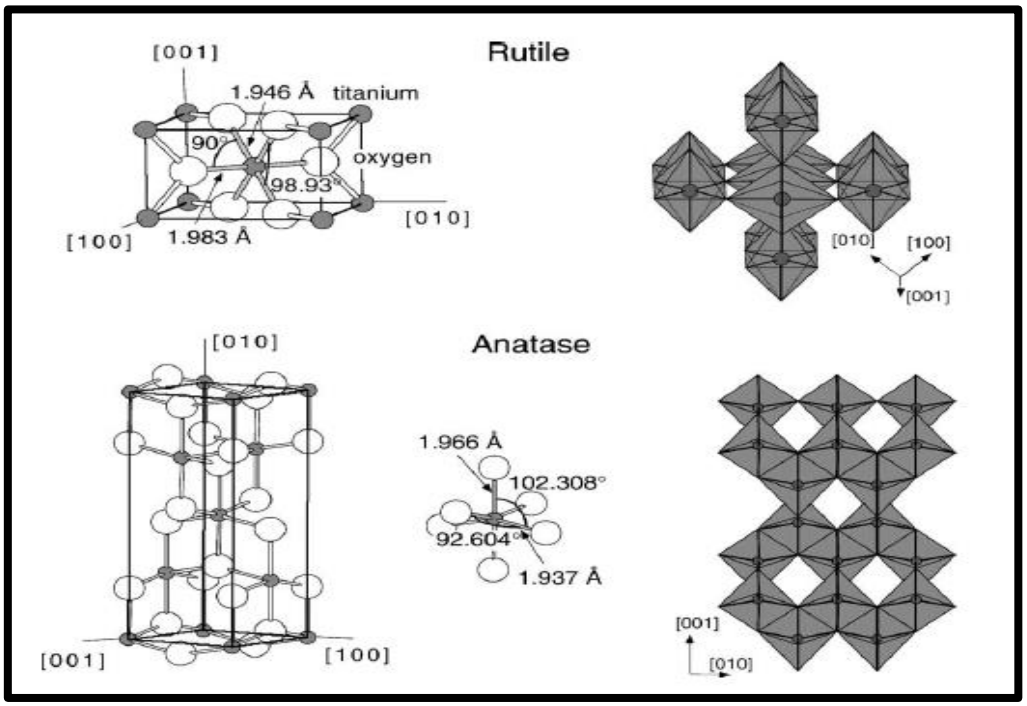

Figure 1.3: Bulk structure of rutile and anatase titanium dioxide showing the bond lengths and angles between atoms [58].

The crystal structure of TiO_2 nanoparticles depends largely on the preparation method. For TiO_2 nanoparticle (<50 nm), anatase seemed more stable and transformed to rutile at >973K. The transformation sequence and thermodynamic phase stability depend on the initial particle size of anatase. The only anatase to rutile phase transformation occurs in the temperature range of 973-1073K.

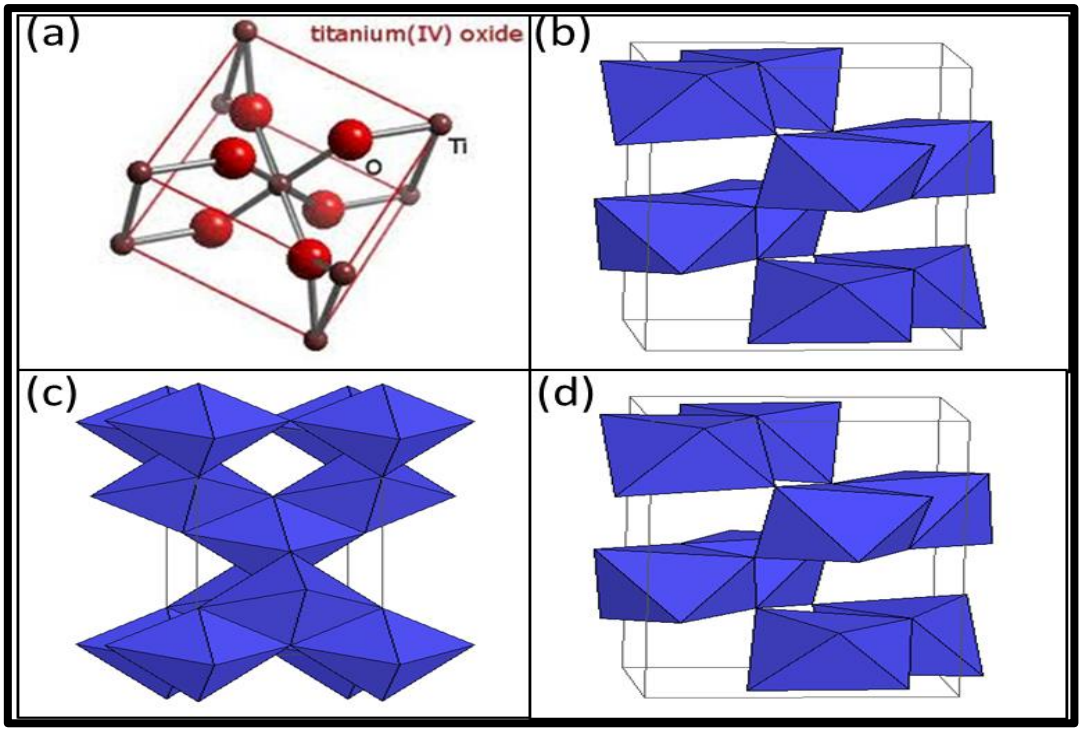

Figure 1.4: (a) Unit cell of the crystalline structure of TiO_2 and crystal structure of (b) Rutile (Tetragonal) TiO_2 (c) Anatase (Tetragonal) TiO_2 (d) brookite (Orthorhombic) TiO_2 [59]

Both anatase and rutile particles sizes increase with the increase in temperature, but with different growth rate. Rutile has a much higher growth rate than anatase. The growth rate of anatase levels off at 800 °C. Rutile particles, after nucleation, grew rapidly, whereas anatase particle size remains practically unchanged with the decrease of initial particle size, the onset transition temperature is decreased [59]. The decreased thermal stability in finer nanoparticles is primarily due to the reduced activation energy as a size related surface enthalpy and increased stress energy.

1.9.2 Properties of TiO_2

The chemical composition of Ti and O in TiO_2 is as given in Table 1.2, which shows the % of content of Ti and O in TiO_2 [60].

Table 1.2 Chemical composition of TiO_2

Chemical Composition	
Element	**Content (%)**
Titanium	59.93
Oxygen	40.55

1.9.3 Key Properties of TiO_2

Physical and mechanical properties of sintered titania are summarised in Table 1.3, while optical and structural properties of titania are provided in Table 1.4.

Table 1.3: Typical physical and mechanical properties of titania [60]

Density	4 g-cm^{-3}
Compressive Strength	680 MPa
Poisson's Ratio	0.27
Shear Modulus	90 GPa
Modulus of Elasticity	230 GPa
Resistivity (25 °C)	10^{12} ohm-cm
Resistivity (700 °C)	2.5 x 10^{4} ohm-cm
Dielectric Constant (1 MHz)	4
Thermal expansion (RT-1000 °C)	9 x 10^{-6}
Melting Point (°C)	1843 °C
Boiling Point (°C)	2972 °C

Table 1.4: The Optical and structural properties of Titania

Phase	**Refractive Index**	**Density ($g\text{-}cm^{-3}$)**	**Crystal Structure**
Anatase	2.49	3.84	Tetragonal
Rutile	2.903	4.26	Tetragonal
Brookite	2.507	4.123	Orthorhombic

1.9.4 Photocatalytic Properties

Titania is used as a photosensitizer for photovoltaic cells and when used as an electrode coating in photoelectrolysis cells, can recover the efficiency of an electrolytic splitting of water into hydrogen and oxygen.

In 1972, Fujishima and Honda [61] discovered the photocatalytic splitting of water on TiO_2 electrodes. This event clears the foundation of a new era in heterogeneous photo-catalysis. Titania is a favourable photocatalyst chemical. Two different crystal structures of TiO_2, rutile and anatase, are generally used in photo-catalysis activity. Photo-catalysis is a photon energy (from the UV in sunlight) used to the medium (catalyst) to support chemical reaction to continue. TiO_2 is a semiconductor in which, the valence band is occupied with electrons. Since the band gap of TiO_2 is 3.20 eV and can use only UV light below 400 nm, several efforts have been made to sensitise larger band gap semiconductors or to use narrow band gap semiconductors that can absorb visible light. Photon or UV light which is below the wavelength of violet (400 nm) has a high destructive energy. When the photon is familiarized to titania, it becomes unstable thus the electron escapes. This electron can break chemical bond since it has a high energy.

This reaction can be very useful to decompose organic material, impurities and bacteria in the air.

1.9.5 Applications

Applications of titania finds so many electrical uses in sensors and electro-catalysis. Some of them are discussed as follows:

1.9.5.1 Oxygen Sensor

Even in slightly reducing atmospheres titania tends to loose oxygen and becomes sub-stoichiometric. In this form, the material becomes a semiconductor and the electrical resistivity of the material can be interconnected to the oxygen content of the atmosphere to which it is exposed. Hence, titania can be used to sense the amount of oxygen (or reducing species) present in atmosphere [62].

1.9.5.2 Pigments

The most important function of titanium dioxide, however, is in powder form as a pigment for providing whiteness and opacity to some products such as paints and coatings (including glazes and enamels), plastics, paper, inks, fibres, food and cosmetics.

Titanium dioxide is mostly used as white pigment and has very high refractive index, more than diamond. The refractive index determines the opacity that the material confers to the matrix in which the pigment is housed. Hence, with its high refractive index, relatively low levels of titania pigment are required to succeed a white opaque coating.

The high refractive index and bright white colour of titanium dioxide make it an effective opacifier for pigments. The material is used as an opacifier in glass and porcelain enamels, cosmetics, sunscreens, paper and paints. One of the major advantages

of the material for wide-open applications is its resistance to discoloration under UV light.

1.9.5.3 Waste water remediation

TiO_2 can be used for waste water treatment and it has following properties:

(i) TiO_2 offers great importance in industries for detoxification or remediation of waste water due to several factors.

(ii) The process occurs under ambient conditions very slowly, direct UV light exposure increases the rate of reaction.

(iii) The development of photocyclized intermediate products, unlike direct photolysis techniques, is avoided.

(iv) Oxidation of the substrates to CO_2 is complete.

(v) The photocatalyst is inexpensive and has a high turnover.

(vi) TiO_2 can be supported on suitable reactor substrates.

1.9.5.4 Antimicrobial Coatings

The photocatalytic activity of titania results in thin coatings of the material exhibiting self-cleaning and disinfecting properties under exposure to UV radiation. These properties make the material application as medical devices, food preparation surfaces, air conditioning filters and sanitary ware surfaces.

1.10 Synthesis Methods of Nanomaterials

Synthesis methods play very important part of research to monitor the size and surface area of nanomaterials. Various synthesis methods are depicted in schematic shown by Figure 1.5.

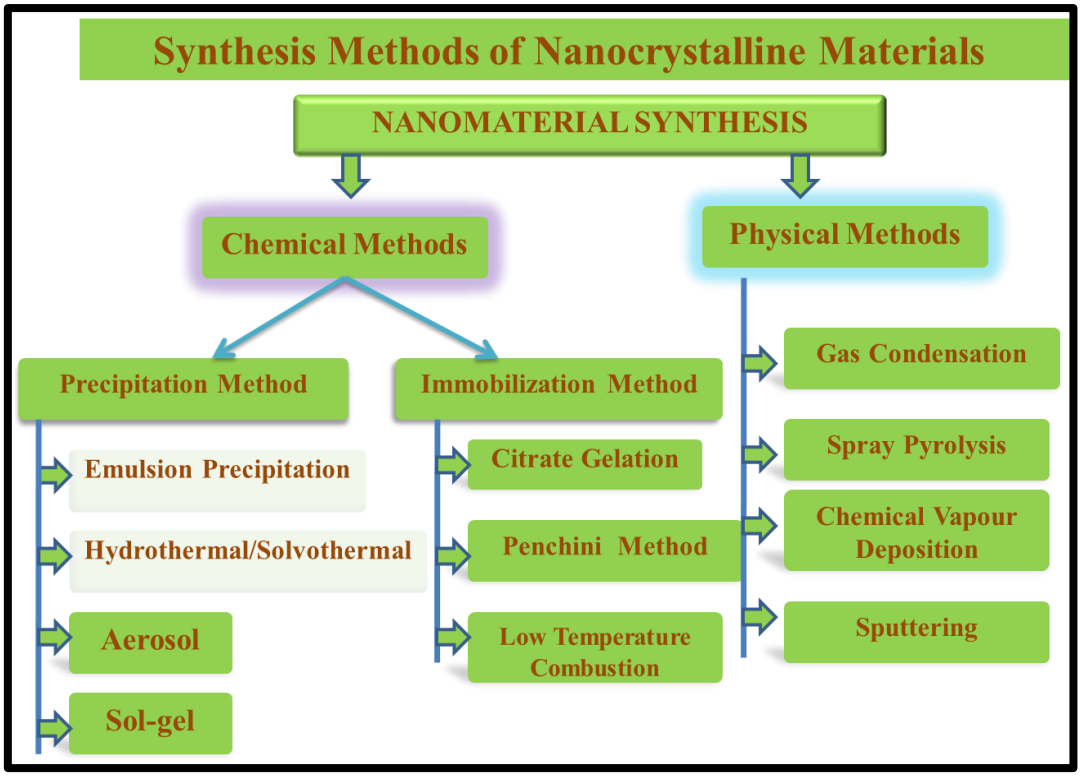

Figure 1.5: Synthesis method of nanocrystalline materials

There are numerous synthesis methods, some of them are described below:

(i) Hydrothermal Synthesis

(ii) Sol-gel Method

(iii) Aerosol Methods

(iv) Low-Temperature Combustion Methods

(v) Emulsion Precipitation method

1.10.1 Hydrothermal Synthesis

Hydrothermal synthesis is a process that employs single heterogeneous phase reactions in aqueous media at a higher temperature and pressure to crystallize and make hydrous ceramic materials directly from solutions [63]. This synthesis offers a low-temperature, direct route to oxide powder with a narrow size distribution avoiding the calcination step. The mechanism of hydrothermal reaction monitors a liquid nucleation model. Complete principles are consisting of theories of chemical equilibrium, chemical

kinetics and thermodynamic properties of the aqueous system under hydrothermal conditions.

This method has various steps as heating metal salts, oxides or hydroxides as a solution of suspension in liquid at controlled temperature and pressure for about 20 hours. The product is washed with de-ionized water to get rid of ions in the solvent and other impurities. After drying in air, fairly well dispersible ceramic nanoparticles are obtained.

The stability and particle size of the final product will depend on pH value, reagent concentrations, reaction temperature and time. Since the mechanism for hydrothermal reactions is different from each other, the corresponding process conditions would vary greatly. Moreover, the hydrothermal synthesis can be enhanced by hybridising it with microwaves, electrochemistry, ultrasound, mechanochemistry and optical radiation.

1.10.2 Sol-gel Method

This method offers specific advantages in preparations of multi-component oxide ceramics [64]. The early formation of a gel provides a high degree of homogeneity and reduces the need of atomic diffusion during the solid state calcinations [65]. Moreover, the processing often starts with metal alkoxides, many of which are liquids or volatile solids that can easily be purified, providing extremely pure oxide precursors. This factor is important for electroceramic synthesis. However, the relatively high cost of the metal alkoxides may be prohibitive for certain applications and the release of large amounts of alcohol during the calcination step requires special safety considerations. The schematic diagram of sol-gel synthesis process is given in Figure 1.6.

A solution of the appropriate precursors (metal salts of metal organic compounds) is formed first, followed by conversion into homogeneous oxide (gel) after hydrolysis and condensation. Drying and subsequent calcination of the gel yields an oxide product. Usually, for the preparation of multi-component oxides, alkoxides are mixed together in

alcohol. Components for which no alkoxides are available are introduced as salts, such as acetates. Hydrolysis is carried out under controlled temperature, pH and concentration of alkoxides, added water and alcohol.

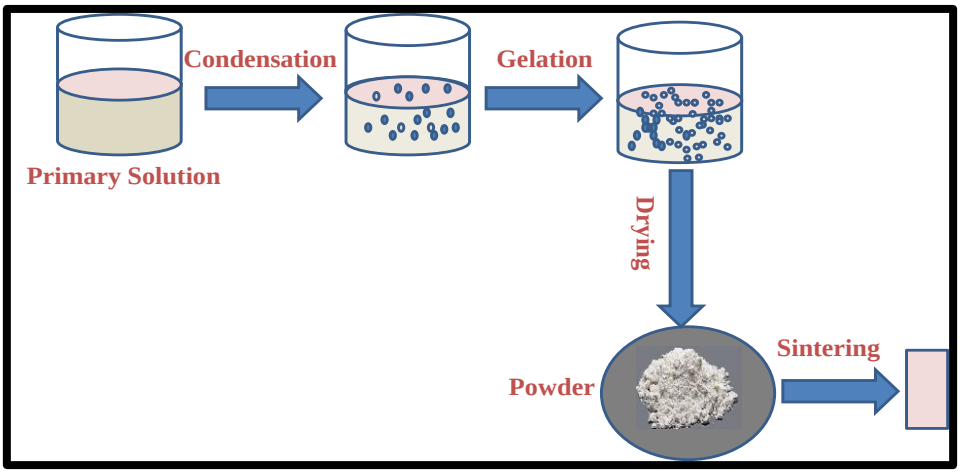

Figure 1.6: Sol-Gel method of synthesis.

1.10.3 Aerosol Method

This method is also defined as a gas phase method. It is thought to be convenient and cost-effective in the large-scale industrial production of multi-component materials [66]. The schematic of aerosol deposition apparatus is shown in Figure 1.7. Aerosols are suspensions of small solid or liquid particle in a gas. There are two routes for the preparation of ultra-fine particles by aerosol processes. The first involves generation of a supersaturated vapour from a reactant followed by homogeneous nucleation (gas-to-particle conversion). The second involves generation of liquid droplets, which undergoes heat treatment to solid particle (liquid-to-particle conversion). In Figure 1.6, the aerosol deposition equipment is composed of two chambers: the aerosol chamber and the deposition chamber. The fine ceramic powders are aerosolized by vibrating the aerosol chamber and pumping an inert gas (Ar) through the fine powder. The aerosol, which is hastened by the pressure difference between the two chambers, is transported through a

tube and is ejected into the deposition chamber through a rectangular-shaped jet. The deposition chamber is evacuated using a rotary pump [66].

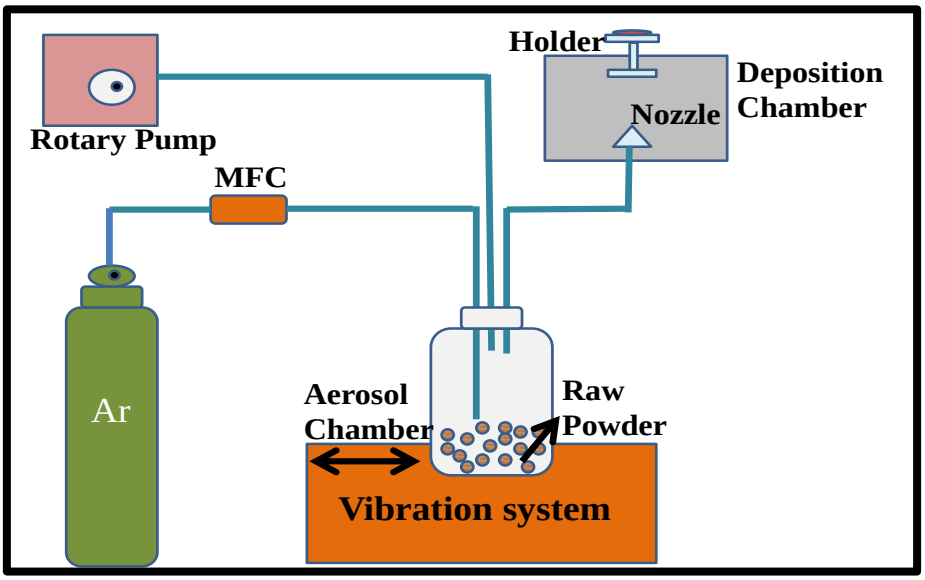

Figure 1.7: Schematic diagram of aerosol deposition apparatus [66].

Spray drying and spray pyrolysis are the most common methods for liquid-to-solid conversion. A metal precursor solution (sol) is made, followed by atomization into droplets, which led into a furnace. Evaporation of the solvent, drying, precipitation, gas phase reactions and pyrolysis occur inside the furnace to form the final product. Spray drying is similar to spray pyrolysis and it is carried out with colloidal dispersion particles. This method has the capability of producing uniformly spherical granules with typical sizes between submicron and millimeter. If the suspension consists of colloidal nanoparticles (primary particles), the resulting granules also comprise the nanoparticles to form nanostructure-granulated powders. Therefore, spray drying may be a suitable process for consolidating nanoparticle into submicron spherical granulates that can be compacted into microscopic shapes.

The ratio between reactants dissolved in the starting solution determines the composition of final particles. The average size and size distribution roughly depend on

the size of the atomised droplets and the precursor concentrations in the starting solution. Properties of precursors, carrier gas flow rate (i.e. residing time in the hot zone) and temperature will mainly affect the morphology of particles and their extent of agglomeration [67].

1.10.4 Low-Temperature Combustion Method

The low-temperature combustion synthesis (LCS) technique has proved to be a novel, extremely facile, time-saving and energy-efficient route for the synthesis of ultra-fine powders [68-70]. This is based on gelling and subsequent combustion of an aqueous solution containing salts of the desired metals and some organic fuels, giving a voluminous and fluffy product with large surface area. The experimental setup of combustion method is given in the Figure1.8. Oxidising metal salts such as metal nitrates, and a combination agent (fuel) such as citric acid, polycyclic acid or urea are used as starting materials. Citric acid is more extensively used since it not only functions as a reductant /fuel agent but also a chelating agent.

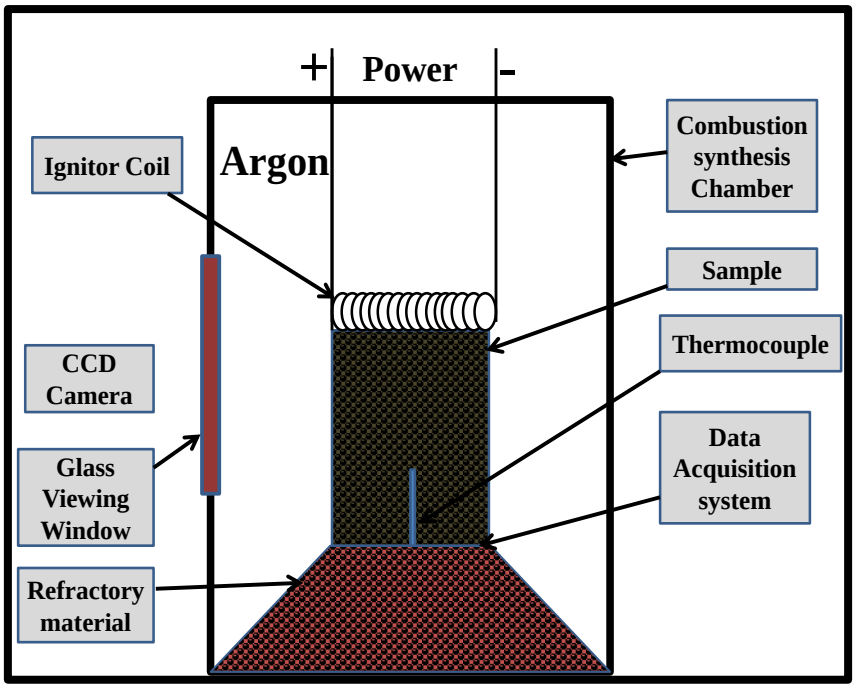

Figure 1.8: Experimental diagram of combustion synthesis setup.

In this thesis work, sol-gel method has been used for the preparation of nanostructured materials. The sol-gel method has received more advantages, however, the cost of precursor materials and metal alkoxides is higher than those of other methods and the right precursors are not always available. Hydrothermal synthesis involves the same principle of hydrolysis of solution species as in the sol-gel method, but without the calcination step. Emulsion precipitation methods are convenient for single component nanoscale ceramic particles, while they are less suitable for producing multi-component ceramics. This is caused by different hydrolysis rates of various precursors and the difficulty to remove surfactants, which are added to keep emulsions stable.

1.10.5 Emulsion Precipitation Method

This method involves the preparation of thermally stable emulsion systems prepared by adding appropriate amounts of surfactants to a water oil system. Within the emulsion system, there are a small number of atoms per droplet. It is necessary that exchange of reactive species take place between droplets in order to form a stable precipitate. From the Einstein-Smoluchowski equation, the normal rate of the particle growth is faster than the equivalent rate of exchange between droplets. Therefore, the nucleation and growth in emulsions are retarded in comparison to those in homogeneous solution, avoiding the formation of large particles. Multi surfactants are effective in forming thermally stable emulsion and controlling droplet size. Other additives play a role as steric particle stabilizer after removal of water. Before the particle dispersion by filtration of decantation of the organic phase, the emulsions are prepared by mixing the oil phase (Cyclohexane or n-heptane) with tergitol surfactants and octan-1-ol as co-surfactant. To the system stoichiometric amounts of water are added followed by vigorous mixing until a translucent emulsion is formed. The emulsion is added drop wise to alcohol solutions of alkoxides and stirred for several hours. After removal of solvents in dispersion the residue

is taken up in acetone to destroy the micelles. The solid product obtained after decantation of the organic phase is dried and transformed to nanocrystalline spinals after calcinations.

This method provides the particular advantage of avoiding agglomeration of the particles formed in the individual bubbles. This in turn makes possible subsequent processing routes at unusually low temperatures. To take full advantage of the method for multi component oxides precipitation routes need to be designed so that an intimate mixture of atoms is formed during precipitation and chemical homogeneity is maintained during subsequent processing. This offers special challenges since emulsion co-precipitations tend to be carried out with sample precursors that do not affect emulsion stability but generally show a tendency to precipitate at different rates leading to at least partial phase segregation.

1.11 Literature Survey

Metal oxides represent an assorted and appealing class of materials which properties covering the entire range from metals to semiconductors and insulators and almost all aspects of material science and physics in areas including superconductivity and magnetism. In the field of chemical sensing, for more than five decades it has been known that the electrical conductivity of semiconductors varies with the composition of the gas atmosphere surrounding them. Gas sensors have a great influence in many areas such as environmental monitoring, domestic safety, public security, automotive applications, and air conditioning in aeroplanes, spacecraft, houses, sensors networks. Due to this huge application range the need of cheap, small, low power consuming and reliable solid state gas sensors, has grown over the years and triggered a huge research worldwide to overcome metal oxide sensors drawbacks, summed up in improving the well-known “3S”: Sensitivity, Selectivity and Stability. In 1991 Yamazoe [71] showed

that reduction of crystallite size caused a huge improvement in sensor performance. In a low grain size metal oxide almost all the carriers are trapped in surface states and only a few thermal activated carriers are available for conduction. In this configuration, the transition from activating to strongly non-activate carrier density, produced by target gases species, has a great effect on sensor conductance. The challenge becomes to prepare materials with a small crystalline size which are stable when operated at high temperature for long periods. From the preparation side, first generation devices are prepared by thick film technology starting from powders. Since sensor performance depends on percolation path of electrons through intergranular regions, by varying small details in the preparation process, each sensor differed slightly in its initial characteristics. Therefore the materials fabrication processes have been improved towards thin film technology, a more automated production method that offers higher reproducibility and compatibility with Si technology, by physical and chemical vapour deposition. However, the technological improvement went along with a reduction of sensing performances due to a lower porosity of the prepared devices. Both thin and thick films electrical properties drift due to grain coalescence, porosity modification and grain-boundary alteration. These effects become more critical because the metal oxide layers must be kept at a relatively high temperature in order to guarantee the reversibility of chemical reactions at the surface. Thus, several solutions have been put forward to stabilise the nanostructure, e.g. addition of a foreign element [72]. An unexpected step forward has been the successful preparation of stable single crystal quasi-one-dimensional semiconducting oxides nanostructures (so called nano-belts, nano-wires or nano-ribbons) by simply evaporating the desired commercial metal oxide powders at high temperatures [71-72]. Their crystallinity assures improved stability and the nanosized lateral dimension the good sensing properties. Their peculiar characteristics and size effects make them interesting

both for fundamental studies and for potential nano-device applications, leading to the third generation of metal oxide gas sensors.

Metal oxide nanoparticles attract great attention in recent years on account of their special electronic and chemical properties. Among the metal oxide semiconductors, TiO_2 has been investigated extensively due to their chemical stability and efficient photo-catalytic properties. TiO_2 has achieved applications in various areas such as optical, piezoelectric, magnetic and gas sensing properties. The worldwide natural gas transport and distribution network is a complex and continuously expanding one. Gas pipelines, as a means of transport, are the safest but this does not mean they are risk-free. Therefore, assuring the reliability of the gas pipeline infrastructure has become a critical need for the energy sector. The main threat considered, when looking for means of providing the reliability of the pipeline network, is the occurrence of leaks. Regardless of their size, pipeline leaks are a major concern due to the considerable effects that they might have. These effects extend beyond the costs involved by downtime and repair expenses and can include human injuries as well as environmental disasters.

Table 1.5: Different metal oxide materials investigated for detection of LPG.

Sensing material	**Gas Concentration**	**Sensor Response**	**Res./Rec. Time (s)**	**Temp. (°C)**	**Authors Name**	**Ref. No.**
γ-Fe_2O_3	1000 ppm	90 %	12/120	RT	I. Ray et. al. (2008)	[73]
$Ni_{1-x}CO_x$-$Mn_xFe_{2-x}O_4$	1000 ppm	1	-	180	Satyanarayana et.al. (2003)	[74]
$BaTiO_3$	1000 ppm	303 %	3/5	350	L.A. Patil et. al.	[75]

					(2014)	
SnO_2	1000 ppm	1.2	-	320	Chakraborty et. al. (2006)	[76]
Ni-SnO_2	1000 ppm	90 %	10	300	Jain et. al. (2006)	[77]
Nano ZnO	200 ppm	0.9	100/100	250	Baruwati et. al. (2006)	[78]
Bulk SnO_2	1000 ppm	3.5	15/120	200	Wagh et. al. (2007)	[79]
TiO_2	1000 ppm	6	-	800	Gunjakar et.al. (2008)	[80]
TiO_2	(0.02-.08) vol.%	35.8 %	165/240	425	More et. al. (2008)	[81]
Ni doped TiO_2	1000 ppm	346 %	12/20	250	L.A. Patil et al. (2013)	[82]
TiO_2	5200 ppm	38.70 %	140/230	400	Dhawale et. al. (2009)	[83]
TiO_2	8000 ppm	18 %	-	400	Le et. al. (2009)	[84]
TiO_2	500 ppm	3.9	45/75	400	Dighavkar et. al. (2009)	[85]

Bulk ZnO	1000 ppm	8.07	18/42	350	Patil et. al. (2009)	[86]
TiO_2	0.1 vol.%	63 %	140/180	27	Dhawale et. al. (2008)	[87]
TiO_2	1040 ppm	55 %	112/131	RT	Bhulekh et. al. (2013)	[88]
TiO_2	1000 ppm	90 %	-	250	Patil et. al. (2013)	[89]
CdO	1040 ppm	44 %	70/80	573	Bhulekh et. al. (2014)	[90]
$ZnTiO_3$	5.0 vol.%	7.32	120/200	RT	B.C. Yadav et. al. (2013)	[91]
SnO_2	200 ppm	.005	-	220	Haridas et al. (2009)	[92]
Titania	5.0 vol.%	1.7	-	400	B.C. Yadav et. al. (2011)	[93]
Pt doped SnO_2	400	3200 %	10/22	120	Garje et. al. (2013)	[94]
$ZnNb_2O_6$	4.0 vol.%	4.8	-	RT	R. Srivastava et. al. (2014)	[95]

NiO	0.3 vol%	36.5 %	13.2/40	698	J.L. Gunjakar et. al. (2008)	[96]
ZnO	1000 ppm	1727 %	2/8	300	L.A. Patil et al. (2010)	[97]
$MgFe_2O_4$	2000 ppm	71 %	38/46	425	Patil et. al. (2012)	[98]
SnO_2	100 ppm	750 %	100/120	260	D. Haridas et al.(2008)	[99]

Table 1.6: Different metal oxide materials investigated for semiconductor sensor for detection of various gases.

Sr. No.	Material	Sensing gas	Temperature (°C)/Volume (ppm)	Sensor Response	Res./Rec. Time (s)	Authors name	Ref. No.
1.	$CoNb_2O_6$	C_2H_5OH	130/120	89%	10/18	C. Balamuruga n et al. (2014)	[100]
2.	$CoNb_2O_6$	NH_3	130/120	38%	13/15	C. Balamuruga n et al. (2014)	[100]
3.	$CoNb_2O_6$	H_2S	150/120	68%	14/25	C. Balamuruga n et al.	[100]

						(2014)	
4.	$CoNb_2O_6$	LPG	150/120	26%	10/10	C. Balamuruga n et al.(2014)	[100]
5.	ZnO	LPG	350/2000	60%	100/70	K.V. Gurav et al.(2014)	[101]
6.	Co:ZnO	H_2 Gas	150/3000	53.7%	120/74	D. Sett. et.al.(2017)	[102]
7.	NiV_2O_6	NH_3	120/100	92 %	9/16	C. Balamuruga n et. al.(2014)	[103]
8	V_2O_5	NH_3	/500	69 %	25/15	A. Dhayal Raj et. al.(2017)	[104]
9	Polyanilin e-pt	NH_3	RT/500	39 %	36/170	C.V. Tuan et al.(2014)	[105]
10	Pd-$LaCo_{0.8}Fe_{0.2}O_3$	NH_3	300/200	97 %	8/20	G.N. Chaudhari et. al.(2010)	[106]
11	Carbon nanotube	NH_3	25/200	65 %	25/15	S.G. Wanga et. al.(2012)	[107]
12	Zr and $CoWO_4$	NH_3	700/1000	50 %	-	Quan Diao et.al.(2012)	[108]
13	$CuNb_2O_6$	NH_3	300/500	56 %	25/15	S.K. Biswas et. al.(2008)	[109]
14	Pt-WO_3	NH_3	350/400	-	60/300	Vibha Srivastava et. al.(2008)	[110]
15	TeO_2	NH_3	170/500	45 %	186/336	T. Siciliano et. al.	[111]

						(2009)	
16	$(Ba_{0.67}Sr_{0.33})TiO_3$	H_2S	350/100	12	3/9	G.H. Jain et.al.(2006)	[112]

1.12 Contemporary Contests and Objective of the Thesis

The Thesis focuses on the fabrication of pure and doped titania as a sensing material for the detection of harmful gases. Nanostructured semiconducting materials are considered to be the most promising materials for the study of sensors because of their higher surface to volume ratio. We have been interested in carrying out our investigations with a new material that possess good sensitivity for the LPG concentration at the LEL level, with properties that are stable over time and thermal cycling after exposure to the various species likely to be present in the ambient.

On the basis of literature survey and up to my knowledge, I found there is no significant work done in the area of design and development of a LPG sensor operable at room temperature. Titania shows very good surface reactivity and it forms composites with other metal oxides very easily. Therefore in this thesis, the synthesis of Titania and their nanocomposites using soft chemical and mechano-chemical routes have been considered. After thorough characterization of synthesised materials, they have been employed as LPG sensor.

The main goal of our present investigation is to design and fabricate an LPG sensor which would be robust, cost effective and more sensitive than previously reported sensors. Here, we wish to elucidate our experimental results of advance stage on LPG sensing of pure and doped titanium oxides at room ambient as LPG sensors operable at room temperature will be most efficient for commercialization point of view.

1.13 Organisation of the Thesis

The present thesis consists of six chapters. **Chapter 1** includes the introduction of nanomaterials, recent development in sensor and its limitations. The sensing principle and extensive survey of literature on the development of LPG sensor and its present status have been discussed. The orientation of work, aims and objectives of the present research investigation are well described at the end of the Chapter. It also deals with the description of synthesis and characterization techniques used in the present research work. The advantage of sol-gel technique over other synthesis methods has been described. **Chapter 2** describes the sol-gel processed grape-like nanostructured Titania based Liquefied Petroleum Gas Sensor. In **Chapter 3**, preparation of PANI doped TiO_2 nanocomposite thin film and its relevance as room temperature liquefied petroleum gas and CO_2 gas sensor is reported. The film of same sensing material has been deposited on the corning glass substrate IDEs using spin coating technique and this was exploited for room temperature detection of LPG. **Chapter 4** deals with the LPG sensing properties of thin film of Zn doped TiO_2 using sol-gel spin coating technique. **Chapter 5** describes the synthesis and characterization of Ag doped TiO_2 nanocomposites via sol-gel method for LPG sensor. **Chapter 6** deals with summary of the work done and the concluding remarks drawn from the present research work. Future scope for further research work in the field of nanosized materials and their composites as LPG sensor has been depicted at the end of this thesis.

1.14 Characterization Techniques

This part has been described in appendix part of thesis.

References

[1] Z. Mohd. Yunus, N. Hamidon, Z. Awang, Gas Sensors: A Review, Sensors & Transducers, 168 (2014) 61-75.

[2] N. Katta, D. C. Meier, K. D. Benkstein, S. Semancik, B. Raman, The I/O transform of a chemical sensor, Sensors and Actuators B 232 (2016) 357-368.

[3] N. Ji, L.J. Ping, D. Huan, P.H. Cheng, Progress on Click Chemistry and Its Application in Chemical Sensors, Chinese Journal of Analytical Chemistry, 43(4) (2015) 609-617.

[4] J. Fraden, Handbook of modern sensors: Physics, designs and applications, AIP Press, second edition, 1997.

[5] D. Compagnone, G.D. Francia, C.D. Natale, G. Neri, R. Seeber and A. Tajani. Chemical Sensors and Biosensors in Italy: A Review of the 2015 Literature, Sensors, 17 (2017) 868.

[6] Y.H. Wang, K.J. Huang, X. Wu, Recent advances in transition-metal dichalcogenides based electrochemical biosensors: A review. https://doi.org/10. 1016 /j.bios.2017.06.0 11.

[7] T. Wang, Y. Zhou, C. Lei, J. Luo, S. Xie, H. Pu, Magnetic impedance biosensor: A review, Biosensors and Bioelectronics 90 (2017) 418-435.

[8] C. Li, W. Yang, Q. Li, TiO_2 based photocatalysts prepared by oxidation of TiN nanoparticles and their photocatalytic activities under visible light illumination, Journal of Materials Science & Technology 2017. https://doi.org/10.1016/j.jmst. 2017.06. 010.

[9] A. Hulnnicki, S. Clab, ind K Ingm. Chemical sensor definitions and classification, Pure & Appl. Chem. 63 (1991) 1247.

[10] R. Gosangi, R.G. Osuna, Active classification with arrays of tunable chemical sensors, Chemometrics and Intelligent Laboratory Systems 132 (2014) 91-102.

[11] J.G. Monroy, E.J. Palomo, E.L. Rubio, J.G. Jimenez, Continuous chemical classification in uncontrolled environments with sliding windows, Chemometrics and Intelligent Laboratory Systems 158 (2016) 117-129.

[12] J. Gebicki, Application of electrochemical sensors and sensor matrixes for measurement of odorous chemical compounds, Trends in Analytical Chemistry 77 (2016) 1-13.

[13] L.A. Mercante, V.P. Scagion, F.L. Migliorini, L.H.C. Mattoso, D.S. Corre, Electrospinning-based (bio) sensors for food and agricultural applications: A review, Trends in Analytical Chemistry 91 (2017) 91-103.

[14] I. Fratoddi, A. Bearzotti, I. Venditti, C. Cametti, M.V. Russo, Role of nanostructured polymers on the improvement of electrical response-based relative humidity sensors, Sensors and Actuators B 225 (2016) 96-108.

[15] L.M. Velazquez, R.D.J.R. Troncoso, G.H. Ruiz, D.M. Sotelo, R.A.O. Rios, Smart sensor network for power quality monitoring in electrical Installations, Measurement 103 (2017) 133-142.

[16] World Bank Group, (1998) Nitrogen oxides, Pollution Prevention and Abatement Handbook World Bank Group Effective July 1998.

[17] F.P. Incropera, D. P. Dewitt, Fundamentals of Heat and Mass Transfer, John Wiley & Sons, Inc 3rd ed., (1990).

[18] http://www.elgas.com.au/blog/453-the-science-a-properties-of-lpg.

[19] J. Brunet, V.P. Gracia, A. Pauly, C. Varenne, B. Lauron, An optimised gas sensor microsystem for accurate and real-time measurement of nitrogen dioxide at ppb level, Sensors & Actuators B 134 (2008) 632-639.

[20] http://www.osha.gov.

[21] R.K. Sonker, B.C. Yadav, Chemical Route Deposited SnO_2, SnO_2-Pt and SnO_2-Pd Thin Films for LPG Detection, Adv. Sci. Lett. 20 (2014) 1023-1027.

[22] https://en.wikipedia.org/wiki/Carbon_monoxide.

[23] Thompson, Mike, Carbon Monoxide Molecule of the Month, Winchester College UK.

[24] http://apps.sepa.org.uk/spripa/pages/ substance information.aspx?pid=129.

[25] https://www.ec.gc.ca/air/default.asp?lang=En&n=0D5AD9F6-1.

[26] L.L.R. Int Panis, The Effect of Changing Background Emissions on External Cost Estimates for Secondary Particulates, Open Environmental Sciences, 2 (2008) 47-53.

[27] LPG is a flammable mixture of hydrocarbon gases, Encyclopedia, 2016.

[28] R.K. Sonker, B.C. Yadav, G.I. Dzhardimalieva, Preparation and Properties of Nanostructured PANI Thin Film and Its Application as Low Temperature NO_2 Sensor, J Inorg. Organomet Polym. 26 (2016) 1428-1433.

[29] M.A. Mir, M.A. Bhat, R.A. Naikoo, R.A. Bhat, M. khan, M. Shaik, P. Kumar, P.K. Sharma, R. Tomar, Utilization of Zeolite/Polymer composites for gas sensing: A review, Sensors and Actuators B 242 (2017) 1007-1020.

[30] G. Korotcenkov, B.K. Cho, Metal oxide composites in conductometric gas sensors: Achievements and challenges, Sensors and Actuators B 244 (2017) 182-210.

[31] I. Fratoddi, I. Venditti, C. Cametti, M.V. Russoa, Chemiresistive polyaniline-based gas sensors: A mini review, Sensors and Actuators B 220 (2015) 534-548.

[32] A. Erol, S. Okur, B. Comba, O. Mermer and M.C. Arikan, Humidity sensing properties of ZnO nanoparticles synthesised by a sol-gel process, Sensors and Actuators B 145 (2010) 174-180.

[33] http://edugreen.teri.res.in/explore/n_renew/lpg.htm.

[34] http://www.elgas.com.au/blog/492-what-is-lpg-lpg-gas-lp-gas.

[35] C.N.R. Rao, S.R.C. Vivekchand, K. Biswas, and A. Govindaraja, Synthesis of inorganic nanomaterials, Dalton Transactions, (2007) 3728-3749.

[36] W. Klonowski, E. Olejarczyk, R. Stepien, A new simple fractal method for nanomaterials science and nanosensors, Materials Science-Poland, 23, 3 (2005) 607-612.

[37] K. Page, T. Proffen, H. Terrones, M. Terrones, L. Lee, Y. Yang, S. Stemmer, R. Seshadri, A.K. Cheetham, Direct observation of the structure of gold nanoparticles by total scattering powder neutron diffraction, Chemical Physics Letters, 393 (2004) 385-388.

[38] A. Busiakiewicz, A. Kisielewska, I. Piwonski, D. Batory, The effect of Fe segregation on the photocatalytic growth of Ag nanoparticles on rutile TiO_2 (001), Applied Surface Science (2017) 378-384.

[39] S.K. Verma, A.K. Tiwari, Application of Nanoparticles in Solar collectors: A Review, materials today proceeding, 2 (2015) 3638-3647.

[40] W. Sangchay, L. Sikong, K. Kooptarnond, Comparison of photocatalytic reaction of commercial P25 and synthetic TiO_2-AgCl nanoparticles., Procedia Engineering 32 (2012) 590-596.

[41] Y. Liu, L. Tian, X. Tan, X. Li, X. Chen, Synthesis, properties, and applications of black titanium dioxide nanomaterials., Science Bulletin 62 (2017) 431-441.

[42] P. Ogrodnik, D. Pieniak, D. Bilski, Reseach on the impact of fireproof impregnation by preservatives containing nanoparticles on the strength of construction timber in increased temperatures. Procedia Engineering 172 (2017) 800-807.

[43] Z. Wang, U. Helmersson, P.O. Kall, Optical properties of anatase TiO_2 thin films prepared by aqueous sol–gel process at low temperature., Thin Solid Films 405 (2002) 50-54.

[44] O. Krsko, T. Plecenik, M. Moško, A. A. Haidry, P. Durina, M. Truchly, B. Grancic, M. Gregor, T. Roch, L. Satrapinskyy, A. Moskova, M. Mikula, P. Kus, A. Plecenik, Highly sensitive hydrogen semiconductor gas sensor operating at room temperature., Procedia Engineering 120 (2015) 618-622.

[45] P. Zhang, H. Qina,, W. Lv, H. Zhang, J. Hu, Gas sensors based on ytterbium ferrites nanocrystalline powders for detecting acetone with low concentrations., Sensors and Actuators B 246 (2017) 9-19.

[46] O. Krsko, T. Plecenik, T. Roch, B. Grancic, L. Satrapinsky, M. Truchly, P. Durina, M. Gregor, P. Kus, A. Plecenik, Flexible highly sensitive hydrogen gas sensor based on a TiO_2 thin film on polyimide foil., Sensors and Actuators B 240 (2017) 1058-1065.

[47] B. Choudhury, S. Bayan, A. Choudhury, P. Chakraborty, Narrowing of band gap and effective charge carrier separation in oxygen deficient TiO_2 nanotubes with improved visible light photocatalytic activity., Journal of Colloid and Interface Science 465 (2016) 1-10.

[48] J Mizsei, Forty years of adventure with semiconductor gas sensors., Procedia Engineering 168 (2016) 221-226.

[49] O. Alev, E. Şennik, N. Kilnic, Z.Z. Ozturk, Gas sensor application of hydrothermally growth TiO_2 nanorods, Procedia Engineering 120 (2015) 1162-1165.

[50] L. Wang, Y. Wang, K.Y.S. Wang, Y. Zhang, C. Wei, A novel low temperature gas sensor based on Pt-decorated hierarchical 3D SnO_2 nanocomposites., Sensors and Actuators B 232 (2016) 9-101.

[51] R.K. Sonker, A. Sharma, Md. Shahabuddin, M. Tomar, V. Gupta, Low temperature sensing of NO_2 gas using SnO_2-ZnO nanocomposite sensor. Adv. Mat. Lett. **4**(3) (2013) 196-201.

[52] R.K. Sonker, A. Sharma, M. Tomar, V. Gupta, and B.C. Yadav, Low Temperature Operated NO_2 Gas Sensor Based on SnO_2-ZnO Nanocomposite Thin Film Advanced Science Letters, 20 (2014) 911-916.

[53] C.A. Betty, S. Choudhury, Charge carrier transport in nanocrystalline SnO_2 thin film sensor and temperature dependence of toxic gas sensitivity, Sensors and Actuators B 237 (2016) 787-794.

[54] R.K. Sonker, S.R. Sabhajeet, S. Singh, B.C. Yadav, Synthesis of ZnO nanopetals and its application as NO_2 gas sensor, Materials Letters 152 (2015) 189-191.

[55] R.K. Sonker, B.C. Yadav, Growth mechanism of hexagonal ZnO nanocrystals and their sensing application, Materials Letters 160 (2015) 581-584.

[56] R.K. Sonker, B.C. Yadav Synthesis of ZnO/CNTs nanocomposite thin film and its sensing, International Journal on Applied Bioengineering, 10 (2016) 1.

[57] R.K. Sonker, B.C. Yadav, A. Sharma, M. Tomar and V. Gupta, Experimental investigations on NO_2 sensing of pure ZnO and PANI–ZnO composite thin films, RSC Adv. 6 (2016) 56149.

[58] X. Chen, S.S. Mao, Titanium dioxide nanomaterials: synthesis, properties, modifications, and applications. Chem Rev 107, 7 (2007) 2891-2959.

[59] http://ruby.colorado.edu/~smyth/min/TiO_2.html.

[60] http://www.azom.com/properties.

[61] A. Fujishima, K. Honda, Electrochemical photolysis of water at a semiconductor electrode, Nature. 238 (1972) 37-38.

[62] L. Gao, Q. Li, Z. Song and J. Wang, Preparation of nano-scale Titania thick film and its oxygen sensitivity, Sens. Act. B 71 (2000) 179-183.

[63] S. Somiya and R. Roy, Hydrothermal synthesis of fine oxide powders, Bulletin of Materials Science, Vol. 23, 6, 12 (2000) 453-460.

[64] M. Nathand, B.A. Parkinson, A Simple Sol-Gel Synthesis of Superconducting MgB_2 Nanowires, Advanced Materials, 18 (2006) 1865-1868.

[65] J.B. Laughlin, J.L. Sarquis, V.M. Jones, and J.A. Cox, Using Sol-Gel Chemistry to Synthesize a Material with Properties Suited for Chemical Sensing, Journal of Chemical Education, 77 (2000) 77-79.

[66] J.J. Huang, Y.P. Fu, J.Y. Wang, Y.N. Cheng, S. Lee, J.C. Hsu, Characterization of Fe-Cr alloy metallic interconnects coated with LSMO using the aerosol deposition process, Materials Research Bulletin 51 (2014) 63-68.

[67] W.Y. Teoh, A Perspective on the Flame Spray Synthesis of Photocatalyst Nanoparticles., Materials 6 (2013) 3194-3212.

[68] I. Salma, W. Maenhaut, G. Zaray, Comparative study of elemental mass size distributions in urban atmospheric aerosol, Aerosol Science, 33 (2002) 339-356.

[69] Z. Wang, W. Weng, D. Ji, G. Shen, P. Du, G. Han, Synthesis and properties of SDC powders and ceramics for low-temperature SOFC by stearic acid process, Journal of Electro ceramics, 21 (2008) 698-701.

[70] K.C. Patil, S.T. Aruna, T. Mimani, Combustion synthesis: an update, Current Opinion in Solid State and Materials Science, 6 (2002) 507-512.

[71] N. Yamazoe, New approaches for improving semiconductor gas sensors, Sens. Actuators B 5 (1991) 7-19.

[72] Z. W. Pan, Z. R. Dai, Z. L. Wang, Nanobelts of semiconducting oxides, Science 291 (2001) 1947.

[73] I. Ray , S. Chakraborty , A. Chowdhury , S. Majumdar, A. Prakash, R. Pyare, A. Sen, Room temperature synthesis of γ-Fe_2O_3 by sonochemical route and its response towards butane, Sensors and Actuators B 130 (2008) 882-888.

[74] L. Satyanarayana, K. Madhusudhan Reddy, S.V. Manorama, Synthesis of nano crystalline a material for Liquefied Petroleum gas sensing, Sensors and Actuators B 89 (2003) 62-67.

[75] L.A. Patil, D.N. Suryawanshi, I.G. Pathan, D.G. Patil, Effect of firing temperature on gas sensing properties of nanocrystalline perovskite $BaTiO_3$ thin films prepared by spray pyrolysis techniques, Sensors and Actuators B 195 (2014) 643-650.

[76] S. Chakraborty, A. Sen, H.S. Maiti, Selective detection of methane and butane by temperature modulation in iron-doped tin oxide sensors, Sensors and Actuators B 115 (2006) 610-613.

[77] K. Jain, R.P. Pant, S.T. Lakshmikumar, Effect of Ni-doping on thick film SnO_2 gas sensor, Sensors and Actuators B 113 (2006) 823-829.

[78] B. Baruwati, D.K. Kumar, S.V. Manorama, Hydrothermal synthesis of highly crystalline ZnO nanoparticles: a competitive sensor for LPG and EtOH., Sensors and Actuators B B119 (2006) 676-682.

[79] M.S. Wagh, G.H. Jain, D.R. Patil, S.A. Patil, L.A. Patil, Surface customization of SnO_2 thick film using RuO_2 as a surfactant for LPG response, Sensors and Actuators B 122 (2007) 357-364.

[80] J.L. Gunjakar, A.M. More, C.D. Lokhande, Chemical deposition of nanocrystalline nickel oxide from urea containing bath and its use in liquefied petroleum gas sensor, Sensors and Actuators B 131 (2008) 356-361.

[81] A.M. More, J.L. Gunjakar, C.D. Lokhande, Liquefied petroleum gas (LPG) sensor properties of interconnected web-like structured sprayed TiO_2 films, Sensors and Actuators B 129 (2008) 671-677.

[82] L.A. Patil, D.N. Suryawanshi, I.G. Pathan, D.M. Patil, Nickel doped spray pyrolyzed nanostructured TiO_2 thin films for LPG gas sensing, Sensors and Actuators B 176 (2013) 514-521.

[83] D.S. Dhawale, R.R. Salunkhe, V.J. Fulari, M.C. Rath, S. Sawant, C.D. Loknande, Liquefied petroleum gas (LPG) sensing performance of electron beam irradiated chemically deposited TiO_2 thin films, Sensors and Actuators B 141 (2009) 58-64.

[84] D.T.T. Le, D.D. Vuong, N.D. Chien, Synthesis and LPG-sensing properties of TiO_2 nanowires, Journal of Physics: Conference Series 187 (2009) 012086.

[85] C.G. Dighavkar, A.V. Patil, R.Y. Borse, Study on gas sensing performance of TiO_2 screen printed thick films, Sensors & Transducers 101 (2009) 73-81.

[86] D.R. Patil, L.A. Patil, Cr_2O_3-modified ZnO thick film resistors as LPG sensors, Talanta, 77 (2009) 1409-1414.

[87] D.S. Dhawale, R.R. Salunkhe, U.M. Patil, K.V. Gurav, A.M. More, C.D. Lokhande, Room temperature liquefied petroleum gas (LPG) sensor based on p-polyaniline/n-TiO_2 heterojunction, Sensors and Actuators B 134 (2008) 988-992.

[88] R.N. Bulakhe, S.V. Patil, P.R. Deshmukh, N.M. Shinde, C.D. Lokhande, Fabrication and performance of polypyrrole (Ppy)/TiO_2 heterojunction for room temperature operated LPG sensor, Sensors and Actuators B 181 (2013) 417-423.

[89] L.A. Patil, D.N. Suryawanshi, I.G. Pathan, D.M. Patil, Nickel doped spray pyrolyzed nanostructured TiO_2 thin films for LPG gas sensing, Sensors and Actuators B 176 (2013) 514-521.

[90] R.N. Bulakhe, C.D. Lokhande, Chemically deposited cubic structured CdO thin films: Use in liquefied petroleum gas sensor, Sensors and Actuators B 200 (2014) 245-250.

[91] B.C. Yadav, A. Yadav, S. Singh, K. Singh, Nanocrystalline zinc titanate synthesised via physicochemical route and its application as liquefied petroleum gas sensor, Sensors and Actuators B 177 (2013) 605-611.

[92] D. Haridas, A. Chowdhuri, K. Sreenivas, V. Gupta, Enhanced LPG response characteristics of SnO_2 thin film based sensors loaded with Pt clusters, an International journal on smart on sensing and intelligent system, 2(2009).

[93] B.C. Yadav, A. Yadav, T. Shukla, S. Singh, Solid-state titania-based gas sensor for liquefied petroleum gas detection at room temperature, Bull. Mater. Sci., 34 (2011) 1639-1644.

[94] A.D. Garje, S.N. Sadakale, LPG sensing properties of platinum doped nanocrystalline SnO_2 based thick films with the effect of dipping time and sintering temperature, Adv. Mat. Lett. 4(1) (2013) 58-63.

[95] R. Srivastava, Nanocomposite $ZnNb_2O_6$ Thick Film as Room Temperature Liquefied Petroleum Gas (LPG) Sensor, American Journal of Sensor Technology, 2 (2014) 25-28.

[96] J.L. Gunjakar, A.M. More, C.D. Lokhande, Chemical deposition of nanocrystalline nickel oxide from urea containing bath and its use in liquefied petroleum gas sensor, Sensors and Actuators B 131 (2008) 356-361.

[97] L.A. Patil, A.R. Bari, M.D. Shinde, V. Deo, Ultrasonically prepared nanocrystalline ZnO thin films for highly sensitive LPG sensing, Sensors and Actuators B 149 (2010) 79-86.

[98] J.Y. Patil, M.S. Khandekar, I.S. Mulla, S.S. Suryavanshi, Combustion synthesis of magnesium ferrite as liquid petroleum gas (LPG) sensor: Effect of sintering temperature, Current Applied Physics 12 (2012) 319-324.

[99] D. Haridas, K. Sreenivas, V. Gupta, Improved response characteristics of SnO_2 thin film loaded with nanoscale catalysts for LPG detection., Sensors and Actuators B 133 (2008) 270-275.

[100] C. Balamurugan, A.R. Maheswari, D.W. Lee, Structural, optical, and selective ethanol sensing properties of p-type semiconducting $CoNb_2O_6$ nanopowder, Sensors and Actuators B 205 (2014) 289-297.

[101] K.V. Gurav, M.G. Gang, S.W. Shin, U.M. Patil, P.R. Deshmukh, G.L. Agawane, M. P. Suryawanshi, S.M. Pawar, P.S. Patil, C.D. Lokhande, J.H. Kim, Gas sensing properties of hydrothermally grown ZnO nanorods with different aspect ratios, Sensors and Actuators B 190 (2014) 439-445.

[102] D. Sett, D. Basak, Highly enhanced H_2 gas sensing characteristics of Co: ZnO nanorods and its mechanism, Sensors and Actuators B 243 (2017) 475-483.

[103] C. Balamurugan, D.W. Lee, A selective NH_3 gas sensor based on mesoporous p-type NiV_2O_6 semiconducting nanorods synthesized using solution method, Sensors and Actuators B 192 (2014) 414-422.

[104] A.D. Raj, T. Pazhanivel, P.S. Kumar, D. Mangalaraj, D. Nataraj, N. Ponpandian, self-assembled V_2O_5 nanorods for gas sensors Curr. Appl. Phys. 10 (2010) 531-537.

[105] C.V. Tuan, M.A. Tuan, N.V. Hieu, T. Trung, Electrochemical synthesis of polyaniline nanowires on Pt interdigitated microelectrode for room temperature NH_3 gas sensor application, Curr. Appl. Phys. 12 (2012) 1011-1016.

[106] G.N. Chaudhari, S.V. Jagtap, N.N. Gedam, M.J. Pawar, V.S. Sangawar, Sol-gel synthesized semiconducting $LaCo_{0.8}Fe_{0.2}O_3$ based powder for thick film NH_3 gas sensor, Talanta 78 (2009) 1136-1140.

[107] S.G. Wanga, Z. Qing, D.J. Yanga, P.J. Sellinb, G.F. Zhong, Multi-walled carbon nanotube-based gas sensors for NH_3 detection, Diam. Relat. Mater. 13 (2004) 1327-1332.

[108] Q. Diao, F. Yang, C. Yin, J. li, S. Yang, X. Liang, G. Lu, Ammonia sensors based on stabilized zirconia and $CoWO_4$ sensing electrode, Solid State Ionics 225 (2012) 328-331.

[109] S.K. Biswas, P. Pramanik, Studies on the gas sensing behavior of nanosized $CuNb_2O_6$ towards ammonia, hydrogen and liquefied petroleum gas, Sens. Actuators B 133 (2008) 449-455.

[110] V. Srivastava, K. Jain, Highly sensitive NH_3 sensor using Pt catalyzed silica coating over WO_3 thick films, Sens. Actuators B 133 (2008) 46-52.

[111] T. Siciliano, M. Di Giulio, M. Tepore, E. Filippo, G. Micocci, A. Tepore, Ammonia sensitivity of RF sputtered tellurium oxide thin films, Sens. Actuators B 138 (2009) 550-555.

[112] G.H. Jain, L.A. Patil, Gas sensing properties of Cu and Cr activated BST thick films, Bull. Mater. Sci., 29 (2006) 403-411.

Chapter-2

Sol-gel processed Grape-like nanostructured Titania based Liquefied Petroleum Gas Sensor

In this chapter thin films of nanostructured TiO_2 have been fabricated by sol-gel spin coating process. The structural, morphological and optical properties of the prepared sensor structure have been studied by X-ray diffraction (XRD), Scanning Electron Microscopy (SEM) and UV-Visible spectroscopy, respectively. XRD revealed the crystallite size as 20 nm. SEM showed the regular and porous grape-like surface morphology before exposure to the LPG. The band gap of the material was found as 3.65 eV. This film was employed for LPG sensing and variations in resistance with exposure of LPG were observed. The maximum sensing response was found as 1.34 for the exposure of 4% vol. of LPG and results were found reproducible.

2.1 Introduction

Liquefied petroleum gas (LPG) sensor has become the interesting topic of research today in observation of fundamental research as well as industrial applications. Gas sensors that utilise metal oxide materials are widely used in industry to monitor combustion processes. While they are inexpensive to robust in high-temperature environments, many of these instruments are not selective towards the species of interest when placed in a stream composed of multiple gases. Metal oxide semiconductors are useful for the detection of combustible gases by the change in the surface conductivity due to exposure togases. The n-type semiconducting materials such as stannous oxide (SnO_2), zinc oxide (ZnO), titanium dioxide (TiO_2) are promising materials for gas and humidity sensors [1-9]. TiO_2 is an important metal oxide for abroad range of gas sensing applications, because of its surface chemistry, charge transport and electrical properties. It is a versatile material widely used in industry, research and environmental cleaning. Titanium dioxide is found in three different phases; rutile (tetragonal), anatase (tetragonal) and brookite (orthorhombic) and each phase has its own structure along with a particular application [10-13]. TiO_2 is a versatile functional material due to its many unusual properties such as hydrophilicity [13], biocompatibility [14], semiconductivity, corrosion resistance, low cost, wide availability, nontoxicity and physicochemically stable nature [15] and also known for its gas sensing behaviour [16-17]. Titanium dioxide has received considerable attention because of its excellent optical, electrical, mechanical and catalytic properties, which makes it technologically useful. Its superior properties are due to chemical and biological inertness, non-toxicity, strong oxidising/reducing power, cost-effectiveness, and long-term stability against photo-corrosion and chemical corrosion. The band gap of titania is about 3.2 eV. The band gap further increases with decreasing

the particle size and hence the utilisation is typically confined within the UV-radiation of the electromagnetic spectrum.

The basic requirement for the sensor is the change in electrical conductivity with exposure to LPG at the surface of semiconducting oxides which depends on their band gaps, surface morphology, size, the diffusion rate of gas and specific surface area. The semi-conducting properties of metal oxides represent the basis for their use as gas sensors since the number of free charge carriers within the metal oxide and thus its electrical conductivity reversibly depends on the interactions with the ambient gas atmosphere.

The LPG sensing mechanism is based on the chemisorption reaction that takes place at the surface of the metal oxide. As a result increasing the specific surface area of the sensing film leads to more sites for adsorption of surrounding gases. The oxygen adsorbed on the surface of the film influences the resistance of the titania based sensor. Initially, oxygen from the atmosphere adsorbs on the surface of the film and extracts electrons from its conduction bands to form O_2^- species on the surface, consequently resistance increases. After that an equilibrium state is achieved between oxygen of TiO_2 and atmospheric oxygen.

2.2 Experimental

2.2.1 Materials

Titanium tetrachloride ($TiCl_4$), propanol, deionized water (DI) and ethanol were used for the material preparation. All chemicals were purchased from Sigma-Aldrich Chemical Co. with 99.99% purity.

2.2.2 Synthesis of nanomaterials

Analytical grade chemical including $TiCl_4$(99.99%) and citric acid purchased from Sigma-Aldrich Co. Limited were used. Also the deionized water and ice cubes were consumed in all preparation methods.

2.2.3 Synthesis Method

The sol gel method is used for the synthesis of TiO_2 powder as shown in flow chart of Figure 2.1 [18].

2.2.4 Thin film deposition technique

Spin coating is a method which is generally employed for the preparation of thin films. A typical process involves depositing a small puddle of a fluid material onto the centre of a substrate and thin spinning the substrate at high speed. Centripetal acceleration will cause most of the resin to spread to, and eventually off, the edge of the substrate leaving a thin film of the material on the surface. Final film thickness and other properties will depend on the nature of the fluid material (viscosity, drying rate, surface tension, etc.) and the parameters chosen for the spin process. Factors such as final rotation speed, acceleration, and fume exhaust affect the properties of the coated films. Spin speed is one of the important factors in spin coating. The speed of the substrate (rpm) affects the degree of radial (centrifugal) force applied to the fluid resin as well as the velocity and characteristic turbulence of the air immediately above it [19].

A thin film of the sample was prepared by spin coating method. For this purpose, the synthesised powder was dissolved in isopropyl alcohol and was then sonicated for 30-40 min. The sonicated solution was stirred at 100 °C for 6 h. Then a drop of the obtained solution was spun on the well-cleaned borosilicate glass substrate using spin coater (METREX). The resulting thin film was dried at 120 °C for 10 min for each time of deposition [9].This drying procedure stabilises the thin film. Further, the film was annealed at 300 °C which converts the anatase phase into rutile with almost uniform and porous structure. The thickness of the film was found 0.4 μm, measured by Accurion variable angle spectroscopic ellipsometer (Nanofilm EP3 Imaging). Further with the help of the silver paste, two electrodes were fabricated on opposite end of the film for signal

registration. Variations in resistance with the variation in concentration of LPG were recorded using Keithley Electrometer [6517 B].

2.3. Characterization of TiO_2

2.3.1. Scanning Electron Microscopy (SEM)

Figure 2.2 (a & b) shows SEM images of theTiO_2 thin film at microscale and nanoscale, respectively. The SEM image at microscale shows that some of the particles combined with each other to form clusters and leaving some spaces as pores. The uniformly distributed pores with random size may also be seen through SEM image at the nanoscale. These pores serve as gas adsorption sites and gas sensitivity depends on their depths and sizes. The gas response of sensors is mainly due to the interactions between target gas and the surface of the sensor. Therefore, it is obvious that for the greater specific surface area for adsorption of LPG, the interactions between the adsorbed gases and the sensor surface would be stronger, as a result, the sensor response will be higher. In the present investigation, the improved sensing performance of sample may be attributed to their porous spherical structure and crystallite size. The pores in irregular nanospheres can act as channels for diffusion of LPG and thus provide more active sites where LPG molecules get absorbed and counter the surface species (O_2, O_2^-, O^-). This improves the reaction of LPG with surface adsorbed oxygen and is an imperative parameter regarding the sensitivity of the sensor. A close look of micrographs give the average pore size 100 nm which may contain many in-situ meso-pores.

2.3.2 X-Ray Diffraction

X-Ray diffraction pattern of as-prepared material shown in Figure 2.3 reveals the anatase phase. The average crystallite size (*D*) of the sensing material can be calculated by the Debye-Scherer's formula, which is given by

$$D = \frac{K\lambda}{\beta cos\theta} \quad (1)$$

Where, K = 0.94 is Scherer's coefficient, which depends on the shape of the crystallite and the type of defects present, λ is the wavelength of X-ray radiation, β is the full width at half maximum (FWHM) of the diffraction peak and θ is the angle of diffraction.

The XRD pattern of the TiO_2 thin film also reveals that the sensing material consists of several peaks. In Figure 2.2(a), the peaks of TiO_2 show less crystalline nature of TiO_2 before annealing. It may be observed that from Figure 2.2(b), the peaks observed at 2θ = 25.29º, 48.49º, 54.73ºand 55.86º correspond to (110), (101), (200), (105) and (211) reflection planes of TiO_2, respectively and are in good agreement with the corresponding values reported for the anatase structure of TiO_2. The average value of crystallite size of TiO_2 was calculated as 20 nm. The reduced crystallite size provides a large surface to volume ratio, hence the ability for adsorption of gas through the pores on the surface of the thin film increases which enhances the sensitivity of the gas sensor.

2.3.3. UV-Visible Spectroscopy

The optical transmission spectra of the as-grown TiO_2 thin film (200 nm) deposited separately on the glass substrate was investigated in the wavelength range of 190 to 1100 nm, and the variation is shown in Figure 2.4. The TiO_2 thin film exhibits a high transmission (>75%) in the visible region and shows a sharp fundamental absorption edge in UV-region at 380 nm. It is known that the properties of optical absorption are relevant to the electronic structure and hence are the key factor in the determination of the band gap. The optical energy band gap was calculated by Tauc relation as given below [20]:

$$\alpha h\nu = A(h\nu - E_g)^{\frac{1}{2}} \quad (2)$$

Where A is a constant, hν is the photon energy, E_g is the energy band gap and α is the absorption coefficient given by:

$$\alpha = 2.303\ (\frac{A_b}{t}) \quad (3)$$

In Eq. (2), A_b is the absorbance and t is the thickness of the film. Optical band gap of the TiO_2 thin film deposited on glass substrate was calculated from the intercept on energy axis obtained by extrapolating the band gap for as-grown TiO_2 thin film and is found as 3.65 eV in the linear portion of the Tauc plot i.e. $(\alpha h\nu)^2$ *vs* photon energy ($h\nu$) as shown inset of Figure 2.4. Estimated value of optical band gap is close to the actual values for TiO_2 thin films (3.2 eV) grown by various other techniques.

2.4. Gas Sensing Measurements

The schematic diagram of LPG sensing set-up is shown in Figure 2.5(a). The sensing film was inserted between the silver electrodes inside the glass chamber having two knobs. One knob is associated with the concentration measuring system (gas inlet) and other is an outlet knob for releasing the gas [21]. Concentration measuring system is shown in Figure 2.5(b), which consists of a glass bottle containing double distilled water, which is saturated with LPG, in order to avoid the possibility of dissolution of inserted gas. At the top of the bottle, the measuring tube (pipette) is connected by a vacuum seal. The cock I is connected to the LPG cylinder and cock II is connected to the inlet of the gas chamber. When the cock I is opened, the LPG from the cylinder is filled in the glass bottle and an equivalent amount of water is displaced in the measuring pipette. When the cock II is opened, the desired amount of gas e.g. 1, 2, 3 and 4 vol.% was entered in the gas chamber. Before passing the LPG into the chamber, the gas chamber with a resistance measuring holder was stabilised for 10-20 minutes. Sensing film with silver contacts was used for measurements of LPG sensing properties. The resistance of the film was taken as stabilised resistance in the presence of air (R_a). When LPG was introduced into the chamber, the variations in electrical resistance with time for different vol.% of LPG were recorded by using Keithley electrometer (Model: 6517 B). Sensitivity of the LPG sensor

is defined as the change in resistance in the presence of gas (R_g) to the resistance in the presence of air (R_a) [22], that is;

$$S = \frac{R_a}{R_g} \tag{4}$$

2.4.1. Gas sensing behaviour of metal oxide

From the band theory for applied sensor, the target gas interacts with the surface of a metal oxide film (through the absorbed oxygen ion by surface) which results in achange in charge carrier concentration of the material [23]. This change in charge carrier concentration alters the conductivity of material. An n-type semiconductor is one where the majority charge carriers are electrons and on interaction with a reducing gas, decrease in conductivity (or increase in resistance) occurs. Conversely, an oxidising gas serves to deplete the sensing layer of charge carrying the electrons resulting in an increase in conductivity. A p-type semiconductor is a material that conducts with holes being the majority charge carriers hence the opposite effects are observed with the material and show an increase in conductivity in the presence of an oxidising gas.

2.4.2. Gas sensing behaviour of TiO_2 thin film

Figure 2.6 illustrates the variations in resistance of the TiO_2 film with time after exposure of different vol.% of LPG at room temperature. The curve for 1 vol.% of LPG shows the slightly increase in the resistance with time after exposure to the gas. Curves for 2 and 3 vol.% of LPG exhibit the improved response and has better sensitivity than 1 vol.%. Further, for 4 vol.% of LPG, the resistance increases sharply with the time after exposure up to 1000 s and then become constant. The sensing response of different vol.% concentration with the response and recovery times is depicted in Table 2.1.

Figure 2.7 exhibits the variations of average sensitivity with a concentration of LPG and it was found that as the concentration of LPG (in vol.%) increases, the average sensitivity of sensor increases linearly up to 4 vol.% of LPG. The linear increment of the

sensitivity of the sensor is a significant factor for the device fabrication. The maximum sensitivity was obtained as ~ 0.65 for 4 vol.% of LPG.

The gas sensing mechanism of TiO_2 thin film based sensor belongs to surface control type, i.e. resistance change is controlled by the contact surface area and the amount of chemisorbed oxygen. LPG consists of CH_4, C_3H_8 and some hydrocarbons. In each composition, the reducing hydrogen species are bound to a carbon atom, therefore, LPG dissociates into the reactive reducing components hardly on the surface of the sensing element. As LPG is exposed to sensing element, the conductivity decreases due to adsorption of oxide and capture more electrons that reduce the current. It was observed that as the concentration of LPG increases, the average sensitivity increases linearly in the beginning and later it becomes saturated. The linear relationship between sensitivity and gas concentration may be attributed to the availability of a sufficient number of sensing sites on the film to act upon the LPG. The low concentration implies a lower surface coverage of gas molecules, resulting in a lower surface reaction between the surface adsorbed oxygen species and the gas molecules. The increase in LPG concentration increases the surface reaction due to a large surface coverage. Further increase in the LPG concentration does not increase the surface reaction and eventually, saturation takes place. Thus, the maximum sensitivity was obtained at higher concentration of LPG i.e. 4 vol.%. The linearity of average sensitivity for the LPG suggests that TiO_2 thin film can be reliably used to monitor the LPG over this range of concentration. As the lower explosive limit (LEL) for LPG is 0.2 vol. % [24], therefore, response is measured up to 4.0 vol.% in order to detect the LPG for safety requirement.

2.4.3. Sensing Mechanism

The oxygen adsorbed on the surface of the film affects the resistance of the titania based sensor. Initially, oxygen molecules from the atmosphere get adsorbed on the

surface of the film and extracts electrons from its conduction bands to form O_2^- species on the surface, after that an equilibrium state is achieved between the lattice oxygen of TiO_2 and atmospheric oxygen and further the value is stabilized.

$$O_2\,(gas) \leftrightarrow O_2\,(ads) \quad \text{(Thin Film Surface)} \tag{5}$$

$$O_2\,(gas) + e^- \leftrightarrow O_2^- \quad \text{(Thin Film Surface)} \tag{6}$$

When the thin film is being exposed to LPG, it reacts with the chemisorbed oxygen. On interaction with hydrocarbons (C_nH_{2n+2}) of LPG, the adsorbed oxygen is removed, forming gaseous species and water vapour. Consequently, the resistance changes, which is due to the change in the width of depletion layer after exposure to LPG. The reaction of LPG molecules with adsorbed oxygen can be explained as follows;

$$C_n\,H_{2n+2} + 2O^- \leftrightarrow H_2O + C_nH_{2n} - O + e^- \tag{7}$$

It is evident from the proposed reaction schemes that a large number of electrons are released upon LPG exposure to TiO_2 surface; particularly in the presence of O_2^- which is responsible for the rapid decrease in conductivity. The improvement in the performance of the sensor towards reducing gases has been reported in Table 2.2.

2.5. Conclusion

In this work, LPG sensor operable at room temperature was fabricated using titanium oxide thin film prepared by sol-gel route successfully. Film thickness was measured as 0.4 μm and average crystallite size was estimated as 20 nm. The maximum sensing response was found as ~ 1.34 for 4 vol.% of LPG with a response and recovery times of 117 sec and 148 sec respectively. This sensor structure may be exploited for the device fabrication for the detection of LPG below LEL. Also by using appropriate dopant, the band-gap of synthesised material can be engineered so that the sensitivity of the sensor may enhance.

References

[1] R. Srivastava, B.C. Yadav, C.D. Dwivedi, R. Kumar, Comparative study of moisture sensing properties of ZnO nanomaterials through hydroxide route by mixing dropwise and sudden, Sens. Trans. J.,80 (2007) 1295-1301.

[2] D.R. Patil, L.A. Patil, Room temperature chlorine gas sensing using surface modified ZnO thick film resistors, Sens. Actuators B: Chem., 123 (2007) 546-553.

[3] A.M. More, J.L. Gunjakar, C.D. Lokhande, Liquefied petroleum gas (LPG) sensor properties of interconnected web-like structured sprayed TiO_2 films.,Sens. Actuators B: Chem.,129 (2008) 671-677.

[4] R.K. Sonker, A. Sharma, M. Tomar, V. Gupta, B.C. Yadav, Nanocatalyst (Pt, Ag and CuO) Doped SnO_2 Thin Film Based Sensors for Low-Temperature Detection of NO_2 Gas, Adv. Sci. Lett.,20 (2014) 1374-1377.

[5] V.R. Shinde, T.P. Gujar, C.D. Lokhande, LPG sensing properties of ZnO films prepared by spray pyrolysis method: effect of molarity of precursor solution, Sens. Actuators B: Chem, 120 (2007) 551-559.

[6] D.R. Patil, L.A. Patil, G.H. Jain, M.S. Wagh, S.A. Patil, Surface activated ZnO thick film resistors for LPG gas sensing, Sens. Trans. J., 74 (2006) 874-883.

[7] R.K. Sonker, A. Sharma, M. Tomar, V. Gupta, B.C. Yadav, Low temperature operated NO_2 gas sensor based on SnO_2-ZnO nanocomposite thin film,Adv. Sci. Lett., 20 (2014) 911-916.

[8] G.N. Chaudhari, P.R. Padole, A.B. Bodade, S.S. Patil, Sensitivity and selectivity of chemically modified nanosized SnO_2 based CO sensors, Indian J. of Phy., 79(10) (2005) 1157-1162.

[9] R.K. Sonker, A. Sharma, Md. Shahabuddin, M. Tomar, V. Gupta, Low-temperature sensing of NO_2 gas using SnO_2-ZnO nanocomposite sensor, Adv. Mat. Lett.,4(2013)196-201.

[10] C. Xiabo, S.S. Mao, Titanium Dioxide Nanomaterials: Synthesis, Properties, Modifications, and Applications, Chem. Rev.,107(2007)2891-2906.

[11] A. Fujishima, K. Honda, Electrochemical photolysis of water at a semiconductor electrode, Nature,238 (1972) 37-38.

[12] U. Diebold, The surface science of titanium dioxide, Surf. Sci. Rep., 28(2003)53-229.

[13] O. Carp, C.L. Huisman, A. Eller, the Photoinduced reactivity of titanium dioxide, Solid State Chem., 32 (2004) 33-177.

[14] A.K. Jha, K. Prasad, Ferroelectric $BaTiO_3$ nanoparticles biosynthesis and characterization, Colloids Surf., 5(2010)330-334.

[15] C.H. Kwon, H. Shin, J.H. Kima, W.S. Choi, K.H. Yoon, Degradation of methylene blue via photocatalysis of titanium dioxide, Mat. Chem. Phys. 86 (2004) 78-82.

[16] L.R. Skubal, N.M. Meshkov, M.C. Vogt, Detection and identification of gaseous organics using a TiO_2 sensor, J. Photochem. Photobiol., 148 (2002) 103-108.

[17] K.R. Meier, M. Gratzel, Redox Targeting of Oligonucleotides Anchored to Nanocrystalline TiO_2 Films for DNA Detection, Chem. Phys. Chem., 3 (2002) 371-374.

[18] B.C. Yadav, N. Verma, S. Singh, Nanocrystalline SnO_2-TiO_2 thin film deposited on the base of the equilateral prism as an optoelectronic humidity sensor, Optics & Laser Technology, 44 (2012) 1681-1688.

[19] B.C. Yadav, R.C. Yadav, S. Singh, P.K. Dwivedi, H. Ryu, S. Kang, Nanostructured cobalt oxide and cobalt titanate thin films as optical humidity sensor: A new approach, Optics and Laser Technology, 49(2013)68-74.

[20] S. Singh, A. Singh, W. Meher, R.R. Yadav, P. Tandon, S.S.A. Rasool, B.C. Yadav, Fabrication of self-assembled hierarchical flowerlike zinc stannate thin film and its application as liquefied petroleum gas sensor, Sens. Actuators B: chem., 205 (2014) 102-110.

[21] R. Srivastava, B.C. Yadav,Nanostructured $ZnFe_2O_4$ thick film as room temperature liquefied petroleum gas sensor, J. Exp. Nanosci., 10(2015)703-717.

[22] B.C. Yadav, R. Srivastava, A. Yadav, V. Srivastava, LPG sensing of nanostructured zinc oxide and zinc niobate, Sensor letters 6 (5) (2008) 714-718.

[23] G.F. Fine, L.M. Cavanagh, A. Afonja, R. Binions, Metal Oxide Semi-Conductor Gas Sensors in Environmental Monitoring, Sensors, 10 (2010) 5469-5502.

[24] B.C. Yadav, A. Yadav, T. Shukla, S. Singh, Solid-state titania-based gas sensor for liquefied petroleum gas detection at room temperature, Sens. Lett.,7 (2009) 1-5.

[25] D.S. Lee, D.D. Lee, S.W. Ban, M. Ban, Y.T. Kim, SnO_2 gas sensing array for combustible and explosive gas leakage., recognition IEEE Sensors Journal, 2 (2002) 140-149.

[26] S. Chakraborty, A. Sen, H.S. Maiti, Selective detection of methane and butane by temperature modulation in iron-doped tin oxide sensors, Sens. Actuators B: Chem., 115(2006)610-613.

[27] L. Satyanarayana, K.M. Reddy, S.V. Manorama, Synthesis of nanocrystalline $Ni_{1-x}Co_xMn_xFe_{2-x}O_4$: a material for liquefied petroleum gas sensing, Sens. Actuators B: Chem., 89(2003)62-67.

[28] N. Iftimie, E. Rezlescu, P.D. Popa, N. Rezlescu, the Gas sensitivity of nanocrystalline nickel ferrite., J. of Optoelectronics & Adv. Mat., 8 (2009)1016-1018.

[29] R.N. Bulakhe, S.V. Patil, P.R. Deshmukh, N.M. Shinde, C.D. Lokhande, Fabrication and performance of polypyrrole (Ppy)/TiO_2heterojunction for room temperature operated LPG sensor, Sens. Actuators B: chem.,181(2013)417-423.

Table 2.1 Sensing response of different concentrations (vol.%)

Volume of LPG	**1 vol.%**	**2 vol.%**	**3 vol.%**	**4 vol.%**
Sensor Response	1.10	1.14	1.17	1.34
Response Time (s)	194	51	98	117
Recovery Time (s)	71	25	204	148

Table 2.2 Summary of the result of LPG sensor based on the TiO_2 film

Sensing material	**Method**	**Doping/ Catalyst**	**Gas conc./ operating Temp.**	**Sensing Response (%)**	**Res./Rec. time (s)**	**Ref. No.**
TiO_2 thin film	CBD	p-poly-aniline	0.1 vol.%/ RT	63	440/180	Lee et. al.2002 [25]
TiO_2 thick film	CBD	Poly-pyrrole	260-1040 ppm/RT	55	112/131	Chakraborty et. al. 2006 [26]
TiO_2 thin film	Spray pyrolysis technique	Ni	1000 ppm/ 250 ^oC	90	300/600	Satyanarayana et. al. 2003 [27]
TiO_2 thin film	Spray pyrolysis deposition	_	0.02-0.08 vol.%/ 698 ^oC	35.8	1650/540	Iftimie et. al. 2009 [28]
TiO_2 thin film	_	Nb	_	18	4000/790	Bulakhe et. al. 2013 [29]
TiO_2 thin film	Sol-Gel	-	4 vol.% /RT	134	117/148	Present Work

Figures:

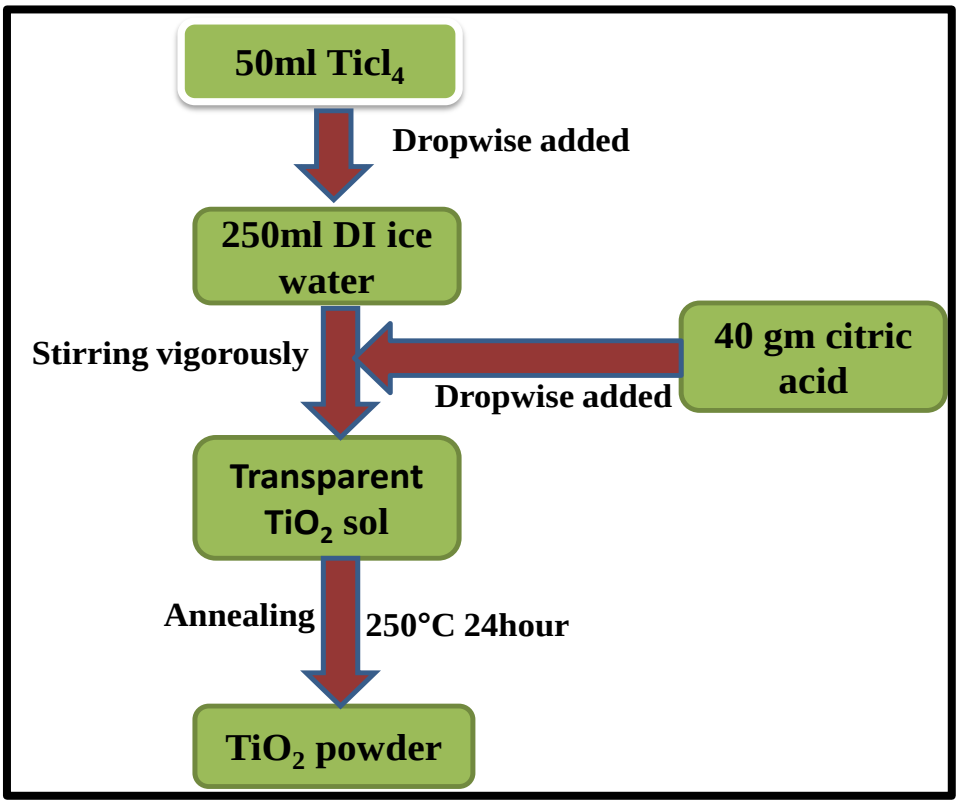

Figure 2.1: Preparation of TiO_2 powder by sol gel technique

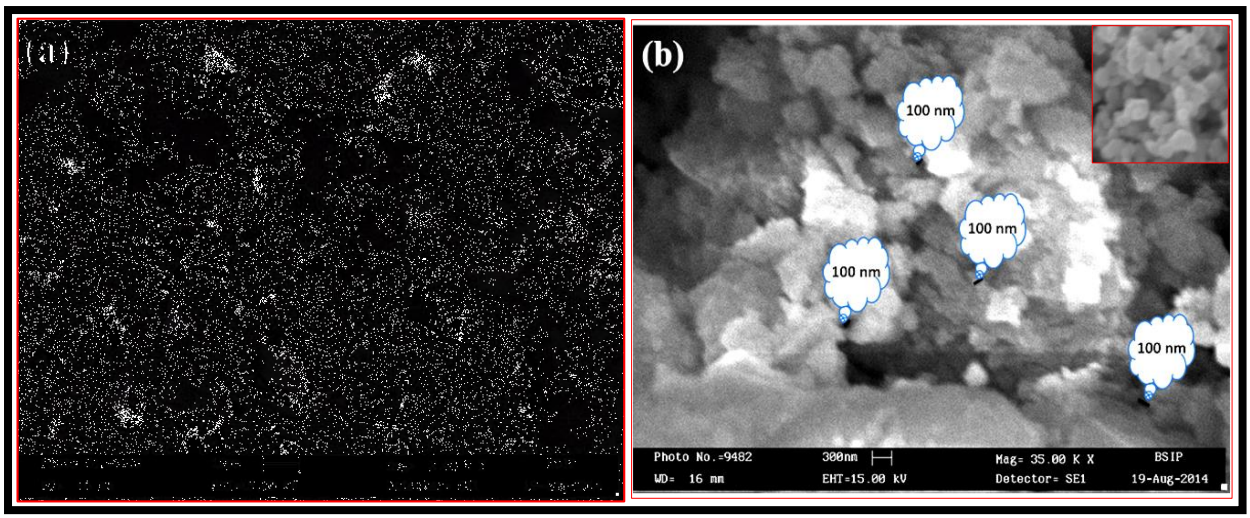

Figure 2.2: SEM image of TiO_2 thin film at **(a)** microscale **(b)** nanoscale

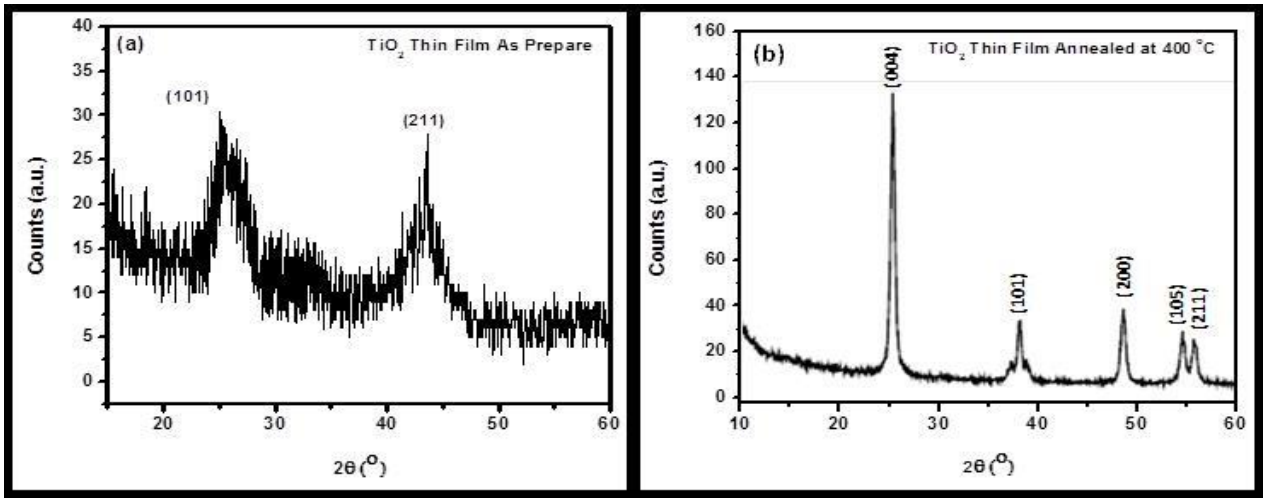

Figure 2.3: X-Ray Diffraction of synthesised TiO_2 thin film (a) as prepared (b) annealed at 400 ºC

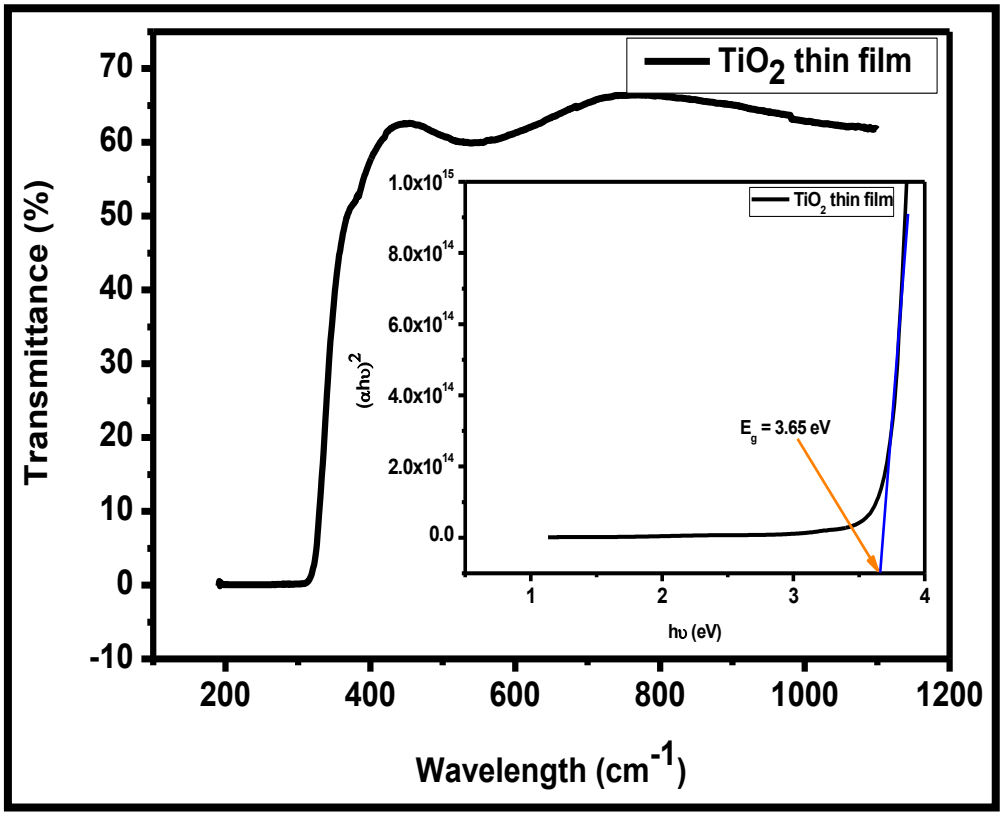

Figure 2.4: Transmittance spectra of TiO_2 thin film and Tauc plot of $(\alpha h\nu)^2$ versus $h\nu$

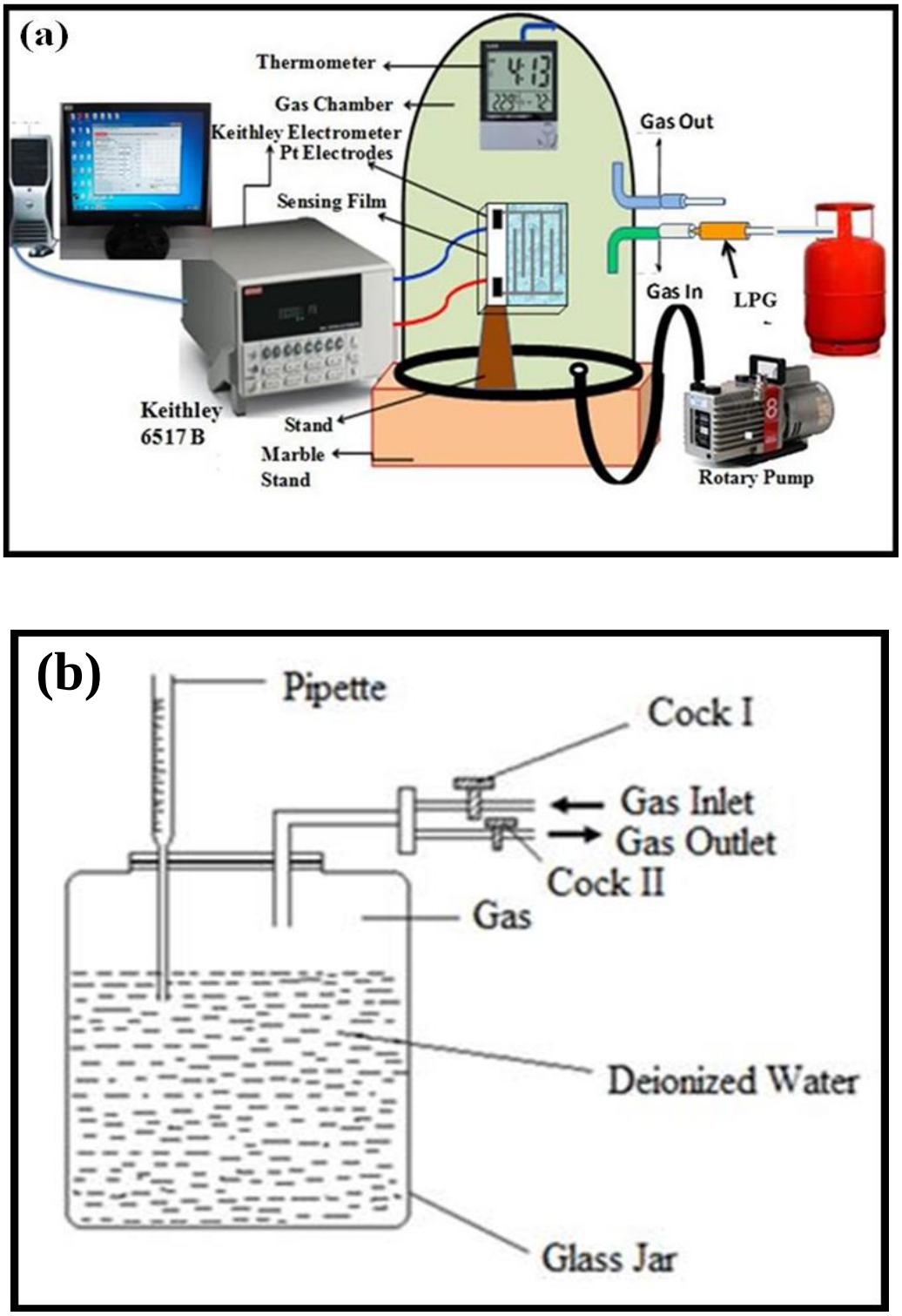

Figure 2.5: (a) Gas sensing set-up: Lab Model (**b)** Concentration measuring system

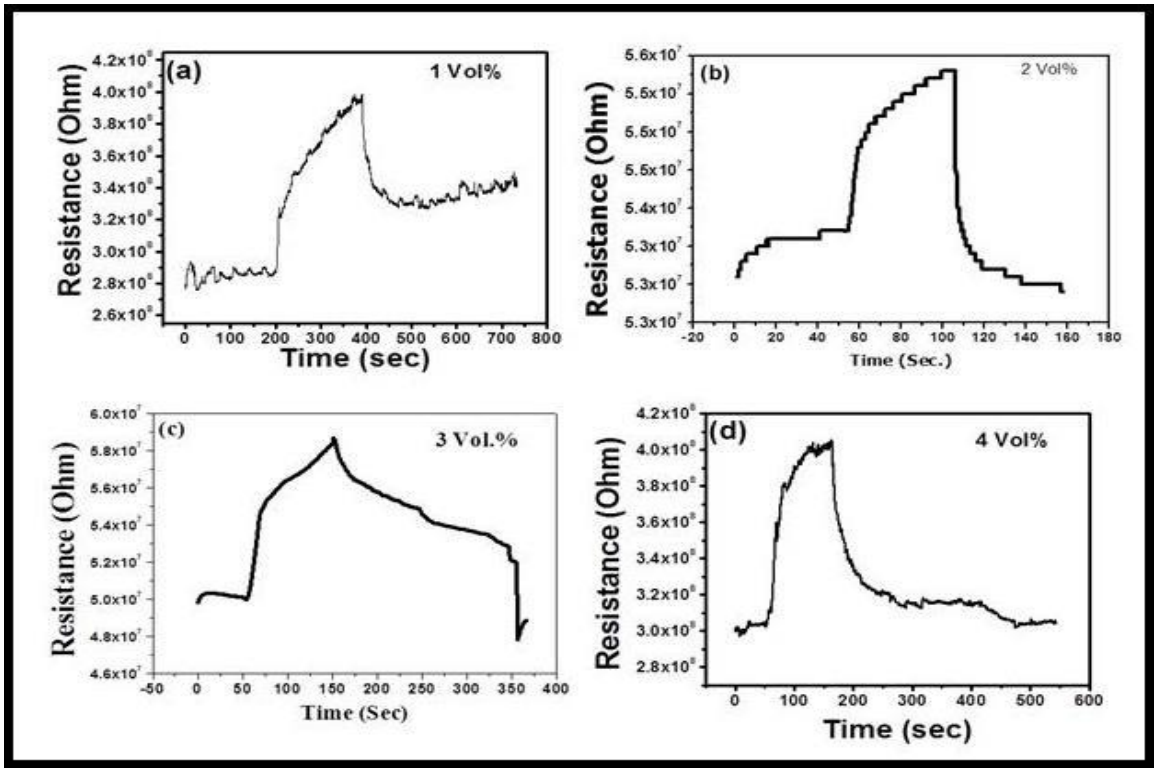

Fig. 2.6: Variations in resistance of TiO_2 thin film with time after exposure for different Vol.% of LPG.

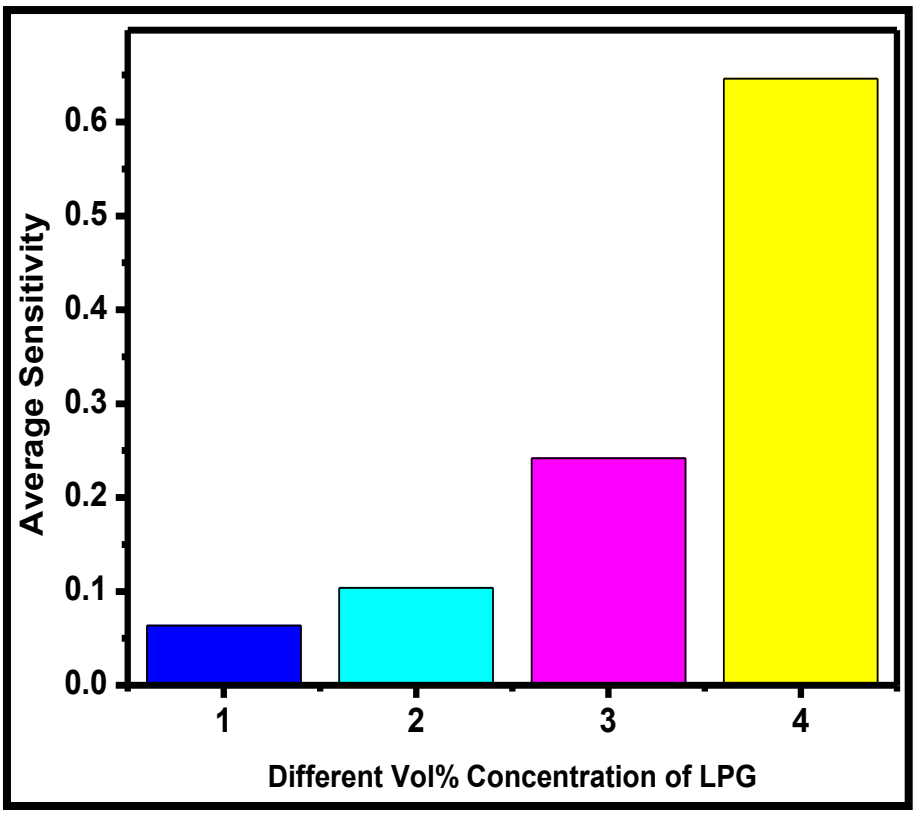

Fig. 2.7: Variations of average sensitivity of TiO_2 thin film with different concentrations of LPG

Chapter-3

Preparation of PANI doped TiO_2 nanocomposite thin film and its relevance as room temperature LPG and CO_2 sensors

Present chapter reports the utility of PANI doped titanium dioxide thin film prepared by spin coating technique as LPG, CO_2 sensing. The increasing needs of carbon dioxide and LPG detection in various fields like air quality control, greenhouse monitoring, bio-related process and industry, home appliance have been demanding high-quality CO_2, LPG sensors in day to day life. Optical properties were investigated using UV-vis absorption spectroscopy. The surface morphology and structure of synthesised material were characterised by TEM and XRD analysis, respectively. The structural analysis confirmed the formation of PANI-TiO_2 having an average crystallite size 7 nm. Variations in resistance with exposure of LPG to the sensing element were observed. Sensor response (S) as a function of time was calculated and its maximum value was found as 2.37 towards 2000 ppm of LPG, response time of the sensor was 120 s. Similarly, the sensor response (S) as a function of time was calculated and its maximum value was found as 53 for 1000 ppm of CO_2. Response and recovery times of the sensor were observed as 552 s and 342 s respectively. The sensor was quite sensitive and results were found reproducible.

3.1 Introduction

Liquefied Petroleum Gas (LPG) contains the hydrocarbons, majority propane and butane. The Lower Explosive Limit (LEL) as specified by National Institute for Occupational Safety and Health (NIOSH) and Occupational Safety and Health Administration (OSHA) standards for chemical hazards is average 20,000 ppm by volume 2.0% in air. The Permissible Exposure Limit (PEL) for LPG as specified by NIOSH and OSHA standards is 1000 ppm [1]. Global warming is a major concern of researchers because of the massive emissions of CO_2. Hence, the detection and control of CO_2 concentrations in the environment are necessary. The various kinds of materials are used for the detection of reducing LPG [2]. Among them, semiconducting metal oxides such as titania (TiO_2) [3], tin dioxide [4], iron oxide [5] and zinc oxide [6] have been studied extensively. TiO_2 as an n-type semiconducting metal oxide with two distinct phases; anatase and rutile, has been used for a broad range of LPG gas sensing [3-4]. PANI has been prepared by oxidation of the aniline or anilinium salts e.g. aniline hydrochloride or aniline sulphate, in aqueous acidic ambient [7]. It is a p-type semiconducting material [8] and has specific redox nature, controllable conductivity, and considerable thermal stability [9-10].

CO_2 sensors can be used in many applications, particularly, in air quality monitoring, agricultural production, clean energy technologies, engine exhausts, and chemical industries. Several types of CO_2 sensors, such as infrared [11-12], surface acoustic wave [13], solid electrolyte [14], capacitive [15-16] and resistive [17-18] sensors have been developed. Toxic gas molecules adsorbed on the surfaces of oxide materials create electron-depleted layers, which increase the sensor resistance. Among these sensing platforms, the resistive sensors based on metal oxides [19-22] have important advantages, such as good reliability, low cost, small size, and its potential in the

development of array-integrated gas sensors. Titanium dioxide based gas and moisture sensors have high sensitivity, good chemical stability and are easy to synthesise; therefore, this material has been extensively studied by earlier researchers [17, 20, 23-30]. In the case of CO_2 gas, the resistive sensor works due to change in electrical conductance of sensing material. As CO_2 is a chemically stable gas, therefore its detection with the resistive methods is more difficult than that of other reducing gases [31]. The demand for a convenient and low-cost sensor for continuously monitoring gaseous emissions from various processes is steeply growing. CO_2 is an oxidising gas. The literature survey shows that various metal oxides and their composites were investigated for developing the CO_2 gas sensor. Among them, semiconducting metal oxides such as CSA-TiO_2 composite [32], Cr-doped TiO_2 [33], SnO_2 thin film [34] and zinc oxide [35-36] have been studied extensively. Table 3.1 describes the sensors developed for the detection of CO_2 but one can find that sensor response is very poor. Also, there is a lack of sensitivity and selectivity.

The dynamical properties of the conductive polymer in the form of thin film coated on a metal oxide nanostructured film as substrate have attracted considerable interest in recent years [37-38].

In this work, for the first time, PANI-TiO2 nanocomposite thin film was prepared on a corning glass substrate and employed as LPG sensor and investigated PANI doped TiO_2 based sensor for the detection of CO_2 gas which can meet the basic requirement of current needs.

3.2 Experimental

3.2.1 Materials

Titanium tetrachloride ($TiCl_4$), propanol, deionized (DI)water, ethanol, aniline, HCl, ammonium persulphate and ammonium hydroxide used for the sensor preparation

were purchased from Sigma Aldrich Chemical Co. with 99.99% purity. Figure 3.1(a) shows the flow chart of the synthesis of TiO_2 nanoparticle solution and preparation of thin film. Figure 3.1(b) shows the flow chart of synthesis of PANI by using precursor aniline.

3.2.2 Synthesis of TiO_2 and Polyaniline

50 ml of $TiCl_4$ aqueous solution was added drop wise to 250 ml of ice-water at room temperature under vigorous stirring to obtain dilute $TiCl_4$ aqueous solution. Then 40 g of citric acid was added to it which made it a transparent solution. After annealing at 250 ºC for 24 h, TiO_2 in powder form was obtained.

3.5 M conc. HCl was added to 500 ml distilled water in a beaker marked as A. 331 ml of distilled water was taken and to it and 0.1 M ammonium persulphate was added and stirred in another beaker marked as B. To beaker A, 0.25 M of aniline was added and stirred for 20 min in ice bath. The drop wise ammonium persulphate solution was then added to the above solution with continuous stirring. After complete addition, the solution was left overnight and then filtered. The precipitate was washed with water repeatedly till the filtrate became colourless and after washing, it was left overnight. The precipitate was then dried at 40-50 ºC and made into fine powder. The fine powder was then washed with methanol, refluxed for 4-5 h at 40-50 ºC. It was again dried at 40-50 ºC to obtain emeraldine salt of PANI. To un-doped emeraldine salt, it was washed with ammonium hydroxide solution (25%) three times, filtered and dried to obtain emeraldine base of PANI [39-40].

3.2.3 Fabrication of PANI-TiO_2 nanocomposite thin film sensor

The prepared PANI (0.061 g) was added into TiO_2 colloidal by 1% and 3% concentration solution. The PANI-TiO2 composite solution was prepared at 100 ºC in air for 4 h. TiO_2 colloidal solution and PANI-TiO2 composite solution were used to deposit the films on corning glass and platinum (Pt) inter digital electrode (IDEs) patterned

corning glass substrates by spin coating technique. The Pt-IDEs [41] were patterned over the corning glass substrates using conventional photolithography technique prior to deposition of sensing layers. The platinum thin film of 90 nm thickness was deposited by RF sputtering using platinum metal target in 100% Ar. In order to improve the adhesion of Pt on corning glass substrate an ultra-thin (10 nm) buffer layer of Titanium was sputtered prior to Pt deposition. After every coating, the samples were pyrolized at 100 ^{o}C to evaporate the precursor. In the present work, thin film prepared using TiO_2 colloidal solution and PANI doped TiO_2 solutions were indexed as pure TiO_2 and PANI-TiO2 respectively. Thickness of the film was measured by using Dektak profile meter (Veeco Dektak 150 surface profiler). For the gas sensing application, films were deposited on inter digital electrode (IDEs) patterned corning glass substrates by spin coating of the respective solutions. Variations in resistance with the variation in concentration of LPG were recorded using Keithley Electrometer [Model: 6517 B].

3.3 Characterization

X-ray diffraction (XRD) studies were carried out using an X-ray diffractometer (X-Pert, PRO PANalytical XRD system, Nether land). The XRD patterns were recorded in the 2θ range of 10-70° with a step width of 0.02° and step time as 0.9 sec using $CuK\alpha_1$ radiation (λ = 0.15418 nm). The morphology of the PANI and PANI-TiO_2 films were examined using Transmission Electron Microscope (Tecnai G2 Spirit, TWIN). UV-Vis spectra of the samples dispersed in de-ionized water in an ultrasonic bath were recorded using Thermo Evolution 201 UV-Visible spectrophotometer.

3.3.1 Scanning Electron Microscopy (SEM)

Figures 3.2 (a-f) shows the SEM images of pure PANI, TiO_2 and PANI-TiO2 composite thin films at different scales and resolutions. The SEM image of the pure PANI film shown in Figure 3.2 (a & b) on 10 μm and 5 μm scales respectively exhibits a fibrous

structure with many pores. Figure 3.2(c) shows the hexagonal shaped surface morphology of the TiO_2 thin film annealed at 500 °C for 2 h. The SEM image of the composite thin film is shown in Figure 3.2 (d & f) on different scales with non-uniform and uniform agglomerate distribution of the PANI in TiO_2 thin film matrix. It can be seen that the PANI chains are closely surrounded by the mesh-like structure built by TiO_2 nanoparticles. The obtained rough and porous morphology of prepared thin films as shown in Figure 3.2(e) provide the high surface to volume ratio which enhanced the sensing response. The elemental analysis of PANI-TiO_2 composite film has been recorded by EDX and is shown in Figure 3.2 (f). Polyaniline layers on the TiO_2 NPs surface are attached together and generate the porous PANI-TiO_2 nanocomposite. In fact, such structure has been created from the TiO_2 NPs present in the course of the enzymatic polymerization process. This is a result of polymer growth on the surface of nanoparticles. In addition, it is easy to control the composite structure using various types and shapes of metal oxide nanomaterials. Since composites made from metal oxide nanomaterials exhibit essential stability (owing to metal oxide nanomaterial structures) and polymer film growth is efficiently stable, this approach can be successfully employed for sensing purposes [42-43].

3.3.2 Transmission Electron Microscopy (TEM)

The TEM images of PANI-TiO_2 nanocomposite are shown in Figure 3.3(a-b). TEM images of the composite samples reveal that the TiO_2 particles were embedded in PANI forming the core-shell structure. Due to the different electron penetrability, the light core was the TiO_2 particles, and the black coloured shell was PANI in the composite.

3.3.3 X-Ray Diffraction

The crystal structure and phase of the composite thin film was analysed using X-ray diffractometer (X-Pert, PRO PANalytical XRD system, Netherland) with CuK_α

radiations as a source having wavelength 1.5418 Å. X-Ray diffraction pattern of as-prepared material shown in Figure 3.4 reveals the tetragonal phase. The average crystallite size (*D*) of the sensing material can be calculated by the Debye-Scherer's formula, which is given by [32]:

$$D = \frac{K\lambda}{\beta cos\theta} \quad (1)$$

Where, K= 0.94 is a Scherer's coefficient, which depends on the shape of the crystallite and the type of defects present, λ is the wavelength of X-ray radiation, β is the full width at half maximum (FWHM) of the diffraction peak and θ is the angle of diffraction.

X-Ray diffraction pattern of composite PANI-TiO_2 as shown in Figure 3.4 reveals that the sensing material consists of peaks observed at 2θ = 25.37º, 38.12º, 48.00º, 54.20º and 62.70º correspond to (101), (112), (200), (211) and (204) reflection planes, respectively and are in good agreement with the corresponding values reported by the JCPDS card no. 01-086-1157. The average crystallite size of the composite film was found 7 nm. The reduced crystallite size provides a large surface to volume ratio, hence the ability for adsorption of gas through the pores on the surface of the thin film increases which enhances the sensitivity of the gas sensor.

3.3.4 UV-Visible Spectroscopy

The optical transmission spectra of the as-grown TiO_2 thin film (200 nm) deposited separately on the glass substrate was investigated in the wavelength range of 190 to 1100 nm, and the variation in % transmittance is shown in Figure 3.5. TiO_2 and PANI-TiO_2 thin films exhibit a high transmission (90-74%) in the visible region and show a sharp fundamental absorption edge in UV region at 340 nm.

The optical energy band gap was calculated by Tauc relation as given below:

$$\alpha h\nu = A(h\nu - E_g)^{\frac{1}{2}} \quad (2)$$

Where, A is a constant, hν is the photon energy, E_g is the energy band gap and α is the absorption coefficient given by:

$$\alpha = 2.303 \left(\frac{A_b}{t}\right) \quad (3)$$

In Eq. 3, A_b is the absorbance and t is the thickness of the film. Optical band gaps of the PANI and (1%) PANI-TiO_2 thin film deposited on corning glass substrates were calculated from the intercept on energy axis obtained by extrapolating the linear portion of the Tauc plot i.e. $(\alpha h\nu)^2$ *vs* photon energy (*hν)* as shown in the inset of Figure 3.5. Estimated value of band gap for the as-grown TiO_2 thin film is found to be 3.88 eV which is close to the actual values for TiO_2 thin films (3.71 eV) grown by various other techniques [44]. The variation in band gap shows the electronic interaction between TiO_2 and PANI confining the formation of the PANI-TiO_2 composite thin film.

3.3.5 FTIR spectra of pure PANI and PANI doped TiO_2 nanocomposites

FTIR spectra of pure PANI and PANI-TiO_2 composites are shown in Figure 3.6. Spectra of Figure 3.6(a) exhibits the characteristic peaks of pure PANI appeared at 1631, 1471, 1292 and 1121 cm^{-1}. Figure 3.6(b) shows that in PANI-TiO_2 composite, the adsorption band of composite exists between 448 and 541 cm^{-1} which are attributed to Ti–O stretching and Ti–O–Ti bridging stretching modes [45]; the bonds at 1211 and 968 cm^{-1} are assigned to C–O–C stretching vibration of benzenoid ring and Ti–O–C stretching mode. The broad bond in the region of 3439 and 2086 cm^{-1} is assigned to the binding vibration of H–O–H and O–H stretching vibration of the physically adsorbed water molecules [46]. The bond at 1043 cm^{-1} is due to a quinoid mode of PANI and the band at 1124 cm^{-1} is assigned to an in-plane bending vibration of C–H which is formed during doping [47]. The bonds at 1633 and 1464 cm^{-1} correspond to the stretching modes of the C=C and C–N bonds of the benzenoid rings; the bonds 1398 and 1257 cm^{-1} correspond to

the amine stretching vibration. These characteristic bonds confirm that PANI has Emeraldine salt phase.

3.4 Gas Sensing

3.4.1 CO_2 gas sensing mechanism

The detail of LPG sensing set-up has already been reported in Chapter 2 (Section 2.4) and when the LPG was introduced to the chamber, the variations in electrical resistance with the time were recorded using the Keithley electrometer (Model: 6517 B).

Figures 3.7(a-d) illustrate the variations in resistance of the film with time after exposure for 2000 ppm of LPG at room temperature. Figure 3.7(a) shows the sensing response of the bare TiO_2 thin film to 2000 ppm of LPG purged in the chamber. It is obvious that the variations in resistance are smaller at the time just after the exposure while after 200 s the resistance increases rapidly. It can also be observed that the pure TiO_2 thin film sensor did not recover back to its initial resistance while as LPG was exposed to doped polyaniline (PANI) in TiO_2; sensor recovered back its initial resistance. From Figure 3.7 (b & c), it is obvious that the sensing responses for PANI-TiO_2 (1%) and PANI-TiO2 (3%) doped thin film at 2000 ppm of LPG are the improvements over the previous. During the three repeated injections of gas, its maximum response did not change. Among all the curves corresponding to the three repetitions, the second one is enlarged in Figure 3.7(d) in order to determine the response time and recovery time of the gas sensor. The gas sensor showed excellent sensing response ~2.37 having response and recovery times as 2.6 and 2.4 min respectively [48].

The resistance of TiO_2 thin film sensor structures in the present study increases when impinging gas (LPG) molecules interact with the sensor surface. When LPG is exposed to the sensing surface, the resistance of film is increased due to capture of

electrons from the adsorption sites on the surface, results the reduction in number of electrons in the conduction band [49].

A space charge region is created between the semiconducting metal oxide layer and the polymer due to electronic interaction between them. Catalyst on the surface of semiconducting oxide act as receptors while the semiconductor oxide as a transducer for the changes taking place at the surface under the adsorption of target gas. The oxidation state of the polymer changes with the gas interaction, inducing the corresponding change in the electronic state of the semiconducting oxide layer. The Schematic diagram of sensing mechanism along with the set-up is shown in Figure 3.8.

Presence of PANI on the surface of TiO_2 thin film in the form of clusters may dissociate the impinging LPG molecules and activate the spillover mechanism. The dissociated reducing gas species spillover onto the surface of the uncovered TiO_2 semiconductor and interact with the adsorbed oxygen present in the form of ions. The reaction of LPG molecules with adsorbed oxygen can be explained as follows;

$$C_n H_{2n+2} + 2O^- \leftrightarrow H_2O + C_nH_{2n} - O + e^- \quad (4)$$

The interaction of the reducing gas species with the chemisorbed oxygen results in the release of trapped electrons, thereby decreasing the electron carrier concentration in the conduction band of the TiO_2 sensing layer.

The schematic diagram of CO_2 sensing set-up is shown in Figure 3.10. The sensing film was inserted between the platinum electrodes inside the glass chamber. Sensing film with IDEs was used for studying the sensing properties of CO_2. The resistance of the film in the presence of air (R_a) was taken as stabilised resistance. When CO_2 was introduced into the chamber, the variations in electrical resistance with the time for CO_2 were recorded by using Keithley electrometer (Model: 6517 B).

The sensing response is defined as the change in resistance in the presence of gas (R_g) to the resistance in the presence of air (R_a) [50], that is;

$$S = \frac{R_g}{R_a} \tag{5}$$

Figures 3.9(a-d) illustrate the variations in resistance of the film with time after exposure to 1000 ppm of CO_2 at room temperature. Figure 3.9(a) shows the increase in resistance with time after exposure of CO_2 gas regain its initial position after removal of the gas. Small variations in resistance result in the variation in sensor response and clearly may be seen by the curves. From Figure 3.9(b & c), it is obvious that the sensing responses for (1%) PANI-TiO_2 and (3%) PANI-TiO_2 doped thin film at 1000 ppm of CO_2 was an improvement over the previously reported work [51]. Figure 3.9(d) shows that during the five repeated injections of gas, its maximum response did not change. The gas sensor showed the excellent sensing response of about 53 with a response and recovery time characteristics, i.e. 9.2 and 5.7 min for 90% of its full response and recovery, respectively.

On the basis of characterization and sensing results obtained, a plausible CO_2 sensing mechanism is discussed here. When CO_2 interacts with metal oxide semiconductor [52-53] following reaction will take place:

$$CO_{2(g)} + OH^- \leftrightarrow HCO^-_{3(surface)} \tag{6}$$

$$HCO^-_{3(surface)} + OH^- \leftrightarrow CO^{2-}_{(bulk)} + H_2O_{(g/surface)} \tag{7}$$

$$CO_2 + O^{2-} \rightarrow CO_3^{2-} \tag{8}$$

The CO_2 sensing mechanism involved in this metal oxide (TiO_2) based resistive sensor device relies on the metal bicarbonate/carbonate ↔ CO_2 equilibrium. This suggests that easy metal hydrogen carbonate formation at the operating temperature of the sensor is a prerequisite for applying TiO_2 as sensing layer in the resistive CO_2 sensor. When target gas (CO_2) was inserted in the chamber, the resistance of the film increases

because of the oxidising behaviour of CO_2 gas. TiO_2 responds to CO_2 gas in the following way:

$$CO_2 + TiO_2 \xrightarrow{\text{adsorption}} Ti^{4+} + CO_3^{2-} + O^{2-} \xrightarrow{\text{desorption}} TiO_2 + CO_2 \qquad (9)$$

On the TiO_2 surface, CO_2 gas reacts with Ti sites and captures electrons from conduction band resulting in a decrease in conductivity thus increasing the resistance of the film [54]. It can also be explained as CO_2 gas is exposed to the pure TiO_2 surface, it reacts with the surface adsorbed active oxygen species and is oxidised in the sensing reaction (the metal surface is reduced). Due to this oxidising process, excess electrons return to the valence band of the material and decrease the resistance of the n-type TiO_2 gas sensor. However, the majority of charge carriers in higher PANI concentrations (1 and 3 % PANI) loaded with TiO_2 are holes. When CO_2 gas was exposed to film at room temperature, the gas molecules react with the adsorbed oxygen species on the surface of the sensor. Therefore, electron-donating nature of the oxygen injects captured electrons (due to the oxidation of CO_2 molecules) back to the valence band, which recombine with the holes and decrease the charge carrier (hole) concentration, leading to an increase in the resistance of 1 and 3 % PANI doped TiO_2 sensor. As shown in Figure 3.9, 1% PANI doped TiO_2 based sensor has a higher response to CO_2. This sensor material may have a sufficient number of active PANI sites on the TiO_2 surface. Furthermore, the dispersed PANI nanoparticles can change the electron Debye length, while the discrete particles simultaneously affect the gas surface properties; leading to the higher CO_2 response of the 1 % PANI doped TiO_2. The enhanced CO_2 sensing properties of the PANI doped material can also be explained by active reaction site generation, the spillover effect, enhancement of chemisorptions and porous flower-like morphology. Table 3.1 gives a comparison of sensing properties to our material and other materials reported in the open literature.

3.4.2 LPG sensing mechanism:

The gas sensing mechanism of TiO_2 thin film based sensor belongs to a surface controlled type, i.e. resistance change is controlled by surface area and the amount of chemisorbed oxygen. LPG consists of CH_4, C_3H_8, and some other hydrocarbons. In each composition, the reducing hydrogen species are bound to carbon atom, therefore, LPG dissociates into the reactive reducing components hardly on the surface of the sensing element. As LPG exposed to sensing element, the conductivity increases due to adsorption of oxide and capture more electrons that contribute to reducing the current [55]. It was observed that as the concentration of LPG increases, the average sensitivity increases linearly in the beginning and later, it becomes saturated. The linear relationship between sensitivity and gas concentration may be attributed to the availability of a sufficient number of sensing sites on the film to act upon the LPG. The low concentration implies a lower surface coverage of gas molecules, resulting in a lower surface reaction between the surface adsorbed oxygen species and the gas molecules. The increase in LPG concentration increases the surface reaction due to a large surface coverage. Further, increase in the LPG concentration does not increase the surface reaction and eventually, saturation takes place.

The response was measured 2.77 up to 1% PANI doped TiO_2 based sensor in order to detect the LPG below LEL for safety requirement. The response and recovery times were obtained as 2.6 min and 2.4 min respectively. The sensing mechanism of LPG is reported in previous chapter 2 with the diagram of experimental set-up.

3.5 Conclusion

PANI-TiO_2 composite thin films were successfully fabricated and employed as LPG sensor at room temperature. PANI-TiO_2 (1%) thin film sensor structure exhibited the maximum sensing response ~ 2.37 with a response and recovery times of 2.6 and 2.4

min, respectively. Thus this sensor structure can be proven as a next step for developing an LPG sensor at commercial level operable at room temperature.

PANI-TiO_2 composite thin films were successfully fabricated and employed as a CO_2 sensor at room temperature. (1%) PANI-TiO_2 thin film sensor structure exhibited the maximum sensing response of ~ 53 with a response and recovery times of 9.2 and 5.7 min, respectively. However, the sensing responses as 1.77 and 7.76 were obtained for pure TiO_2 and PANI-TiO_2 (3%) sensor structures respectively towards 1000 ppm of CO_2 gas. Thus this sensor structure can be reliably used for the detection of CO_2 gas. (1%) PANI-TiO_2 thin film sensor structure exhibited the maximum sensing response of ~ 2.37 with a response and recovery times of 2.6 and 2.4 min.

References:

[1] https://www.osha.gov/dts/chemicalsampling/data/CH_249630.html

[2] S. Singh, B.C. Yadav, M. Singh, and R. Kothari, A review report on nanostructured ferrites as liquefied petroleum gas sensor, Inter. J. of Science, Technology & Society, 1, 1 (2015) 5-21.

[3] N. Verma, S. Singh, R. Srivastava, B.C. Yadav, Fabrication of iron titanium oxide thin film and its application as opto-electronic humidity and liquefied petroleum gas sensors, Optics & Laser Technology, 57 (2014) 181-188.

[4] R.K. Sonker, B.C. Yadav, Chemical Route Deposited SnO_2, SnO_2-Pt and SnO_2-Pd Thin Films for LPG Detection, Advanced Science Letters, 20 (2014) 1023-1027.

[5] R.K. Sonker, B.C. Yadav, Low temperature study of nanostructured Fe_2O_3 thin films as NO_2 sensor, Materials Today: Proceedings, 3 (2016) 2315-2320.

[6] R.K. Sonker, B.C. Yadav, A. Sharma, M. Tomar, V. Gupta, Experimental investigations on NO_2 sensing of Pure ZnO and PANI-ZnO composite thin films, RSC Advances, 6 (2016) 56149-58.

[7] J. Stejskal, R.G. Gilbert, Polyaniline. Preparation of conducting polymer, Pure Appl. Chem., 74 (2002) 857-867.

[8] D.N. Huyen, N.T. Tung, N.D. Thien, L.H. Thanh, Effect of TiO_2 on the gas sensing features of TiO_2/PANI nanocomposites, Sensors, 11 (2011) 1924-1931.

[9] A.H. Gemeay, R.G.E. Sharkawy, I.A. Mansour, A.B. Zaki, Preparation and characterization of polyaniline/manganese dioxide composites and their catalytic activity, J. Colloid Interface Sci., 308 (2007) 385-394.

[10] R.K. Sonker, B.C. Yadav, G. Dzhardimalieva, Preparation and Properties of Nanostructured PANI Thin Film and Its Application as Low Temperature NO_2 Sensor, J. Inorg. Organomet. Polym., 26 (2016) 1428-1433.

[11] M.I. Baraton, FTIR surface study of nanosized ceramic materials used as gas sensors, Sens. Actuators B: Chem., 31 (1996) 33-38.

[12] L. Joly, B. Parvitte, V. Zeninari, G. Durry, Development of a compact CO_2 sensor open to the atmosphere and based on near-infrared laser technology at 2.68m, Appl. Phys. B 86 (2007) 743-748.

[13] M.S. Nieuwenhuizen, A.J. Nederlof, A SAW gas sensor for carbon dioxide and water, Preliminary experiments, Sens. Actuators B: Chem., 2 (1990) 97-101.

[14] Y. Sadaoka, NASICON based CO_2 gas sensor with an auxiliary electrode composed of Li_2CO_3 metal oxide mixtures, Sens. Actuators B: Chem., 121 (2007) 194-199.

[15] K.G. Ong, C.A. Grimes, A carbon nanotube-based sensor for CO_2 monitoring, Sensor, 1 (2001) 193-205.

[16] A. Marsal, A. Cornet, J.R. Morante, Study of the CO and humidity interference in La doped tin oxide CO_2 gas sensor, Sens. Actuators B: Chem., 94 (2003) 324-329.

[17] B.C. Yadav, K. Agrahari, S. Singh, T.P. Yadav, Fabrication and characterization of nanostructured indium tin oxide film and its application as humidity and gas sensors, J. of Mat. Science: Mat. in Electronics, 27 (2016) 4172-4179.

[18] A. Marsal, G. Dezanneau, A. Cornet, J.R. Morante, A new CO_2 gas sensing material, Sens. Actuators B: Chem. 95 (2003) 266-270.

[19] R.K. Sonker, B.C. Yadav, Low temperature study of nanostructured Fe_2O_3 thin films as NO_2 sensor, Materials Today: Proceedings, 3 (2016) 2315-2320.

[20] B.C. Yadav, N. Verma, S. Singh, Nanocrystalline SnO_2-TiO_2 thin film deposited on base of equilateral prism as an opto-electronic humidity sensor, Optics & Laser Tech., 44 (2012) 1681-1688.

[21] R.K. Sonker, B.C. Yadav, A. Sharma, M. Tomar, V. Gupta, Experimental investigations on NO_2 sensing of Pure ZnO and PANI-ZnO composite thin films, RSC Advances, 6 (2016) 56149-56158.

[22] Y.K. Mishra, G. Modi, V. Cretu, V. Postica, O. Lupan, T. Reimer, Direct growth of freestanding ZnO tetrapod networks for multifunctional applications in photocatalysis, UV photodetection and gas sensing, ACS Appl. Mater. Interfaces **7** (2015) 14303-14316.

[23] M. Enachi, O. Lupan, T. Braniste, A. Sarua, L. Chow, Y.K. Mishra, Integration of individual TiO_2 nanotube on the chip: Nanodevice for hydrogen sensing, physica status solidi (RRL) Rapid Research Letters, 9 (2015) 171-174.

[24] B.C. Yadav, R. Srivastava, C.D. Dwivedi, Synthesis and characterization of ZnO-TiO_2 nanocomposite and its application as a humidity sensor, Philosophical Magazine, 88 (2008) 1113-1124.

[25] J. Jawalkar, P. More, S.R. Damkale, R. Kumar, B.C. Yadav, A.K. Vishwanath, S.H. Sonawane, P.K. Khanna, Effect of Organic Chromophore on Nano-Sized TiO_2:Optical Properties and Humidity Sensing, I. Jour. of Green Nanotechnology: Phy. and Chemistry, 1 (2009) 40-50.

[26] P. More, R. Kumar, B.C. Yadav, P.K. Khanna, Synthesis and Optical Properties of Anatase-TiO_2 Nanoparticles in Commercial Poly(methyl methacrylate): A Green Approach for Wider Acceptability?, I. Jour. of Green Nanotechnology: Mat. Sci. & Eng., 1 (2009) 3-10.

[27] C. Xiang, Z. She, Y. Zou, J. Cheng, H. Chu, S. Qiu, A room-temperature hydrogen sensor based on Pd nanoparticles doped TiO_2 nanotubes, Ceramics International, 40 (2014) 16343-16348.

[28] H. Lee, S. In, M.W. Horn, Plasmonic enhancement of CO_2 conversion to methane using sculptured copper thin films grown directly on TiO_2, Thin Solid Films, 565 (2014) 105-110.

[29] Z. Han, J. Wang, L. Liao, H. Pan, S. Shen, J. Chen, Phosphorus-doped TiO_2 as oxygen sensor with low operating temperature and sensing mechanism, Applied Surface Science, 273 (2013) 349-356.

[30] D. Biskupski, B. Herbig, G. Schottner, R. Moos, Nanosized titania derived from a novel sol-gel process for ammonia gas sensor applications, Sens. Actuators B: Chem., 153 (2011) 329-334.

[31] R.K. Sonker, B.C. Yadav, Chemical Route Deposited SnO_2, SnO_2-Pt and SnO_2-Pd Thin Films for LPG Detection, Adv. Sci. Lett. 20 (2014) 1023-1027.

[32] S. Hafeez, X, Fan, A. Husain, C. F. Martin, CO_2 adsorption using TiO_2 composite Polymeric membranes: A kinetic study, Journal of environmental Sciences 35 (2015) 163-171.

[33] D. Madare, N. Cornei, C. Mita, D. Florea, A. Stancu, A. Manole, C. Adomnitel, Low temperature TiO_2 based gas sensors for CO_2, Ceramic International 42 (2016) 7353-7359.

[34] R.K. Sonker, A. Sharma, M. Tomar, V. Gupta, B. C. Yadav, Low temperature operated NO_2 gas sensor based on SnO_2–ZnO nanocomposite thin film, Adv. Sci. Lett. 20 (2014) 911-916

[35] R.K. Sonker, B.C. Yadav, Growth mechanism of hexagonal ZnO nanocrystals and their sensing application, Materials Letters., 160 (2015) 581-584.

[36] Y.J. Jeong, C. Balamurugan, D.W. Lee, Enhanced CO_2 gas-sensing performance of ZnO nanopowder by La loaded during simple hydrothermal method, Sens. Actuators B: Chem., 229 (2016) 288-296.

[37] Y.J. Jeong, X. Shi, A. Lu, J. Cai, L. Zhang, H. Zhang, J. Li, X. Wang, Rheological behaviours and miscibility of a mixture solution of polyaniline and cellulose, dissolved in an aqueous system, Bio-macromolecules, 13 (2012) 2370-2378.

[38] A.G. MacDiarmid, Synthetic metals: a novel role for organic polymers (Nobel lecture), Angew. Chem. Int. Ed. 40 (2001) 2581-2590.

[39] B.C. Yadav, N. Verma, S. Singh, Nanocrystalline SnO_2-TiO_2 thin film deposited on the base of the equilateral prism as an optoelectronic humidity sensor, Optics & Laser Technology, 44 (2012) 1681-1688.

[40] R.K. Sonker, B.C. Yadav, Development of Fe_2O_3–PANI nanocomposite thin film based sensor for NO_2 detection, J. Taiwan Ins. of Chemical Eng.77 (2017) 276-281.

[41] R.K. Sonker, S.R. Sabhajeet, B.C. Yadav, PANI-TiO2 nanocomposite thin film prepared by spin coating technique as room temperature CO_2 gas sensing, J. Mater Sci: Mater Electron, 27 (2016) 11726-11732.

[42] R.K. Sonker, A. Sharma, M. Shahabuddin, M. Tomar, V. Gupta, Low temperature sensing of NO_2 gas using SnO_2-ZnO nanocomposite sensor, Adv. Mat Lett, 4 (2013) 196-201.

[43] H. Xu, X. Chen, J. Zhang, J. Wang, B. Cao, D. Cui, NO_2 gas sensing with SnO_2-ZnO/PANI composite thick film fabricated from porous nanosolid, Sens. Actuators B: Chemi., 176 (2013) 166-173.

[44] S. Radhakrishnan, C.R. Siju, D. Mahanta, S. Patil, G. Madras, Conducting polyaniline-nano-TiO_2 composites for smart corrosion resistant coatings, Electrochimica Acta, 54 (2009) 1249-1254.

[45] A.G. Yavuz, A. Gok, Preparation of TiO_2/PANI composites in the presence of surfactants and investigation of electrical properties, Synthetic Metals, 157 (2007) 235-242.

[46] J.G. Yu, Y.R. Su, B. Cheng, M. Zhou, Enhanced photocatalytic activity of TiO_2 (P25) by hydrothermal treatment, J. Mol. Catal. A-Chem., 258 (2006) 104-112.

[47] D.S. Warren, A.J. Mc-Quillan, Influence of adsorbed water on phonon and UV-induced IR absorptions of TiO_2 photocatalytic particles films, J. Phys. Chem. B, 108 (2004) 19373-19379.

[48] R.K. Sonker, B.C. Yadav, S.R. Sabhajeet, Preparation of PANI doped TiO_2 nanocomposite thin film and its relevance as room temperature liquefied petroleum gas sensor, Mater Sci: Mater Electron, (2017) DOI 10.1007/s10854-017-7309-4.

[49] B.C. Yadav, K.S. Chauhan, S. Singh, R.K. Sonker, S. Sikarwar and R. Kumar, Growth and characterization of sol–gel processed rectangular shaped nanostructured ferric oxide thin film followed by humidity and gas sensing, J. Mater. Sci: Mater Electron, 28 (2017) 5270-5280.

[50] M. Singh, B.C. Yadav, A. Ranjan, R.K. Sonker, M. Kaur, Detection of liquefied petroleum gas below lowest explosion limit (LEL) using nanostructured hexagonal strontium ferrite thin film, Sens. Actuators B: Chemi., 249 (2017) 96-104.

[51] I. Karaduman, M. Demir, D.E. Yıldız, S. Acar, CO_2 gas detection properties of a TiO_2/Al_2O_3 heterostructure under UV light irradiation., Phys. Scr. 90 (2015) 055802.

[52] D.H. Kim, J.Y. Yoon, H.C. Park, K.H. Kim, CO_2-sensing characteristics of SnO_2 thick film by coating lanthanum oxide, Sens. Actuators B: Chem., 62 (2000) 61-66.

[53] J. Herrán, G.G. Mandayo, E. Castaño, Solid state gas sensor for fast carbon dioxide detection, Sens. Actuators B: Chem., 129 (2008) 705-709.

[54] J. Herrán, G.G. Mandayo, I. Ayerdi, E. Castaño, Influence of silver as an additive on $BaTiO_3$-CuO thin film for CO_2 monitoring, Sens. Actuators B: Chem., 129 (2008) 386-390.

[55] B.C. Yadav, A. Yadav, T. Shukla, S. Singh, Experimental investigations on solid state conductivity of cobalt zincate nanocomposite for liquefied petroleum gas sensing, Sens. Lett. 7 (2009) 1.

[56] J. Herrán, G.G. Mandayo, I. Ayerdi, E. Castaño, Influence of silver as an additive on $BaTiO_3$–CuO thin film for CO_2 monitoring, Sens. Actuators B: Chem., 129 (2008) 386-390.

[57] A. Chapelle, F.O. Hassani, L. Presmanes, A. Barnabe, P. Tailhades, CO_2 sensing properties of semiconducting copper oxide and spinel ferrite nanocomposite thin film, Applied Surface Science, 256 (2010) 4715-47159.

[58] T. Krishnakumar, R. Jayaprakash, T. Prakash, D. Sathyaraj, N. Donato, S. Licoccia, et al., CdO-based nanostructures as novel CO_2 gas sensors, Nanotechnology, 22 (2011) 325501.

[59] C.J. Chiang, K.T. Tsai, Y.H. Lee, H.W. Lin, Y.L. Yang, C.C. Shih, et al., In situ fabrication of conducting polymer composite film as a chemical resistive CO_2 gas sensor, Microelectronic Engineering, 111 (2013) 409-415.

[60] K. Fan, H. Qin, L. Wang, L. Ju, J. Hu, CO_2 gas sensors based on $La_{1-x}Sr_xFeO_3$ nanocrystalline powders, Sens. Actuators B: Chem., 177 (2013) 265-269.

[61] M. Habib, S.S. Hussain, S. Riaz, S. Naseem, Preparation and Characterization of ZnO Nanowires and their Applications in CO_2 Gas Sensors, Materials Today: Proceedings, 2 (2015) 5714-5719.

[62] Y.J. Jeong, C. Balamurugan, D.W. Lee, Enhanced CO_2 gas-sensing performance of ZnO nanopowder by La loaded during simple hydrothermal method, Sens. Actuators B: Chem, 229 (2016) 288-296.

Table 3.1: Literature survey of the gas sensing

Material	**Gas**	**Operating Temp. (°C)**	**Gas (ppm)**	**Sensor Response**	**Response Time**	**Recovery Time**	**Ref.**
Ag-$BaTiO_3$-CuO	CO_2	250	5000	0.28	15 min	10 min	[56]
CuO-$Cu_xFe_{3-x}O_4$	CO_2	250	5000	0.50	9.5 h	-	[57]
CdO	CO_2	250	5000	0.01	3.33 min	5 min	[58]
PEDOT-BPEI	CO_2	RT	1000	0.03	-	60 min	[59]
$La_{1-x}Sr_xFeO_3$	CO_2	380	2000	0.25	11 min	15 min	[60]
ZnO	CO_2	200	3000	0.03	8 s	40 s	[61]
ZnO-La (50%)	CO_2	400	5000	0.65	90 s	38 s	[62]
(1%) PANI-TiO_2	CO_2	RT	1000	53	9.2 min	5.7 min	Present work
(3%) PANI-TiO_2	LPG	RT	2000	2.77	156 s	140 s	Present work

Figures:

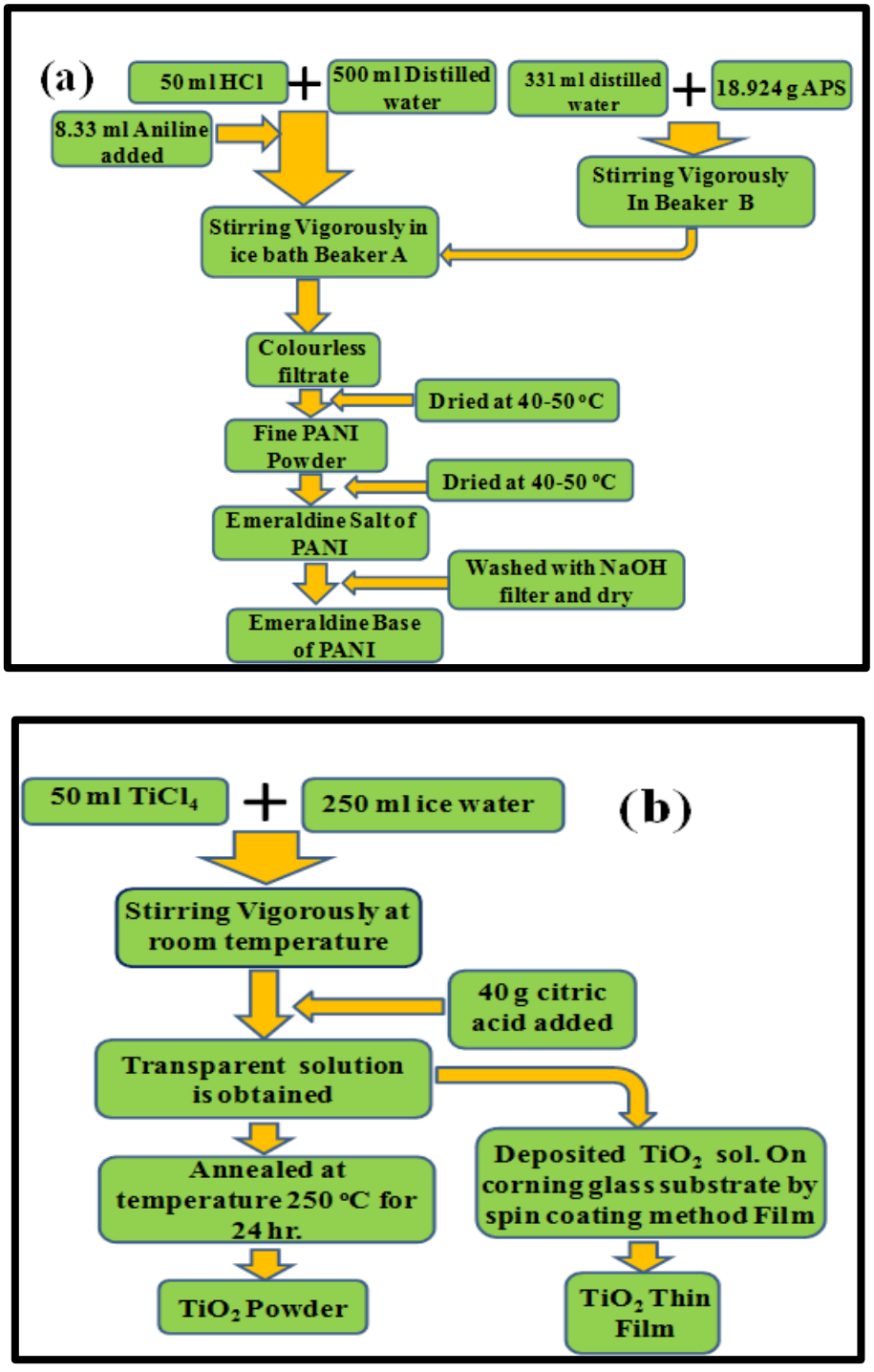

Figure 3.1: (a) Flowchart of the synthesis of TiO_2 nanoparticle thin film and **(b)** Flow chart of synthesis of PANI by using precursor aniline

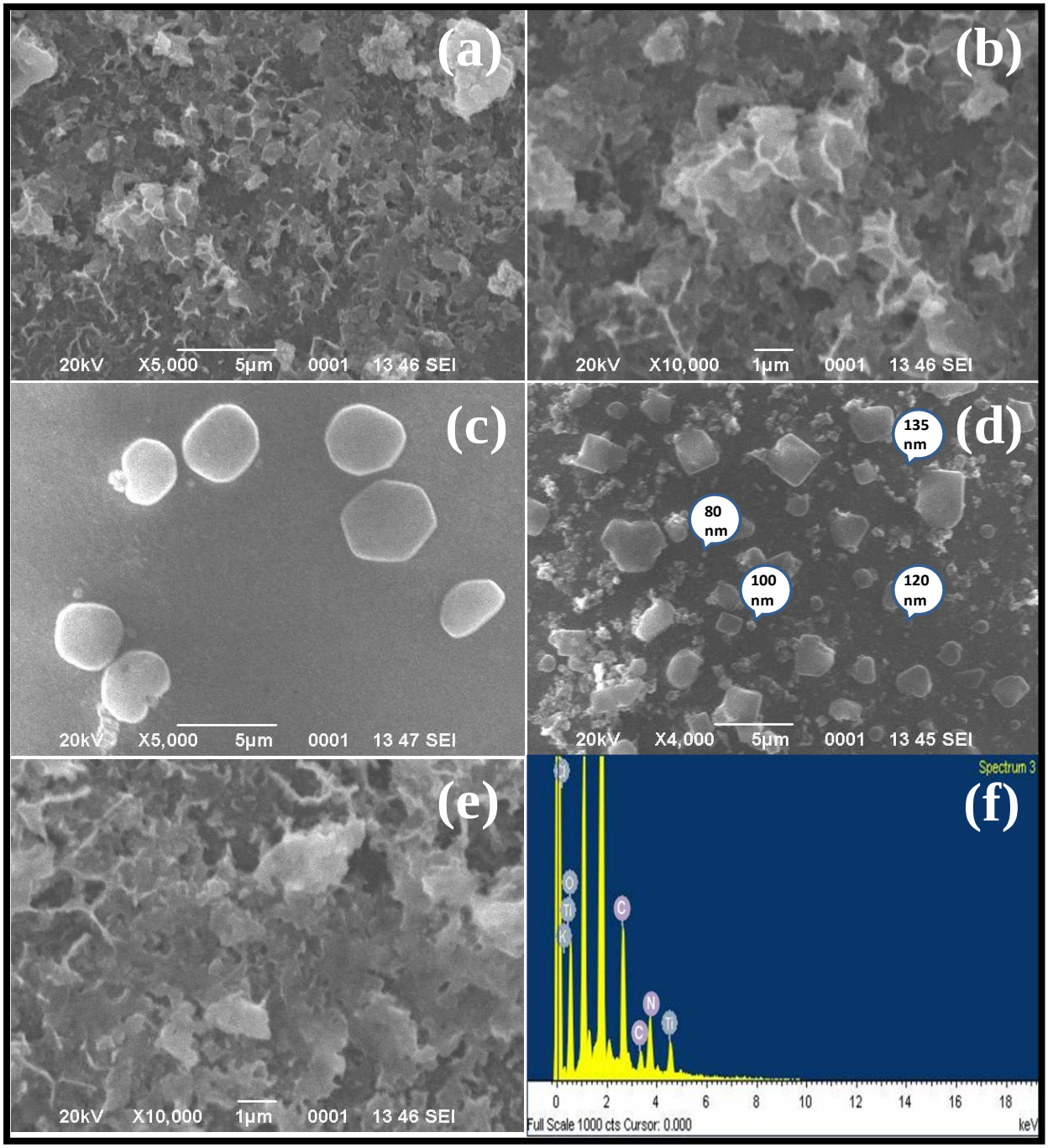

Figure 3.2: SEM image of (a) and (b) Pure PANI, (c) Pure TiO_2 thin film, (d) and (e) PANI-TiO_2 composite thin film and (f) EDX of composite thin film

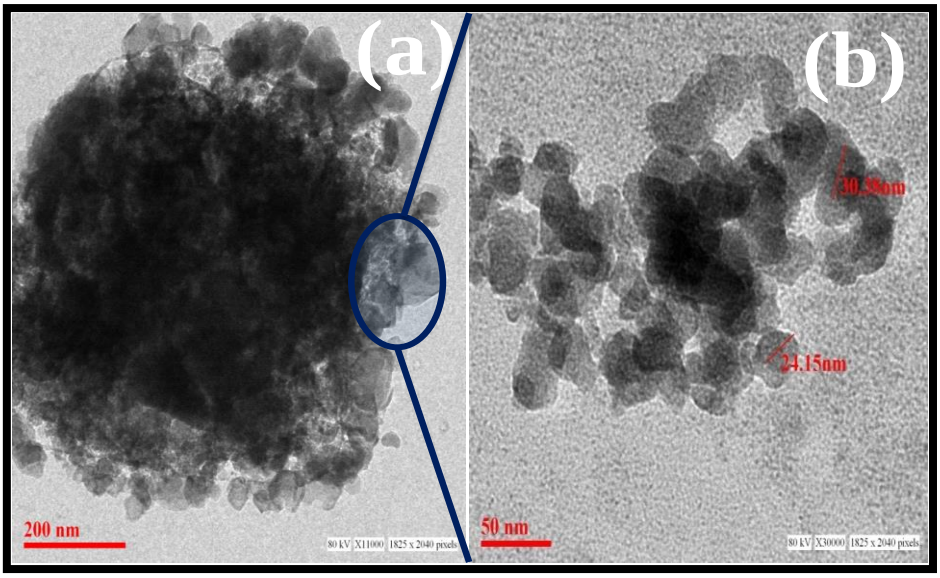

Figure 3.3: (a) & (b) TEM image of PANI-TiO_2 composite film with different magnification x 11,000 and x 30,000

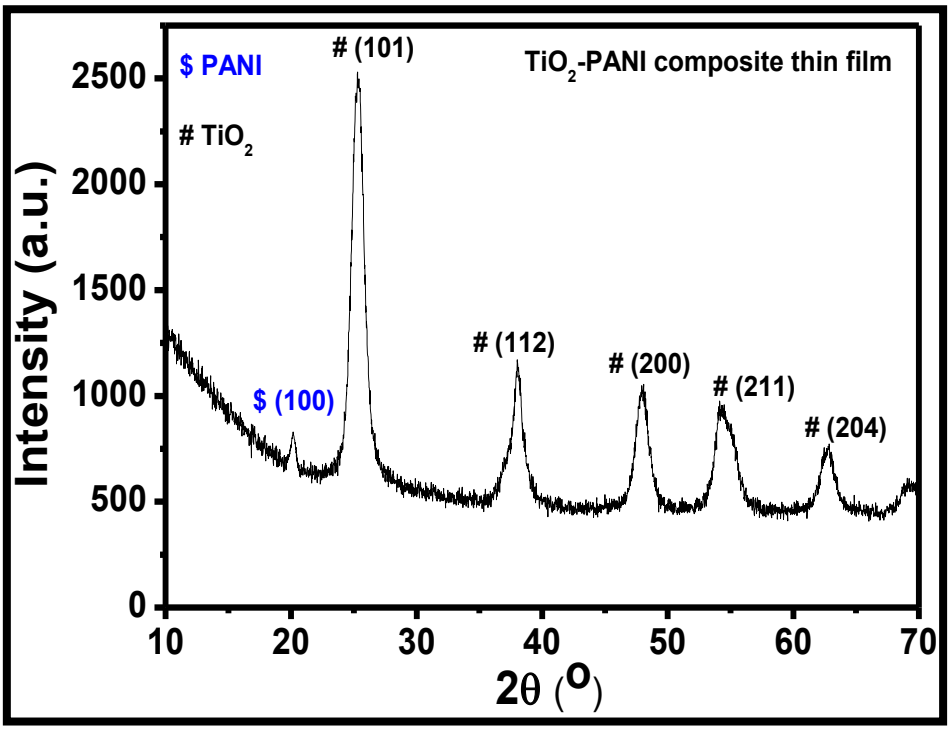

Figure 3.4: XRD structure of PANI-TiO_2 composite film

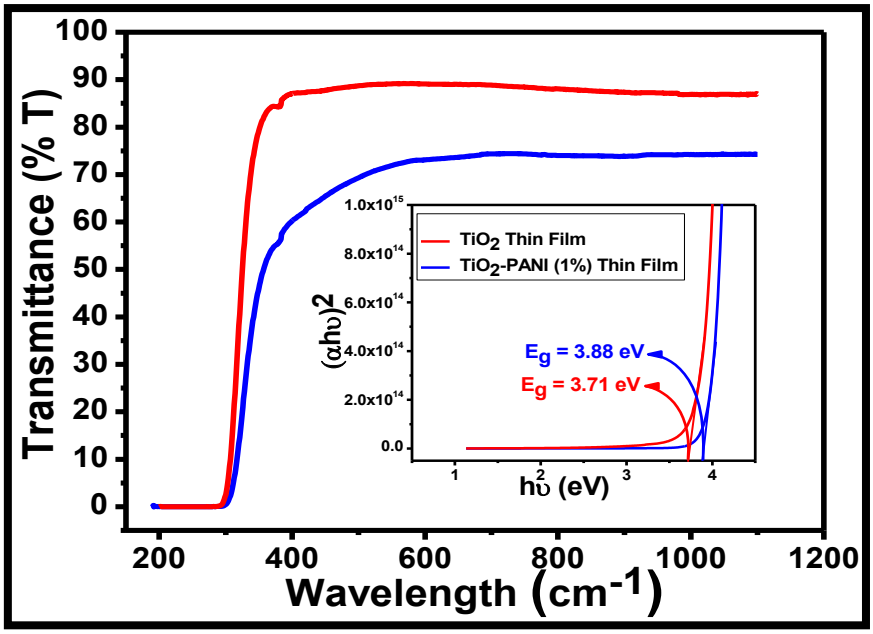

Figure 3.5: UV-visible transmittance spectra of TiO_2 and (1%) PANI-TiO_2 thin film and inset shows the Tauc plot of $(\alpha h\nu)^2$ versus hν

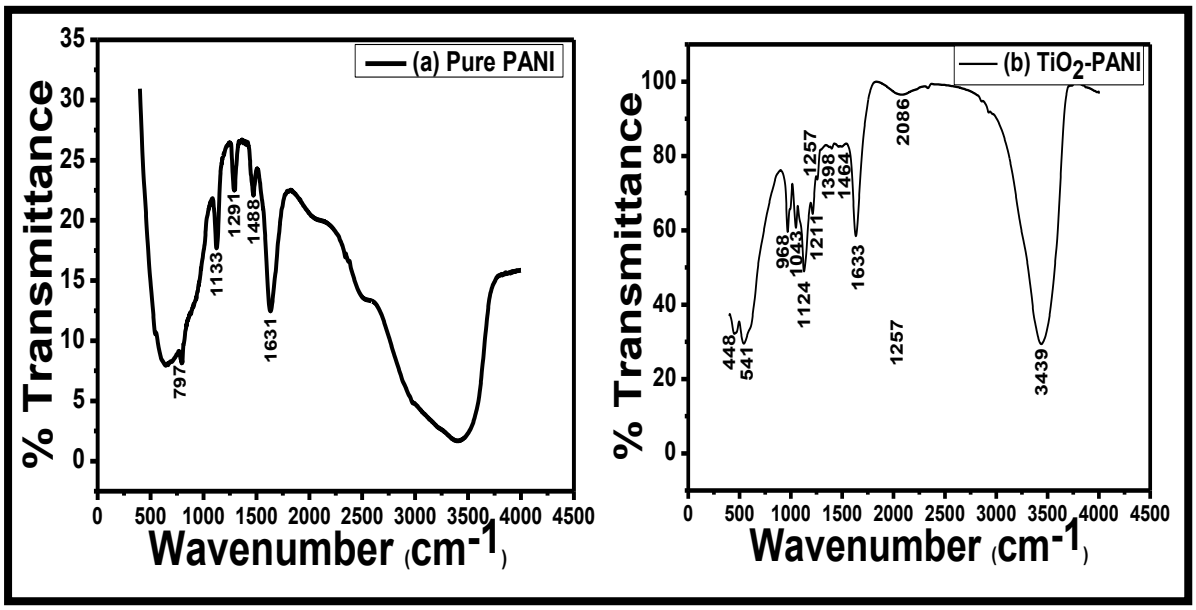

Figure 3.6: FTIR spectra of (a) PANI and (b) PANI-TiO_2 composite

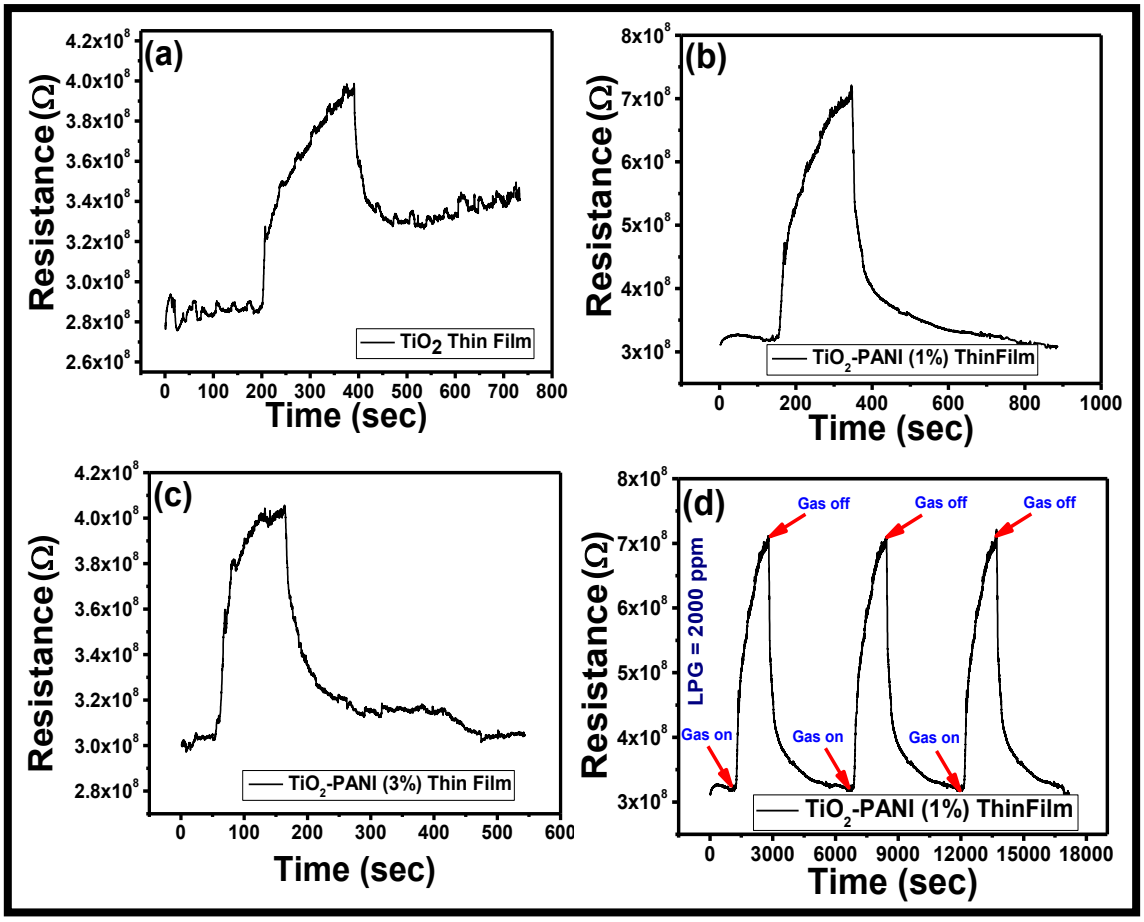

Figure 3.7: (a) The dynamic response curve of TiO_2 film after the exposure of LPG, (b) The dynamic response curve of TiO_2 PANI (1%) film, (c) The dynamic response curve of TiO_2 PANI (3%) film and (d) TiO_2 PANI (1%) reproducibility curve for 2000 ppm LPG

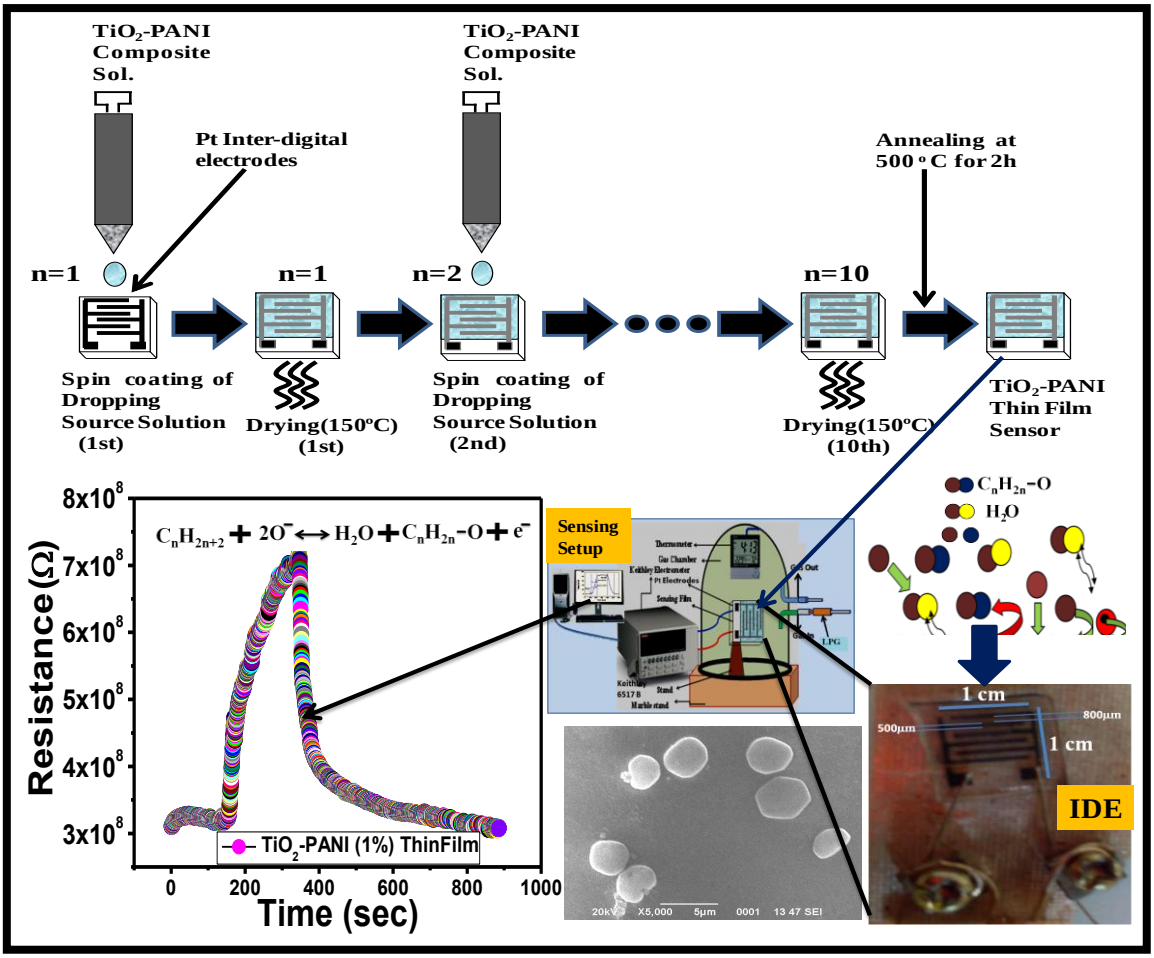

Figure 3.8: Schematic diagram of LPG sensing mechanism

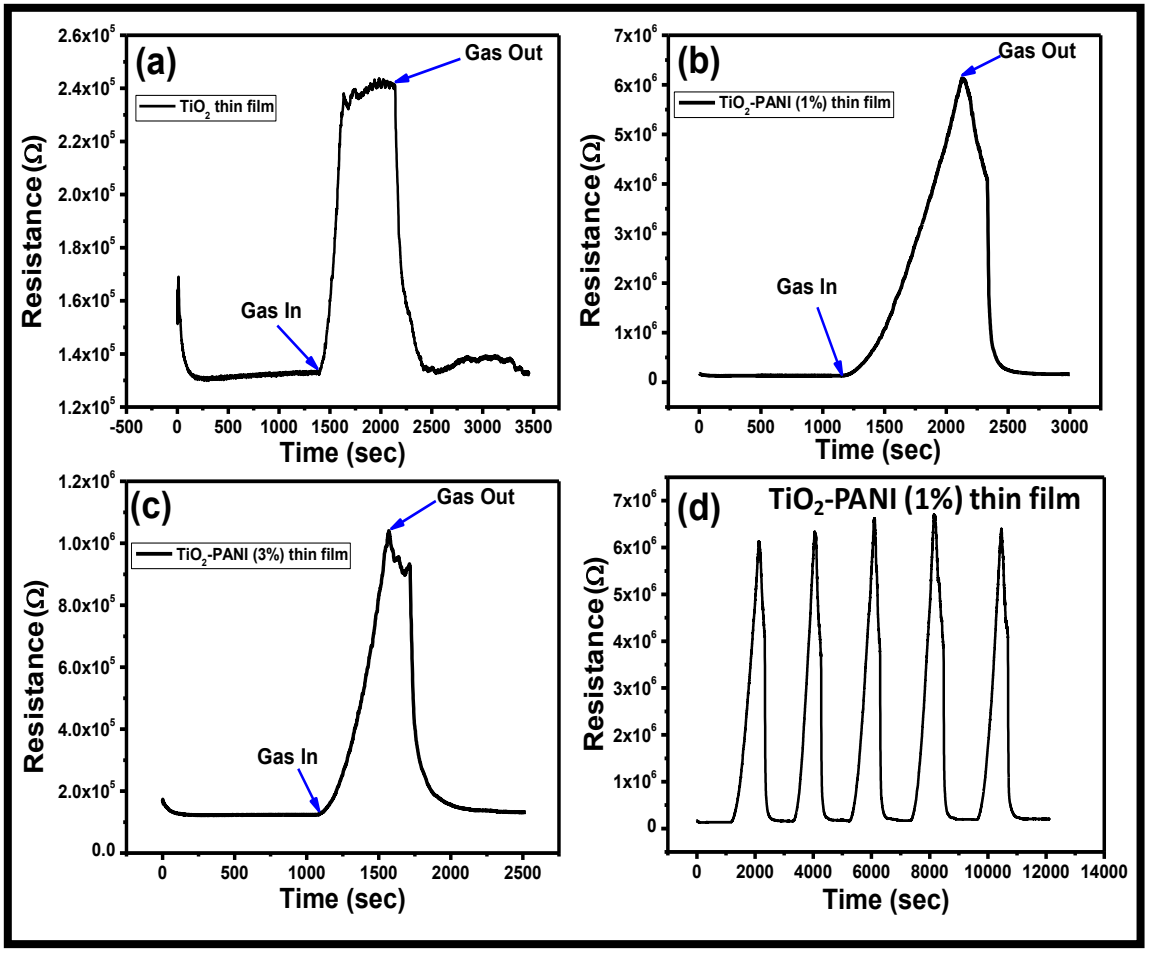

Figure 3.9: (a) The dynamic response curve of TiO_2 film, **(b)** The dynamic response curve of (1%) PANI-TiO_2 film, **(c)** The dynamic response curve of (3%) PANI-TiO_2 film and **(d)** (1%) PANI-TiO_2 reproducibility curve for 1000 ppm CO_2 gas

Chapter 4

Zn-doped TiO_2 nanoparticles employed as room temperature Liquefied Petroleum Gas Sensor

Present chapter reports the performance of a room temperature liquefied petroleum gas (LPG) sensor based on Zn-doped titanium dioxide heterojunction thin film prepared by spin coating technique. The surface morphology and structure of synthesised material were characterised by SEM and XRD. The structural analysis confirmed the formation of Zn doped TiO_2 having an average crystallite size 76 nm with tetragonal rutile structure. Optical properties were investigated using UV–vis absorption spectroscopy. Energy band gap of material was estimated as 3.26 eV. Variations in resistance with the exposure of LPG to the sensing element were observed. Sensor response (S) as a function of time was calculated and its maximum value was 2.92 towards 1.5 vol.% LPG, response time of the sensor was 120 s. The sensitivity of the LPG sensor at 1.5 vol.% was found as 0.4625. The sensor was moderately sensitive to LPG and results were found reproducible.

4.1 Introduction

The interest in the fundamental research of TiO_2 material in last decade has been drastically increased for its important optical and electronic properties. It has proven itself as one of the promising excellent candidates to replace the toxic and expensive material such as GaN, AlN, SnO_2 etc. for the application of gas sensors [1-3]. A lot of efforts have been made in developing new sensing material with improved sensing properties by Zn doped TiO_2. Various doping methods have been extensively utilised for modifying the electronic structure of TiO_2 nanoparticles to achieve a new or improved catalytic activity and other chemical and physical properties. They have many reports on transition metals [4-5], noble metals [6-7] and rare earth metals [8-12] doping in TiO_2. Generally, Titanium Oxide exists in three types of polymorphs as anatase, rutile, and brookite. Rutile phase is stable for TiO_2 at comparatively low temperatures. Thin films are much suitable for LPG sensors as the gas sensing properties are surface phenomenon [13]. The thin film gas sensing material has good sensitivity and selectivity over the thick film and pellet based sensors [14].

Synthesis of TiO_2 films have been reported by many researchers using different chemical methods like chemical deposition, successive ionic layer adsorption and reaction (SILAR), electrodeposition, doctor blade, and chemical bath deposition [14-22]. Among these methods, sol-gel is the most favourable due to easiness, cost effectiveness and production on large scale. This work focuses mainly on the effect of doping of Zn in TiO_2 and their sensing properties. The sensitivity, response time and recovery time of LPG sensor have been investigated.

4.2 Experimental

Analytical grade chemical including $Zn(NO_3).6H_2O$, $TiCl_4$ (99.99%) and urea were purchased from the Sigma-Aldrich Co. Limited and used without extra purification.

Absolute ethanol (99.99%) was purchased from Merck. The deionized water was used in all preparation methods.

4.2.1 Synthesis Method

13 g of $Zn(NO_3).6H_2O$, 1.1 ml $TiCl_4$ and 3 g urea were dissolved in 100 ml of deionized water and stirred vigorously. The resulting mixture was placed at 60 °C for 6 h in a microwave oven. A part of resultant gel was used for the preparation of thin film by spin coating method. The remaining part was then dried at 85 °C and ground to a fine powder and calcined in a muffle furnace at 500°C for 5 h.

4.3 Characterization

X-ray diffraction pattern of Zn-doped TiO_2 powder was analysed at Geological survey of India by using XRD. The morphology of Zn-doped TiO_2 was investigated using SEM. UV-Vis spectrum of the sample was taken out by using UV-Vis spectrophotometer (Evolution thermal scientific-201).

4.3.1 X-Ray Diffraction

The crystal structure and phase identification of material were analysed using X-ray Diffractometer (Xpert, PRO PANalytical XRD system, Netherlands) with Cu K_α radiations as a source having wavelength 1.5418 Å. X-Ray diffraction pattern show amount of crystallisation of the sample. The average crystallite size (D) of the sensing material can be calculated by the Debye-Scherrer's formula, which is given by the following equation:

$$D = K\lambda/\beta\cos\theta \quad (1)$$

Where, K= 0.94 is Scherrer's coefficient, which depends on the shape of the crystallite and the type of defects present, λ is the wavelength of X-ray radiation, β is the full width at half maximum (FWHM) of the diffraction peak and θ is the angle of diffraction. Figure

4.1 shows the XRD pattern of the zinc doped TiO_2 recorded for $2\theta = 20°$ to $70°$. This pattern reveals that the sensing material consists some peaks of Zn and TiO_2. The value of crystallite size of Zn-doped TiO_2 calculated from Scherrer's formula is found to be 76 nm. XRD JCPDS reference code 01-077-0442 confirmed that the rutile phase of TiO_2 is present in the sample. Also the wurtzite phase of ZnO was established with the reported JCPDS data (Card No. 5-664).

4.3.2 Scanning Electron Microscopy (SEM)

The surface morphology of the prepared thin films was analysed using scanning electron microscope (SEM, LEO-Cambridge) and shown in Figure 4.2(a-c). SEM images show the porous nature of the films. Figure 4.2(a) shows the SEM image of thin film of pure TiO_2 having a rectangular shape of TiO_2 nanoparticles on the glass substrate. The rectangular shape of an individual grain may be seen in Figure 4.2(b). The porosity of the material is an imperative parameter regarding gas sensing point of view as the thin film has a number of active sites.

When some amount of Zn is doped in pure TiO_2, the morphology of TiO_2 particles has been transformed, which shows the regular structure of the thin film due to decrease in pH value from 10 to 6 of the sample. The doping of Zn increased the reaction with water, so the space needed for $[TiO_6]^{n+}$ unit adjustment has become larger. The effect of pH is greater than that of the effect of water. By the doping of Zn, surface area was found increased and particle size was reduced which would improve the sensitivity of gas.

4.3.3 UV-Visible Spectroscopy

The optical absorbance spectra of the grown Zn-doped TiO_2 thin film deposited separately on the glass substrate was measured by thermal evolution-201, UV-visible spectrometer in the wavelength range of 190 to 1100 nm, and the variation is shown in Figure 4.3(a). This spectrum reveals that the sample has a low absorbance in the visible

and near infrared regions. The enhanced absorption is observed in the neighbourhood of λ = 400 nm. The optical data were analysed using the equation for near edge absorption [23]:

$$\alpha h\nu = k(h\nu - E_g)^n \quad (2)$$

Where, k is a constant, hν is the photon energy and E_g is the energy band gap, n is a pure number which depends on the nature of electronic transition responsible for the absorption. The band gap is obtained by extrapolating the linear portion of the Tauc plot of $(\alpha h\nu)^2$ *vs* photon energy (hν) on the X-axis. Our experimental result presented in Figure 4.3(b) shows that optical absorption for the sample described by the Eq. (1) with n = 1/2 is the direct transition type. The direct band gap observed by Tauc plot of Zn-doped TiO_2 thin film is found as 3.26 eV.

The structure of TiO_2 in sol-gel contains many hydroxyl groups, which are used by both Ti and Zn. When the solution was heated above 80°C, the hydroxyl groups present in solution eliminated and ZnO formed together with the structure of TiO_2. Therefore, the energy band gap of the Zn-doped TiO_2 changed. Metal ion (Zn^{2+}) dopants influenced the photoreactivity of the TiO_2 by acting as electron or hole traps and by altering the e^-/h^+ pair recombination rate through the following process:

$$M^{n+} + e_{cb}^- \rightarrow M^{(n-1)+} \text{ (electron trap)} \quad (3)$$

$$M^{n+} + h_{vb}^+ \rightarrow M^{(n+1)+} \text{ (hole trap)} \quad (4)$$

The dimensions of the semiconductor can be on the order of nanometers and the energy shifts according to the quantum size effect. The shift of the conduction band (CB) may accelerate the reduction ($E_M^{n+}/M^{(n-1)+} < E_{cb}$), while that of the valance band (VB) may increase the oxidation reaction ($E_M^{n+}/M^{(n+1)+} < E_{vb}$) [24]. Therefore, the band gap

energy of the Zn-doped TiO_2 sample is small 3.26 eV as compared to the bare TiO_2 (4.07 eV).

4.4 Gas sensing measurements

The schematic diagram of LPG sensing set-up is shown in Figure 2.5 (a) and described in detail in Chapter 2, subheading 2.5. The sensing film was inserted between the silver electrodes inside the glass chamber having two knobs. One knob is associated with the concentration measuring system (gas inlet) and other is an outlet knob for releasing the gas. Concentration measuring system is shown in Figure 2.5 (b), which consists of a glass bottle containing double distilled water, which is saturated with LPG, in order to avoid the possibility of dissolution of inserted gas. At the top of the bottle, the measuring tube (pipette) is connected by a vacuum seal. The cock I is connected to the LPG cylinder and cock II is connected to the inlet of the gas chamber. When the cock I is opened, the LPG from the cylinder is filled in the glass bottle and an equivalent amount of water is displaced in the measuring pipette. When the cock II is opened, a desired amount of gas e.g. 0.5, 1.0, 1.5 and 2.0 vol.% is entered to the gas chamber. Before passing the LPG in the chamber, the gas chamber with a resistance measuring holder was stabilised for 10-20 minutes.

Sensing film with silver contacts was used for measurements of LPG sensing properties. The stabilised resistance of the film was taken as stabilised resistance in the presence of air (R_a). Now, this was exposed to LPG and variations in electrical resistance with the time for different vol.% of LPG were recorded by using Keithley electrometer (Model: 6517A). Sensitivity of the LPG sensor is defined as the change in resistance in the presence of gas (R_g) to the resistance in presence of air (R_a) that is

$$S = \frac{R_a}{R_g} \tag{5}$$

Figure 4.4 illustrates the variations in resistance of the film with time after exposure for different vol.% of LPG at room temperature. The curve for 0.5 vol.% of LPG shows a small variation in resistance with time after exposure and inset figure shows an increase in the resistance after exposing the gas. The curve for 1.0 & 1.5 vol.% of LPG exhibits the improved response and has better sensitivity than 0.5 vol.%. Further, for 2.0 vol.% of LPG resistance increases sharply with time after exposure up to 300 s and then become constant. The sensing response for different vol.% concentration has been depicted in Table 4.1.

Figure 4.5 exhibits the variations of average sensitivity with the variation of concentration of LPG and it was found that as the concentration of LPG (in vol.%) increases, the average sensitivity of sensor increases linearly up to 1.5 vol.% of LPG, later it increases slowly. The linear increment of the sensitivity of the sensor is a vital factor for device fabrication. The maximum sensitivity was obtained for 1.5 vol.% of LPG as ~ 0.4625 GΩ/min.

It is important to investigate the surface reaction between Zn-doped TiO_2 and LPG molecules for better understanding of the sensing mechanism. Gas-sensing mechanism of Zn-doped TiO_2 based sensor belongs to the surface-controlled type, the resistance change is controlled by the species and amount of chemisorbed oxygen on the surface. The gas sensing mechanism of Zn-doped TiO_2 thin film based sensor belongs to a surface controlled type, i.e. resistance change is controlled by surface area and the amount of chemisorbed oxygen. LPG consists of CH_4, C_3H_8, and some other hydrocarbons. In each composition, the reducing hydrogen species are bound to carbon atom therefore, LPG dissociates into the reactive reducing components hardly on the surface of the sensing element. As LPG exposed to sensing element, the conductivity increases due to adsorption of oxide and capture more electrons that contribute to reducing the current. It

was observed that as the concentration of LPG increases, the average sensitivity increases linearly in the beginning and later, it becomes saturated. The linear relationship between sensitivity and gas concentration may be attributed to the availability of a sufficient number of sensing sites on the film to act upon the LPG. The low concentration implies a lower surface coverage of gas molecules, resulting in a lower surface reaction between the surface adsorbed oxygen species and the gas molecules. The increase in LPG concentration increases the surface reaction due to a large surface coverage. Further, increase in the LPG concentration does not increase the surface reaction and eventually, saturation takes place [25].

Thus, the maximum sensitivity was obtained at higher concentration of LPG i.e. 1.5 vol.%. The linearity of average sensitivity for the LPG suggests that the Zn-doped TiO_2 nanocomposite thin film can be reliably used to monitor the LPG over this range of concentration. As the lower explosive limit (LEL) for LPG is < 2.0 vol.% discussed in Table 1.1 therefore, the response is measured up to 2 vol.% for fulfilling the safety requirement.

The equilibrium of the chemisorption process results in stabilization of surface resistance (R_a). Figure 4.6 shows the proposed model of stabilization curve of Zn-doped TiO_2 in different steps as: (a) at higher operating temperature, thermal excitation of conduction electrons in the metal oxide, (b) the electron donated by the metal oxide to the oxygen, (c) oxygen atoms get chemisorbed on the surface of metal oxide and the stabilization curve is shown in graph. When the sensor is exposed to the atmosphere containing inflammable gases such as LPG at elevated temperature, the O^- adsorbate reacts with the inflammable gas and releases the electrons to the conduction band. The oxygen adsorbed on the surface of the film influences the resistance of the Zn-doped TiO_2 based sensor. Initially, oxygen from the atmosphere adsorbs on the surface of the film and

extracts electrons from its conduction bands to form O_2^- species on the surface, consequently resistance increases. After that an equilibrium state is accomplished between the oxygen of Zn-doped TiO_2 and atmospheric oxygen. The sensing mechanism of LPG is also given in Chapter 2 with its experimental set-up. When the thin film is exposed to LPG, it reacts with the chemisorbed oxygen. On interaction with hydrocarbons of LPG, the adsorbed oxygen is removed, forming gaseous species and water vapour. Consequently, the resistance changes, which is due to the alteration in the width of depletion layer after exposure to LPG [25].

4.5 Conclusion

Zn-doped TiO_2 thin film was successfully fabricated and characterised using SEM, XRD and UV-Vis Spectrophotometer. SEM showed rectangular particles regularly distributed on the surface of the film. XRD revealed the nanostructured crystals with minimum size as 76 nm. The Tauc plot obtained from the UV-Vis spectrum gave the energy band gap of sensing material as 3.26 eV. Zn-doped TiO_2 thin film based LPG sensor was thoroughly investigated below LEL concentration to LEL at room temperature. Sensor response was found maximum as 2.92 for 1.5 vol.% of LPG and results were found reproducible after 2 months.

References

[1] K. H. Baik, J. Kim, S. Jang, Highly sensitive nonpolar a-plane GaN based hydrogen diode sensor with textured active area using photo-chemical etching, Sensors and Actuators B: Chemical, Volume 238 (2017) 462-467.

[2] G. Sun, P. Zhao, W. Zhang, H. Li, C. He, Adsorption of gas molecules on armchair AlN nanoribbons with a dangling bond defect by using density functional theory., Materials Chemistry and Physics 186 (2017) 305-311.

[3] W. Zhang, B. Yang, J. Liu, X. Chen, X. Wang, C. Yang, Highly sensitive and low operating temperature SnO_2 gas sensor doped by Cu and Zn two elements., Sensors and Actuators B 243 (2017) 982–989.

[4] R.J. Wu, Y.L. Sun, C.C. Lin, H.W. Chen, M. Chavali, Composite of TiO_2 nanowires and Nafion as humidity sensor material, Sens. Actuators B, 115 (2006) 189–204.

[5] H. Tang, K. Prasad, R. Sanjines, F. Levys, TiO_2 anatase thin films as gas sensors, Sens. Actuators B, 26 (1995) 71–75.

[6] C.M. Carney, S. Yoo, A.A. Sheikh, TiO_2–SnO_2 nanostructures and their H_2 sensing behaviour, Sens. Actuators B, 108 (2005) 29–33.

[7] W. Choi, A. Termin and M.R. Hoffmann, The role of Metal ion dopants in quantum-sized TiO_2; the correlation between photoreactivity and charge carrier recombination dynamics, J. Phys. Chem., 98 (1994) 13669–13679.

[8] D.H. Kim, S.I. Woo, S.H. Moon, H D. Kim, B.Y. Kim, J. H. Cho, Y.G. Joh and E. C. Kim, Effect of Co/Fe co-doping in TiO_2 rutile prepared by solid state reaction, Solid State Commun., 136 (2005) 554–558.

[9] H. Chen, S. Chen, X. Quan, H. T. Yu, H. M. Zhao and Y.B. Zhang, Fabrication of TiO_2-Pt coaxial nanotube array Schottky structures for enhanced photocatalytic degradation of phenol in aqueous solution, Journal of Phys. Chem. C., 112 (2008) 9285–9290.

[10] J.L. Chen, E. Loso, N. Ebrahim and G.A. Ozin, Synergy of slow photon and chemically amplified photochemistry in platinum nanocluster-loaded inverse titania opals, Journal of American Chemical Society. 130 (2008) 5420–5421.

[11] K.T. Ranjit, I. Willner, S.H. Bossmann and A.M. Braun, Lanthanum oxide doped titanium dioxide photocatalysts: Effective catalysts for the enhanced degradation of the salicylic acid and t-cinnamic acid, J. Catal., 204 (2001) 305–313.

[12] Y. Zhang, H. Xu, Y. Xu, H. Zhang, and Y. Wang, The effect of lanthanide on the degradation of RB in nanocrystalline Ln/TiO_2 aqueous solution, J. Photochem. Photobiol. A: Chem., 170 (2005) 279–285.

[13] Y. Xiaoli, J. He, D.G. Evans, X. Duan and Y. Zhu, Effect of TiO_2 thin film thickness and specific surface area by low-pressure metal–organic chemical vapour deposition on photocatalytic activities, Applied Catalysis B Environmental., 55 (2005) 243–252.

[14] Y. Xie, C. Yuan, and X. Li, Photosensitized and photocatalyzed degradation of azo dye using Lnn^{+}-TiO_2 sol in aqueous solution under visible light, Material Science Engineering B., 117 (2005) 325–333.

[15] K.V. Baiju, P. Periyat, W. Wunderlich, P.K. Pillai, Mukundan P. and Warrier K.G.K., Enhanced photoactivity of neodymium doped mesoporous titania synthesised through aqueous sol–gel method. Journal of Sol–Gel Science and Technology. 43 (2007) 283.

[16] C.D. Lokhande, E.H. Lee, K.D. Jung, O.S. Joo, Room temperature chemical deposition of amorphous TiO_2 thin films from Ti(III) chloride, J. Mater. Sci. 39 (2004) 2915–2918.

[17] S.S. Kale, R.S. Mane, H. Chung, M.Y. Yoon, C.D. Lokhande, S.H. Han, Use of successive ionic layer adsorption and reaction (SILAR) method for amorphous titanium dioxide thin films growth, Appl. Surf. Sci. 253 (2006) 421-424.

[18] C.D. Lokhande, S.K. Min, K.D. Jung, O.S. Joo, Cathodic electrodeposition of amorphous titanium oxide films from an alkaline solution bath, J. Mater. Sci. 39 (2004) 6607–6610.

[19] S. D. Burnside, V. Shklover, C. Barbe, P. Comte, F. Arendse, K. Brooks, and M. Gratzel, Self-Organization of TiO_2 Nanoparticles in Thin Films., Chem. Mater. 10 (1998) 2419-2425.

[20] S. Karuppuchamy, K. Nonomura, T. Yoshida, T. Sugiura, H. Minoura, Cathodic Electrodeposition of TiO_2 Thin Films for Dye-Sensitized Photoelectrochemical Applications., Solid State Ionics 151 (2002) 19-27.

[21] J. Wang , H. Wang, J. Yu, Synthesis of 1-D porous TiO_2 on fly ash carriers through surface modification method., Journal of Physics and Chemistry of Solids 107 (2017) 7-13.

[22] A. Elfanaoui1, A. Ihlal, A. Taleb, L. Boulkaddat, E. Elhamri, M. Meddah1, K. Bouabid and X. Portier, The synthesis of the TiO_2 thin film by Chemical Bath Deposition (CBD) method, M. J. Condensed matter 13 (2011) 95-99.

[23] J.C. Tauc, Optical Properties of Solids, North-Holland, Amsterdam (1972) 372.

[24] T. B. Nguyen, M. J. Hwang, K. S. Ryu, Synthesis and High Photocatalytic Activity of Zn-doped TiO_2 Nanoparticles by Sol-gel and Ammonia-Evaporation Method., Bull. Korean Chem. Soc. 33 (2012) 1.

[25] R.K. Sonker, B.C. Yadav, Chemical Route Deposited SnO_2, SnO_2-Pt and SnO_2-Pd Thin Films for LPG Detection, Adv. Sci. Lett. 20 (2014) 1023-1027.

[26] R.N. Bulakhe, C.D. Lokhande, Chemically deposited cubic structured CdO thin films: Use in liquefied petroleum gas sensor, Sensors and Actuators B 200 (2014) 245-250.

[27] D.S. Dhawale, R.R. Salunkhe, U.M. Patil, K.V. Gurav, A.M. More, C.D. Lokhande, Room temperature liquefied petroleum gas (LPG) sensor based on p-polyaniline/n-TiO_2 heterojunction, Sensors and Actuators B 134 (2008) 988-992.

[28] B.C. Yadav, T. Shukla, S. Singh, T.P. Yadav, Titania Prepared by Ball Milling: Its Characterization and Application as Liquefied Petroleum Gas Sensor, Synthesis and Reactivity in Inorganic, Metal-Organic, and Nano-Metal Chemistry 45 (2015) 487-494.

[29] B. Baruwati, D.K.K. Sunkara, V. Manorama, Hydrothermal synthesis of highly crystalline ZnO nanoparticles: A competitive sensor for LPG and EtOH, Sensors and Actuators B 119 (2006) 676-682.

[30] S.S. Joshi, C.D. Lokhande, S.H. Han, A room temperature liquefied petroleum gas sensor based on all-electrodeposited n-CdSe/p-polyaniline junction, Sensors and Actuators B 123 (2007) 240-245.

[31] P.P. Sahay, R.K. Nath, Al-doped zinc oxide thin films for liquid petroleum gas (LPG) sensors, Sensors and Actuators B 133 (2008) 222-227.

[32] R.B. Waghulade, P.P. Patil, R. Pasricha, Synthesis and LPG sensing properties of nano-sized cadmium oxide, Talanta 72 (2007) 594-599.

[33] V.R. Shinde, T.P. Gujar, C.D. Lokhande, LPG sensing properties of ZnO films prepared by spray pyrolysis method: Effect of molarity of precursor solution, Sensors and Actuators B 120 (2007) 551-559.

[34] R.R. Salunkhe, C.D. Lokhande, Effect of film thickness on liquefied petroleum gas (LPG) sensing properties of SILAR deposited CdO thin films, Sensors and Actuators B 129 (2008) 345-351.

[35] R.R. Salunkhe, V.R. Shinde, C.D. Lokhande, Liquefied petroleum gas (LPG) sensing properties of nanocrystalline CdO thin films prepared by chemical route: Effect of molarities of precursor solution, Sensors and Actuators B 133 (2008) 296-301.

[36] D. Haridas, K. Sreenivas, Vinay Gupta, Improved response characteristics of SnO_2 thin film loaded with nanoscale catalysts for LPG detection, Sensors and Actuators B 133 (2008) 270-275.

[37] B. Thomas, K.K. Radha, Influence of Cs doping in spray deposited SnO_2 thin films for LPG sensors, Sensors and Actuators B 133 (2008) 404–413.

[38] K.V. Gurav, S.W. Shin, U.M. Patil, P.R. Deshmukh, M.P. Suryawanshi, G.L. Agawane, S.M. Pawar, P.S. Patil, J.Y. Lee, C.D. Lokhande, J.H. Kim, Cu_2ZnSnS_4 (CZTS)-based room temperature liquefied petroleum gas (LPG) sensor., Sensors and Actuators B 190 (2014) 408-413.

Table 4.1: Sensing response of different vol.% concentration

Concentration of LPG	**0.5 vol. %**	**1.0 vol. %**	**1.5 vol. %**	**2.0 vol. %**
Sensor Response	1.37	1.43	2.92	2.76
Response Time (s)	315	208.8	120	330
Recovery Time (s)	252	171	102	225

Table 4.2: Summary of result for LPG sensor based on semiconductor TiO_2 thin film

Material	**Concentration of Gas**	**Sensor response**	**Res./Rec. Time(s)**	**Temp. (°C)**	**Ref. No.**
CdO	1040 ppm	44%	41/39	300	[26]
Pani-TiO_2	0.1 vol%	63%	140/180	27	[27]
TiO_2	5 vol.%	1100 %	100/250	RT	[28]
Pd doped TiO_2	200 ppm	20%	100/80	250	[29]
n-CdSe/p-polyaniline	.08 vol.%	70%	100/200	27	[30]
Al-doped ZnO	1 vol%	89%	-	325	[31]
CdO	75 ppm	341%	5/10	450	[32]
ZnO	200 ppm	43 %	84/90	400	[33]
CdO	.08 vol.%	18.75 %	20/30	425	[34]
CdO	0.2 vol%	23.28 %	70/80	425	[35]
SnO_2	100 ppm	750 %	100/-	260	[36]
Cs-doped SnO_2	1000 ppm	93.40%	60/-	345	[37]
Cu_2ZnSnS_4	1200 ppm	19.30%	70/40	RT	[38]
Zn doped TiO_2	1.5 vol%	292.0%	120/102	RT	Present work

Figures

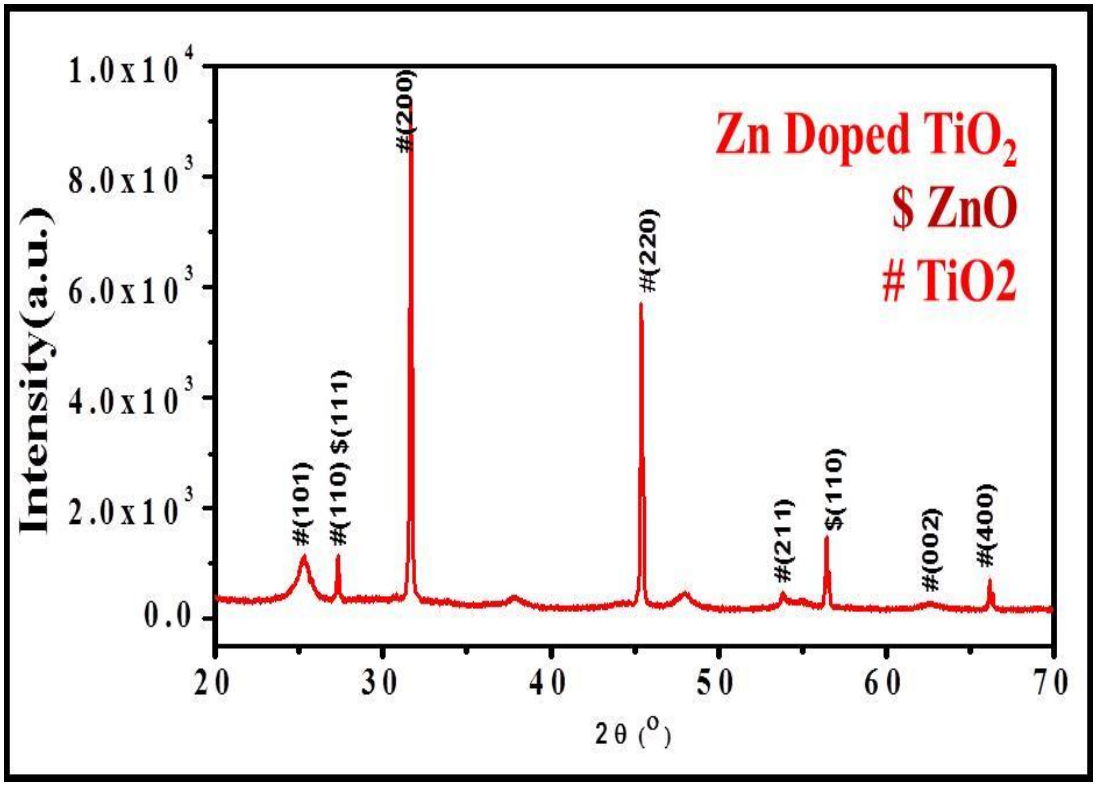

Figure 4.1 XRD pattern of Zn-doped TiO_2 powder.

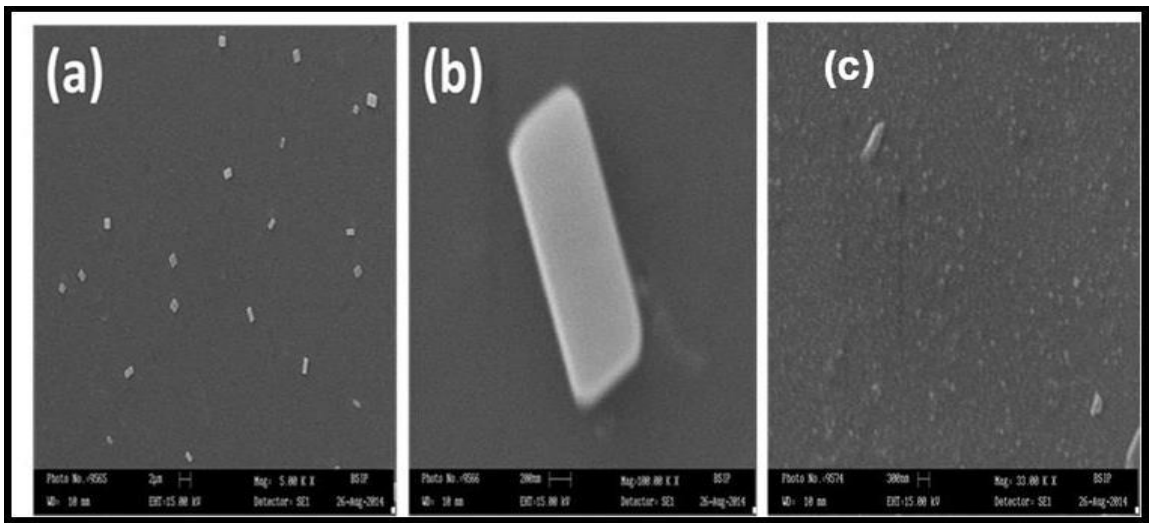

Figure 4.2: (a), (b) SEM images of Pure TiO_2 Thin film on the scale 2 µm, 200 nm and (c) Zn-doped TiO_2 thin film at 300 nm scale.

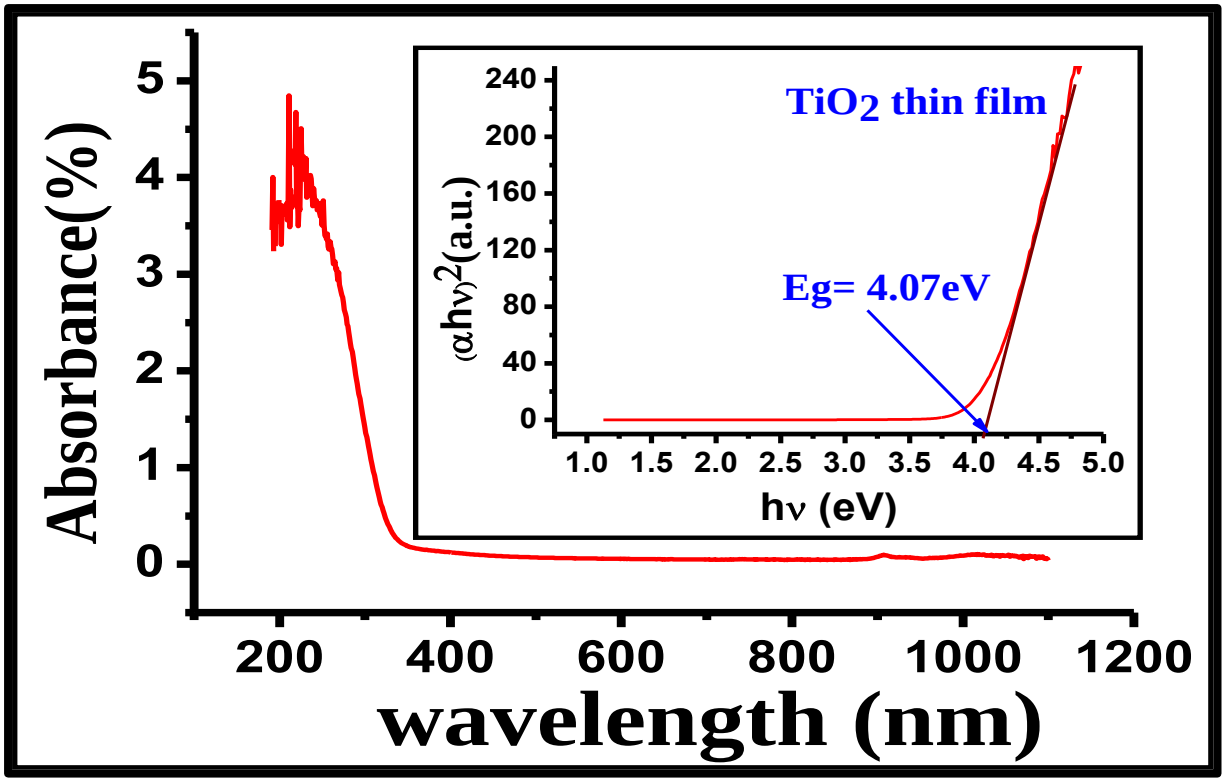

Figure 4.3(a) : UV-visible Absorbance spectra of TiO_2 thin film and inset shows the Tauc plot of $(\alpha h\nu)^2$ versus $h\nu$

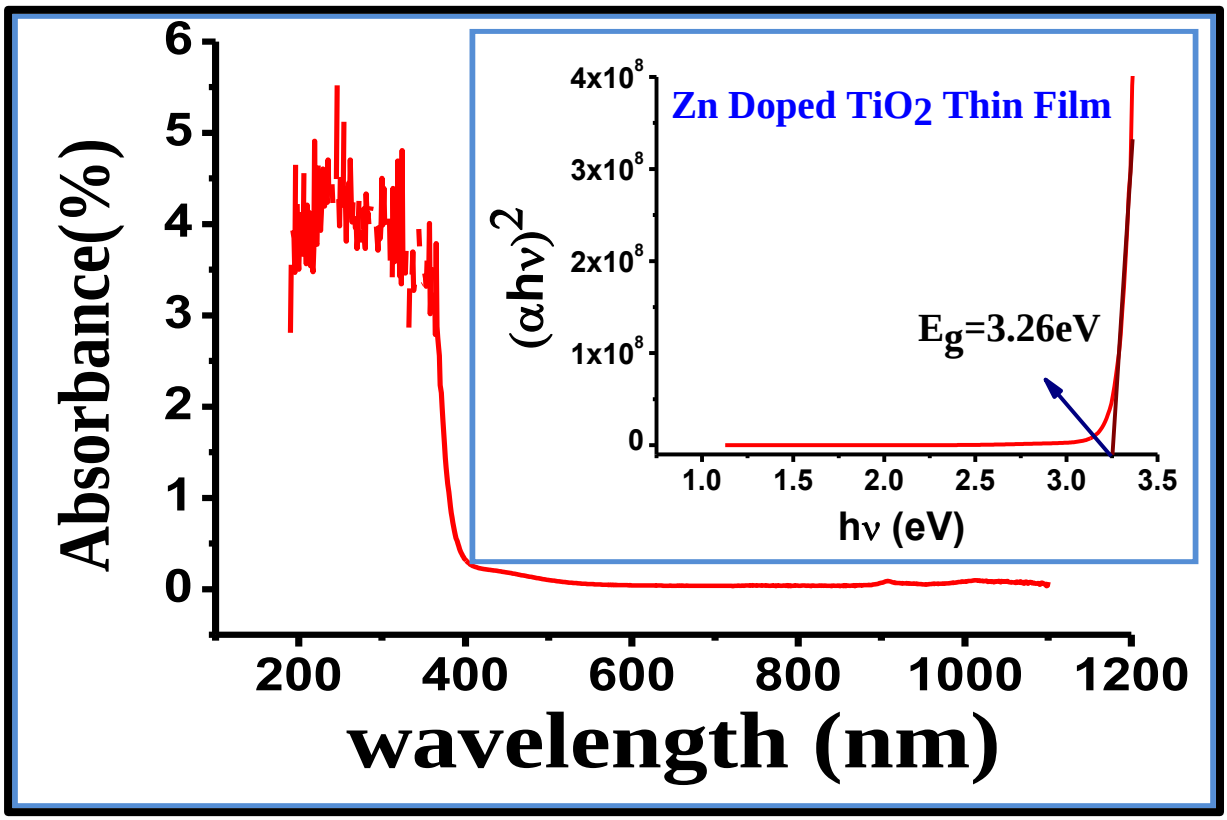

Figure 4.3(b): UV-visible Absorbance spectra of Zn doped TiO_2 thin film and inset shows the Tauc plot of $(\alpha h\nu)^2$ versus $h\nu$

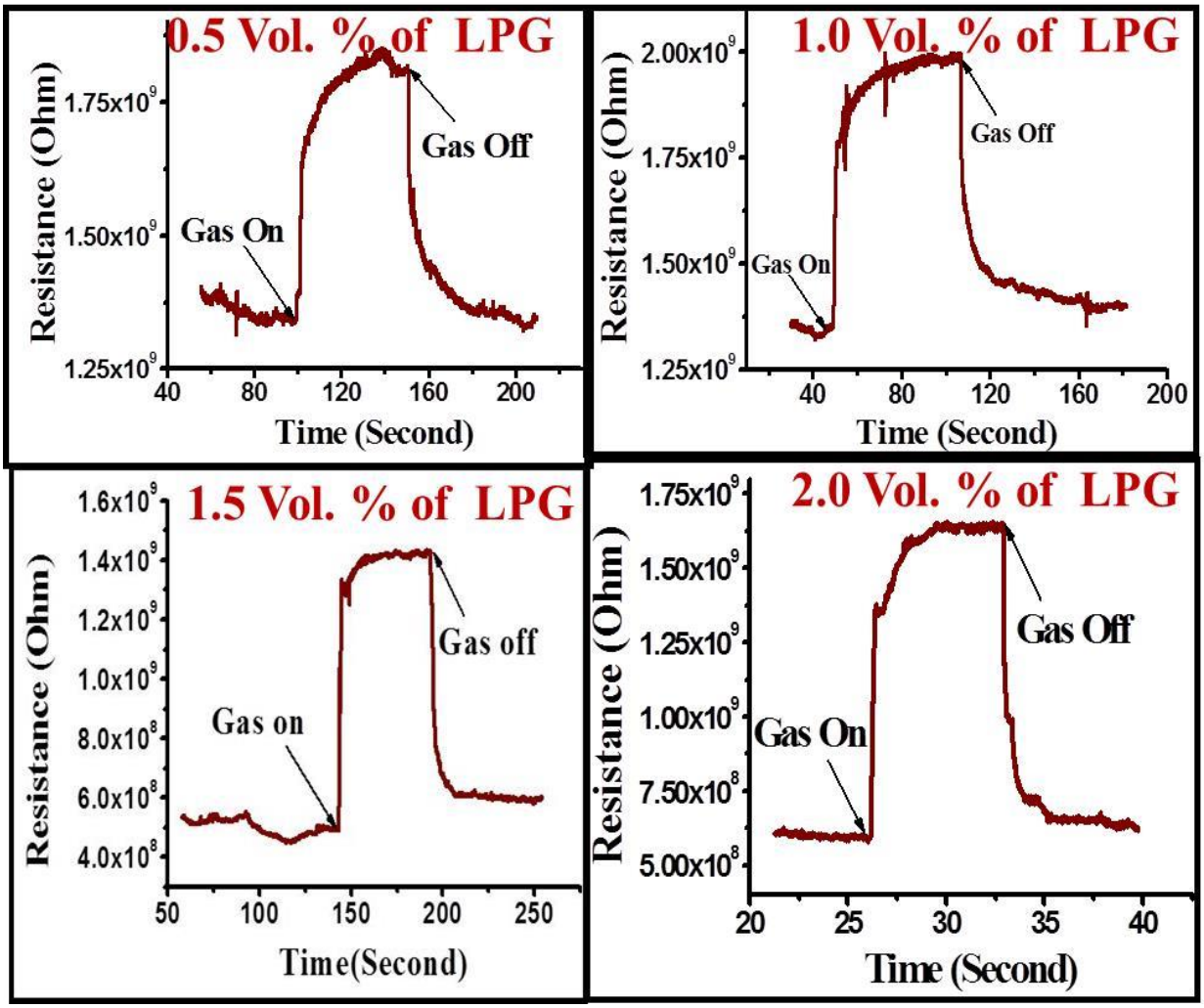

Figure 4.4: Variations in resistance of Zn-doped TiO_2 thin film with time after exposure for different Vol% of LPG.

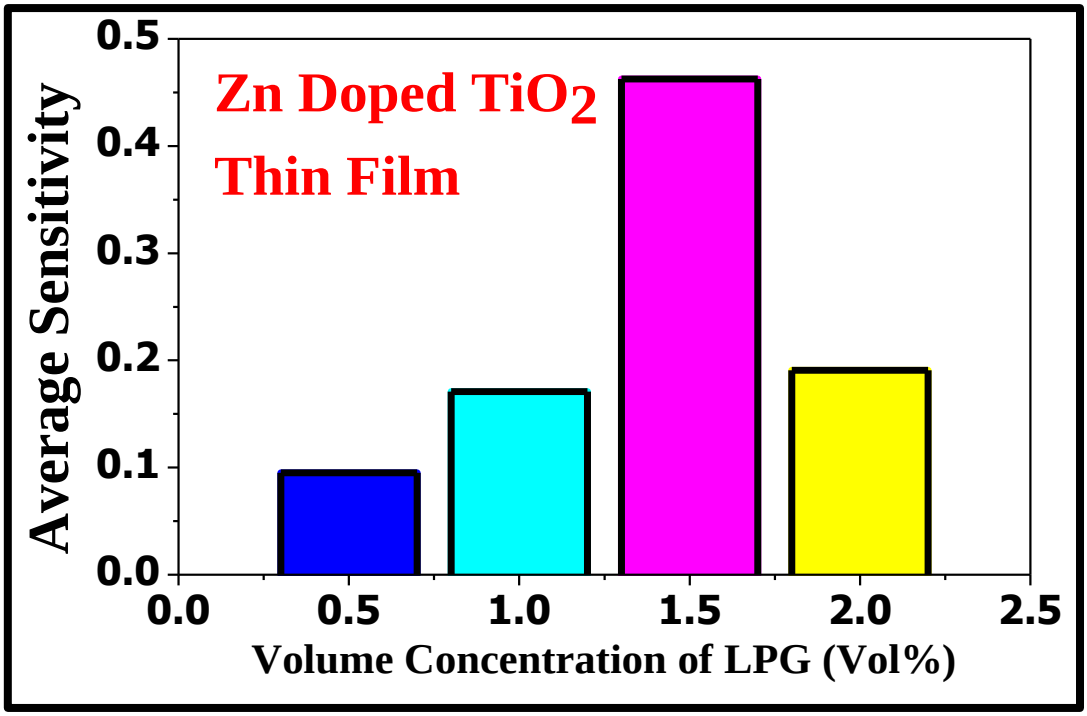

Figure 4.5: Variations of average sensitivity of Zn-doped TiO_2 thin film with different volume concentrations of LPG.

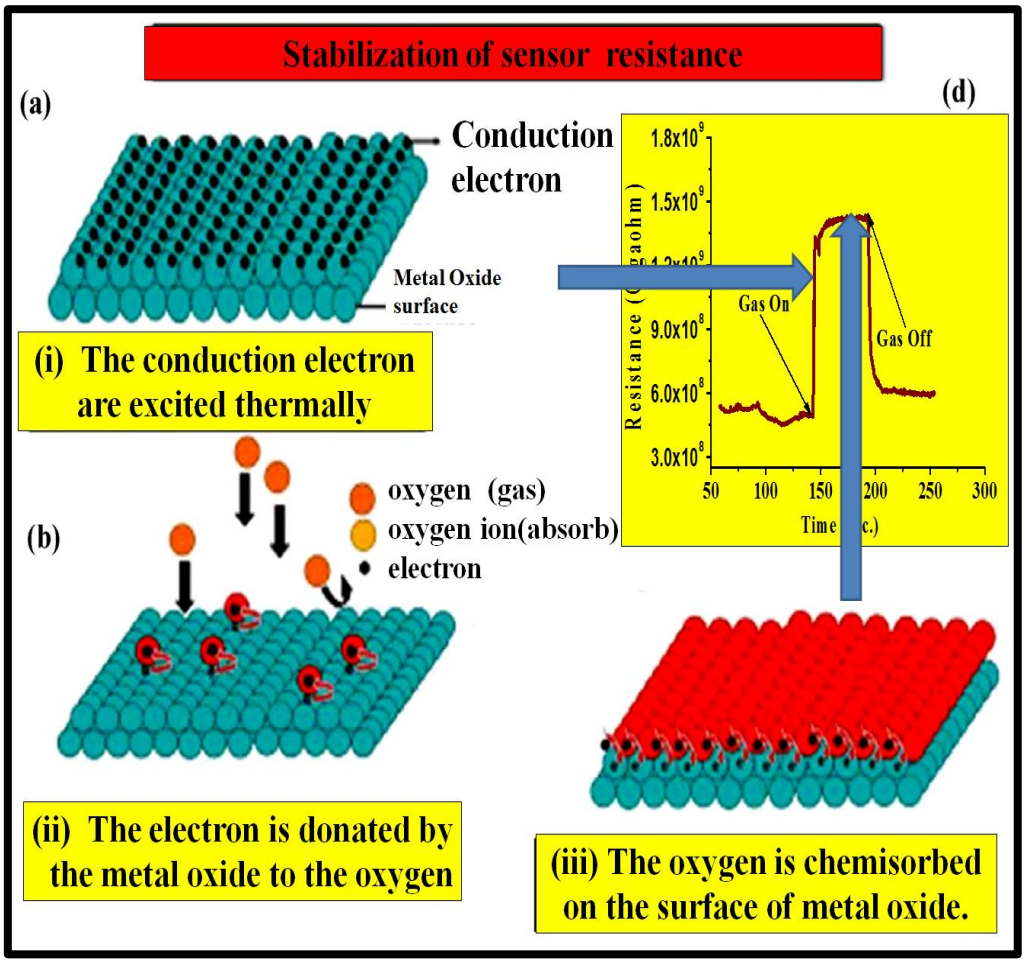

Figure 4.6 Stabilization of sensor resistance

Chapter 5

Synthesis and characterization of Ag-doped TiO_2 nanocomposites via sol-gel method for LPG sensor

This chapter reports the synthesis of Ag-doped TiO_2 nanocomposite via sol-gel method, its characterization and application as liquefied petroleum gas (LPG) sensor. The synthesised material was characterised using XRD and confirmed the creation of (Ag-TiO_2) nanocomposite. The minimum crystallite size was found as ~ 81 nm. XRD pattern shows the tetragonal crystalline nature of the material. The material was investigated through SEM and UV-Vis spectrophotometer. The thin film was fabricated for the sensing analysis. Further at room temperature, the film was exposed to LPG in a gas chamber under controlled conditions and variation in resistance with the concentration of LPG was observed. The maximum value of sensor response of solid state thin film based sensor was found 3.82 for 2 vol.% of LPG.

5.1 Introduction

The occurrence of toxic and pollutant gases in the home and at the workplace, in addition to outside, poses professional and health risks and thus gas sensing devices are necessary at such places. This concern has attracted extensive research interest in recent years towards developing gas sensors for various pollutant and toxic gases. Among the solid-state chemical sensors, the semiconductor metal oxide sensors have become the most hopeful devices due to the advantages of small size, low cost, good reversibility, high sensitivity and the possibility of integration [1]. Many semiconductor oxides such as SnO_2 [1–3], ZnO [4], Fe_2O_3 [5], In_2O_3 [6–8], WO_3 [9] and CuO [10] have been explored to sense poisoning and toxic gases such as toluene, H_2S, ethanol, CO, CO_2, NO_2, LPG, etc. Between these oxide materials, SnO_2 had always been the material of select and demanded to be the best in gas sensing but nevertheless, attempts in the direction of making TiO_2 equally promising were always there [11–14].

Titanium dioxide (TiO_2) is broadly investigated because of good chemical stability, non-toxicity, availability and low cost. Also, TiO_2 has been used as the material choice for photo-catalytic applications in environmental remediation long time [15-17] but looking into its flexibility, it seems to be equally favorable for gas sensing applications especially for reducing gases because it is an n-type semiconductor and at room temperature there is change in electrical resistance. On the basis of detection effects of the noble metals on metal oxides through chemical and electronic interactions, the base materials have been improved with these metals in order to improve their gas sensing characteristics. Wang et al. reported the effect of the addition of Ag, Au, Pd and Pt on the sensing properties of Fe_2O_3 sensors towards H_2S gas [18]. Gong et al. investigated the effect of the Ag-doped SnO_2 as H_2S sensor [19]. Joshi et al. studied the electronic interaction, size, and surface induced effects as the result of Ag metal additives

responsible for enhancing the gas sensing response of ethanol gas in In_2O_3: Ag composite nanoparticles layers [7-8]. Also, there have been precise contemporary reports of gas sensing properties of Ag nanoparticles embedded-ZnO nanorods synthesized by photochemical method [20] and Ag-doped TiO_2 prepared by Liquid Phase Deposition (LPD) towards NH_3 gas sensing [21]. Going through these reports and more on gas sensing applications involving Ag, it was observed that high amounts of dopant Ag was employed. Wang et al. used 0.25–5 wt% Ag in α-Fe_2O_3 sensors towards H_2S gas [18]. Singh et al. prepared In_2O_3: Ag composite nanoparticles layers with 15 wt% Ag in dip-coating method [8]. Ag-loaded TiO_2 powders were synthesized by sol–gel technique with Ag content of 0.1 mol%. Ag–TiO_2 catalysts have higher surface area and higher adsorption capacity than the bare-TiO_2, which was attributed to the more active site provided by Ag for TiO_2.

5.2. Experimental

5.2.1 Materials

Titanium tetrachloride ($TiCl_4$) (99.99%) and silver nitrate ($AgNO_3$) (99.99%) were purchased from Sigma Aldrich. Absolute ethanol (99.99%) was purchased from Merck.

5.2.2 Synthesis of Ag-doped TiO_2 nanoparticles

The synthesis of Ag-doped TiO_2 was done and described as follows in two steps:

(i) Preparation of TiO_2 nanoparticles: 3.9 ml of $TiCl_4$ into 10 ml of absolute ethanol was added slowly. This reaction was performed under vigorous stirring under fume hood at room temperature because of the exothermic reaction, the high volatility of $TiCl_4$ and the release of hydrogen chloride thereafter. Then, water was added dropwise to the mixture. The above solution changed from a colourless to a yellow viscous solution which produced TiO_2 nano-powder after drying it at 85 °C in an oven for 15 h. Finally, the

obtained TiO_2 nano-powder was calcined in a furnace at a temperature of 500 °C. The initial heating rate was maintained at 5 °C/min.

(ii) Afterwards, 10 mL silver nitrate solution (0.1M) was added dropwise to this solution of TiO_2 prepared above. The obtained paste was eventually dried at 85°C overnight. The dried gel was then ground to a fine powder and calcined in a muffle furnace at 500°C for 5 h. 0.1M Ag Doped TiO_2 powder was obtained by using a sol-gel method.

5.2.3 Fabrication of Ag-TiO_2 nanocomposite thin film sensor

A thin film of Ag doped TiO_2 material was prepared on a borosilicate glass substrate by using spin coating method. The first glass substrate was cleaned by using isopropyl alcohol, acetone, and deionized water. The glass slide was then sonicated in deionized water and absolute ethanol, respectively. A dispersed solution of the synthesized Ag-TiO_2 nanoparticles was prepared by sonicating 1 mg of the sample in 5 ml absolute ethanol. The cleaned glass substrates were coated by casting Ag-TiO_2 solution and dried at 100°C temperature to allow solvent evaporation.

5.3 Characterization of Ag-doped TiO_2 thin film

5.3.1 Scanning Electron Microscopy (SEM)

The surface morphology of the synthesized TiO_2 and silver doped TiO_2 powder was investigated by using scanning electron microscope (SEM, LEO-Cambridge) at Birbal Sahani Institute of Paleabotany (BSIP), Lucknow, U.P., India as shown in Figure 5.1. The SEM image shows that the distribution of Ag on the surface of TiO_2 is not uniform. Silver doped TiO_2 contains irregularly shaped particles due to aggregation of little crystals. Also, the figure shows that the densities of nanoparticles increase on increasing the silver content in TiO_2 lattice [22]. Spongy and porous structure causes more surface area at high hardness which is more efficient for adsorption [23]

5.3.2 X-ray diffraction

X-ray diffraction pattern was obtained by using X-ray diffractometer (Xpert, PRO PANalytical XRD system, Netherlands) with Cu-K_α radiations as a source at Department of Minerals, Geological Survey of India (GSI), Lucknow, U.P., India having wavelength 1.5418 Å. X-Ray diffraction pattern shows the amount of crystallization of the sample. The average crystallite size (D) of the sensing material can be calculated by the Debye-Scherrer's formula, which is given by the following equation:

$$D = \frac{K\lambda}{\beta \cos\theta} \quad (1)$$

Where, K= 0.94 is Scherrer's coefficient, which depends on the shape of the crystallite and the type of defects present, λ is the wavelength of X-ray radiation, β is the full width at half maximum (FWHM) of the diffraction peak and θ is the angle of diffraction. Figure 5.2 shows the XRD pattern of Ag doped TiO_2 sample and confirmed the rutile phase of TiO_2 with characteristic diffraction peaks of 2θ values at about 27.259(110), 35.76(101), 53.89(211), 54.7(105) and anatase phase at angle 25.3(101) by the JCPDS reference no. 010761941 and 010894921. Ag is found at angle 38.1(111). Thus the prepared Ag-TiO_2 powder was a crystalline phase material and the average crystallite size for the 25.3(101) plane was found as approximately 81 nm.

5.3.3 UV-Visible Spectroscopy

The optical absorption spectra of undoped and silver-doped titanium dioxide sample by an UV⁻Vis spectrophotometer in the range of 190-1100 nm at 400 °C are presented in Figure 5.3. It can be seen from the figure that the intensive absorptions are present in the range of about 240-380 nm. The recorded spectral data of undoped TiO_2 showed the strong cut-off at 410 nm; where the absorbance value is low. It can be seen that the absorption edge shifted towards the longer wavelength side for all Ag-doped

samples. The reason for this hypsochromic shift [24] in optical energy gap is that the energy level for Ag^{+}/Ag lies below the conduction band edge (E_{cb}) and above the valence band edge (E_{vb}) of TiO_2. The introduction of such energy levels in the bandgap induces the hypsochromic shift in transition and the visible light absorption through a charge transfer between a dopant conduction band and valence band or the d–d transition in the crystal field. A small red shift observed from Figure 5.3 and 5.4 indicates the decrease of band gap energies for Ag-doped TiO_2 to TiO_2 thin film. This would contribute to an enhanced photocatalytic activity. The fundamental absorption, which corresponds to the transmission from valance band to the conduction band, is used to determine the band gap of the material. The direct band gap energy can be estimated from a plot of $(\alpha h\nu)^2$ versus photon energy ($h\nu$). The energy band gap was determined by using the relationship:

$$(\alpha h\nu)^2 = A(h\nu - E_g) \quad (2)$$

Where, $h\nu$ = photon energy. Where A is a constant, $h\nu$ is the photon energy, E_g is the energy band gap and α is the absorption coefficient given by:

$$\alpha = 2.303\left(\frac{A_b}{t}\right) \quad (3)$$

A_b is the absorbance and t is the thickness of the film. The exponent 'n' depends on the type of transition and it may have values 1/2, 2, 3/2, and 3 corresponding to the allowed direct, allowed indirect, forbidden direct, and forbidden indirect transitions, respectively. The plots of $(\alpha h\nu)^2$ versus $h\nu$ for 0.1 M Ag doped TiO_2 are presented in Figure 5.4. The value of band gap was determined by extrapolating the straight line portion of $(\alpha h\nu)^2 = 0$ on the X- axis.

The optical absorbance spectra of the as-grown Ag-doped TiO_2 thin films deposited separately on the glass substrate was measured by Thermo evolution 201 UV-visible spectrophotometer in the wavelength range of 190 to 1100 nm, and the variation is shown

in Figure 5.3 and 5.4. This spectrum reveals that the sample has a low absorbance in the visible and near infrared regions. The enhanced absorption is observed in the neighbourhood of λ=400 nm. The optical data were analysed using the equation for near edge absorption [25]:

$$\alpha h\nu = k(h\nu - E_g)^n \quad (4)$$

Where, k is a constant, hν is the photon energy and E_g is the energy band gap, n is a pure number which depends on the nature of electronic transition responsible for the absorption. The band gap is obtained by extrapolating the linear portion of the Tauc plot of $(\alpha h\nu)^2$ *vs* photon energy (hν) on the X-axis. Our experimental result shows that optical absorption for the sample described by the equation (1) with n = 1/2 as shown in Figure 5.3 and 5.4 indicating the direct transition mechanism in the samples. The direct band gap observed by Tauc Plot in Figure 5.4 of 0.1 M Ag-doped TiO_2 thin film is found as 3.21 eV in comparison to 3.32 eV for TiO_2 as shown in Figure 5.3. The optical band gap of thermally treated Ag-TiO_2 film is smaller than those of pure titania due to effect of Ag nanoparticles. The observed decrease of E_g with silver addition is reported by other authors [26]. The shift of band gap is probably due to the interaction of Ag ions with TiO_2 [27] or formation of impurity band inside the TiO_2 band gap [28, 29].

5.4 Gas Sensing

5.4.1 Gas sensing measurements

The schematic diagram of LPG sensing set-up is shown in Figure 2.5 (a) in chapter 2. The sensing film was inserted between the silver electrodes inside the glass chamber having two knobs. One knob is associated with the concentration measuring system (gas inlet) and other is an outlet knob for releasing the gas.

Concentration measuring system is shown in Figure 2.5 (b) in chapter 2, which consists of glass bottle containing double distilled water, which is saturated with LPG, in order to avoid the possibility of dissolution of inserted gas. At the top of the bottle, the measuring tube (pipette) is connected by a vacuum seal. The cock I is connected to the LPG cylinder and cock II is connected to the inlet of the gas chamber. When the cock I is opened, the LPG from the cylinder is filled in the glass bottle and an equivalent amount of water is displaced in the measuring pipette. When the cock II is opened, a desired amount of gas e.g. 0.5, 1.0, 1.5 and 2.0 vol.% is entered into the gas chamber. Before passing the LPG in the chamber, the gas chamber with a resistance measuring holder was stabilised for 10-20 minutes.

Sensing film with silver contacts was used for measurements of LPG sensing properties. The stabilised resistance of the film was taken as stabilised resistance in the presence of air (R_a). Now, this was exposed to LPG and variations in electrical resistance with the time for different vol.% of LPG were recorded using the Keithley electrometer (Model: 6517A). Sensitivity of the LPG sensor is defined as the change in resistance in the presence of gas (R_g) to the resistance in presence of air (R_a) that is

$$S = \frac{R_a}{R_g} \tag{5}$$

Figure 5.6 illustrates the variations in resistance of the film with time after exposure for different vol.% of LPG at room temperature. The curve for 0.5 vol.% of LPG shows a small variation in resistance with time after exposure and inset Figure shows an increase in the resistance after exposing the gas. The curve for 1.0 & 1.5 vol.% of LPG exhibits the improved response and has better sensitivity than 0.5 vol.%. Further, the maximum sensing response of sensor was recorded 3.82 for 2 vol.%, the response and recovery characteristics of the sensor were found to be 13.2 s and 6.6 s respectively. The sensing response for different vol.% concentration has been depicted in Table 5.1.

When the Ag doped TiO_2 film gas sensor is exposed to air, oxygen gets chemisorbed on the surface of the oxide material, captures electron from the adsorption sites on the surface and depending on the temperature forms either O_2^-, O^- or O^{2-}. For a sensor operating at room temperature, formation of O^{2-} is favoured. Corresponding reaction kinematics is as given below:

$$O_2(gas) \leftrightarrow O_2(ads) \tag{6}$$

$$O_2(ads) + e^- \rightarrow {O_2}^- \tag{7}$$

This electron extraction tends to increase the resistance (for an n-type material such as TiO_2 in which majority charge carriers are electrons). Oxygen vacancies can be the best position for the adsorption of oxygen on the surface of the nanostructure and subsequent formation of the O_2^- depletion layer. Electron-transfer from conduction band to the chemisorbed oxygen results in a decrease in electron concentration on the film surface. As a consequence, an increase in the resistance of the TiO_2 film was observed. After some time the resistance of the film gets stabilized through above chemisorption reactions and stabilized resistance in the presence of air (R_a). Thus, the maximum sensitivity was obtained at higher concentration of LPG i.e. 2.0 vol.%. The linearity of average sensitivity for the LPG suggests that the Ag-doped TiO_2 nanocomposite thin film can be reliably used to monitor the LPG over this range of concentration. As the lower explosive limit (LEL) for LPG is ~ 2.0 vol.%, therefore, the response is measured up to 2.0 vol.% in order to detect the leakage of LPG below LEL for ensuring the safety.

When the Ag doped TiO_2 sensor is exposed to LPG, it reacts with the chemisorbed oxygen and a surface charge layer would be formed as per the following reaction [30].

$$C_nH_{2n+2} + {O_2}^- \rightarrow C_nH_{2n}O + H_2O + e^- \tag{8}$$

Where, C_nH_{2n+2} represent hydrocarbons. Due to the ejection of the electrons (charge carriers), the resistance of the film decreases after it comes in contact with LPG. It is obvious that the variations in resistance are smaller at the time just after the exposure while after 30 s the resistance increases rapidly. From Figure 5.5, it is obvious that the sensing response for Ag-TiO_2 thin film at 2.0 vol.% of LPG are the improvements over the previous published work [31-36]. During the three repeated injections of gas, its maximum response did not change. The gas sensor showed excellent sensing response ~ 3.82 having response and recovery times as 13.2 and 6.6 s for 2.0 vol.% of LPG respectively. Average sensitivity of sensor increases with increase in vol.% of LPG as shown in Figure 5.6 having highest value 42.76 at 2 vol.% of LPG. Working mechanism of 0.1 M Ag doped TiO_2 thin film as a LPG sensor is presented through schematic in Figure 5.7.

5.5 Conclusion

Ag-doped TiO_2 thin film based LPG sensor was thoroughly investigated and gave best sensing response as 3.82 for 2 vol.% at room temperature. Ag-doped TiO_2 thin film was successfully fabricated and characterised using SEM, XRD and UV-Vis spectrophotometer. SEM showed that particles were irregularly distributed on the surface of the film. XRD revealed the nanostructured crystals with minimum crystallite size as 81 nm. The Tauc plot obtained from UV-Vis spectrum gave the energy band gap of sensing material as 2.6 eV. Sensor response was found best for 2.0 vol.% of LPG as 3.82. Response and recovery time were found as 13.2 s and 6.6 s respectively. Average sensitivity of sensor increases with increase in vol.% of LPG and its highest value was found as 42.76 for 2 vol.% of LPG.

References

[1] R.K. Joshi, F. E. Kruis, Size selected $SnO_{1.8}$: Ag mixed nanoparticle films for ethanol, CO and CH_4 detection, J. Nanomater. (2007) DOI: http://dx.doi.org/10.1155/2007/ 67072.

[2] A. Srivastava, K. Jain, Rashmi, A.K. Srivastava, S.T. Lakshmi kumar, Study of structural and microstructural properties of SnO_2 powder for LPG and CNG gas sensors, Mater. Chem. Phys. 97 (2006) 85-90.

[3] R.K. Joshi, F.E. Kruis, O. Dmitrieva, Gas sensing behavior of $SnO_{1.8}$: Ag films composed of size-selected nanoparticles, J. Nanoparticle Res. 8 (2006) 797-808.

[4] N. Koshizaki, T. Oyama, Sensing characteristics of ZnO-based NO sensor, Sens. Actuators B 66 (2000) 119-121.

[5] L.H. Huo, Q. Li, H. Zhao, L .J. Yu, S. Gao, J.G. Zhao, Sol-gel route to pseudocubic shaped α-Fe_2O_3 alcohol sensor: preparation and characterization., Sens. Actuators B 107 (2005) 915-920.

[6] V.N. Singh, B.R. Mehta, R.K. Joshi, F.E. Kruis, Size-dependent gas sensing properties of indium oxide nanoparticles layers, J. Nanosci. Nanotechnol. 7 (2007) 1930-1935.

[7] V.N. Singh, B.R. Mehta, R.K. Joshi, F.E. Kruis, S.M. Shivaprasad, Enhanced gas sensing properties of In_2O_3: Ag composite nanoparticles layers, electronic interaction, size and surface induced effects, Sens. Actuators B 125 (2007) 482-488.

[8] V.N. Singh, B.R. Mehta, R.K. Joshi, F.E. Kruis, Effect of silver addition on the ethanol sensing properties of Indium Oxide nanoparticle layers optical absorption study., Hindawi Publishing Corporation, J. Nanomater. (2007). doi:10.1155/2007/ 28 031.

[9] X.L. Li, T.J. Lou, X.M. Sun, Y.D. Li, Highly sensitive WO_3 hollow-sphere gas sensors, Inorg. Chem. 43 (2004) 5442-5449.

[10] T. Cheng, Z.Y. Fang, Q.X. Hu, K.D. Han X.Z. Yang, Y.J. Zhang, Low temperature Co-Oxidation over CuO/Fe_2O_3 catalysts., Catal. Commun. 8 (2007) 1167-1171.

[11] H.M. Lin, C.H. Keng, C.Y. Tung, Gas sensing properties of nanocrystalline TiO_2., Nanostruct. Mater. 9 (1997) 747-750.

[12] A. Teleki, S.E. Pratsinis, K. Kalyanasundaram, P.I. Gouma, Sensing of organic vapors by flame-made TiO_2 nanoparticles., Sens. Actuators B 119 (2006) 683-690.

[13] I.A. Al-Homoudi, J.S. Thakur, R. Naik, G.W. Auner, G. Newaz, Anatase TiO_2 films based CO gas sensor: film thickness, substrate and temperature effects, Appl. Surf. Sci. 253 (2007) 8607-8614.

[14] R. Rella, J. Spadavecchia, M.G. Manera, S. Capone, A. Taurino, M. Martino, A.P. Caricato, T. Tunno, Acetone, and ethanol solid-state gas sensors based on TiO_2 nanoparticles thin film deposited by matrix assisted pulsed laser evaporation, Sens. Actuators B 127 (2007) 426-431.

[15] A. Kumar, N. Mathur, Photocatalytic oxidation of aniline using Ag-loaded TiO_2 suspensions, Appl. Catal. A: Gen. 275 (2004) 189-197.

[16] A. Kumar, N. Mathur, Photocatalytic degradation of aniline at the interface of TiO_2 suspensions containing carbonate ions, J. Colloid Interface Sci. 300 (2006) 244-253.

[17] N. Bahadur, K. Jain, A.K. Srivastava, Govind, R. Gakhar, D. Haranath, M.S. Dulat, Effect of nominal loading of Ag and Ni on the crystalline structure and photocatalytic properties of mesoporous titania, Mater. Chem. Phys. 124 (2010) 600-608.

[18] Y. Wang, Y. Wang, J. Cao, F. Kong, H. Xia, J. Zhang, B. Zhu, S. Wang, S. Wu, Low-temperature H_2S sensors based on Ag-loaded α-Fe_2O_3 nanoparticles, Sens. Actuators B 131 (2008) 183-189.

[19] J. Gong, Q. Chen, M.R. Lian, N.C. Liu, R.G. Stevenson, F. Adami, Micromachined nanocrystalline silver loaded SnO_2 H_2S sensor, Sens. Actuators B 114 (2006) 32-39.

[20] Q. Xiang, G. Meng, Y. Zhang, J. Xu, P. Xu, Q. Pan, W. Yu, Ag nanoparticle embedded-ZnO nanorods synthesized via a photochemical method and its gas-sensing properties, Sens. Actuators B: Chem. 143 (2010) 635-640.

[21] V.B. Georgieva, P.L. Stefchev, P.K. Stefanov, Z.G. Raicheva, M.J. Atanassov, Y.V. Lazarov, Study of the Ag-loaded effect on the LPD-TiO_2 gas sensing properties, AIP Conf. Proc. 1203 (2010) 1068-1073.

[22] S. Perumal, C.G. Sambandam, A.P. Mohamed, Synthesis and characterization studies of solvothermally synthesized undoped and Ag-doped TiO_2 nanoparticles using toluene as a solvent, Journal of engineering research and applications, 4(7)(2014) 184-187.

[23] H. Younas, I.A. Qazi, I. Hashmi, M.A. Awan, A. Mahmood and H.A. Qayyum, Visible light photocatalytic water disinfection and its kinetics using Ag-doped Titania nanoparticles, Environmental science, and pollution research, 21(1), (2014) 740-752.

[24] Kamlet, J. Mortimer, R. W. Taft, (1976). "The solvatochromic comparison method I. The beta-scale of solvent hydrogen-bond acceptor (HBA) basicities", Journal of the American Chemical Society, 98 (2) 377–383. ISSN 0002 7863. doi:10.1021/ja00418a 009.

[25] J. C. Tauc, Optical Properties of Solids, North-Holland, Amsterdam (1972) 372.

[26] C. Zhao, A. Krall, H. Zhao, Q. Zhang, Y. Li, Ultrasonic spray pyrolysis synthesis of Ag/TiO_2 nanocomposite photocatalysts for simultaneous H_2 production and CO_2 reduction, Inter. J. Hydrogen Energy 37 (2012) 9967-9976.

[27] K. Lalitha, J.K. Reddy, M.V.P. Sharma, V.D. Kumari, M. Subrahmanyam, Continuous hydrogen production activity over finely dispersed Ag_2O/TiO_2 catalysts from methanol:water mixtures under solar irradiation: a structure-activity correlation, International Journal Hydrogen Energy 35 (2010) 3991.

[28] N. Sobana, M. Muruganadham, M. Swaminathan, Nano-Ag particles doped TiO_2 for efficient photodegradation of direct azo dyes, Journal of Molecular Catalysis A-Chemical 258 (2006) 124.

[29] N. Sobana, K. Selvam, M. Swaminathan, Optimization of photocatalytic degradation conditions of direct red 23 using nano-Ag doped TiO_2, Separation and Purification Technology 62 (2008) 648.

[30] R.K. Sonker, B.C. Yadav, Chemical Route Deposited SnO_2, SnO_2-Pt and SnO_2-Pd Thin Films for LPG Detection, Adv. Sci. Lett. 20 (2014) 1023-1027.

[31] A.M. More, J.L. Gunjakar, C.D. Lokhande, Liquefied petroleum gas (LPG) sensor properties of interconnected web-like structured sprayed TiO_2 films, Sens. Actuators B 129 (2008) 671-677.

[32] D.S. Dhawale, R.R. Salunkhe, U.M. Patil, K.V. Gurav, A.M. More, C.D. Lokhande, Room temperature liquefied petroleum gas (LPG) sensor based on p-polyaniline/n-TiO_2 heterojunction, Sens. Actuators B 134 (2008) 988–992.

[33] R.N. Bulakhe, S.V. Patil, P.R. Deshmukh, N.M. Shinde, C.D. Lokhande, Fabrication and performance of polypyrrole (Ppy)/TiO_2 heterojunction for room temperature operated LPG sensor, Sensors and Actuators B 181 (2013) 417-423.

[34] L.A. Patil, D.N. Suryawanshi, I.G. Pathan, D.M. Patil, Nickel doped spray pyrolyzed nanostructured TiO_2 thin films for LPG gas sensing, Sensors and Actuators B 176 (2013) 514-521.

[35] E.R. Kumar, R. Jayprakash, G.S. Devi, P.S. Prasada Reddy, Magnetic dielectric and sensing properties of manganese substituted copper ferrite nanoparticles, Journal of magnetism and magnetic materials 355 (2014) 87-92.

[36] D.S. Dhawale, R. R. Salunkhe, V.J. Fulari, M.C. Rath, S.N. Sawant, C.D. Lokhande, Liquefied petroleum gas (LPG) sensing performance of electron beam irradiated chemically deposited TiO_2 thin films., Sensors and Actuators B 141 (2009) 58-64.

Table 5.1: Sensing response of different vol.% concentration

Concentration of LPG	**0.5 vol.%**	**1.0 vol.%**	**1.5 vol.%**	**2 vol.%**
Sensor Response	2.37	2.77	3.64	3.82
Response Time (s)	4.2	7.7	9.4	13.2
Recovery Time (s)	25	5.2	14.4	6.6

Table 5.2 Summary of result for LPG sensor based on MOS thin film

S. No.	**Material**	**Temp. (°C)**	**Volume Conc.**	**Sensor Response**	**Res./Rec. time(s)**	**Ref. no.**
1.	TiO_2	698	.08 vol%	35.8%	165/240	[31]
2.	p-Pani/ n-TiO_2	27	0.1 vol%	63%	140/180	[32]
3.	TiO_2	RT	1040 ppm	55%	112/131	[33]
4.	TiO_2	250	1000 ppm	90%	12/20	[34]
5.	$CuFe_2O_4$	300	1000 ppm	0.28	10/20	[35]
6.	Cu doped CdO	425	5200 ppm	38.7%	450/250	[36]
7.	Ag-TiO_2	RT	0.2 vol%	382%	13.2/6.6	Present work

Figures:

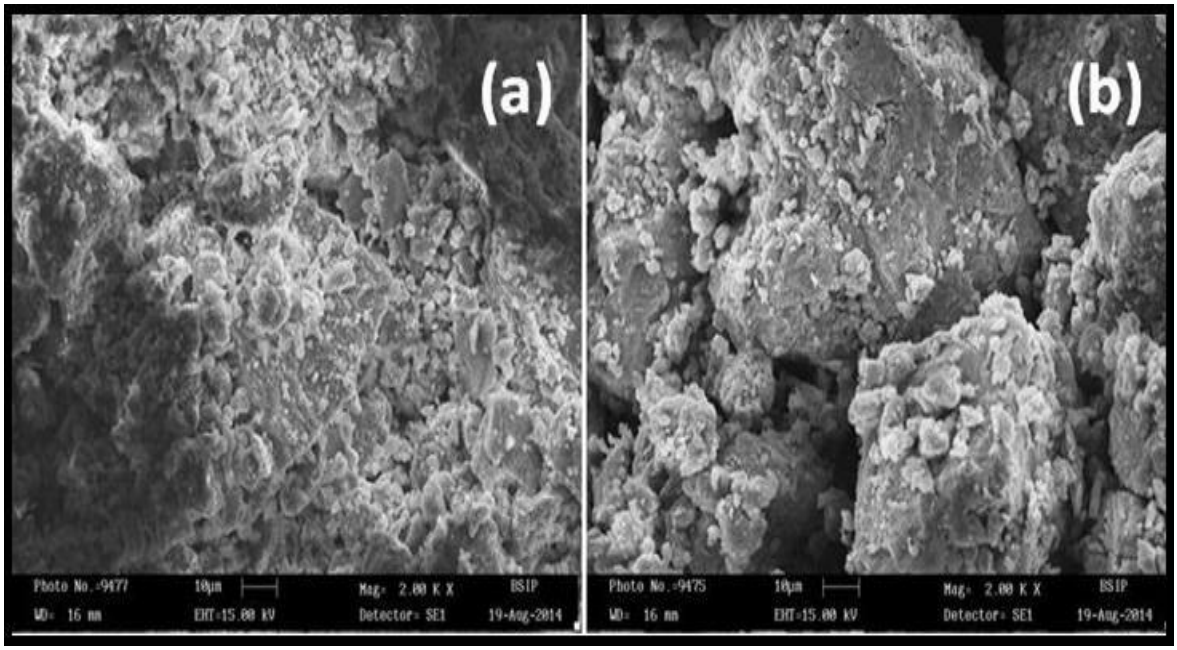

Figure 5.1 SEM images of (a) Bare TiO_2 (b) 0.1M Ag Doped TiO_2

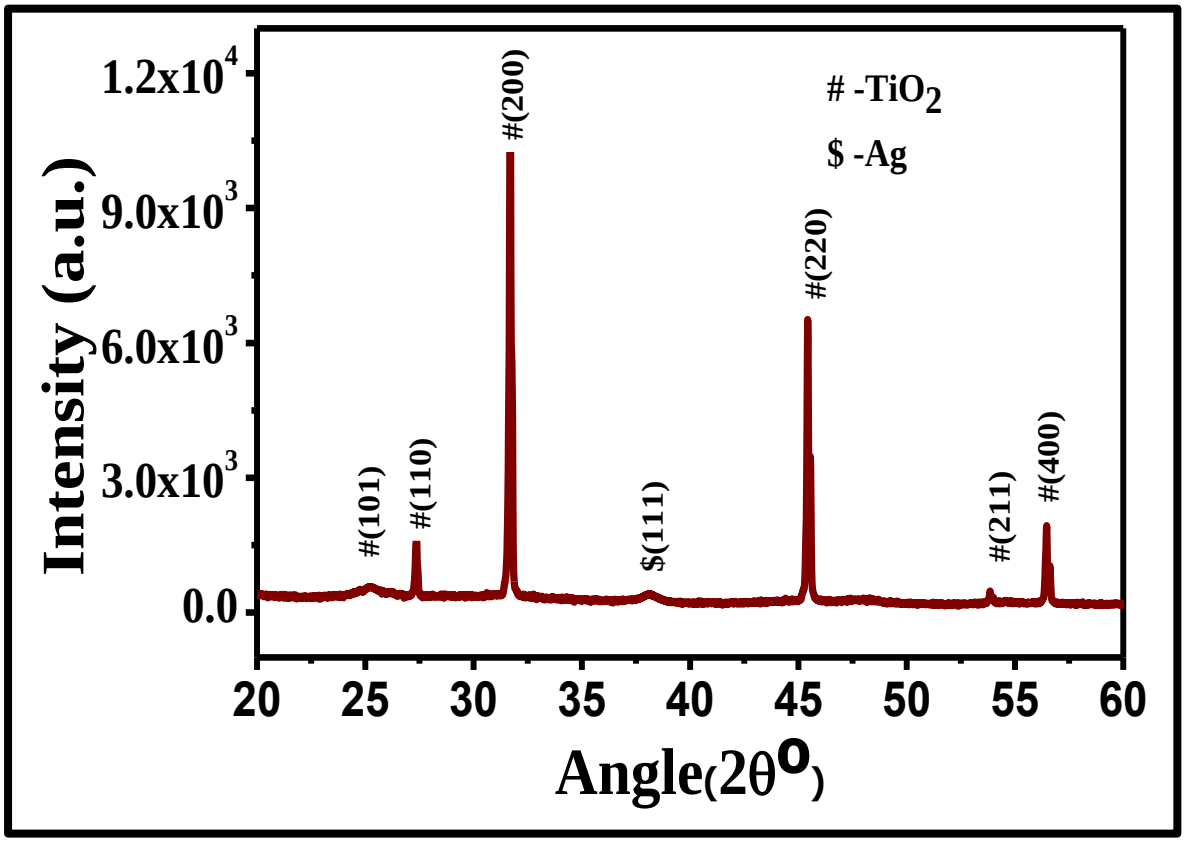

Figure 5.2 XRD pattern 0.1M Ag Doped TiO_2

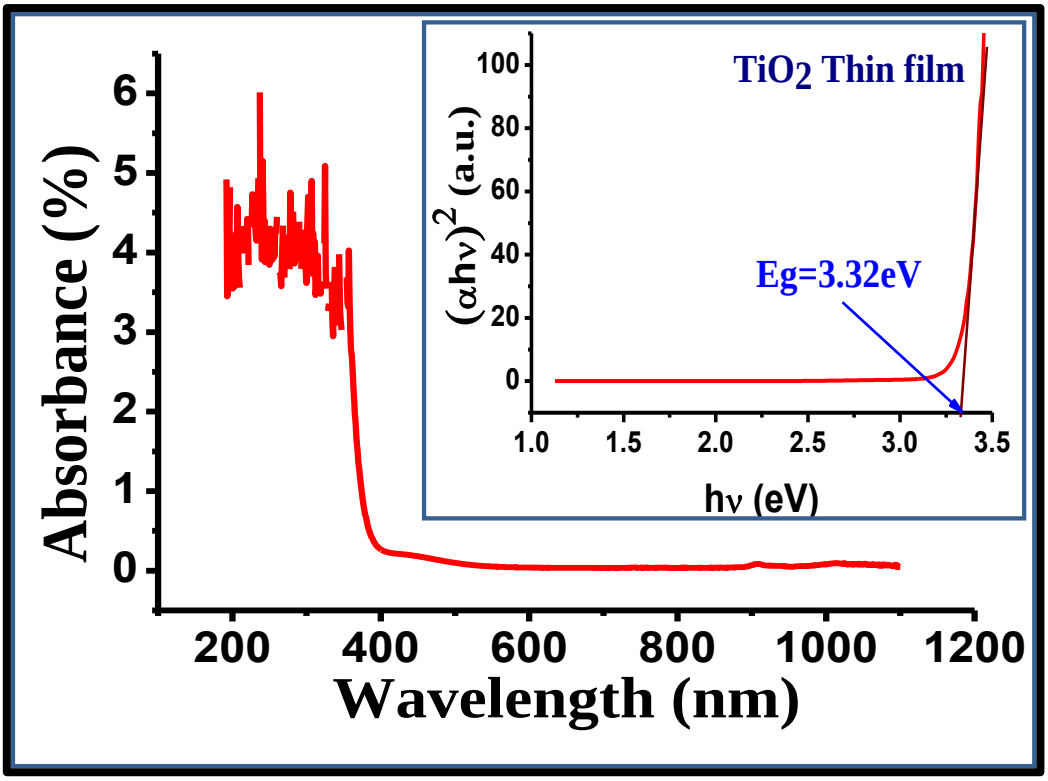

Figure 5.3: UV-visible Absorbance spectra of TiO_2 thin film and inset shows the Tauc plot of $(\alpha h\nu)^2$ versus $h\nu$

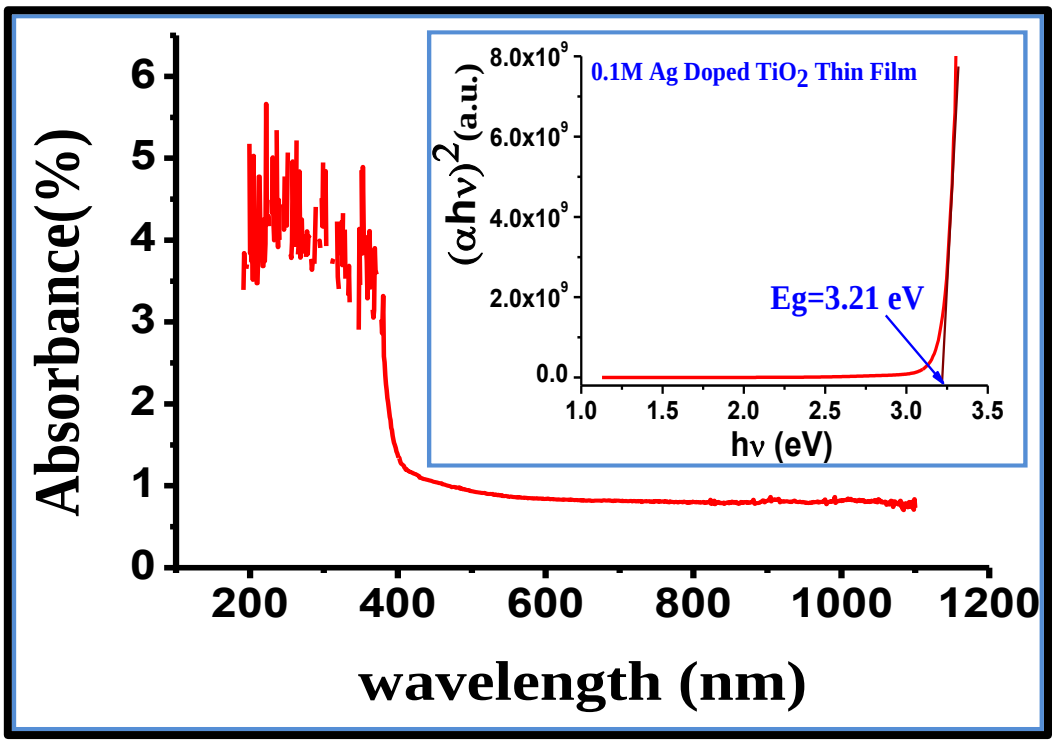

Figure 5.4: UV-visible Absorbance spectra of 0.1M Ag Doped TiO_2 thin film and inset shows the Tauc plot of $(\alpha h\nu)^2$ versus $h\nu$

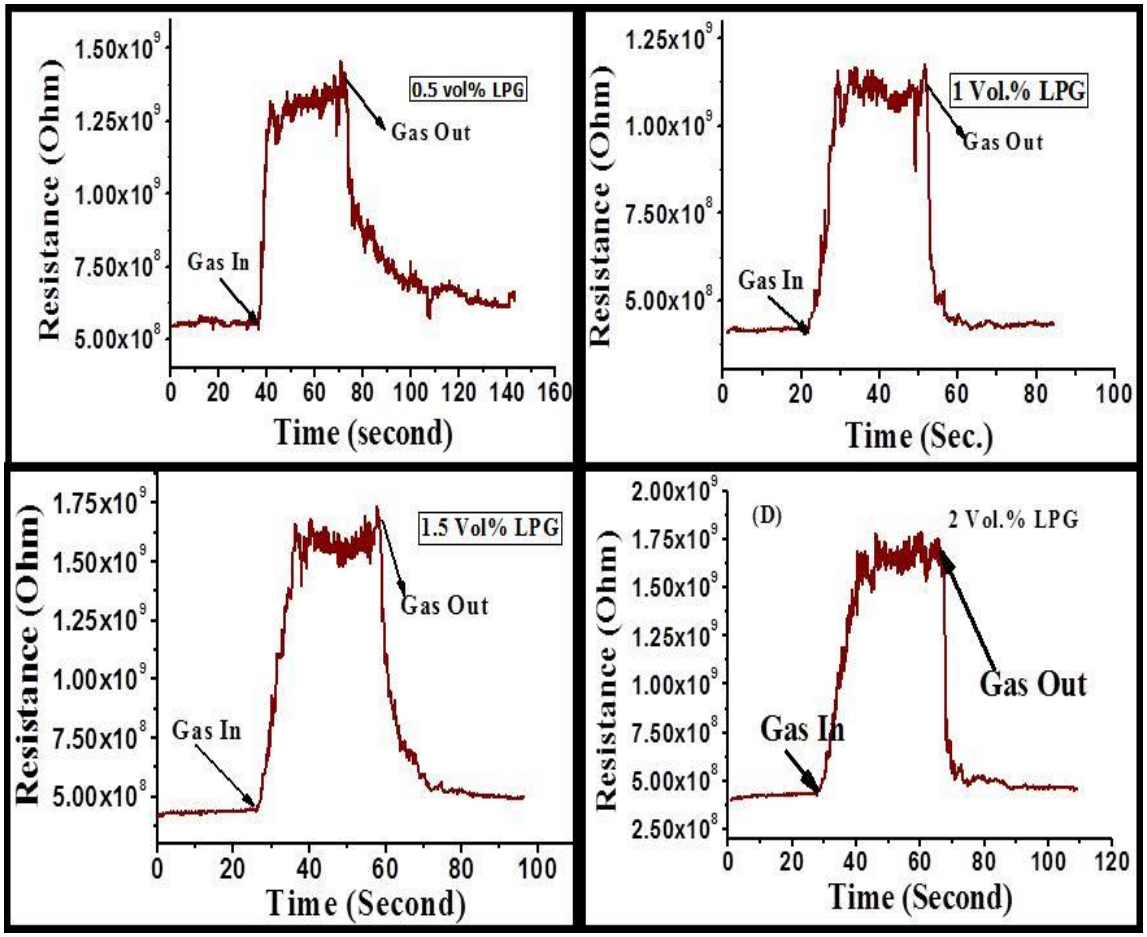

Figure 5.5: Variations in resistance of Ag doped TiO_2 thin film with time after exposure for different vol.% of LPG.

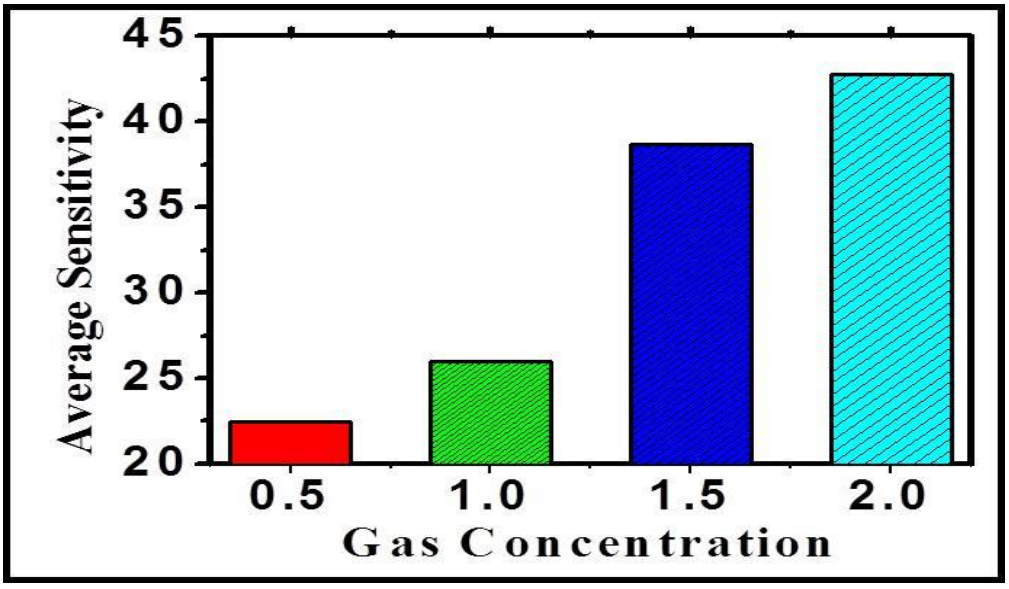

Figure 5.6 Variation of Sensitivity vs different gas concentration.

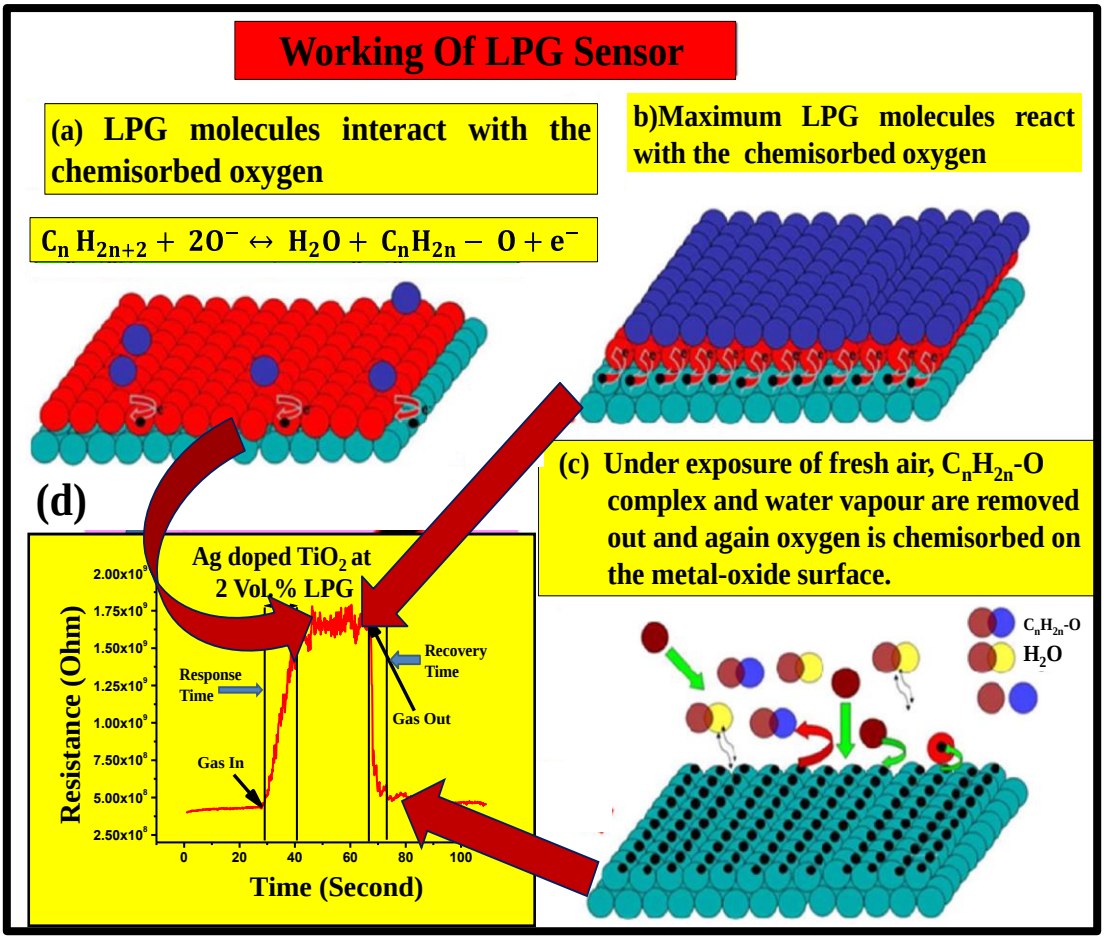

Figure 5.7: Schematic diagram working of LPG sensor for 0.1 M Ag doped TiO_2 Thin film.

Chapter 6

Concluding Remarks and Scope of Further Research

A systematic study of synthesis, characterization and LPG sensing properties of titanium oxide, PANI doped TiO_2, Zn doped TiO_2 and Ag doped TiO_2 is summarised in the present chapter. This chapter also provides the guidelines for further research work in the field of nanosized materials and their composites as LPG sensor.

6.1 Conclusion

Titanium dioxide is an important metal oxide for broad range of gas sensing applications, because of its surface chemistry, charge transport and electrical properties. It is a versatile material widely used in industry, research and ecological cleaning. Titanium dioxide is found in three different phases; rutile (tetragonal), anatase (tetragonal) and brookite (orthorhombic) and each phase has its own structure along with a specific application [1-4]. It is a versatile functional material due to its many unusual properties such as high refractive index, hydrophilicity [4], biocompatibility [5], semiconductivity, corrosion resistance, low cost, wide availability, nontoxicity and physicochemically stable nature [6] and also known for its gas sensing behavior [7-8]. Titanium dioxide has received considerable attention because of its excellent optical, electrical, mechanical, and catalytic properties, which makes it technologically useful. Its superior properties are due to chemical and biological inertness, non-toxicity, strong oxidizing/reducing power, cost-effectiveness and long-term stability against photo and chemical corrosions. The band gap of titania is about 3.2 eV. The band gap further increases with decreasing the particle size and hence the utilization typically confined within the UV-radiation of electromagnetic spectrum.

Basic requirement for a sensor is the sequential change in electrical conductivity with exposure of LPG to surface of semiconducting oxides which depends on their band gaps, surface morphology, size, diffusion rate of gas and specific surface area. The semi-conducting properties of metal oxides represent the basis for their use as gas sensors, since the number of free charge carriers within the metal oxide and thus its electrical conductivity reversibly depends on the interactions with the ambient gas atmosphere.

Since the LPG sensing mechanism is based on the chemisorption reaction that takes place at the surface of the metal oxide. Thus increasing the specific surface area of the sensing film leads to more sites for adsorption of surrounding gases. The oxygen adsorbed on the surface of the film influences the resistance of the titania based sensor. Initially oxygen from the atmosphere adsorbs on the surface of the film and extracts electrons from its conduction bands to form O_2^- species on the surface, consequently resistance decreases. After that an equilibrium state is achieved between oxygen of TiO_2 and atmospheric oxygen.

Usage of nanotechnology in engineering materials for sensor applications may improve the working detection limit of gas sensors to lower temperatures. This will be achieved predominantly by alterations of the space charge layers for each grain and enhancing other electronic properties of the material. The large surface to volume ratio of nanomaterials can be used as an advantage to contribute in gas sensor development. The surface reaction on the gas sensor is improved when the number of defect sites for reaction is augmented. The large surface area to volume ratio of nanocrystalline structures increases the opportunity for this surface reaction to occur. This in turn will increase the sensitivity of the gas sensor. The surface of nanomaterials can comprise much of the actual material making them ideal for gas sensors. Chapter-1 includes the introduction of nanomaterials, recent development in sensor and its limitations. The sensing principle and extensive survey of literature on the development of LPG sensor and its present status have been discussed. The orientation of work, aims and objectives of the present research investigation are well described at the end of the Chapter. It also deals with the description of synthesis and characterization techniques used in the present research work. The advantage of sol-gel technique over other synthesis methods has been described. Chapter 2 describes the sol-gel processed grape-like nanostructured Titania

based Liquefied Petroleum Gas Sensor. In Chapter 3, preparation of PANI doped TiO_2 nanocomposite thin film and its relevance as room temperature liquefied petroleum gas and CO_2 gas sensor is reported. The film of same sensing material has been deposited on the corning glass substrate with IDEs using spin coating technique and this was exploited for room temperature detection of LPG. Chapter 4 deals with the LPG sensing properties of thin film of Zn doped TiO_2 using sol-gel spin coating technique. Chapter 5 describes the synthesis and characterization of Ag doped TiO_2 nanocomposites via sol-gel method for LPG sensor. Chapter 6 deals with summary of the work done and the concluding remarks drawn from the present research work. Future scope for further research work in the field of nanosized materials and their composites as LPG sensor has been depicted at the end of this thesis.

A study of synthesis, characterization and sensing properties of pure and doped TiO_2 is summarized as followed:

6.2 Grape-like nanostructured Titania based Liquefied Petroleum Gas Sensor

Liquefied petroleum gas (LPG) sensor has become the interesting topic of research today in observation of fundamental research as well as industrial applications. Gas sensors that utilize metal oxide materials are widely used in industry to monitor combustion processes while they are inexpensive and robust in high temperature environments, many of these instruments are not selective towards the species of interest when placed in a stream composed of multiple gases. Metal oxide semiconductors are useful for the detection of combustible gases by the change in the surface conductivity due to exposure of gases. TiO_2 is an important metal oxide for broad range of gas sensing

applications, because of its surface chemistry, charge transport and electrical properties. It is a versatile material widely used in industry, research and environmental cleaning.

In this work, LPG sensor operable at room temperature was fabricated using titanium oxide thin film prepared by spin coating method successfully. Film thickness was measured as 0.4 μm and average crystallite size was estimated as 21 nm by X-Ray Diffraction pattern. The average sensitivity of sensor increases linearly up to 4 vol.% of LPG. The linear increment of the sensitivity of the sensor is a significant factor for the device fabrication. The maximum sensitivity was obtained as ~ 0.65 for 4 vol.% of LPG. In present investigation the improved sensing performance of sample may be attributed to their porous spherical structure and crystallite size. The pores in irregular nanospheres can act as channels for diffusion of LPG, and thus provide more active sites where LPG molecules get absorbed and counter the surface species (O_2, O_2^-, O^-). This improves the reaction of LPG with surface adsorbed oxygen and is an imperative parameter regarding the sensitivity of the sensor.

The maximum sensing response was found as ~ 2.8 for 4 vol.% of LPG with a response and recovery times of 240 sec and 248 sec respectively. This sensor structure may be exploited for the device fabrication for the detection of LPG below LEL. TiO_2 thin film exhibits a high transmission (>75%) in the visible region and show a sharp fundamental absorption edge in UV region at 380 nm. The band gap for as-grown TiO_2 thin film is found to be 3.65 eV in the linear portion of the Tauc plot. Also by using appropriate dopant, the band-gap of synthesized material can be engineered so that the sensitivity of the sensor may enhance. The complete sketch of LPG sensing experiment along with the gas concentration measurement set-up is depicted in Figure 6.1.

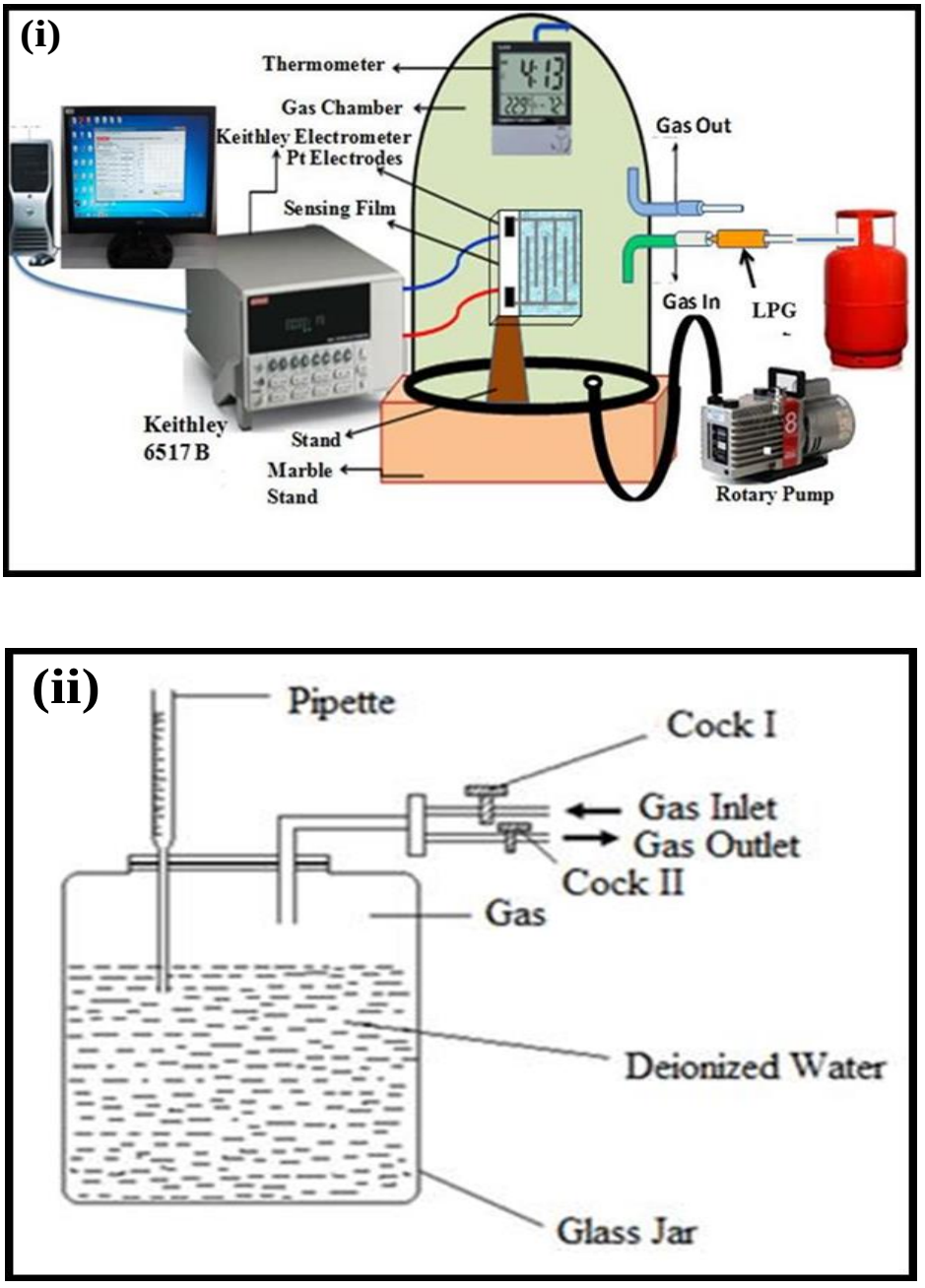

Figure 6.1: (i) Gas sensing Set-up: Lab Model (**ii)** Concentration measuring system

6.3 Preparation of PANI doped TiO_2 nanocomposite thin film and its relevance as room temperature liquefied petroleum gas and CO_2 sensor

Present work reports the utility of PANI doped titanium dioxide thin film prepared by spin coating technique as LPG and CO_2 sensing. The increasing requirements of carbon dioxide detection in various fields like air quality control, greenhouse monitoring

and bio-related processes have been demanding high-quality CO_2 sensors in day to day. Optical properties were investigated using UV–vis absorption spectroscopy. The surface morphology and structure of synthesised material were characterised by TEM and XRD analysis, respectively. The structural analysis confirmed the formation of TiO_2-PANI having an average crystallite size is 7 nm. Variations in resistance with exposure of LPG to the sensing element were observed. Sensor response (S) as a function of time was calculated and its maximum value was found as 2.37 towards 2000 ppm of LPG, response time of the sensor was 2 min. Similarly, the sensor response (S) as a function of time was calculated and its maximum value was found as 53 for 1000 ppm of CO_2. Response and recovery times of the sensor were observed as 9.2 min and 5.7 min respectively. The sensor was quite sensitive and results were found reproducible. Preparation of PANI-TiO_2 film, experimental set-up, LPG sensing mechanism and its characteristics are briefly presented through schematic in Figure 6.2.

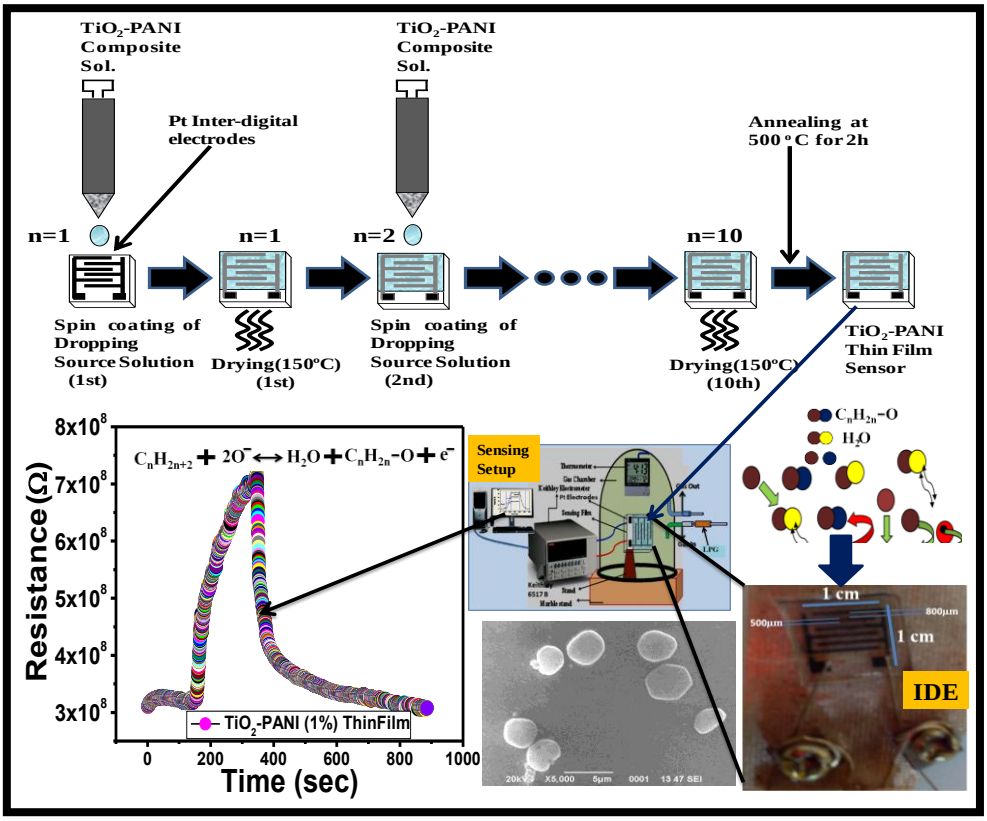

Figure 6.2: Schematic diagram of LPG sensing mechanism

6.4 Zn doped TiO_2 nanoparticles employed as room temperature Liquefied Petroleum Gas Sensor

This chapter reports the performance of a room temperature liquefied petroleum gas (LPG) sensor based on Zn doped titanium dioxide hetrojunctions thin film prepared by spin coating technique. The surface morphology and structure of synthesized material were characterized by SEM and XRD analysis respectively. The structural analysis confirmed the formation of Zn doped TiO_2 having an average crystallite size 76 nm with tetragonal rutile structure. Optical properties were investigated using UV–vis absorption spectroscopy. Energy band gap of material was estimated as 3.26 eV. Variations in resistance with the exposure of LPG to the sensing element were observed. Sensor response (S) as a function of time was calculated and its maximum value was found as 2.92 towards 1.5 vol.% LPG, response time of the sensor was 120 s.

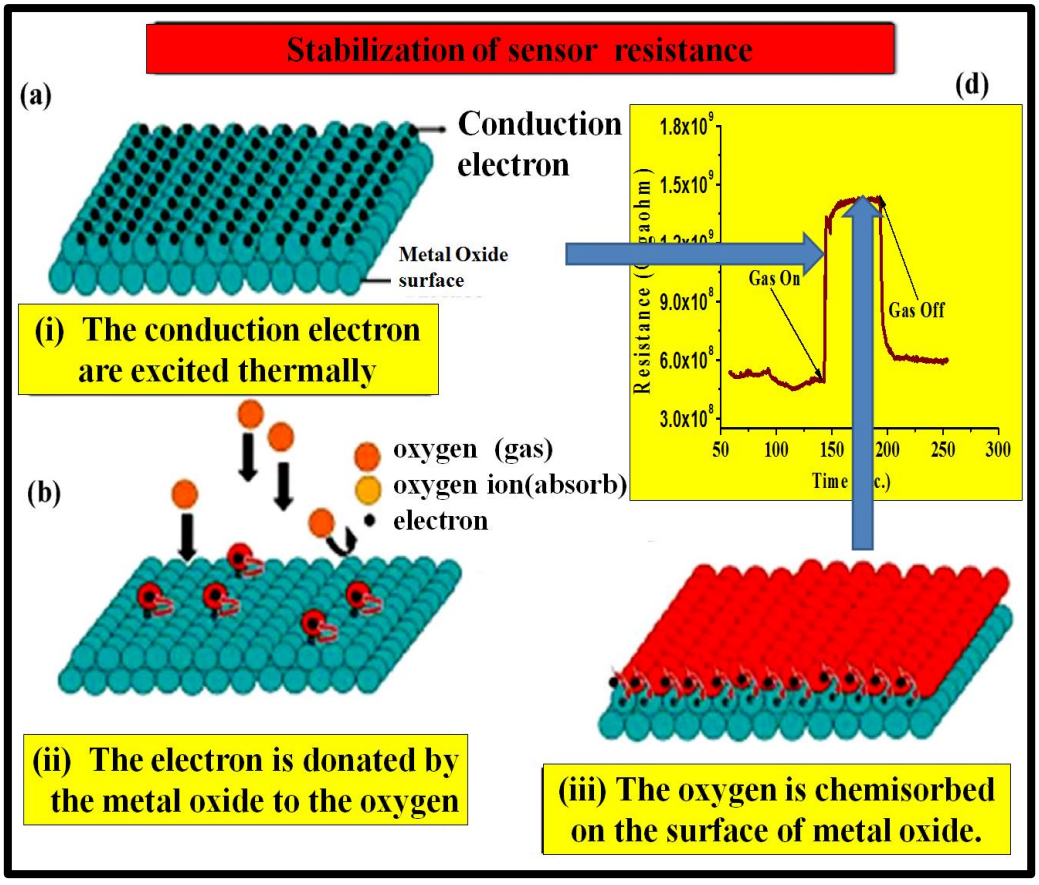

Figure 6.3 Stabilization of sensor resistance

The sensitivity of the LPG sensor at 1.5 vol.% was found as 0.4625. The sensor was moderately sensitive to LPG and results were found reproducible. The stabilization mechanism of sensor resistance is shown in Figure 6.3.

6.5 Synthesis and characterization of Ag doped TiO_2 nanocomposites via sol-gel method for LPG sensor

This chapter reports the synthesis of Ag doped TiO_2 nanocomposite via sol-gel method, its characterization and application as liquefied petroleum gas (LPG) sensor. The synthesized material was characterized using XRD which confirmed the creation of (Ag-TiO_2) nanocomposite. Minimum crystallite size was found as ~ 81 nm. XRD pattern show the tetragonal crystalline nature of anatase material.

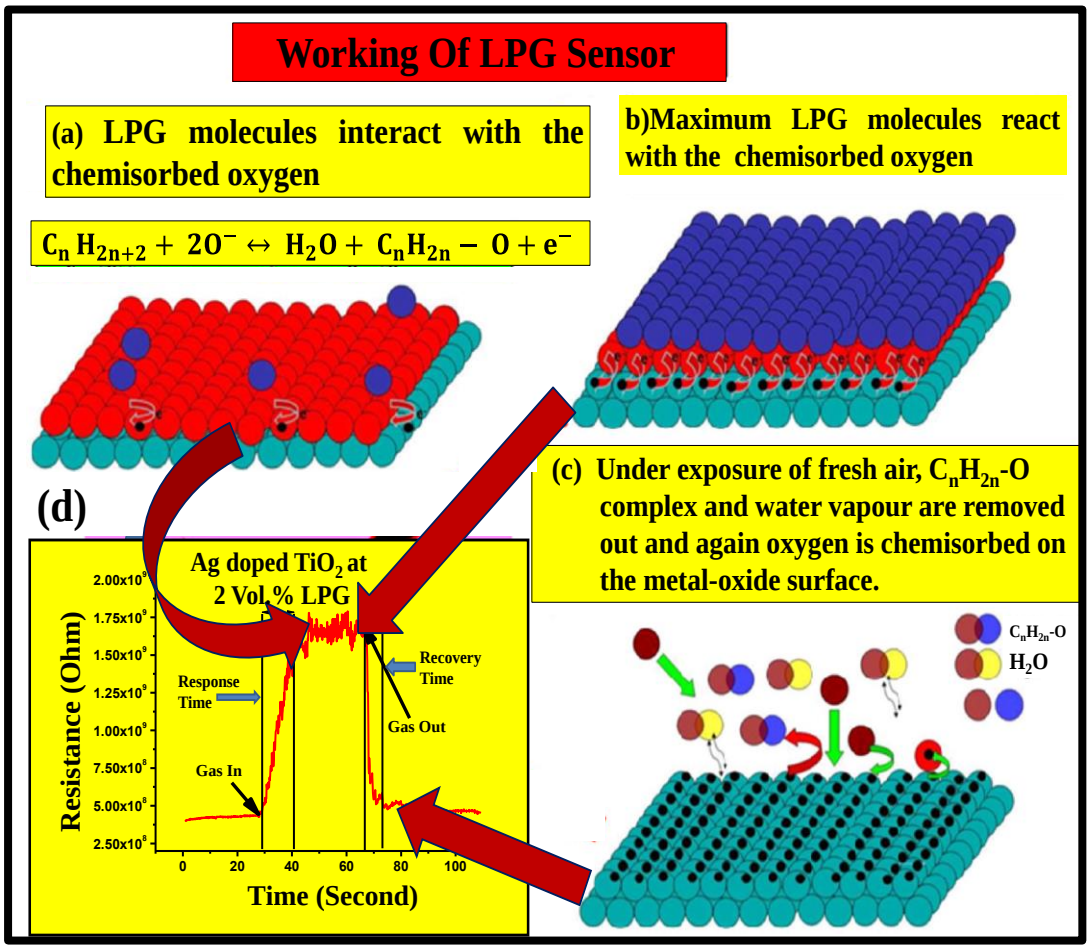

Figure 6.4: Schematic diagram showing the working of LPG sensor using 0.1 M Ag doped TiO_2 thin film.

The material was investigated through SEM, and UV-Vis spectrophotometer. The thin film was fabricated for the sensing analysis. Further at room temperature, the film was exposed to LPG in a gas chamber under controlled conditions at room temperature and a variation in resistance with the concentrations of LPG was observed. The maximum value of sensor response of solid state thin film based sensor was found 3.82 for 4 vol.% of LPG, respectively. The schematic diagram of working of LPG sensor using 0.1 M Ag doped TiO_2 thin film has been presented in Figure 6.4.

A chapter wise sketch of the thesis including the materials, percentage sensor response, crystallite size and concerned journals is depicted in Table 6.1. The main goal of our research work carried out was to design and fabricate a LPG sensor which would be robust, cost effective and more sensitive than previously reported sensors.

Table 6.1: A chapter wise sketch of the Thesis.

Chapters	**Sensing Materials**	**Target Gas**	**Concentration of gas**	**Sensor Response**	**Response time(s)**	**Recovery time(s)**
Chapter 1	Introduction					
Chapter 2	TiO_2	LPG	4.0 vol. %	1.34	117	148
Chapter 3	PANI-TiO_2	LPG	2000 ppm	2.77	156	140
Chapter 4	Zn doped TiO_2	LPG	1.5 vol. %	2.92	120	102
Chapter 5	Ag-TiO_2	LPG	2.0 vol. %	3.82	13.2	6.6
Chapter 6	Concluding Remarks					

From the Table 6.1, we conclude that the nanocrystalline Ag doped titanium oxide is an excellent material for LPG sensing application at room temperature and using this material a commercialized model of LPG sensor applicable for both indoor and outdoor detection of LPG may be designed. Thus various configurations/systems described in the thesis and the detailed specifications given for each of them are expected to prove beneficial in fabricating a sturdy, robust and cost-effective LPG sensor suitable for operation over the entire range; from lower explosive limit (LEL) to upper explosive limit (UEL).

6.6 Scope and suggestions of work for further research

(i) In future, I want to study the effect of swift heavy ion irradiation and gamma irradiation on metal oxide semiconductor and effect on the sensitivity and sensor response of gas sensor by using other harmful gases in environment. Growth simulations and reconstructions of the different surface species under different irradiation conditions would give rise to even more specific engineering of nanomaterials than what is currently known to the world of research within nanotechnology. Radiation effect evaluation on the sensing mechanism would be very fruitful in the selection of the material to be used for the fabrication of a gas sensor in future.

(ii) Detailed analysis of the evolution of the surface reactions with respect to temperature needs to be carried out, in order to exactly understand the reaction products from the surface interaction. Temperature Programmed Desorption (TPD) experiments give valuable information on the formation and desorption of reaction products on the surface. Controlled TPD experiments, at the sensing temperatures need to carry out for understanding the surface chemistry.

(iii) TiO_2 thin film based LPG sensor has been prepared using sol-gel technique. To improve the sensing response parameters, there is scope for integration of best identified modifiers like WO_3, TeO_2 and Al_2O_3 for the fast detection of LPG gas for the outdoor applications.

(iv) Theoretical modelling on sensing mechanism of LPG and other oxidising gases with the metal oxides may be under taken for further investigations.

(v) The presence of crystallographic defects affects the sensing mechanism of gas sensors. A quantitative study that links the presence of these defects and the density of states in the energy gap with the sensitivity of the sensors has to be done. A detailed XPS study before and after sensing of all gas analyte would confirm the reaction mechanism with those gases. An in-situ XPS with gas atmosphere control would give better idea as to what happens to the electronic structure of the metal oxide during high temperature gas interaction and also an idea of how the shear planes grow and whether this leads to an increase in the density of states in the gap.

References:

[1] C. Xiabo, S.S. Mao, Titanium Dioxide Nanomaterials: Synthesis, Properties, Modifications, and Applications, Chem. Rev., 107 (2007) 2891-2906.

[2] A. Fujishima, K. Honda, Electrochemical photolysis of water at a semiconductor electrode, Nature, 238 (1972) 37-38.

[3] U. Diebold, The surface science of titanium dioxide, Surf. Sci. Rep., 28 (2003) 53-229.

[4] O. Carp, C.L. Huisman, A. Eller, Photoinduced reactivity of titanium dioxide, Solid State Chem., 32 (2004) 33-177.

[5] A.K. Jha, K. Prasad, Ferroelectric $BaTiO_3$ nanoparticles: biosynthesis and characterization, Colloids Surf., 5 (2010) 330-334.

[6] C. H. Kwon, H. Shin, J. H. Kima, W. S. Choi, K. H. Yoon, Degradation of methylene blue via photocatalysis of titanium dioxide, Mat. Chem. Phys. 86 (2004) 78-82.

[7] L.R. Skubal, N.M. Meshkov, M.C. Vogt, Detection and identification of gaseous organics using a TiO_2 sensor, J. Photochem. Photobiol, 148 (2002) 103-108.

[8] K.R. Meier, M. Gratzel, Redox Targeting of Oligonucleotides Anchored to Nanocrystalline TiO_2 Films for DNA Detection, Chem. Phys. Chem., 3 (2002) 371-374.

APPENDIX

Experimental Methods and Characterization Techniques

This chapter gives an account of experimental facilities used throughout the whole thesis work have been presented. The synthesis part shows the chemical route of the synthesis of metal oxides whereas the characterization part shows the experimental techniques used such as TEM, SEM, FTIR, UV-Visible, spectroscopy and XRD etc.

A.1 Introduction

Sensor characterization is an important feature to identify the various aspects of performance of gas sensor and the experimental part plays very critical role in the outcome of any research work. This Chapter describes the methodology and various experimental techniques used in the preparation and modification of nanostructured Titania, polyaniline (PANI) doped Titanium Di-oxide (TiO_2-PANI), Zn doped Titanium Di-oxide (Zn-TiO_2), and Silver doped Titanium Di-oxide (Ag-TiO_2) composite thin films. These films were characterized using Fourier transform infrared (FT-IR), UV-Vis spectroscopy, SEM, XRD and TEM. These techniques have been described in detail in this chapter.

A.2 Methodology of present work

The methodology adopted in the present thesis is summarized as following:

- Synthesis of Titania as thin film by sol-gel technique.
- Synthesis of conducting PANI doped TiO_2 as thin film by sol-gel technique.
- Synthesis of conducting Zn doped TiO_2 as thin film by sol-gel technique.
- Synthesis of conducting Ag doped TiO_2 as thin film by sol-gel technique

A.2.1 Methods

A.2.1.1 Sol-gel Techniques

A solution (sol) is a dispersion of the solid particles (~ 0.1-1 μm) in a liquid where only the Brownian motions suspend the particles. A gelation (gel) is a state where both liquid and solid are dispersed in each other, which forms a solid network containing liquid components. The schematic flow chart of sol-gel process is shown in Figure A.1.1. The sol-gel coating process usually consists of 4 steps [1-2].

1. The desired colloidal particles are dispersed in a liquid to form a sol.

2. The deposition of sol produces the coatings on the substrate by spraying, dipping or spinning.
3. The particles in sol are polymerized through the removal of the stabilizing components and produce a gel in a state of a continuous network.
4. The final heat treatment pyrolyze the remaining organic or inorganic components and form an amorphous or crystalline coating.

The increasing demand for multifunctional materials requires a stronger multidisciplinary approach as well as the merging of the traditional scientific disciplines (chemistry, physics, and biology) into new cross-boundary technologies. Moreover, these novel technologies have to be able to bridge the gap between polymers, ceramics or metals, between organic and inorganic materials, or between the mineral and biological world. Sol-gel technology might offer a solution. The first experiment on sol-gel was performed in the fifties of the previous century. By their inorganic nature, sol-gel layers are extremely strong and wear resistant. Therefore, very thin 'nanometric' layers surface to obtain the desired effects. Since several years, there is an increasing demand of sol-gel technology in the application of device fabrication. However, the formula and methods used in other industrial branches have to be adapted to the raw materials and specific properties [3-4]. In the present work, sol-gel technique will be exploited for the synthesis and deposition of TiO_2, TiO_2-PANI, Zn-TiO_2 and Ag-TiO_2 thin films.

A.2.2 Fabrication Techniques for Thin Film

A.2.2.1 Sputtering

In an alternating electric field, electrons oscillate to and fro and during their motion they collide with other atoms. The ordered motion changes to random motion due to the collisions. The energy of electrons increases sufficiently to produce ionization collision,

which further releases more electrons. The high voltage, essential in dc-sputtering for the generation of secondary electrons to sustain the discharge is not required in rf sputtering. The electrons in the plasma will have sufficient energy to directly ionize gas atoms, reducing the dependence on the secondary generation of electrons at the cathode. At an operating frequency of 13.56 MHz, the ions in the plasma can no longer move quickly enough to offset the changing field, due to which only a little accumulation of positive ions occur during the portion of the cycle in which the target electrode is acting as a cathode. However, due to the high mobility of electrons, the electron current in the target surface is initially much higher than the ion current. This results in a fixed negative dc bias on the target with respect to the plasma. The value of the bias potential is close to half of the peak-to-peak rf voltage on the target surface. The positive ions from the plasma are accelerated towards the target essentially by the bias potential (V_b) rather than the rf potential, and bombard the target surface with energy of the order of V_b electron volts to sputter out the atoms. The rf diode sputtering unit were used for preparation of Pt interdigited electrodes (IDTs) shown in Figure A.1.2 and a platinum IDTs shown in Figure A.1.3.

A.2.2.2 Spin coating unit

Preparation of a highly cross-linked solid thin film, onto substrates can be achieved by mean of hydrolysis and condensation of the molecular precursor using the spin coating technique. The substrate is placed on the chunk table and hold by vacuum (~10^{-2} mTorr), so as to keep it stable while providing rotation. Once the substrate is fixed on the chuck, the filtered precursor solution is drop casted on the substrate using the pipette in measured quantity and allowed to spin at a particular rpm in spin coater (Figure A.1.4). Typical spinning speed is ranging from 500 to 6000 rpm, depending on the properties of the fluid as well as the substrate. To achieve a required thickness of film along with uniformity the combination of spin speed and time are selected and optimized. In the spin-up stage, the

liquid flows radially outwards by means of centrifugal force acting outwards giving rise to the formation of uniform thin film.

A.3 Thin Film Characterization techniques

Synthesis of TiO_2, TiO_2-PANI, Zn-TiO_2 and Ag-TiO_2 composite thin films were characterized by various characterization techniques to study the optical properties, surface morphology and electrical and dielectric properties using XRD, FTIR, UV-Visible Spectroscopy, Scanning Electron Microscopy (SEM), TEM.

A.3.1 Structural Characterization

A.3.1.1 X-ray diffraction

X-ray diffraction (XRD) is an indispensable characterization tool for the study of crystallographic structure of matter and has been extensively used for the investigation of the orientation of deposited material, determination of grain size, estimation of stress etc. The periodic and regular arrangement of atoms in the crystal acts as scattering centers, because the interplanar spacing is of the order of the wavelength of X-rays. In a typical powder XRD system monochromatic X-ray radiation is incident on the powder specimen at an angle θ, called the Bragg's angle, and the intensity of the diffracted beam is measured simultaneously. For a given angle of incidence (θ), only those reflections from a crystal plane will be detected in the scattered beam which satisfies the Bragg's diffraction condition:

$$n\lambda = 2d \sin\theta \quad (1)$$

where, n is the order of diffraction, 'λ' is the wavelength of X-rays (λ = 1.54056 Å for Cu K_α radiation), and 'd' is the inter-planar spacing.

In the present work, a Bruker D 80 X Ray diffractometer is used to study the crystallographic structure of the metal oxide (TiO_2) and various materials doped metal oxide thin films shown in Figure A.1.5. The specimen is mounted at the center of the diffractometer

and is rotated continuously around an axis parallel to the film surface. The X-ray beam after passing through the collimator strikes the specimen. The diffracted radiations are detected by the detector which converts it into a corresponding electrical signal. The various reflections obtained in the XRD spectra of a sample corresponding to the crystal planes (*hkl*) could be indexed after matching with the standard data available for same material composition. Subsequently, the value of interplanar spacing distance (d_{hkl}) corresponding to a particular plane (*hkl*) can be estimated using equation given. For a tetragonal lattice, the interplanar distance (d_{hkl}) is given by [6]:

$$\frac{1}{d_{hkl}} = \frac{h^2}{a^2} + \frac{k^2}{b^2} + \frac{l^2}{c^2} \quad (2)$$

A.3.1.2 Lattice parameter and crystallite size calculation

Powder X-ray Diffraction (XRD) is a versatile non-destructive and an efficient analytical technique used to identify and characterise the unknown crystalline material [5-7]. X-ray Diffraction (XRD) provides information on structures, phases, preferred crystal orientations (texture) and other structural parameters such as average grain size, crystallinity, strain, crystal defects and relative abundance of materials. X-ray Diffraction peaks are produced by constructive interference of monochromatic beam scattered from each set of lattice planes at specific angles. The peak intensities are determined by the atomic decoration within the lattice planes. Consequently, the XRD pattern is the fingerprint of periodic atomic arrangements in a given material. An on-line search of a standard database for Powder X-ray diffraction pattern enables quick phase identification for a large variety of crystalline samples.

The average crystallite size (X) of the synthesized material (in thin film, ceramic or powder form) can be calculated from the full width at half maximum (FWHM) of the dominant peak in the XRD spectra using the well-known Scherrer's formula given by

$$X = 0.94\,\lambda/(\beta\, cos\theta) \tag{3}$$

Where β is the full width at half maximum FWHM (in radians) of the dominant XRD peak and λ is the wavelength of X-rays (1.5406 Å for Cu $K\alpha_1$ radiation).

A.3.2 Optical characterization

A.3.2.1 Fourier Transform Infrared (FTIR) Spectroscopy

Fourier transform infrared spectroscopy is a useful method for the characterization of conducting polymers because it does not require polymers to be soluble in any other solvent. It is primarily used for the detection of functional groups but analysis of spectra in the lower frequency finger print region can give evidence of degree of polymerization. The absorption versus frequency characteristics of light transmitted through a specimen irradiated with a beam of infrared radiation provide a detail of molecular structure. The infrared radiation is absorbed when a dipole vibrates naturally at the same frequency in the absorbing material. The pattern of vibrations is unique for a given molecular structure. The intensity of absorption is related to the quantity of absorber. Figure A.1.6 (a) shows the Schematic for Michelson interferometer and Figure 1.6 (b) shows the Perkin Elmer GX 2000 FTIR spectrometer. Therefore, infrared spectroscopy allows the determination of components or groups of atoms/molecules that absorb the radiation in the infrared frequency range, permitting identification of the molecular structure [8-13].

Crystalline and molecular strain can also be measured with instruments of high spectral resolution. Copolymer dispersions can be determined as block copolymers absorb additively and alternating copolymers which deviate from this addictively due to interaction

of neighboring groups. In general, the spectrometer with a dispersive prism or grating has been largely superseded by a moving mirror is used in an interferometer to produce an optical transform of the infrared signal. Numerical Fourier analysis is able to give the relation of intensity and frequency, i.e., the IR spectrum. FTIR technique can be used to analyze gases, liquids and solids with minimal preparation of sample. FTIR technique has been applied to study many such systems which include adsorption on polymer surfaces, chemical modification and irradiation of polymers and oxidation of rubbers [14]. Moreover, the application of infrared spectroscopy to the study of polymers has been reviewed by Bower and Maddams [10].

In particular, π-conjugated delocalized electron system shows an interesting class of long molecules (macromolecules/polymer) where the extent of delocalization of π-electron cloud affects position of bands for a particular bond and helps in distinguishing two different types of bonds even for polymeric chains having same type of constituents. By knowing the absorption position (cm^{-1}) of a particular bond attached to π–conjugated chain, an idea about extent of effective π–electron delocalization can be known which ultimately shows the quality of electronic polymer. In the present thesis work, FTIR spectra have been recorded on the instrument name as Frontier 88277 FT-IR spectrophotometer mode in the wave number range 400–4000 cm^{-1} (Figure A.1.6). The spectroscopic grade KBr disks have been used for collecting the spectra with a resolution of 4 cm^{-1} and performing 32 scans. It gives idea about different functional groups and their arrangements (symmetrical or asymmetrical) present in the polymeric chain and shows very sharp changes when the nature and conformation of inherent polymeric chains change.

A.3.2.2 UV-VIS Spectroscopy

As mentioned in the previous sections, UV-Vis spectroscopy is a useful technique for characterization of TiO_2 due to presence of various dopants. A molecule or macromolecule

leads to transitions between the electronic energy levels of the molecule or macromolecule in the spectra range ultraviolet (200-400 nm)/visible (400-800 nm) radiation [15-16] and shows the absorption of radiation in the range. The excited state so formed is in a very short time (~ 10-15 s) resulting that the atoms of the molecule do not move following the Franck-Condon principle. There are many factors such as, solvents, substituents, position/conformation of substituents, etc. which influence the relative energies of molecular orbitals. The knowledge of these factors is the essence of electronic spectroscopy. The strength of electronic spectroscopy lies in its ability to measure the extent of multiple bond or aromatic conjugation within molecules or macromolecules.

The longer the conjugation, longer will be the maximum wavelength of the absorption spectrum. Non-bonding electrons in oxygen, nitrogen and sulfur atoms may also be involved in extending π-conjugation of multiple-bond systems. The progression in electronic spectra of a π-conjugated polymer continues with increased conjugation to a limit of 550-600 nm (more than 20 double bonds in conjugation). Addition for each substituent –R alkyl (5 nm), –Cl, –Br (5 nm), –CH=CH– additional π-conjugation (30 nm), etc., is in accordance with Woodward's rules. These rules are empirically based on similar model compounds and will only hold good for other compounds whose structures are close to those of the models. Photograph of Thermo Scientific Evolution-201 Spectrophotometer shown in Figure A.1.7 (a) and Figure A.1.7 (b) Schematic of the optical system indicating: D2: Deuterium lamp, WI: Halogen lamp, M1-M5: Mirrors (M3 is half-mirror), S1: Entrance slit, G: Diffraction grating, S2: Exit slit, F: Filter, W: Window plate, Reference cell, Sample cell, Lens 1, Lens 2P.D.: Photodiodes.

Application of electronic spectroscopy is of importance in the exploration of electronic property of semiconducting polymers [17-18]. The intensity and λ_{max} values increase with increasing π–conjugation and electron donating substituents which is regularly

attached to main π–conjugated backbone of polymer. It can also be shown that the angular strain or steric overcrowding (caused by bulky and irregularly attached side groups) can disturb the planar geometry and distribution of the chromophore. For example, π-conjugation is reduced by lowering π-orbital overlap. Electronic spectroscopy is so sensitive to the distribution of the chromophore that one can turn this to an advantage in demonstrating that the distortion present in the molecule is caused by the influence of steric inhibition of resonance in the π-conjugation.

In the present work, UV-visible spectra of polyaniline, Ag, Zn doped TiO_2 have been recorded on Thermo Scientific Evolution-201. In order to prepare a sample for measurement, the known amounts of samples have been dissolved in chloroform and measurements have been performed in a single quartz curette with 1 cm path length.

A.3.3 Surface morphological characterization

A.3.3.1 Transmission electron microscopy (TEM)

Transmission electron microscopy (TEM) has been used to study size, shape and distribution of materials at nanoscale [19]. The schematic diagram of a typical transmission electron microscope has been represented by Figure A.1.8 [20]. A thin solid specimen (< 200 nm) is bombarded in vacuum with a highly focused, mono energetic beam of electrons in TEM. The smaller de Broglie wavelength associated with high energy electron beam is responsible for high resolution and its ability to focus the electron beam. As an example, the electrons having energy of 100 keV corresponds to de Broglie wavelength of 3.7×10^{-3} nm. In general, TEM is expected with the electron beams having energy in the range of 20-200 keV. The spatial resolution is large enough for higher energy electron beam. In the energy range, the beam has enough high energy to propagate through the specimen. A series of electromagnetic lenses are used to magnify the transmitted electron signals [19].

There are two modes of TEM which are employed to study a desired specimen they are: image and diffraction. The image mode contrast must be induced in order to produce image for analysis of materials. There are many contrast forming mechanisms. The interpretation of images is complicated due to the interplay of the different mechanisms. The most commonly used imaging techniques in TEM are mass thickness imaging, diffraction imaging and phase contrast imaging. In diffraction imaging mode, the pattern of the diffracted electrons is obtained from the electron illuminated sample.

When the electron beam is incident on the sample, the scattering events occur because all the illuminated parts of the sample act as scattering sources. Interference between scattering beam causes coherently scattered beams when Bragg's law is fulfilled. The scattered beams are recorded in the form of a "*spot*". This spot pattern of diffracted electron beam from the selected sample area is called the selected area electron diffraction (SAED) pattern and provides the information about the crystalline and crystal orientation. The dependence of electron transpiring lies as the sample thickness, as a thick sample would cause too many interactions leaving no intensity in the transmitted beam. On the other hand a thick sample also increases the risk that an electron is scattered on multiple occasions and the resulting image would be difficult to interpret. In the work presented in this thesis the samples for TEM imaging have been prepared by dispersing powder sample in isopropanol using sonication and a small drop of that solution was casted onto the carbon coated copper grid. In the present thesis work, TEM has been used to analyze the shape, size and particle size distribution of PANI-TiO_2 nanoparticles.

- **High resolution transmission electron microscopy (HRTEM)**

If a scattered electron beam is a sharp spot diffracted from a single crystal, the phase contrast image that forms only when it is recombined with the unscattered beam is an image

of the crystal lattice planes that produce the scattering by Bragg diffraction. The resulting image of the crystal lattice can be obtained when several beams are recombined.

This specialized phase contrast technique has been utilized for the study of atomic scale structure in many types of crystalline metals and ceramics. It is called high resolution electron microscopy (HREM) which allows the direct imaging of defects and interfaces at the atomic scale [21-23]. However, this technique is difficult to apply for the study of polymeric materials due of their instability in the electron beam as the high resolution images require high beam intensities.

High-resolution electron microscopy can provide information that is difficult to obtain in any other way but it needs skill and experience. In case of polymers, lattice fringe images have been obtained from a wide range of polymers. In the present thesis, the particle size, the morphology of polyaniline (PANI) doped Titanium dioxide (TiO_2), have been examined using a high-resolution transmission electron microscope (HRTEM, Tecnai G2 F30 S-Twin) operating at an accelerating voltage of 300 kV, having a point resolution of 0.2 nm and a lattice resolution of 0.14 nm (Figure A.1.9).

A.3.3.2 Scanning Electron Microscopy (SEM)

Scanning Electron Microscopy (SEM) is a very useful technique and widely accepted to study the surface morphology, surface topography, composition and other properties such as electrical conductivity of the samples. It offers a better resolution than that of optical microscope. It can have resolution of a few nanometers and provides high magnification [24]. The schematic of scanning electron micrograph is shown in Figure A.1.10 [25].

In a typical SEM instrument, Tungsten or LaB_6 is used to emit monochromatic electrons with the energy range of 10-30 keV. These electrons are focused by magnetic field which acts as condenser lenses to form a beam with a very fine spot size ~ 1 to 5 nm. Then

beam passes through a pair of scanning coils in the objective lenses, which deflects the beam in a raster fashion over the sample surface. This beam of primary electrons interacts with sample volume, the thickness of which ranging from less than 100 nm to 5 μm. The signals secondary electrons, internal currents, photon emission etc. so generated are detected by appropriate detectors. The cathode ray is used to generate the final image on the screen. In addition, SEM can provide information about the sample composition near the surface. This is known as Energy Dispersive Spectroscopy [26-27].

In the present work, SEM has been used to study the morphology of nanostructured polyaniline (PANI) doped Titanium dioxide (TiO_2), TiO_2, Ag doped TiO_2 and Zn doped titanium dioxide (TiO_2) composite.

A.4 Electrical studies

A.4.1 Electrical Characterization

The gas sensing characteristic properties of prepared sensors were studied in a specially designed by a glass test chamber. Different concentrations of LPG were introduced into the glass test chamber for interaction to the material though the flowmeter. The response of a gas sensor is tested by measuring the resistance or conductance of the sensor element in the air and in the presence of analyte gas. The sensor resistance can also be calculated by measuring the current along the sensor.

Sensing film with silver contacts was used for measurements of LPG sensing properties. The stabilised resistance of the film was taken as stabilised resistance in the presence of air (R_a). Now, this was exposed to LPG and variations in electrical resistance with the time for different vol.% of LPG were recorded by using Keithley electrometer (Model: 6517A). The gas sensing measurements were carried out in a static mode. At the

time of recovery of the sensor, target gas was flushed out of the test chamber (by creating vacuum again) and the clean dry air was introduced. Target gas (LPG) of specific concentration was introduced into the test chamber and changes in the sensor resistance were recorded for every vol.% of LPG. The gas sensing mechanism of TiO_2 thin film based sensor belongs to a surface controlled type, i.e. resistance change is controlled by surface area and the amount of chemisorbed oxygen. LPG consists of CH_4, C_3H_8, and some other hydrocarbons. In each composition, the reducing hydrogen species are bound to carbon atom therefore, LPG dissociates into the reactive reducing components hardly on the surface of the sensing element. As LPG exposed to sensing element, the conductivity increases due to adsorption of oxide and capture more electrons that contribute to reducing the current. It was observed that as the concentration of LPG increases, the average sensitivity increases linearly in the beginning and later, it becomes saturated. The linear relationship between sensitivity and gas concentration may be attributed to the availability of a sufficient number of sensing sites on the film to act upon the LPG. The low concentration implies a lower surface coverage of gas molecules, resulting in a lower surface reaction between the surface adsorbed oxygen species and the gas molecules. The increase in LPG concentration increases the surface reaction due to a large surface coverage. Further, increase in the LPG concentration does not increase the surface reaction and eventually, saturation takes place.

The oxygen adsorbed on the surface of the film influences the resistance of the TiO_2 based sensor. Initially, oxygen from the atmosphere adsorbs on the surface of the film and extracts electrons from its conduction bands to form O_2^- species on the surface, consequently resistance increases. After that an equilibrium state is achieved between the oxygen of TiO_2 and atmospheric oxygen.

$$O_2\,(\text{gas}) \leftrightarrow O_2\,(\text{ads}) \qquad \text{(Thin Film Surface)} \qquad (2)$$

$$O_2\,(\text{gas}) + e^- \leftrightarrow O_2^- \qquad \text{(Thin Film Surface)} \qquad (3)$$

When the thin film is exposing to LPG, it reacts with the chemisorbed oxygen. On interaction with hydrocarbons of LPG, the adsorbed oxygen is removed, forming gaseous species and water vapour. Consequently, the resistance changes, which is due to the change in the width of depletion layer after exposure to LPG. The overall reaction of LPG with the chemisorbed oxygen may take place as shown below [29]:

$C_4H_{10}+13O^- \rightarrow 4CO_2+5H_2O+13e^-$ (4)

$C_4H_{10}+\frac{13}{2}O_2^- \rightarrow 4CO_2+5H_2O+\frac{13}{2}e^-$ (5)

$C_4H_{10}+13O^{2-} \rightarrow 4CO_2+5H_2O+26e^-$ (6)

$C_3H_8+10O^- \rightarrow 3CO_2+4H_2O+10e^-$ (7)

$C_3H_8+5O_2^- \rightarrow 3CO_2+4H_2O+10e^-$ (8)

$C_3H_8+10O^{2-} \rightarrow 3CO_2+4H_2O+20e^-$ (9)

A.4.2 Gas injection and calibration of sensor for different gas concentration

The gas for which the sensing parameter of the sensor element is to be studied is injected into the glass chamber, through the gas inlet from ppm level in the air ambient, by using medical practitioner's syringe. The required gas concentration inside the system is achieved by injection a predefined known volume of the test gas. The volume of chamber is 5 liters. The gas concentration in ppm can be determined as:

$$concentration\ of\ gas\ (ppm) = \frac{volume\ of\ ejected\ gas\ (ml)}{volume\ of\ chamber\ (L)} \times 10^6$$

The gas calibration chart based on the above equation is given in Table No.1.

Table 6.1 Conversion chart of ml to ppm level of the gas

Quantity of gas ejected in chamber (ml)	0.05	0.1	0.2	0.3	0.4	0.5
Concentration of gas in chamber (ppm)	5	10	20	30	40	50

A.4.3 Gas Sensing Parameters

It is very much important to understand the sensing parameters of a good sensor. These are defined as:

- Sensing response,
- Operating temperature,
- Response time and
- Recovery time

There are some of the salient parameters that are associated with measurement of response characteristics of a gas sensor.

(a) Sensing Response

The response (*S)* of a gas sensor to a target gas at a given temperature T is determined from the measured value of resistance of the sensing element (Zn, PANI, Ag doped TiO_2 bare TiO_2 thin film) in the absence (R_a) and presence of the sensing gas (R_g). The sensor response *S* is defined as:

$$S = \frac{R_g - R_a}{R_a} \tag{9}$$

Where $R_g >> R_a$ for oxidizing gases, and therefore to a good approximation

$$S \approx \frac{R_g}{R_a} \tag{10}$$

(b) Response Time (T_{res})

The response time is defined as the time taken by the sensor to acquire 90% of its maximum resistance value in the presence of target oxidizing gas.

(c) Recovery time (T_{rec})

The recovery time is defined as time taken by the sensor to reacquire about 10% higher value of its initial resistance in the presence of atmospheric air.

The typical variation in the response (S) of a gas sensor with temperature for a specific concentration of target gas is shown in Figure A.1.11. The maximum in the response (S_{max}) at a certain critical temperature (T_{opt}) is referred to as the operating temperature of the sensor.

Response (t_{res}) and recovery (t_{rec}) time characterization of a typical sensor are shown in Figure A.1.12 which gives a clear picture about the increase in resistance value for any oxidizing gas comes in contact with n-type semiconducting sensing layer. The sample regains its original resistance value (R_a) as soon as the sensing gas is expelled out from its vicinity.

References:

[1] C.J. Brinker and G.W. Sherer, Sol-Gel Science, The Physics and Chemistry of Sol-Gel Processing, Academic Press, San Diego, 1990.

[2] C.J. Brinker, A.J. Hurd, P. R. Schunk, C.S. Ashely, R.A. Cairncross, J. Samuel, K. S. Chen, C. Scotto and R. A. Schwartz, "Sol-Gel Derived Ceramic Films Fundamentals and Applications", K. Stern (Ed.), Metallurgical and Ceramic Protective Coatings, Chapman & Hall, London, (1996) 112.

[3] T. Troczynski and Q. Yang, Process for Making Chemically Bonded Sol-Gel Ceramics, U.S. Pat. No. 6, 284 (2001) 682.

[4] T. Olding, M. Sayer and D. Barrow, Ceramic sol-gel composite coatings for electrical insulation, Thin Solid Films 398 (2001) 581-586.

[5] H. Chung Frank, K. Deane, Smith, Industrial application of X-ray Diffraction, Technology & Industrial Arts, (2000) ISBN 0824719921.

[6] N.A. Aqeeli, G.M. Suarez and R.A.L. Drew, XRD and TEM characterization of Al-Mg based nanocomposite alloys, Reviews on Advanced Materials Science, 18 (2008) 23-235.

[7] S. Cornaby, A.R. Mena, P.W. Moody, T. Hughes, A. Straddling, T. Grow, Simultaneous XRD/XRF With Low-Power X-ray Tubes**,** International Centre for Diffraction Data, Volume 45, (2002).

[8] H.W. Siesler, K.H. Moritz, Infrared and Raman Spectroscopy of Polymers (Marcel Dekker, New York, 1980).

[9] P.C. Painter, M.M. Coleman, J.L. Koenig, The Theory of Vibrational Spectroscopy and its Application to Polymers (John Wiley, New York, (1982) 530).

[10] D.L. Bower, W.F. Maddams, The Vibrational Spectroscopy of Polymers (Cambridge University Press, Cambridge, 1989).

[11] E.C. Faulques, D.L. Perry and A.V. Yeremenko, Eds. Spectroscopy of Emerging Materials., Springer, Sudak, Crimea, Ukraine (2004) 414.

[12] J.L. Koenig, Infrared and Raman Spectroscopy of Polymers, Rapra Technology, Shropshire UK, (2001) 154.

[13] P.R. Griffith, Chemical Infrared Fourier Transform Spectroscopy, Wiley, New York, (1975).

[14] L.H. Lee, Ed. Characterization of Metal and Polymer Surfaces: Polymer Surfaces, Academic Press, New York, (1977).

[15] P. Atkins, J. de Paula, Physical Chemistry, Oxford University Press, 7th Edition, (2002) 291.

[16] C.N. Banwell, E.M. McCash, Fundamentals of Molecular Spectroscopy, Tata McGraw-Hill Publishing Company Limited, New Delhi, 4th Edition, (1994).

[17] K. Kaeriyama, "Handbook of Organic Conducting Molecules and Polymers", John Wiley & Sons, Chichester, H. S. Nalwa (Ed.), 2 (1997) 271.

[18] E.J. Samuelsen, J. Mardalen, "Handbook of Organic Conducting Molecules and Polymers", John Wiley & Sons, Chichester, Nalwa H.S. (Ed.) 3 (1997) 81.

[19] D.B. Williams, Transmission electron microscopy, A textbook for material science, Plenum Press. New York and London, (1996).

[20] http:/www.steve.gb.com/image/science/transmission_electron_mocroscope.png.

[21] P. Buseck, J. Cowley, L. Eyring, Eds. High-Resolution Transmission Electron Microscopy and Associated Techniques, Oxford University Press, Oxford, (1988).

[22] J.C.H. Spence, High-Resolution Electron Microscopy, 3rd ed., Oxford University Press, Oxford, (2003).

[23] F. Ernst, M. Ruhle, Eds. High-Resolution Imaging and Spectrometry of Materials Springer, New York, (2003).

[24] G. Lawes, Scanning electron microscopy and X-ray microanalysis: Analysis chemistry by open learning, John Willey and Sons, (1987).

[25] www.purdue.edu/REM/rs/sem.htm.

[26] C. Juan, C.M. Lino, A. Pena, J.C. Molto, J. Manes, I. Silveira, Determination of ochretoxin A in maize bread samples by LC with fluorescence detection, Talanta 73 (2007) 246-250.

[27] N. Axelrod, E. Axelrod, A. Gutina, A. Puzenko, P. Ben Ishai, and Yu Feldman, Dielectric spectroscopy data treatment: I. Frequency domain, Meas. Sci. Tech. 15 (2004) 755-764.

[28] Elton N. Kaufmann, (ed) Characterization Of Materials Vol.1, John Wiley & Sons Inc., Hoboken, New Jersey, 2003.

[29] R.K. Sonker, B.C. Yadav, Chemical Route Deposited SnO_2, SnO_2-Pt and SnO_2-Pd Thin Films for LPG Detection, Adv. Sci. Lett. 20 (2014) 1023-1027.

Figures:

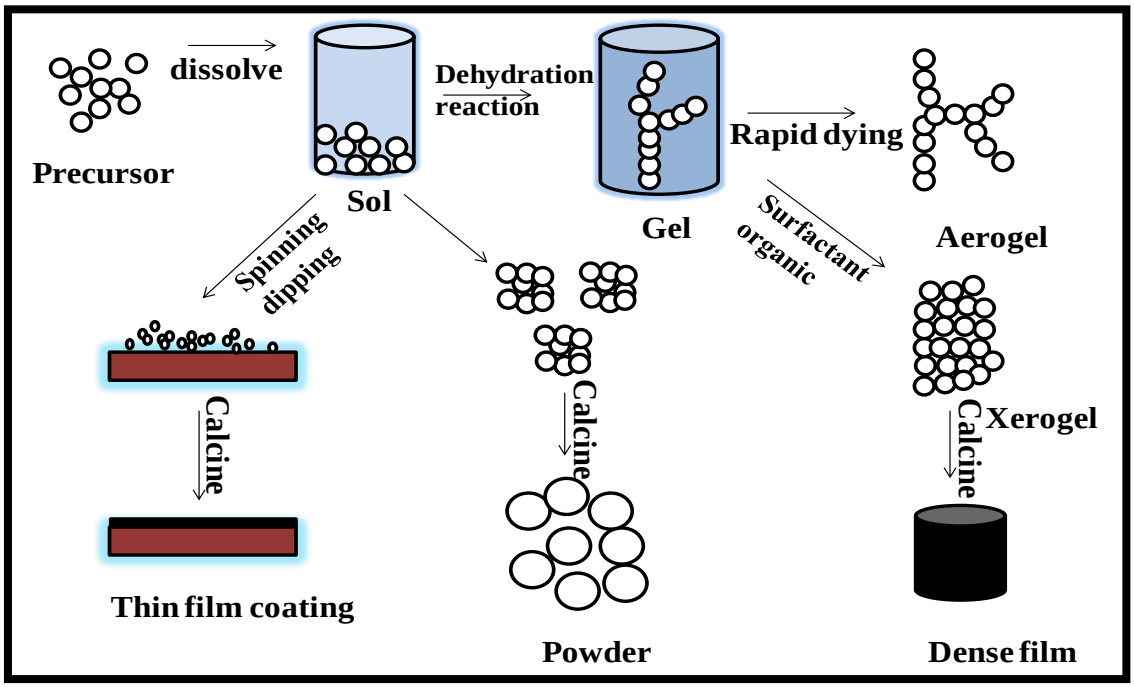

Figure A.1.1: Sol- Gel Process

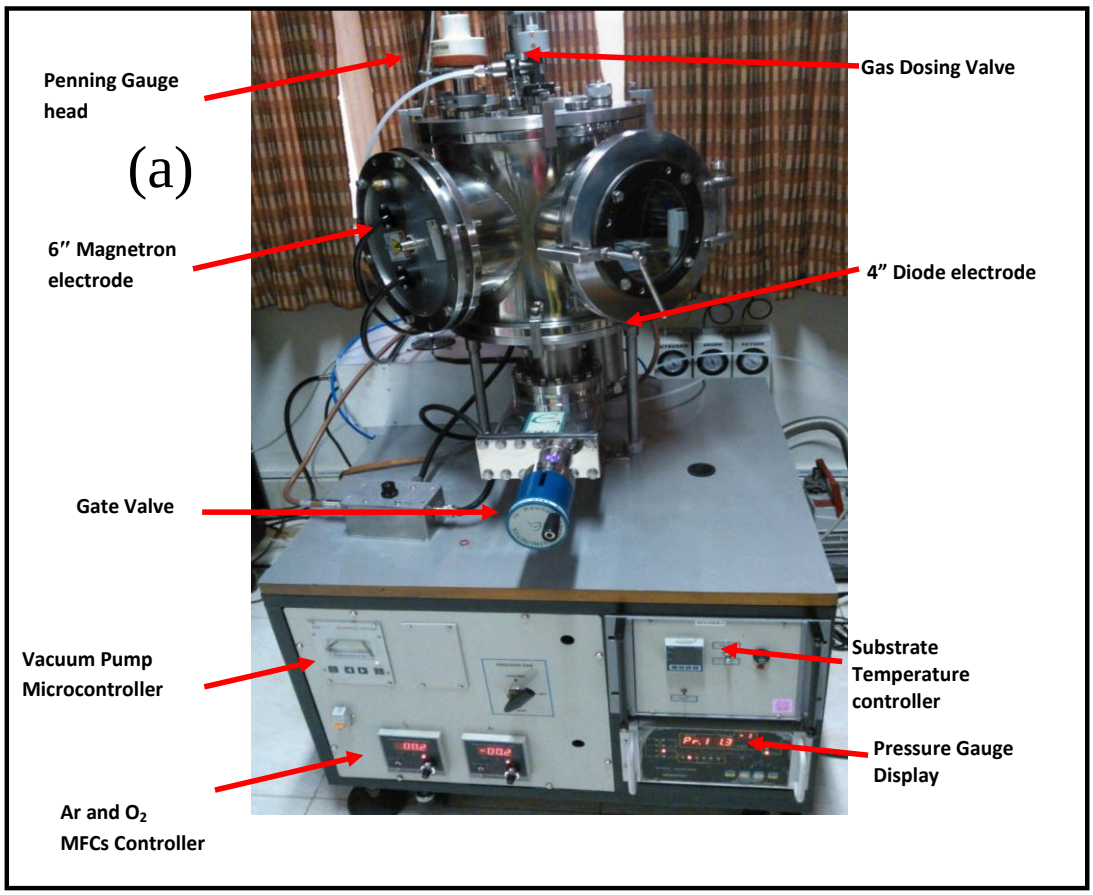

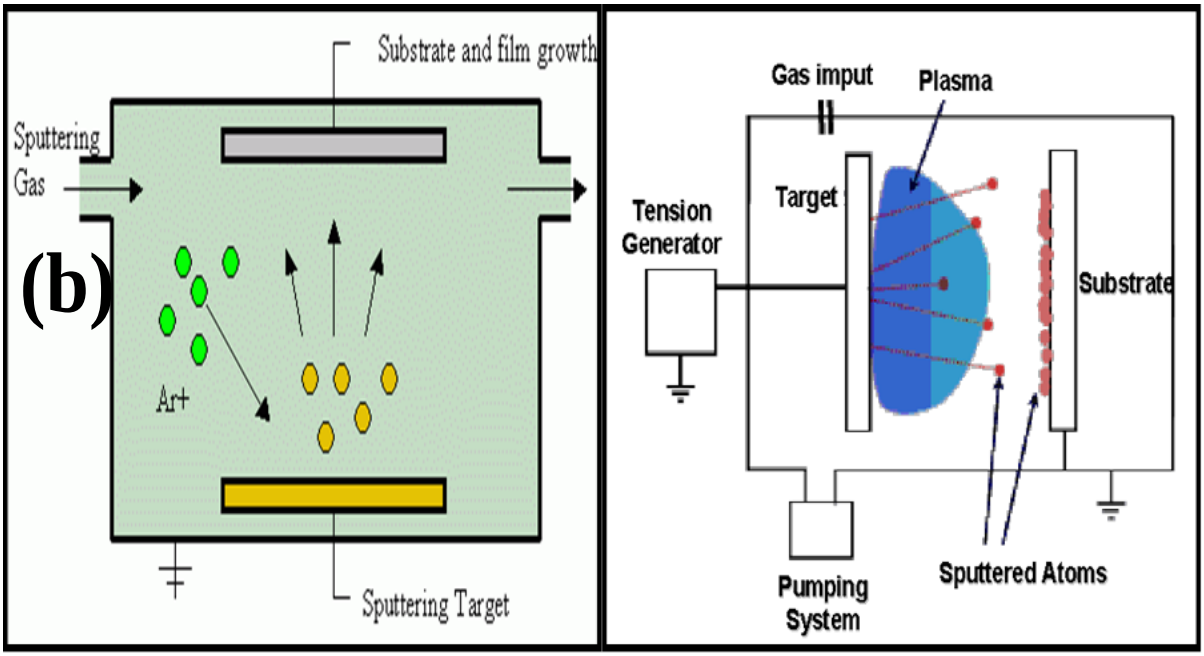

Figure A.1.2: (a) Photograph of the rf diode sputtering unit and (b) Schematic diagram of sputtering technique.

Table 6.2 Platinum & Titanium thin film deposition parameter

Parameters	Platinum	Titanium
Target	Platinum foil	Titanium
Gas composition	100% Ar	100% Ar
Sputtering pressure	10 m Torr	10 m Torr
TS distance	7.5 cm	7.5 cm
RF Power	100 W	150 W
Substrate Temperature	No heating	No heating

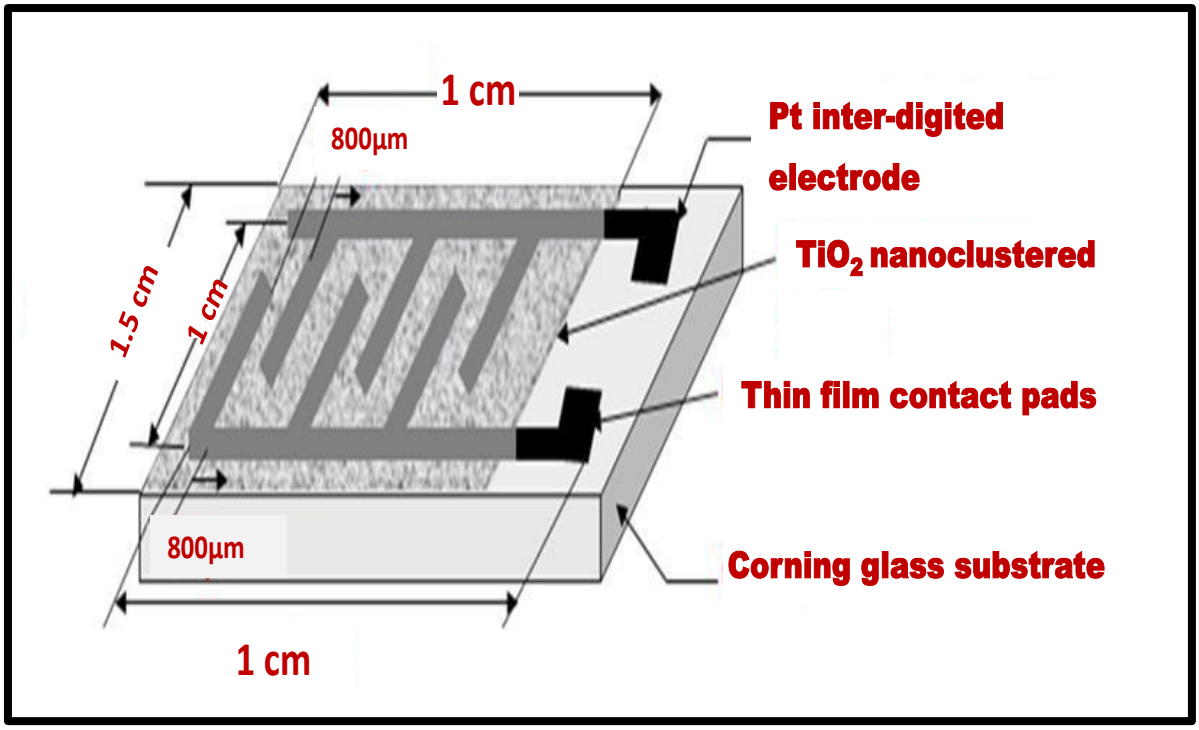

Figure A.1.3: Platinum IDTs on glass substrate

Figure A.1.4: Photograph of spin coater used in the preparation of thin film

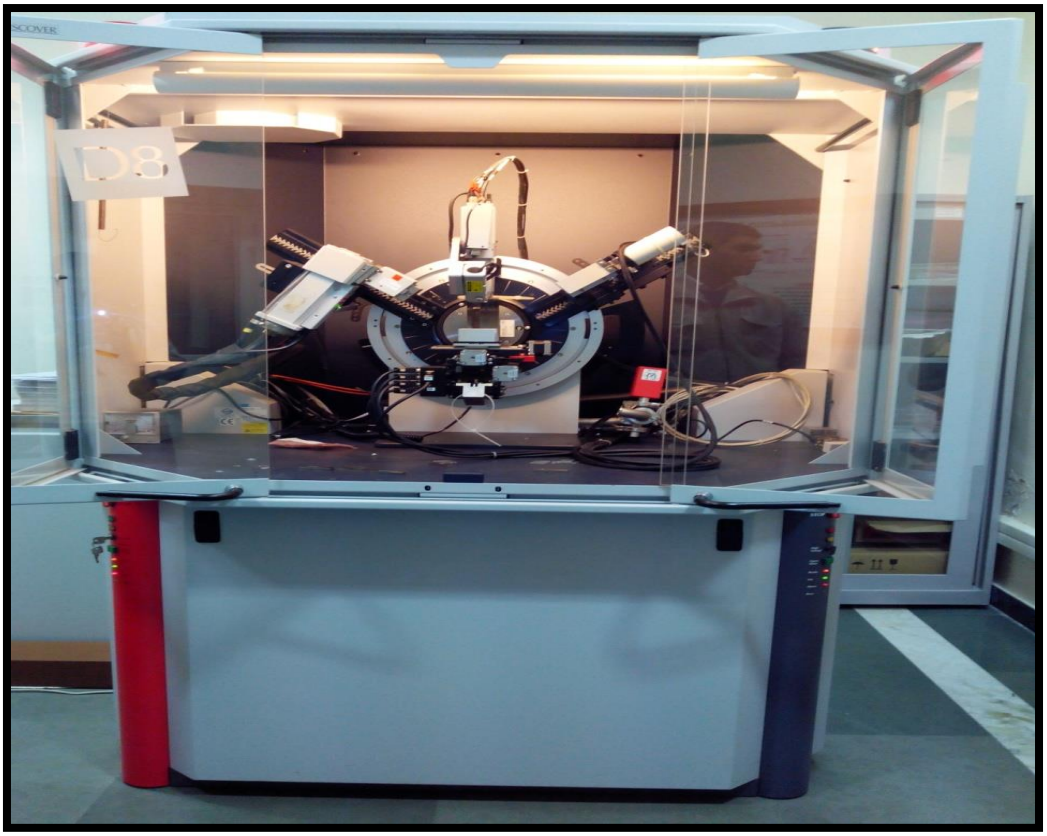

Figure A.1.5: Photograph of X-Pert, PRO PANalytical XRD system, Nether land.

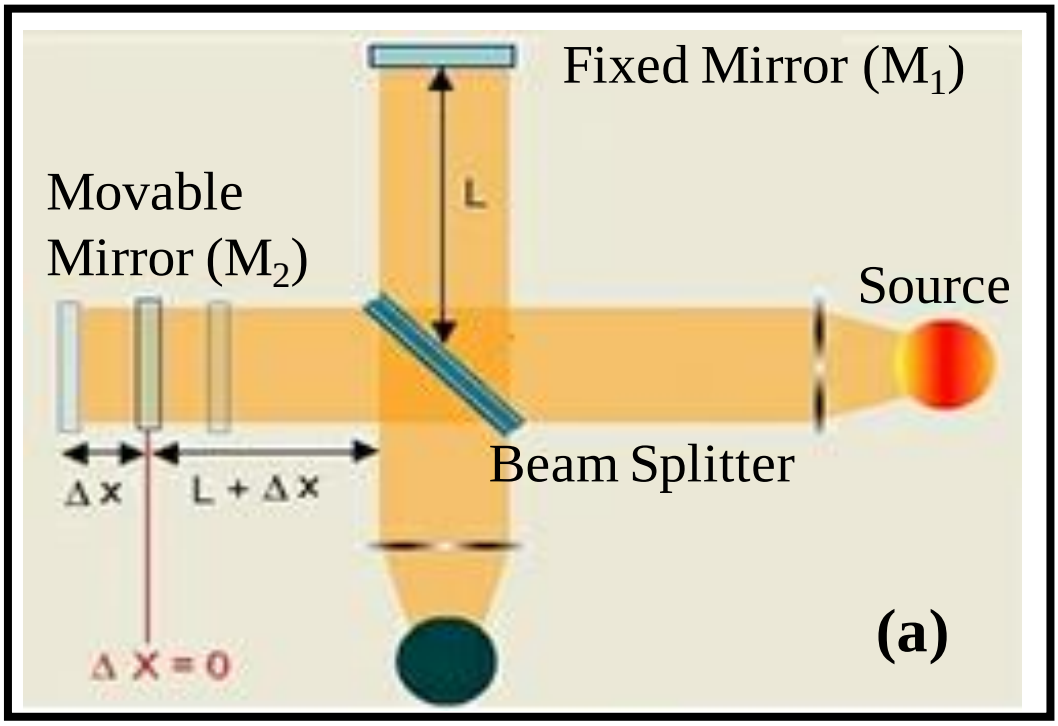

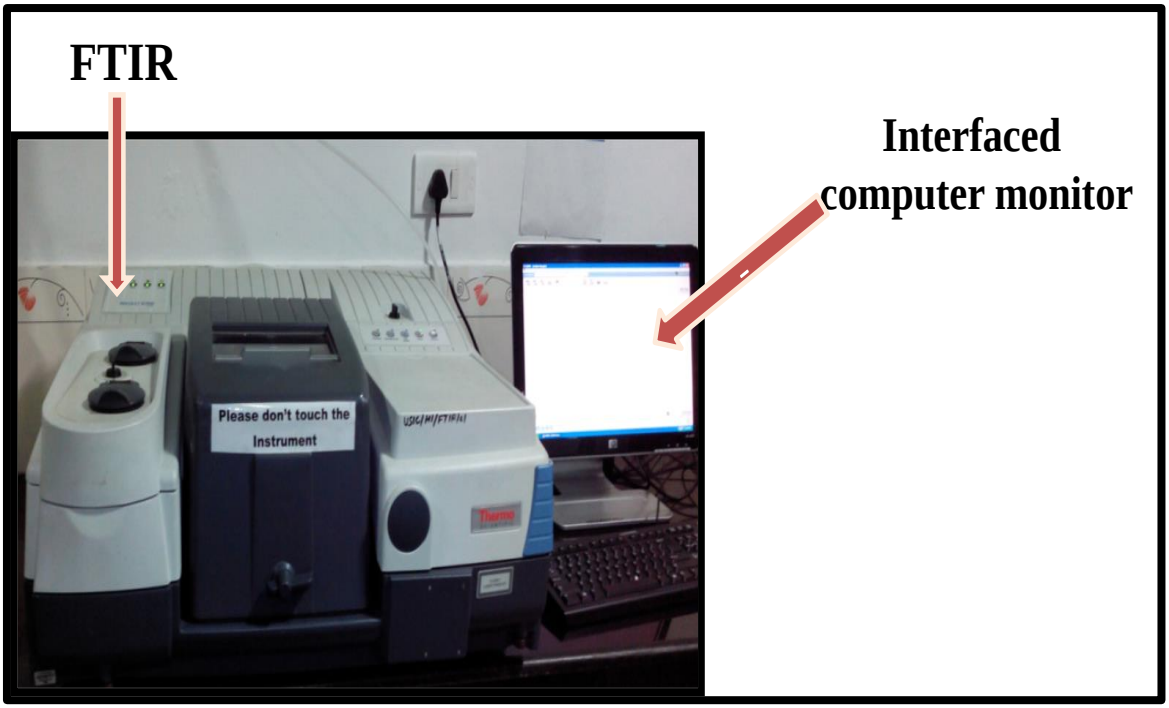

Figure A.1.6: (a) Schematic for Michelson interferometer and (b) FTIR spectrometer

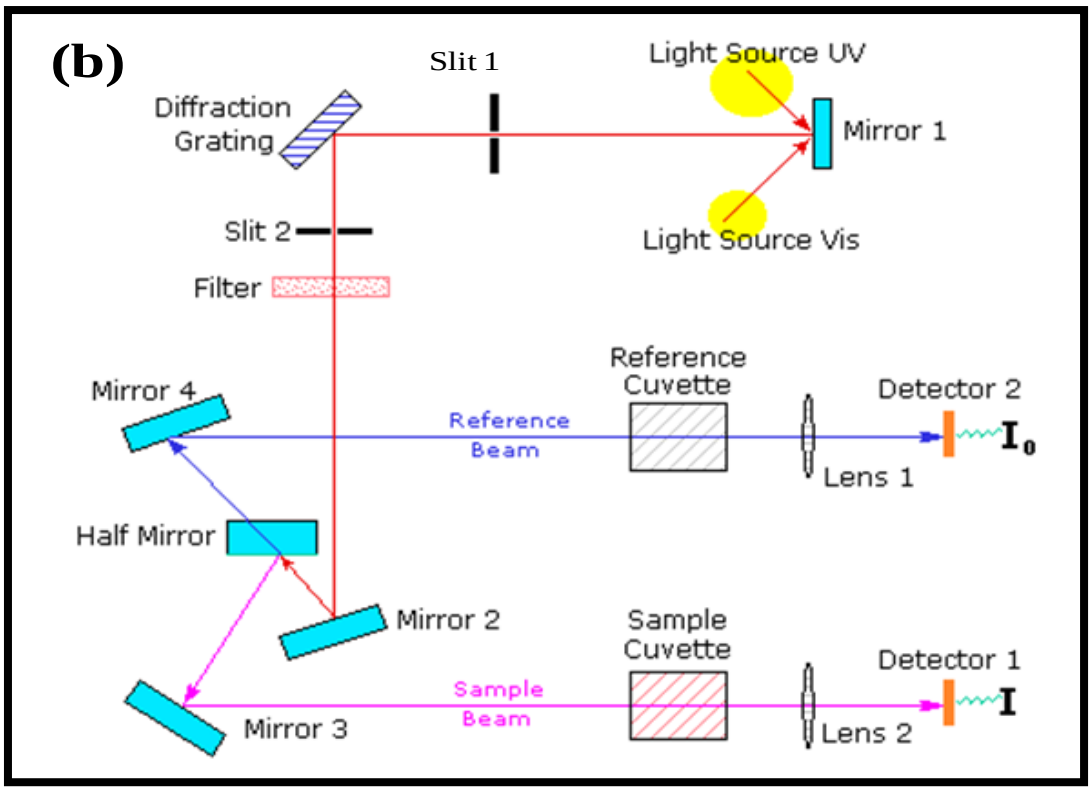

Figure A.1.7: (a) UV-Visible spectrophotometer (Thermo scientific Evolution 201) and (b) Schematic of the optical system

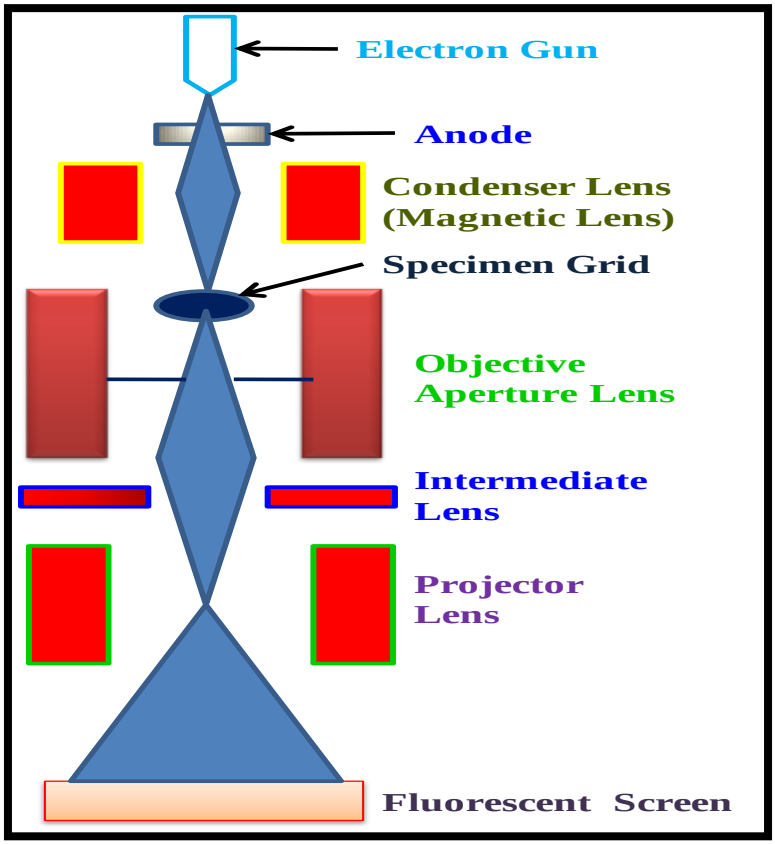

Figure A.1.8: Schematics diagram of Transmission Electron Microscope (TEM)

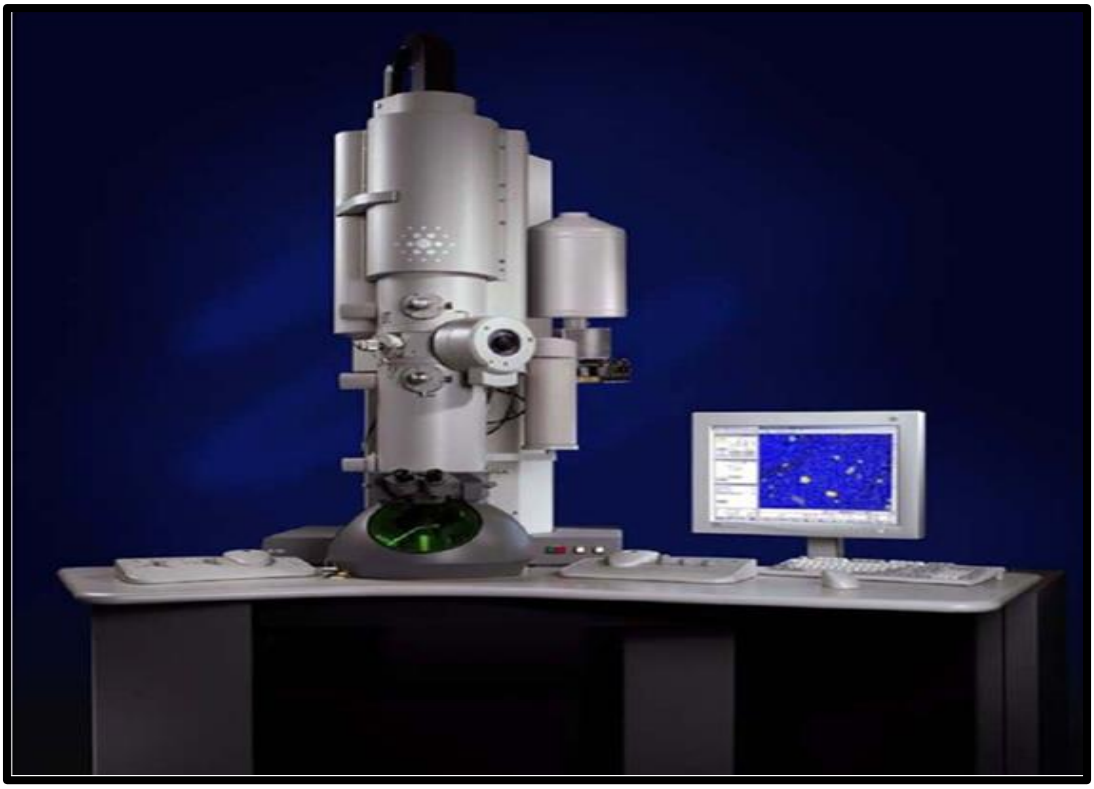

Figure A.1.9: Photograph of High-Resolution Transmission Electron Microscope (Philips T20ST, operated at 200 kV)

Figure A.1.10: (a) Photograph of Scanning Electron Microscopes (JEOL, JSM-6490LV)

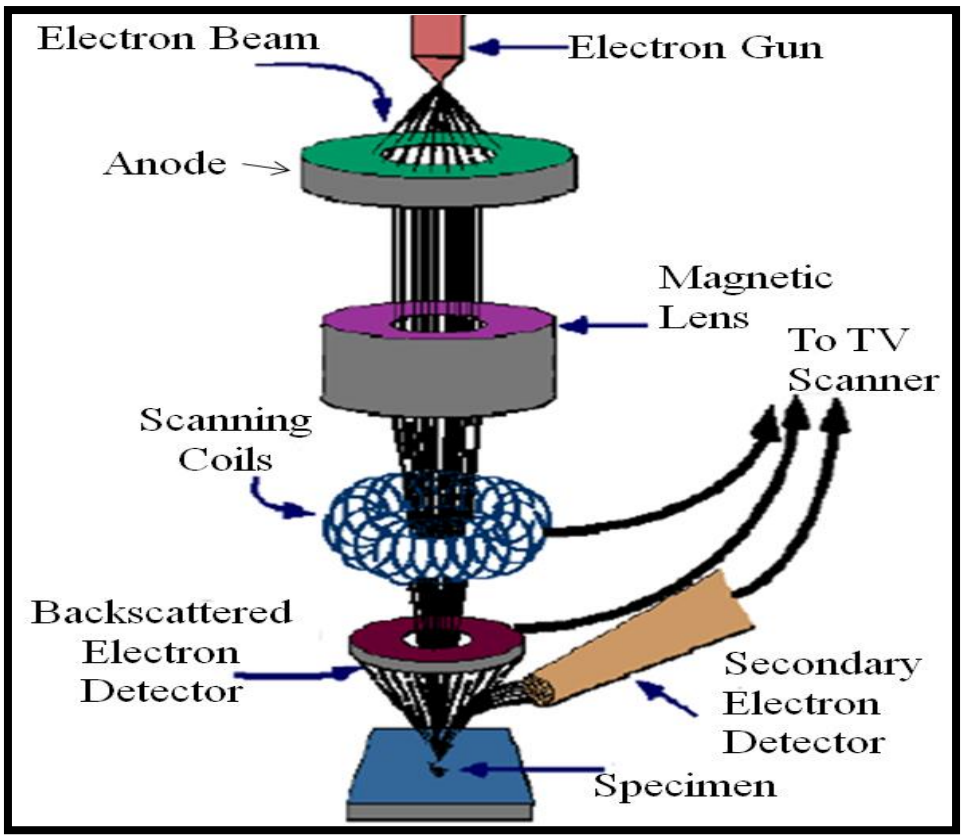

Figure A.1.10: (b) Schematics of Scanning Electron Microscope (SEM)

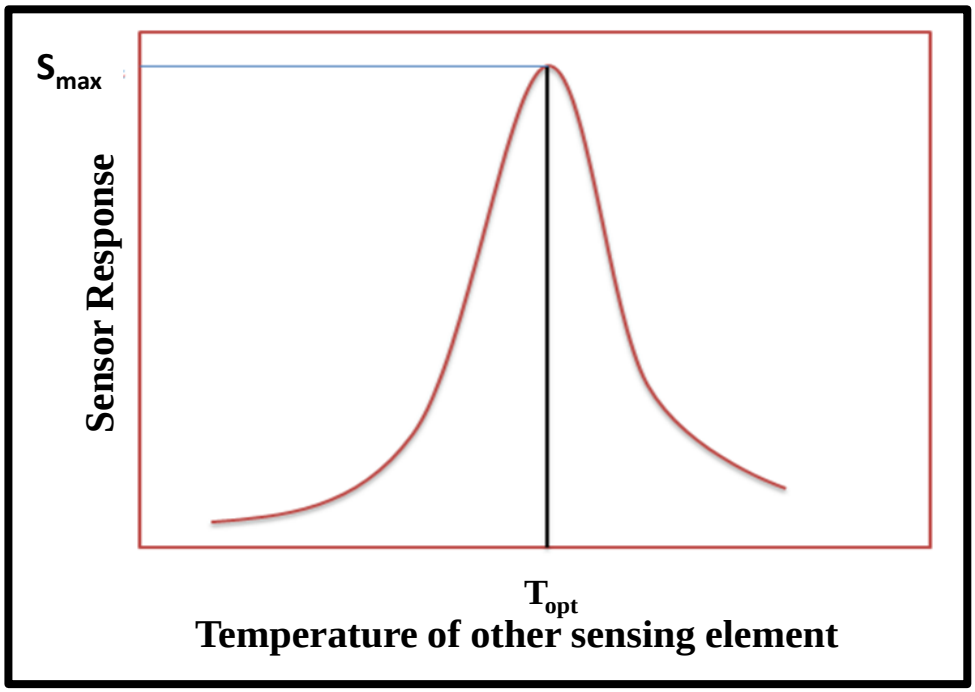

Figure A.1.11: Variation of sensor response with temperature for a typical sensor

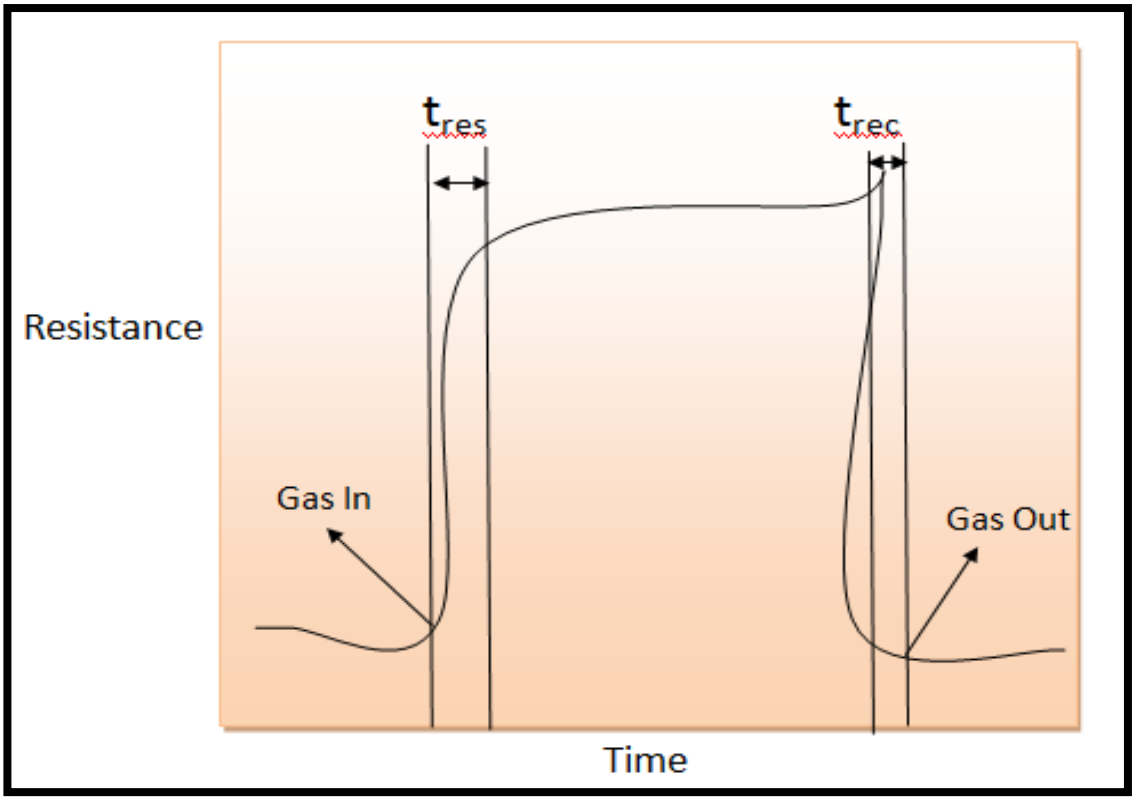

Figure A.1.12: Sensor response as a function of time, defining response time and recovery time of a typical sensor in response to an oxidizing gas

J Mater Sci: Mater Electron
DOI 10.1007/s10854-017-7309-4

Preparation of PANI doped TiO_2 nanocomposite thin film and its relevance as room temperature liquefied petroleum gas sensor

Rakesh K. Sonker[1,2] · B. C. Yadav[1] · S. R. Sabhajeet[1]

Received: 11 March 2017 / Accepted: 6 June 2017

Abstract Present work reports the utility of PANI doped titanium dioxide thin film prepared by spin coating technique as LPG sensing. Optical properties were studied using UV–Vis absorption spectroscopy and FTIR spectroscopy. The surface morphology and structure of synthesized material were characterized by SEM and XRD analysis, respectively. The structural analysis confirmed the formation of TiO_2–PANI having an average crystallite size 21 nm. Variations in the resistance with exposure of LPG to the sensing element were observed. Sensor response (S) as a function of time was calculated and its maximum value was found as 2.37 towards 2000 ppm of LPG, response time of the sensor was 2 min. The sensor was quite sensitive to LPG and results were found reproducible.

1 Introduction

Liquefied petroleum gas (LPG) contains the hydrocarbons, majority propane, and butane. The lower explosive limit (LEL) as specified by National Institute for Occupational Safety and Health (NIOSH) and Occupational Safety and Health Administration (OSHA) standards for chemical hazards is average 20,000 ppm by volume 2.0% in air. The permissible exposure limit (PEL) for LPG as specified by NIOSH and OSHA standards is 1000 ppm [1]. The various kinds of materials are used for the detection of reducing LPG gas [2]. Among them, semiconducting metal oxides such as titania (TiO_2) [3], tin dioxide [4], copper ferrite [5] and zinc oxide [6] have been studied extensively. TiO_2 as an n-type semiconducting metal oxide with two distinct phases; anatase and rutile, has been used for a broad range of LPG gas sensing [3, 4]. PANI has been prepared by oxidation of the aniline or anilinium salts e.g. aniline hydrochloride or aniline sulphate, in aqueous acidic ambient [7]. It is a p-type semiconducting material [8] and has specific redox nature, controllable conductivity, and considerable thermal stability [9, 10].

In this work, for the first time, TiO_2–PANI nanocomposite thin film was prepared on a corning glass substrate and employed as LPG sensor.

2 Experimental

Titanium tetrachloride ($TiCl_4$), propanol, deionized water (DI), ethanol, aniline, HCl, ammonium persulphate (APS) and ammonium hydroxide used for the sensor preparation were purchased from Sigma Aldrich Chemical Co. with 99.99% purity. 500 ml distilled water was dissolved with 50 ml HCl followed by 8.33 ml Aniline. After vigorous stirring in ice bath, it was indexed as part (I). 18.924 gm APS was mixed in 331 ml distilled water and after vigorous stirring the solution was indexed as part (II). Now Part I was added with part II followed by vigorous stirring for 2 h. A colour less filtrate was obtained. After drying it at 40–50 °C for 4–5 h, emeraldine salt of PANI was prepared. Later it was washed with NaOH and filtered. Filtrate was

✉ B. C. Yadav
balchandra_yadav@rediffmail.com

Rakesh K. Sonker
rakesh.sonker81@gmail.com

[1] Nanomaterials and Sensor Research Laboratory, Department of Applied Physics, Babasaheb Bhimrao Ambedkar University, Lucknow, Uttar Pradesh 226025, India

[2] Department of Physics and Astrophysics, University of Delhi, Delhi 110007, India

Published online: 10 June 2017

J Mater Sci: Mater Electron (2016) 27:7852–7863
DOI 10.1007/s10854-016-4776-y

Fabrication and characterization of nanostructured (Sn–Ti)O_2 pellets and films for liquefied petroleum gas sensing

B. C. Yadav[1,2] · Nidhi Verma[1] · Tripti Shukla[1] · Satyendra Singh[3] · S. R. Sabhajeet[2]

Received: 8 January 2016 / Accepted: 2 April 2016 / Published online: 12 April 2016

Abstract Present paper reports the synthesis of nanostructured (Sn–Ti)O_2 via physicochemical method, its characterization and performance as liquefied petroleum gas (LPG) sensor. The synthesized material was characterized using XRD that confirmed the formation of (Sn–Ti)O_2 nanocomposite. Minimum crystallite size was found as 7 nm. The material was also investigated through SEM, DSC, FTIR, PL and UV–Vis spectrophotometer. Further, the pellet, thick and thin films were fabricated for the sensing analysis. Pellets (9 mm diameter, 4 mm thickness) of (Sn–Ti)O_2 nanocomposite were made by hydraulic pressing machine by applying uniaxial pressure of 616 MPa, thick films (thickness ~2 μm) were made by screen printing technique and thin films were prepared using a Photo resist spinner unit. Further at room temperature, the pellet and films were exposed to LPG in a gas chamber under controlled conditions at room temperature and variations in resistance with the concentrations of LPG were observed. The maximum value of sensitivity of solid state pellet, thick and thin films based sensors were found 7, 9 and 39 for 5 vol% of LPG, respectively. Sensing characteristics were found to be reproducible, after 6 months of their fabrication, indicating the stability of the sensors.

✉ B. C. Yadav
balchandra_yadav@rediffmail.com

[1] Nanomaterials and Sensors Research Laboratory, Department of Physics, University of Lucknow, Lucknow, U.P. 226007, India

[2] Department of Applied Physics, School for Physical Sciences, Babasaheb Bhimrao Ambedkar University, Lucknow, U.P. 226025, India

[3] Department of Physics, University of Allahabad, Allahabad 211002, U.P., India

1 Introduction

A great deal of research efforts has been directed towards the development of portable sensors for practical applications ranging from toxic gas detection to manufacturing process monitoring [1–5]. Hazardous gases, specifically liquefied petroleum gas (LPG), have been widely used for several industrial and domestic applications [6–10]. Research on gas sensing materials has been focused on the design of higher performance and elevated efficiency gas sensing materials. Gas sensors using metal oxide semiconductors are the fundamentals of smart device as both the structure and morphology of these materials can be controlled precisely and so they are referred to as a functional oxides. The structures of functional oxides are very diverse and varied, and there are infinite new phenomena and applications [11–16]. They have been researched for several decades owing to their advantage such as low cost fabrication, the high sensitivity and possibility of miniaturization. n-type semiconductor such as SnO_2 has been used for the detection of inflammable and toxic gases such as NO_x, CH_4, or CO [17–24]. In more recent research the interest is shifted to some other promising metal oxide such as ZnO, Fe_2O_3, SnO_2, In_2O_3 and TiO_2 with interesting properties as a gas sensing material [25–29]. Among these TiO_2 is a promising material for gas sensor. So far TiO_2 based devices have attracted much attention as gas sensors because of their chemical response to different adsorbed gases, high chemical stability, amenability to doping, no toxicity and low cost. TiO_2 gas sensor can be used not only for detecting the leakage of inflammable gases and toxic

J Mater Sci: Mater Electron (2016) 27:11726–11732
DOI 10.1007/s10854-016-5310-y

TiO_2–PANI nanocomposite thin film prepared by spin coating technique working as room temperature CO_2 gas sensing

Rakesh K. Sonker[1] · S. R. Sabhajeet[1] · B. C. Yadav[1]

Received: 20 May 2016 / Accepted: 2 July 2016 / Published online: 14 July 2016

Abstract Present work reports the performance of a semiconducting PANI doped TiO_2 nanocomposite thin film and its application in CO_2 sensing. The TiO_2–PANI nanocomposite layer was deposited on a simplified test device. Optical properties were investigated using UV–Vis absorption spectroscopy. The surface morphology and structure of synthesized material were characterized by TEM and XRD analysis, respectively. The structural analysis confirmed the formation of TiO_2–PANI having an average crystallite size 7 nm. Variations in resistance with the exposure of CO_2 to the sensing element were observed. Sensor response (S) as a function of time was calculated and its maximum value was found as 53 for 1000 ppm of CO_2. Response and recovery times of the sensor were observed as 9.2 and 5.7 min respectively. Sensor was found reproducible.

1 Introduction

CO_2 is the main greenhouse gas which causes global climatic changes on larger scale. Recently, detection of greenhouse gases has become essential to control the damage causing to the environment and quality of life. Global warming is a major concern of researchers because of the massive emissions of CO_2. Hence, the detection and control of CO_2 concentrations in the environment is necessary. CO_2 sensors can be used in many applications, particularly, in air quality monitoring, agricultural production, clean energy technologies, engine exhausts, and chemical industries. Several types of CO_2 sensors, such as infrared [1, 2], surface acoustic wave [3], solid electrolyte [4], capacitive [5, 6] and resistive [7, 8] sensors, have been developed. Toxic gas molecules can be adsorbed on the surfaces of oxide materials create electron-depleted layers, which increase the sensor resistance. Among these sensing platforms, the resistive sensors based on metal oxides [9–12] have important advantages, such as good reliability, low cost, small size, and its potential in the development of array-integrated gas sensors. Titanium dioxide based gas and moisture sensors have high sensitivity, good chemical stability and are easy to synthesize; therefore, this material has been extensively studied by earlier researchers [7, 10, 13–20]. In case of CO_2 gas, the resistive sensor works due to change in electrical conductance of sensing material. As CO_2 is a chemically stable gas, therefore its detection with the resistive methods is more difficult than that of other reducing gases [21]. The demand for convenient and low-cost sensor for continuously monitoring gaseous emissions from various processes is steeply growing. Literature survey shows that various metal oxides and their composites were investigated for developing the CO_2 gas sensor. Among them, semiconducting metal oxides such as CSA–TiO_2 composite [22], Cr doped TiO_2 [23], SnO_2 thin film [24] and zinc oxide [25, 26] have been studied extensively. Table 1 describes the sensors developed for the detection of CO_2 but one can find that sensor response is very poor and without the sensitivity and selectivity.

The dynamical properties of conductive polymer in the form of thin film coated on a metal oxide nanostructured film as substrate have attracted considerable interest in recent years [27, 28].

✉ B. C. Yadav
balchandra_yadav@rediffmail.com

Rakesh K. Sonker
rakesh.sonker81@gmail.com

[1] Nanomaterials and Sensor Research Laboratory, Department of Applied Physics, Babasaheb Bhimrao Ambedkar University, Raebareli Road, Lucknow, Uttar Pradesh 226025, India

Materials Letters 152 (2015) 189–191

Contents lists available at ScienceDirect

Materials Letters

journal homepage: www.elsevier.com/locate/matlet

Synthesis of ZnO nanopetals and its application as NO_2 gas sensor

Rakesh K. Sonker [a], S.R. Sabhajeet [a], Satyendra Singh [b], B.C. Yadav [a,*]

[a] Department of Applied Physics, School for Physical Sciences, Babasaheb Bhimrao Ambedkar University, Lucknow 226025, Uttar Pradesh, India
[b] Department of Physics, University of Allahabad, Allahabad 211002, Uttar Pradesh, India

ARTICLE INFO

Article history:
Received 8 February 2015
Accepted 24 March 2015
Available online 2 April 2015

Keywords:
ZnO nanopetal
NO_2 gas sensor
Chemical route

ABSTRACT

In the present work an effort has been made to fabricate nanopetal structured thin film of zinc oxide using chemical route for the efficient and fast detection of NO_2 gas at lower operating temperature. The thin film of ZnO was fabricated on the surface of corning glass substrate and Pt inter digital electrodes (IDEs) were grown over the thin film. The as prepared ZnO sensor showed a high sensing response of $\sim 1.19 \times 10^2$ towards 20 ppm of NO_2 gas at room temperature with an average response and recovery time of $\sim$1.42 min and 1.71 min, respectively. The obtained results were found reproducible and no ageing effect was observed.

1. Introduction

ZnO is one of the n-type semiconducting oxide materials utilized widely in the fields of transparent conducting electrodes, varistors, sensors and optoelectronic devices [1,2]. Especially, this oxide material has been extensively studied for its potential use in semiconductor type gas and UV sensors, since it has considerable sensitivity to CO or NO_x gases [3–5]. Oxidizing gas molecules adsorbed on the surfaces of oxide materials and creates electron-depleted layers, which increase the sensor resistance. There are two different types of contact between the particles of sensing materials [6]: the two-dimensional (2-D) contact between necked particles and point-to-point contact between ordinary particles. When the particles are necked together significantly and the sizes of the necked part become comparable to the thickness of the resistive electron depleted layer, the conductive channel through the neck determines the total resistivity (neck model). When the particle sizes are significantly larger than the thickness of the electron depleted layer, the conductive channel through the neck becomes too wide for the channel to control the electrical resistivity of the particles chain. In this condition, the point-to-point contacts between the grain boundaries dominate the total resistivity, giving rise to gas sensitivity independent of the particle size. Metal-oxide semiconductors such as SnO_2, TiO_2 and ZnO have high sensitivity, good chemical stability and are easy to synthesize; therefore, these semiconductors have been extensively studied to determine their suitability for use as NO_2 gas sensors [7,8].

In the present work, we have investigated ZnO in order to develop a highly responsive sensor which is robust, small sized, having long life and operable at low temperature with sufficient sensitivity for the detection of nitrogen dioxide in low concentrations.

2. Experimental

2.62 g zinc nitrate hexahydrate was dissolved into 100 ml of distilled water. In order to make the gel of the zinc oxide 100 ml of diluted ammonia solution (3% concentration, labelled as A) was added to zinc nitrate precursor under continuous stirring. This gel was used for the fabrication of thin film. Later for increasing the pH value, concentrated ammonia solution (25% concentration, labelled as B) was added to it that results in the precipitation of the material. The obtained precipitate was separated by centrifugation at 5000 rpm for 10 min and then dispersed in 50 ml of 1,4-butanediol. The solution with the dispersed $Zn(OH)_2$ was heated at 150 °C for 36 h in a closed glass bottle.

The morphology and size distribution of as-prepared ZnO nanostructures were observed by scanning electron microscope (SEM, TESCAM MiraIII). The crystallinity and structure were investigated by an X-ray diffractometer (X-Pert PRO PANalytical). Optical characterization was carried out by the UV–vis Spectrophotometer. For studying the gas sensing properties, the home-made gas dilution system was utilized [9]. The total amount of gas flow rate of the diluted NO_2 gas by dry air is 5000 ml/min and the volume of chamber is 5000 ml. The ZnO nanopetal (NP) array sensor was inserted between the two electrodes and the diluted NO_2 gas was injected into the test chamber. Variations in the electrical resistance of the sensor were measured with a Keithley (6517B) electrometer interfaced with a personal computer. The sensing response of prepared sensor structure towards oxidizing NO_2 gas is given as follows [10]:

$$S = \frac{R_g}{R_a} \quad (1)$$

where R_a and R_g are the values of resistance of the sensor in the presence of atmospheric air and target gas, respectively. The response time was measured as the time taken by the sensor to acquire the 90%

* Corresponding author. Mobile: +91 9450094590.
E-mail address: balchandra_yadav@rediffmail.com (B.C. Yadav).

http://dx.doi.org/10.1016/j.matlet.2015.03.112
0167-577X/